The University Of Sheffield.

Physical Layer Techniques for Indoor Wireless Visible Light Communications

Ravinder Singh

A thesis submitted for the degree of

Doctor of Philosophy in Engineering

The University of Sheffield

Faculty of Engineering

Department of Electronic and Electrical Engineering

Dec 2015

Acknowledgements

It has been a privilege to be a student under the supervision of Professor Timothy O'Farrell and Professor John David.

I would like to thank Professor Timothy O'Farrell for his continuing guidance and support. I have benefited immensely from his technical expertise, research direction and commitment.

I would also like to thank Professor John David, the former head of EEE department, for providing me with this opportunity to research at the University of Sheffield. Professor David is one of the kindest human being I have had the opportunity to work with. He has been very supportive ever since I have arrived in the UK.

I am very grateful to have received immense amount of technical advice from Prof John Cioffi of Stanford University on vector coded multi-carrier signalling, which is detailed in Chapter 3 of this thesis. I would like to thank Dr Atsuya Yokoi of Samsung Research Institute, Yokohama, for his invaluable help in understanding the IEEE standardised CSK systems. I would also like to thank Prof Sarah Wilson of Santa Clara University and Prof Jeffrey Carruthers of Boston University for their detailed explanation on the optical channels.

I am very grateful to have worked along all my colleagues in communications research group. Dr Salim Abukharis, Dr Charles Turyagyenda and Dr Siyi Wang were very supportive since the beginning of my research.

At last, I would like to thank all my family members for their continuous support and encouragement throughout my education. I am grateful to have support from my Fiancee, Amanpreet Kaur, and would like to thank her for always standing by me.

~ This thesis is dedicated to my beloved mother and father ~

Abstract

The growing demand for bandwidth-hungry applications and increasing number of smart interconnected devices has increased the data traffic on radio access networks. Subsequently, the saturating spectral efficiencies in crowded radio frequency spectrum has impelled the researchers to exploit the optical spectrum for communications. In particular, many developments in the visible light communication (VLC) as a combined lighting and communications system have taken place.

Despite abundant optical bandwidth, the data transmission rates and power efficiencies in VLC are partly limited by the electrical channel bandwidth and the type of signalling sets which can be used in this intensity modulated, direct detected system. In order to improve the power and spectral efficiencies, this thesis focuses on physical layer (PHY) techniques. The state-of-the-art single channel modulations (SCM) based on M-PAM, multi-channel modulations (MCM) based on OFDM, and IEEE standardised multi-colour modulations are investigated comprehensively through simulations and theoretical analysis, over representative VLC channels considering the optical properties of front-end devices.

The bit error performances and spectral efficiencies of DC-biased and non DC-biased MCM systems are compared. A new vector coding based MCM is proposed to optimally utilise the channel state information at the transmitter as an alternative to optical OFDM. The throughputs, peak-to-average power ratios and DC-bias requirements of SCM and MCM systems are investigated which show that the lower DC-bias requirements reduce power consumed for the same throughput in SCM systems when compared to MCM systems. A new quad-chromatic colour shift keying (CSK) system is proposed which reduces power requirements and complexity, enhances throughput and realises a four-dimensional signalling to outperform the IEEE standardised tri-chromatic CSK system.

For improved power efficiency and throughput of VLC PHY, use of rate-adaptive binary convolutional coding and Viterbi decoding is proposed along with frequency domain channel equalisation to mitigate temporal dispersion over representative VLC channels.

A List of Abbreviations

APD: Avalanche Photo-Detector
APP: *A Posteriori* Probability
ADC: Analogue to Digital Converter
AR: Aggregate Rate
AWGN: Additive White Gaussian Noise
ACO-OFDM: Asymmetrically Clipped Optical OFDM
ADO-OFDM: A Clipped DC-biased Optical OFDM

BB: Bipolar Baseband
BC: Binary Convolutional
BCYR: Blue Cyan Yellow Red
BER: Bit Error Rate
BPSK: Binary Phase Shift Keying

CAGR: Compound Annual Growth Rate
CDF: Cumulative Distribution Function
CB: Colour Band
CBC: Colour Band Combination
CC: Colour Calibration
CP: Cyclic Prefix
CSK: Color Shift Keying
CSI: Channel State Information
CIE: Commission Internationale de l'Eclairage
CIL: Cross-talk and Insertion Loss
CIM: Colour Intensity Modulation
CIR: Channel Impulse Response
CWCV: Central Wavelength Chromaticity Value

DAC: Digital to Analogue Converter
DCO-OFDM: Direct-current-biased Optical OFDM
DCO-PAM: Direct-current-biased Optical PAM
DCO-VC: Direct-current-biased Optical VC
DD: Direct Detection
DFT: Discrete Fourier Transform
DFE: Decision Feedback Equalisation
DPPM: Differential Pulse Position Modulation
DPIM: Digital Pulse Interval Modulation

DMT: Discrete Multi-tone
DR: Dynamic Range

E/O: Electrical-to-Optical
Eb/No: Energy Per Bit to Noise Power Spectral Density Ratio

FD: Frequency Domain
FDE: Frequency Domain Equalisation
FEC: Forward Error Correction
FFT: Fast Fourier Transform
FIR: Finite Impulse Response
FOV: Field of View

GF: Galois Field

HD: Hard Decision

IEEE: Institute of Electrical and Electronics Engineers
IM: Intensity Modulation
IM/DD: Intensity Modulation/ Direct Detection
IDFT: Inverse Discrete Fourier Transform
IFFT: Inverse Fast Fourier Transform
ISI: Inter-symbol Interference
IR: Infra-red

JEITA: Japan Electronics and Information Technology Industries Associations

LED: Light Emitting Diode
LD: Laser Diode
LLR: Log Likelihood Ratio
LOS: Line-of-sight
LTE: Long-term Evolution

MAP: Maximum *a posteriori* Probability
MCM: Multi-channel Modulation
M-CSK: M-ary Color Shift Keying
M-QAM: M-ary Quadrature Amplitude Modulation
M-PAM: M-ary Pulse Amplitude Modulation
M-PPM: M-ary Pulse Position Modulation
MIMO: Multiple Input Multiple Output
MSM: Multiple Sub-Carrier Modulation
MM: Metameric Modulation

MMSE: Minimum Mean Square Equalisation

NLOS: Non Line-of-Sight
NRZ: Non Return to Zero

OWC: Optical Wireless Communication
OFDM: Orthogonal Frequency Division Multiplexing
OOK: On-off Keying
O/E: Oprical-to-Electrical
OLED: Organic Light Emitting Diode
OC: Optical Concentrator
OCC: Optical Camera Communication

PSD: Power Spectral Density
PD: Photo Detectors
PHY: Physical Layer
PAM: Pulse Amplitude Modulation
PPM: Pulse Position Modulation
PAPR: Peak-to-average Power Ratio

QPSK: Quaternary Phase Shift Keying
QLED: Quad-chromatic LED
QAM: Quadrature Amplitude Modulation

RAC: Rate Adaptive Coded
RF: Radio Frequency
RGB: Red Green Blue
RS: Reed-Solomon
Rx: Receiver

SEE-OFDM: Spectrally and Energy Efficient OFDM
SCM: Signal Channel Modulation
SD: Soft Decision
SNR: Signal to Noise Ratio
SISO: Single Input Single Output
SPD: Spectral Power Distribution
SVD: Singular Value Decomposition

TLED: Tri-chromatic LED
TD: Time Domain
Tx: Transmitter

U-OFDM: Unipolar Optical OFDM
UE: User Equipment
UV: Ultraviolet

VC: Vector Coding
VLC: Visible Light Communication
VLCC: Visible Light Communication Consortium
V2V: Vehicle to Vehicle
V2I: Vehicle to Infrastructure

WDM: Wavelength Division Multiplexing
WIC: Wireless Infra-red Communication
WUC: Wireless Ultraviolet Communication
WLAN: Wireless Local Area Network
Wi-Fi: Wireless Fidelity
WiMAX: Worldwide Interoperability for Microwave Access

ZFE: Zero Forcing Equalisation

Contents

List of Figures

List of Tables

Chapter 1

Introduction

Communication has played an important role in the advancement of every aspect of the human life. Early humans used fire, sound and sign languages to communicate and with evolution more sophisticated techniques were developed to support the growth in human knowledge about themselves and the world around them. The idea of transmitting data over long distances and at fast transmission rates led to the development of the modern communication modes such as telegraphy, telephones, cellular phones and optical fibres. However, the demands for higher data transmission rates to support bandwidth hungry applications and the number of smart interconnected devices are ever growing. This has kept the communications researchers continuously advancing the existing as well as innovating new information transmission technologies.

The limited radio frequency (RF) spectrum impelled the researchers to exploit the abundant visible, infrared and ultraviolet parts of the optical spectrum for wireless communication which led to the development of optical wireless communication (OWC) systems. The visible spectrum in particular has been of more interest due to the advantage of combining the lighting and communication through single source, the light emitting diode (LED).

This thesis is focused on the design of physical layer (PHY) techniques for wireless visible light communications (VLC). This includes the study of the state-of-the-art single & multi channel modulation schemes for VLC and modifying the existing and/or developing new modulation methods to improve the power efficiency for sufficiently low bit error probabilities and limited bandwidths. The use of forward error correction (FEC) coding and channel equalisation techniques for both single and multi channel modulation has been explored to further improve the system power or spectral efficiencies. Both line-of-sight (LOS) and non-LOS (NLOS) wireless VLC channels have been used to evaluate the performance of different PHY configurations. The optical properties of different

transceiver components have been taken into account to investigate their impact on the PHY performance.

This Chapter provides an introduction to this thesis and the research carried out in designing novel physical layer techniques for wireless visible light communication. The requirements and applications of VLC systems are detailed in the beginning of the chapter. Later, the aim and objectives of the research are presented. Original research contributions are then introduced and a list of publications is presented. At last the chapter details the outline of the thesis.

1.1 VLC Requirements and Applications

As per CISCO forecast shown in Fig. 1.1, the compound annual growth rate (CAGR) of mobile data traffic is 61% [11]. At the same time the CAGR for wired and Wi-Fi devices are 12% and 25%, respectively [11], indicating a large increment in the global IP traffic by 2018. On the other hand the RF spectrum is very limited and the spectral efficiency gains are saturating [12][13]. This indicates that there could be a significant network capacity shortfall in the very near future. Researchers around the world are exploring different solutions to improve the capacity of the networks using technologies such as massive MIMO and mmWave [14]. Another solution to overcome the foreseen capacity crunch is to make use of hundreds of THz of unlicensed bandwidth available in the visible spectrum for indoor wireless communication. This will not only provide spectrum relief to the RF network but will also make mobile communication simpler, energy efficient and less prone to interference [12]. The indoor VLC could enable the end users to directly connect to the high speed fiber optic network. The indoor environment also allows VLC to achieve high data rates due to the availability of high signal to noise ratio (SNR). In a typical office environment, *Grubor et al* has found the electrical SNRs to be greater than 60dBs throughout the entire office [15].

Table 1.1 compares current RF and VLC technologies. It is clear that the data rate and range of RF communication technology are superior to current VLC systems as proposed in [16][17]. The RF technology is well understood and developed. Whereas VLC is a relatively new concept, it has the potential to achieve much higher data rates with the use of multiple multi-colour light sources (LEDs) [16][17], MIMO [18] and frequency domain equalisation techniques, with the use of multi-gigahertz laser diodes (LDs) [19]. Additionally, techniques like fibre-wireless-fibre coherent wavelength division multiplexing (WDM) [20] can also be used in VLC systems for further enhance the data rates. Switching the LED at high frequencies reduces its output power levels. However, Through the use of an array of LED, the general illumination conditions can be satisfied.

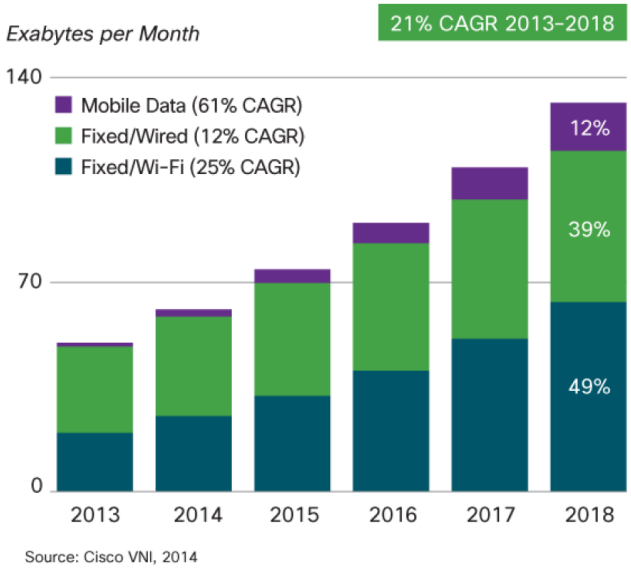

Figure 1.1: Global IP Traffic: Wired and Wireless (Source: CISCO VNI 2014)

Another big advantage of VLC is the energy consumption of the solid-state lighting devices. If every single light bulb is replaced by a VLC system the overall energy saving through a combined lighting and communication system will be significant as an LED bulb consumes 95% less power than an incandescent bulb [21].

Table 1.1: Key Characteristics of RF and VLC Technologies

Characteristics	**IEEE 802.11ac/ad System**	**VLC Prototype**[1]	**Potential VLC System**
Data Rate	7 Gbit/s	5.6 Gbit/s	10s of Gbit/s
Range	10m	1.5m	10m
BER	$\leq 10^{-6}$	$\leq 3.8 * 10^{-3}$	$\leq 10^{-6}$
Achetecture	Single Cell	Single Cell	Single Cell
Concept/ Technology	Well understood and developed	New and less developed	–

In what follows, further advantages of VLC are listed:

[1]This system is based on SISO setup with WDM [16]

- Unregulated and unlicensed wide spectrum;
- Security and immunity to interference in indoor environment as visible light is confined within walls;
- Simple and small system circuitry can be made out of inexpensive components;
- Free from multipath fading (but not multipath intersymbol interference (ISI)) [22];
- High data transmission rates achievable as high SNRs in indoor environments.

However, there are some shortcomings of VLC too, such as:

- Short range of operation;
- Limited electrical bandwidth of optical front-ends ;
- Poor bit error rates (BERs) of the existing prototypes;
- Unproven multicell operation;
- The need for extensive backhaul.

1.1.1 Applications

There are various applications of VLC systems of which some are detailed below:

- ***A smart home/office network***: Wireless communication through LEDs brings lighting and communication together for a home/office environment. The advancements in solid state lighting are improving the energy efficiencies of the LEDs. Use of visible spectrum for indoor wireless communication provides RF spectrum relief, particularly in 2.4 and 5 GHz bands, which can be used for other purposes.
- ***Hybrid RF-VLC systems***: The upcoming generations of wireless and mobile communication systems is likely to be highly heterogeneous where multiple access technologies will co-exist to enhance the user experience. A hybrid RF-VLC system, in such a scenario, could prove to be a highly energy efficient and reliable method for wireless communication where the two technologies piggyback on each other's strengths.
- ***Intelligent transport systems***: Vehicle to vehicle (V2V) and vehicle to infrastructure (V2I) communication can also be achieved through VLC to send useful information regarding traffic, road works and accidents & emergencies.

- ***Embedded displays***: LED displays such as computer/tablet monitors, televisions, advertisement/information boards etc. can be used to transmit display related detailed information to the viewers.
- ***Location-based service in shopping malls and supermarkets***: VLC can be used to broadcast product information as well as for navigation purpose inside a supermarket or a shopping mall.
- ***Commercial aviation***: The pre-installed LED lighting system on aeroplanes can also be used to provide communication services as visible light is safe and free of interference. Additionally, use of pre-installed LED lighting would mean minimum extra communication equipment on-board.
- ***Interference free communication system for hospitals and healthcare centres, petrol stations, oil refining cites***: VLC is very attractive in environments where the use of RF systems is prohibited. In hospitals and healthcare centres, VLC can provide interference free communication particularly near MRI scanners . Similarly due to risk of explosions, the use of RF systems is banned near petrol stations and oil refining sites where visible light can provide both light and communication.
- ***Underwater communication***: Visible light allows communication up to longer distances under water when compared to radio waves. This is because water containing dissolved salts conducts electricity well and it absorbs electromagnetic waves quickly. An underwater communication system that uses green light can operate up to a distance of 30 metres has been described in [23].

1.2 Research Motivation and Objectives

Aim

The aim of this research was to explore and extend the transmission capabilities of the standardised and non-standardised, single and multiple channel modulation techniques for VLC systems, such that the challenges with respect to the physical layer design of VLC systems can be addressed for the deployment of visible light access points within an indoor environment to support energy efficient, very high data rate, and secure wireless communication for enterprise & home networks.

Motivation

As detailed in the VLC system requirements, the looming RF network capacity crisis has led researchers to develop VLC systems and exploit the optical spectrum for indoor wireless communications. This and the potential of VLC systems to reduce the global energy consumption and carbon emissions, by combining lighting and communication has motivated the author to study the VLC systems and propose novel techniques to improve the communication capabilities of VLC to support the ever growing high data rate demands.

In principle, the PHY design of RF and VLC systems is very similar, however, the use of LED as a source and photo detector (PD) as a receiver forces the VLC systems to use intensity modulation (IM) and direct detection (DD). This means that the transmit signal in VLC is different from that used in the RF communications as it has to be a real and unipolar waveform. This reduces the dynamic range of the VLC signals and limits them to be of real and unipolar form, which makes the power and spectral enhancements in VLC systems even more challenging.

The author was motivated to explore both single (phosphor coated blue) and multi colour (red, green and blue) optical signalling techniques as the different types of light sources can be exited with various signal sets to realise wireless communication as well as lighting simultaneously. Additionally, in some VLC applications, signalling schemes will be required to have a precise control over the output colour of the LEDs, whereas, in other applications the output might just have to be white light. Therefore, both types of signalling schemes were explored in this thesis such that contributions can be made across different types of VLC physical layers.

Objectives

In order to achieve the aim, research had set different objectives which are detailed as following:

1. ***Single and Multi Channel Modulations***: This involved studying the existing single channel modulation (SCM) and multi channel modulation (MCM) schemes through developing physical layer simulators in MATLAB to identify their strengths & weaknesses, and compare their performance using additive white Gaussian noise (AWGN), LOS and NLOS VLC channels. Despite its origins in RF communications, various modified OFDM MCM schemes have been proposed for VLC where the indoor optical wireless channel does not vary with time as fast as the RF channels do. Therefore, an objective of this research was to explore the use of an ideal MCM

scheme under known channel conditions called vector coding (VC) for VLC and carry out the following investigations:

- Simulate VC using baseband modulation scheme which is appropriate for IM/DD channel e.g. multi-level pulse amplitude modulation, and compare its performance against optical OFDM schemes, in representative VLC channels.
- Compare the throughput performance of SCM and MCM schemes over VLC channels and analyse the effects of different channel delay spreads on both techniques.

2. ***Investigation of Color Shift Keying***: Research also involved investigation into modulation schemes which are specifically designed for multi-colour light sources, such as colour shift keying (CSK) for VLC. CSK which is standardised in IEEE 802.15.7, provides a maximum data rate of 96 Mbit/s [8]. This is limited by the electrical bandwidths of the front-end devices specified in the standard. The idea was to improve the data rates of CSK systems assuming the same electrical bandwidths. The following steps describe how the investigation into CSK was approached:

   - Develop CSK simulators and evaluate the performance of standardised VLC modulation scheme.
   - In order to improve the data rates, design higher order modulation e.g. 64-CSK, 256-CSK, 1024-CSK and 4096-CSK.
   - The standardised CSK uses three colour LEDs (RGB LEDs). Develop methods to include more colour channels into CSK to extend its signal space for improved performance.
   - Improve Gray mapping in multilevel CSK constellations as the standardised system constellations have neighbour symbols with more than one bit Hamming distances.

3. ***Forward Error Correction Coding***: FEC coding is an important part of the PHY in wireless communications, which enhances the system performance by making it more resilient to bit errors occurring during a transmission. As mentioned earlier, due to restrictions on the transmit signal of IM/DD VLC systems, enhancing their power and spectral requirements becomes more important. Therefore, a study in to FEC coding schemes for the investigated VLC modulation schemes was also planned, such that these scheme can approach their theoretical capacities. Well-know industry standard binary convolutional (BC) codes with a Viterbi decoder was chosen to be used with the existing and new VLC modulation modes. As specified by the IEEE

802.15.7, the objective involved investigation of the Reed-Solomon (RS) codes for CSK and to compare their performance against that of the BC coded counterparts.

4. ***Channel Equalisation***: The existing optical MCM systems deploy frequency domain (FD) channel equalisation to mitigate the effects of channel dispersion leading to inter symbol interference (ISI). An objective of this research was to investigate use of different FD channel equalisation techniques for all the considered SCM modulation schemes, in order to improve their performance while operating over dispersive VLC channels. This would also allow a fair performance comparison between SCM and MCM schemes.

1.3 Original Contributions

As an outcome of this research the following original contributions are made:

1. ***Performance evaluation of CSK PHY of IEEE 802.15.7:*** The investigation of IEEE standardised tri-chromatic[1] LED (TLED) CSK system involves extensive simulations and theoretical analyses to define a baseline system performance for CSK developers. The bit & packet error performances of nine different colour band combinations of CSK are examined based on chromatic and signal space detection at the receiver side. The multi-colour channel cross-talk and insertion losses which arise due to the properties of optical devices are modelled and taken into account for the completeness of performance evaluation (see Chapter 5).

2. ***Design and evaluation of an enhanced CSK (QLED) system:*** A novel quad-chromatic[2] LED (QLED) CSK to enhance the performance of multi-colour VLC systems is proposed. Being a three colour system, the standardised TLED CSK possesses a triangular chromatic symbol constellation with limited space. The QLED system with the addition of an extra colour enhances the Euclidean distance between CSK symbols and enables 2^{nd} order Gray mapping, leading to a reduction of up to 5 dB in system SNR requirements (in comparison to TLED CSK). The QLED scheme enables the use of very high level modulation orders for CSK e.g. 4096-CSK, while providing control over the output light and M-QAM like simple Gray mapping methods (see Chapter 5).

3. ***Channel coding and equalisation for improved performance of CSK schemes:*** While operating over indoor VLC channels, the TLED and QLED CSK

[1] Three colours
[2] Four colours

schemes suffer from irreducible bit error rate in uncoded & unequalised formats due to ISI. Especially, the higher modulation modes are affected due to ISI, which limits the throughput of these multi-colour systems even when strong line-of-sight (LOS) is available between the transmitter and receiver. Extensive study of rate-adaptive coded CSK systems with frequency domain equalisation (FDE) is carried out through simulations and theoretical analyses. This study shows that the CSK systems improve their throughput by up to 200% with the use of a binary convolutional encoder, Viterbi decoder and FDE while operating over hybrid (LOS+Diffuse) and purely diffuse VLC channels for a limited system bandwidth of 24 MHz (see Chapter 6).

4. ***Comparative study of DC-biased and non DC-biased multi-channel VLC systems for high spectral efficiency:*** The uncoded DC-biased & non DC-biased multi channel modulation schemes are studied based on simulations and analytical formulations. The spectral efficiencies and BER performances of the two schemes are compared and the investigation concludes that despite their high DC-bias requirements, the DC-biased multi-channel modulation schemes will achieve high spectral efficiencies with lower system complexity and power requirements in comparison to the non DC-biased multi-channel modulation schemes which become very complex to model as the spectral efficiency increases above 3 bit/s/Hz (see Chapter 3).

5. ***A new multi-channel modulation scheme for VLC:*** Vector coding is utilised to develop a novel DC-biased optical multi-channel signalling scheme for VLC which is named DCO-VC. The DCO-VC scheme uses channel state information at the transmitter for optimal channel partitioning which is well suited to the static nature of indoor VLC channel. The throughput performance of the DCO-VC scheme is studied through simulations and theoretical analyses over AWGN, hybrid and diffuse channels and compared to the existing optical multi-channel modulation schemes, such as DCO-OFDM (see Chapters 3 & 4).

6. ***Throughput enhancement of single and multi channel VLC signalling schemes:*** In order to improve the capacity of the DC-biased single and multi channel systems while operating over representative VLC channels, use of punctured binary convolutional codes and Viterbi decoder with both hard and soft decision detections is considered. The analyses of results show that the rat-adaptive FEC coding schemes provide SNR gains of up to 9 dB for the single and multi channel systems. The effects of signal clipping at the transmitter due to limited dynamic range are studied and the peak-to-average power ratios (PAPRs) of both the single

and multi-channel schemes are compared. Due to low DC-bias requirements for a low bit error rate, the single channel system proves to be much more power efficient than the multi-channel systems.

1.3.1 Publications

The investigations made throughout this research led to following publications:

Refereed Journal Papers

1. Singh, R., O'Farrell, T., David, J.P.R., "An Enhanced Color Shift Keying Modulation Scheme for High-Speed Wireless Visible Light Communications," in IEEE Journal of Lightwave Technology, vol.32, no.14, pp.2582-2592, July 2014.

2. Singh, R., O'Farrell, T., David, J.P.R., "Rate-Adaptive Coded Colour Shift Keying with Frequency Domain Equalisation for VLC," (**under review**) in IEEE Journal of Lightwave Technology.

3. Singh, R., O'Farrell, T., David, J.P.R., 'Rate-Adaptive Coded Single and Multi-channel Signalling for Visible Light Communications," (**under review**) in IEEE Transaction on Vehicular Technology.

Conference Papers

1. Singh, R., O'Farrell, T. and David, J.P.R., "Performance evaluation of IEEE 802.15.7 CSK physical layer," In IEEE Globecom Workshops (GC Wkshps), 2013, December, (pp. 1064-1069).

2. Singh, R., O'Farrell, T. and David, J.P.R., "Higher Order Colour Shift Keying Modulation Formats for Visible Light Communications," In IEEE Vehicular Technology Conference (VTC Spring), 2015, May, (pp. 1-5).

3. Singh, R., O'Farrell, T. and David, J.P.R., "Analysis of Forward Error Correction Schemes for Colour Shift Keying Modulation," In IEEE Annual Symposium on Personal, Indoor and Mobile Radio Communications (PIMRC), 2015, September.

1.4 Thesis Outline

This thesis is comprised of seven chapters. The first chapter provides an introduction to the research undertaken and summarises the importance of VLC technology in wireless communications. The research aim and objectives are also presented in the first chapter

together with the motivation behind the research. This chapter ends by summarising the research contributions and listing the publications.

Chapter 2 presents an overview of VLC systems. The background and a literature review of VLC techniques is provided in this chapter. A general VLC system set-up is introduced. The front-end optoelectronic devices used in VLC are characterised in this chapter. Different indoor channel models used throughout the research are also detailed with their channel impulse responses, which includes the LOS and NLOS channels. The noise at the receiver, insertion losses and colour cross-talk, which affect the performance of VLC systems are also modelled. The chapter finishes by reviewing the VLC signalling schemes and standards developed so far.

The thesis starts by detailing the investigations made in to the conventional non-standardised single and multi channel VLC modulation schemes. A performance comparison of pulse amplitude modulation (PAM) based single channel modulation and OFDM based multi channel modulation schemes is provided in Chapter 3. The optical OFDM schemes include both the DC-biased and non DC-biased systems. The focus in this chapter is on the analytical and simulations based bit error rate comparison: a) between single and multi channel modulations and b) between different types of multi channel modulation schemes. A comparison between the peak-to-average power ratios of considered systems is also presented. The spectral efficiencies of all the considered systems are also compared. The newly developed DC-biased optical vector coding multi channel modulation schemes is also introduced in this chapter. A bench mark performance of single and multi channel schemes using an AWGN channel is provided in this chapter, which serves as a basis to the investigations carried out in Chapter 4.

Chapter 4 evaluates the performance of DC-biased single and multi channel modulation schemes using the representative VLC channels introduced in Chapter 2, first in uncoded modes and later through the use of punctured binary convolutional codes with a Viterbi decoder. This investigation is carried out to enhance the throughput of each system for their operation over a variety of indoor LOS and NLOS channels. The throughputs of uncoded and coded systems are compared with their theoretical capacities obtained from a modified Shannon's formulas. Both hard and soft decision detections at the receiver of each system are investigated. Both simulation and theoretical performance analysis are presented. This chapter also investigates the effects of signal clipping which arise due to the limited dynamic range of the VLC transmitters, for both the uncoded and coded systems.

Having investigated the most commonly used single and multi channel VLC modulation schemes, this thesis then studies another single channel modulation scheme named colour shift keying, which is a modified unipolar PAM scheme specifically designed to

have precise control over the output light of a multi-colour VLC source. Chapter 5 begins by studying the IEEE standardised CSK system through simulations and analytical formulations for bit error probabilities for an AWGN channel. The colour and signal space detections along with nine different standardised colour band combinations of CSK systems are investigated. Chapter 5 then details the working of a new four colour based CSK modulation scheme and evaluates its bit error rate performance in order to make a comparison with the standardised three colour CSK systems studied earlier in the chapter. The bit error probabilities of both the standardised and new CSK systems are then evaluated considering the colour cross-talk and insertion losses that arise due to the optical characteristics of the front-end devices such as LEDs, PDs and filters. The use of a colour calibration technique to mitigate the effects of cross-talk is also investigated in Chapter 5. This chapter ends by comparing the performance of CSK systems with a WDM system which has the ability to concurrently transmit data through multiple colour channels.

After characterising the uncoded CSK systems over the AWGN channels with colour cross-talk and insertion losses, this thesis then evaluates the performance of BC coded and FD equalised CSK systems over both LOS and NLOS VLC channels in Chapter 6. This chapter begins by analysing the performance of the coded and uncoded CSK systems over an AWGN channel through simulations and theoretical approximations. As a FEC scheme, both standard specific RS and proposed BC codes are used. After confirming the working of coded CSK over AWGN channel, indoor environment based LOS and NLOS channels are then included into the investigations and throughput performance of uncoded-CSK, coded-CSK and coded-CSK systems with a FD zero forcing equaliser is evaluated. Investigations in this chapter show the importance of channel coding and equalisation for CSK systems in order to maximise their throughputs. Finally, Chapter 7 summarise all the research outcomes and gives concluding remarks.

Chapter 2

An Overview of VLC Systems

2.1 Introduction

The VLC, like infrared (IR) [22] and ultraviolet (UV) [24], is an optical wireless communication (OWC) technique [13], which utilises the visible part ($\sim 380-700$ nm) of the optical spectrum to convey information wirelessly [25]. The very first idea of using visible light for information transmission came into existence back in 1870s when Alexander Graham Bell and his assistant Charles Sumner Tainter modulated the sun light falling on a mirror with a person's voice [26]. Later in 1880, the first VLC device, named Photophone, was revealed which successfully communicated up to a distance of 700 ft. [26]. However, the reliance on the sun light was the major disadvantage of the Photophone. In modern VLC systems, the optical source/transmitter (Tx) is realised by light emitting diode (LED) and the optical receiver (Rx) by a PIN photo-detector (PD) or avalanche photo-detector (APD).

The first ever indoor OWC system was proposed by Gfeller and Bapst in 1979 [27], which was based on the use of IR radiations. Since then, extensive research on IR wireless communication devices has been carried out over almost two decades. However, with the rapid advancements in the solid-state devices to provide highly energy efficient lighting [28] and their ability to combine lighting and communication through a single medium has worked as a catalyst to boost research in VLC [29]. VLC has been the centre of attention for the past decade due to its ability for save energy in comparison to RF communication systems and to provide spectrum relief to wireless communications. According to a study in [21], if every light bulb in the world is turned into a VLC access point, approximately 900 kWhr of power can be saved.

Research on VLC started in Keio University, Japan with the objectives to develop, plan and standardise VLC systems [30]. There are various research organisations and

groups that have worked on VLC, such as visible light communications consortium (VLCC) [30], Japan electronics and information technology industries associations (JEITA), home gigabit access (OMEGA) [31] and the task group IEEE 802.15.7. VLC standardisation started in 2007, when JEITA issued two standards, CP-1221 and CP-1222. The first IEEE VLC standard, the IEEE 802.15.7, was published in 2011 with various physical layers (PHYs) and medium access control (MAC) layers with data rates ranging from 11.67 kbit/s to 96 Mbit/s [8][32].

This chapter provides an overview of VLC system development since their introduction in 2000 [33]. Details of front-end electrical-to-optical and optical-to-electrical devices are presented, which includes LEDs, PDs, optical filters and concentrators. Different types of optical wireless channel models used in this research are introduced, which include LOS, NLOS and hybrid channels. The multicolour channel cross-talk and insertion losses, which arise due to the characteristics of optical front-end devices, are also introduced. A model of noise processes at the receiver is also presented. The chapter ends by describing the development of standards and various single and multi channel modulation techniques that have been developed so far for VLC.

2.2 A General VLC Link

Fig. 2.1 illustrates a basic VLC link which consists of a light source, optical wireless channel and an optical receiver. In VLC, the light source is realised using white LED, which is either a blue LED with phosphor coating or an RGB (Red-Green-Blue) LED. The optical receiver is usually a PD or APD. A VLC system, like IR [34] and UV [24] OWC systems, is an IM/DD system [26], where the data is encoded to various intensity levels of the source. A positive and real valued electrical signal $m(t)$ modulates the intensity of the LED(s) which radiates an optical signal $x(t)$ that propagates through the optical wireless channel.

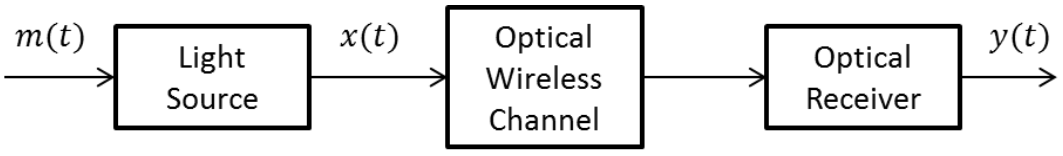

Figure 2.1: A General Schematic of a Visible Communication Link

The optical receiver at the receiving end detects instantaneous intensity changes in the light falling across its surface and outputs an electrical signal $y(t)$, which is corrupted with additive white Gaussian noise (AWGN) [22] and processed to detect the original modulating signal $m(t)$. Given the channel impulse response $h(t)$ of the optical wireless

channel, the VLC systems can be mathematically summarised by [35]:

$$y(t) = \Re(x(t) * h(t)) + n(t), \tag{2.1}$$

where " * " denotes convolution, $\Re$ is the responsivity of the PD and *n(t)* is the AWGN. A complete system equation must also include the electrical response of the source and receiver, and the optical properties of the source and optical filters. In this thesis, the optical properties of the front-end devices are taken into account in the forthcoming chapters. However, the frequency response of the source and receiver is assumed to be flat given the low bandwidths used during the simulations. The details on different indoor optical wireless channels and the AWGN are given in section 2.4 and section 2.5, respectively. In addition to the responsivity of the PD, VLC systems suffer insertion losses and colour cross-talk due to the optical properties of LEDs and optical filters. These losses are detailed in section 2.4.4.

2.3 VLC Electro/Optic Devices

In VLC and in other forms of OWC, the transmitter is an electrical-to-optical (E/O) converting device and the receiver is an optical-to-electrical (O/E) converting device [10]. In this section, details of different types of VLC transmitters and receivers are provided and a comparison of these front-end devices is made based on some key characteristics such as, modulation bandwidth, field-of-view (FOV) (directionality), cost and E/O and O/E conversion efficiency.

2.3.1 Source

LEDs and Laser Diodes (LDs) are the two main types of sources considered in OWC, and the former type of source is generally considered in VLC due to its wide FOV, which makes it a better candidate for the indoor lighting application. However, LDs based VLC systems have recently been explored in order to achieve very high data rates [36][19]. Although LD can provide higher modulation bandwidth [9], when compared to LED, due to their narrow FOV, a complete line-of-sight (LOS) configuration between the transmitter and receiver is required, and eye safety becomes more critical due to large amount of optical power being focused into a certain direction. Therefore, LEDs are generally preferred for VLC over LDs. A characteristic comparison between the two sources is made in Table 2.1.

These optical sources are operated in a forward bias condition and recombination of free carriers in the depletion region generate photons. This phenomenon is know as

Table 2.1: Key Characteristics of Optical Sources [9]

Characteristics	**LED**	**LD**
Modulation Bandwidth	∼KHz to ∼MHz	∼MHz to ∼GHz
FOV	Broad (∼60°)	Narrow(<10°)
Cost	Low	Moderate to High

electroluminescense [37]. In VLC, the LED drive current is varied to modulate the message data over the intensity of light emitted by the semiconductor device. A direct band gap semiconductor material is generally considered for LEDs in order to enhance the probability of recombination [10], hence higher probability of photon emission. The central wavelength, λ_c, of an LED is based on the band gap energy (E_g) of the material used, and the two terms are related as [38]:

$$\lambda_c = \frac{h_p c}{E_g}, \tag{2.2}$$

where h_p is the Planck's constant and c is the velocity of light in vacuum. For more details on the physics of the LEDs and LDs, reader is referred to [37],[38].

In VLC, one of the most important characteristic of a light source is its modulation or cut-off bandwidth. The modulation bandwidth is a function of the capacitance of an LED, radiation lifetime, temperature and the amplitude of current pulse [37]. It defines how fast the data can be transmitted without severe degradation. If a light source is switched at a rate equivalent to its cut-off frequency, its output radiation levels will be halved. As the switching rate increases above cut-off the LED response is further degraded. The modulation bandwidth of LDs is much higher than LEDs due to lower recombination time [37]. However, an advanced form of LEDs known as μ-LEDs is able to achieve modulation bandwidths in range of hundreds of MHz [39]. One drawback of μ-LEDs is their small FOV, which requires LOS for data transmission. Equalising for the frequency response of LEDs allows switching the device above its cut-off bandwidth [28], which is an attractive technique to enhance the data-rates in VLC.

A big advantage of LEDs, from lighting perspective, is their energy efficiency when compared to incandescent bulbs and fluorescent tubes [40]. For an indoor illumination requirement between 400-600 lumens (lux), the commercial LED light bulbs use 6-9 Watt electrical power [41] and have wallplug efficiency of ∼1/3 which is increasing above 50% as per recent research [42]. On the other hand LEDs tend to be more expensive than

incandescent and fluorescent bulbs. However, mass production is expected to continue driving down the cost of LEDs.

There are two main[1] types of LEDs currently being considered in VLC for downlink, which are phosphor coated blue LEDs and multicolour LEDs. The use of IR diode is generally proposed for uplink [16]. A description of these sources is given in the next sub-section.

Phosphor Coated Blue LED

These are essentially blue LEDs with λ_c of $\sim$450nm. The LED is coated with phosphor, which irradiates yellow light and the mixture is perceived as white light by the human eye. A problem with this type of LED is the slow response time of the phosphor compared to the blue LED which limits the modulation bandwidth of the device to $\sim$2 MHz [46] and hence the data rate. To transmit data at a rate equal to the cut-off bandwidth of the blue LED, a blue optical bandpass filter at the receiver side can be used at the cost of reduced signal power that is available to the PDs due to the transmissivity of the optical filter.

Due to simple design and low manufacture cost these LEDs are preferred for illumination and communication when compared to multicolour LEDs. However, to enable display screen data communication and for very high data-rates, the multicolour LEDs become more useful as colour shift keying modulation and wavelength division multiplexing (WDM) can be used.

There exist some eye safety concerns related to the white LEDs known as thermal and photochemical hazards [47]. The probability of occurrence and the potential damage that these hazards may cause depends up on various factors such as, the intensity of light, the wavelength, the exposure time and the area of the retina exposed [47]. The blue and some part of green light is of key concern due to high energy content [47]. There are international (IEC 62471), European (EN 62471) and USA (ANSI/IESNA RP-27) standards that the LED manufactures must comply with for eye safety.

Multicolour LED

The multicolour LEDs are different from phosphorescent LEDs in a way that they produce white light by mixing the light from different colour sources such as red, green and blue (RGB) primary colour sources. Each colour source in a multicolour LED uses semiconductor material with a different band gap and hence have a different λ_c in their spectral power distribution (SPD). These LEDs have the capability of reproducing not just white

[1]Relatively new type of LED named organic LEDs (OLEDs) [43, 44, 45] have also been considered for VLC recently, however, not used in this research.

but also various other colours, which can be represented by chromaticity values, by electronically varying the intensities of colour sources [8]. Details of multicolour LED based modulations are provided in Chapter 5.

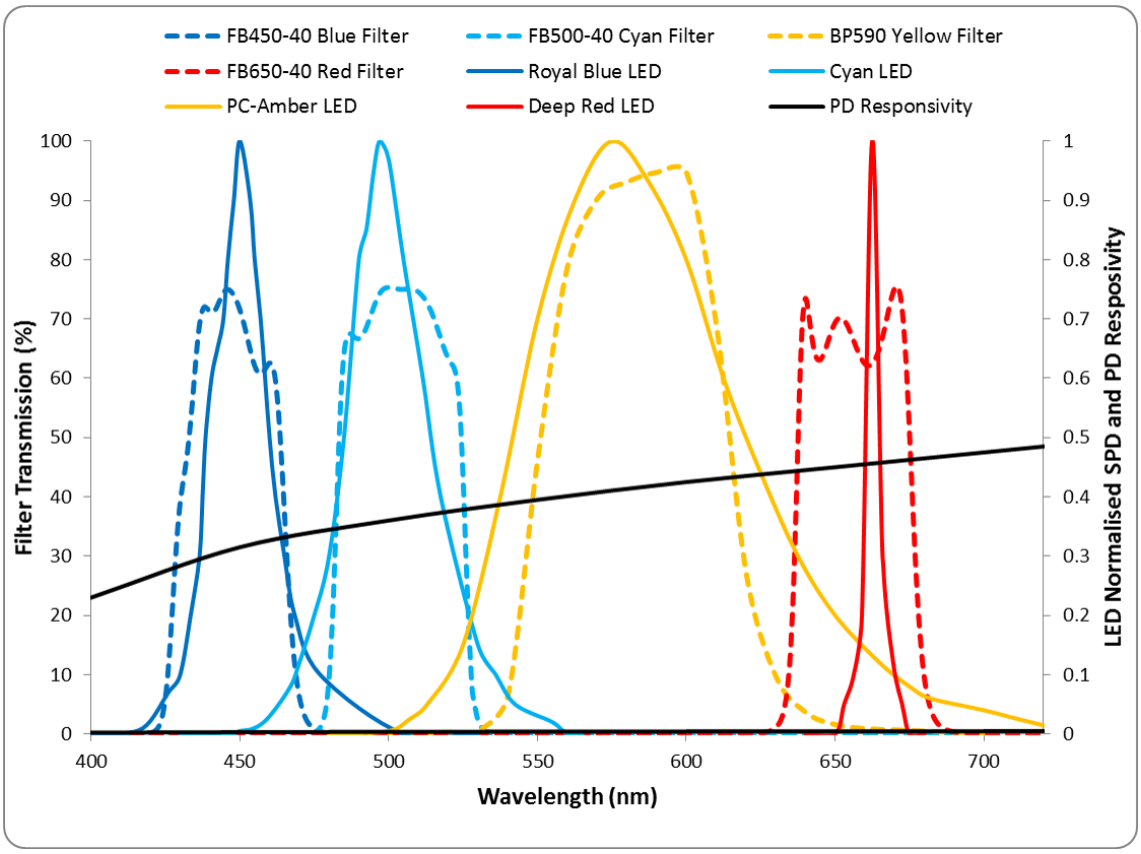

Figure 2.2: Spectral properties of multicolour LEDs [1], optical colour filters [2][3][4][5]) and a PD [6]. Filter transmission is also known as transmissivity.

In Fig.2.2, the normalised SPD of four commercially available different colour LEDs is shown [1]. As we can see each source has different central wavelength. However, there is a significant amount of spectral overlap between different colours. This spectral overlap can have significant effect on the performance of a VLC system where intensities in individual colour bands are required at the receiver. There are different ways to reduce the effect of spectral overlap in multicolour based VLC systems which are discussed later in this chapter and in Chapter 5. Despite the problem, multicolour LEDs have the potential to enable multiple parallel transmissions in VLC through WDM.

IR LEDs

Although this research is focused on VLC systems, it is worth mentioning IR LEDs which act as sources in wireless infrared communications because the uplink in OWC could utilise the infrared spectrum to avoid interference. The IR LEDs operate based on the same principle of electroluminescense. The 780-950nm band in near infrared spectrum is mostly preferred in IR communications due to cost effective LEDs and PDs in this region [10].

One key point to mention here is the health and safety issues regarding the IR LEDs. The optical power that these sources can operate at is limited due to eye and skin safety issues [48][10]. The IEC standard has classified various types of optical sources according to their maximum average optical power that can be used [49]. This limits the operational range or the maximum data rate of the communication system especially with the LED sources in the 780-950nm range [50][51].

2.3.2 Detector

PDs are generally considered in a VLC receiver to detect the intensity changes in the light falling across their surface and translate these change via their output current which is directly proportional to the light intensity. These devices are generally operated in reverse bias condition, and free electron-hole pairs are generated depending on the energy of light or photons that hit the PD surface, which constitute the photo-current [10]. The PD photo-current, I_p, can be given as [10]:

$$I_p = qQ_e \frac{P_i}{h_p \nu}, \tag{2.3}$$

where q is the charge of an electron, P_i is the incident optical power, ν is the optical frequency and Q_e is the quantum efficiency which represents the probability of a photon creating an electron-hole pair. $h_p\nu$ gives the photon energy. The ratio I_p/P_i gives the conversion efficiency or responsivity of the PD, which can be given as [10]:

$$\Re = \frac{I_p}{P_i} = \frac{qQ_e}{h_p \nu}, \tag{2.4}$$

$\Re$, PD surface area (A_{PD}) and capacitance are the key parameter of PDs that define its performance. Generally, high $\Re$, large A_{PD} and low junction capacitance are sought for good performance. However, there is a trade-off between the capacitance and A_{PD}, which are directly proportional to each other. Large A_{PD} is required to collect more optical power, however, this increases the capacitance too which reduces the attainable receiver

bandwidth or response time. Therefore, sometimes use of an array of PDs is suggested to enhance the sensitivity of the receiver in trade of increased device size and cost.

There are two types of PDs which are widely used in VLC research: a *p-i-n* PD and an avalanche PD (APD). In both PDs, incident light is absorbed in the intrinsic region where free carriers are generated which are swept to the junctions by the built-in E-field in this region [37][10]. The maximum $\Re$ a *p-i-n* can have is equal to $q/h_p\nu$, when Q_e is unity [37]. An APD differs from a *p-i-n* in a way that it offers much higher $\Re$ through a phenomenon known as *impact ionization* which provides internal current gain [52]. Therefore, APD may be preferred over a *p-i-n* to improve the sensitivity of a receiver. However, there is excess shot noise associated to the APDs due to large amount of current flowing in the device, when compared to a*p-i-n* PD [10]. Overall, the *p-i-n* PDs are less expensive than APDs due to simpler manufacturing. Some key characteristics of the two detectors are shown in Table 2.2. In this thesis, the optical properties of the PC10-6b PD by First Sensor [6] were used for the performance evaluation of different VLC systems. The responsivity of the PD10-6b is shown in Fig. 2.2.

Table 2.2: Key Characteristics of Optical Detectors [10]

Characteristics	***p-i-n* PD**	**APD**
Modulation Bandwidth	Tens of MHz to Tens of GHz	Hundreds of MHz to Tens of GHz
Photo-current Gain	1	10^2 to 10^4
Additional Circuitry	None	High Bias Voltage and Temperature Compensation
Cost	Low	Moderate to High

Optical Concentrators

An option to collect more power at the receiver is through the use an optical concentrator which increases the effective surface area of the PD where A_{PD} can be kept small [22][18]. Use of non-imaging lens is usually suggested as an optical concentrator. However, for a MIMO system is has been found that the imaging lens improves the system performance and enhances the receiver's mobility [18]. In this thesis, the performance of considered VLC systems is studied without the use of optical concentrators to provide a benchmark performance of investigated physical layers.

Optical Filters

Optical filters are generally used in front of the PDs at the receiver to filter our any unwanted radiation mixed with the desired optical signal which carries the information. In VLC, bandpass optical filters are used to isolate different multicolour bands at the receiver side while working with multicolour LEDs. On the other hand, while working with a phosphor coated blue LED, a blue bandpass filter is used to remove the slow phosphorescent potion of the optical spectrum (∼500-700nm) thereby benefiting from faster switching rates [46]. This reduces the optical power incident on the PD by approximately 50%. However, the overall modulation bandwidth is enhanced from 2 MHz to 20 MHz as shown in [46].

The RGB LEDs produce white light by mixing the light from different colour sources. Therefore, the modulation bandwidth is not limited as in phosphor based LEDs. However, some modulation schemes, such as WDM and colour shift keying (CSK), require the information in each colour-band to be decoded separately at the receiver, in which case the use of optical filters become essential as the PDs can detect a wide range of optical signals. The PD10-6b, whose responsivity is shown in Fig.2.2, can receive light from the entire visible spectrum.

Fig. 2.2 shows the transmissivity of four multicolour optical bandpass filters with certain λ_c. It is apparent from Fig. 2.2 that filtering leads to power loss as the transmissivity is generally below 1 (~ 0.70). However, optical filters with superior transmissivity are also available as shown in [16]. Clearly these filters have very low spectral overlap and can provide a good isolation between different colour bands. However, the LEDs can have a large spectral overlap. The normalised SPDs of multicolour LEDs with different centre wavelengths are also shown in Fig. 2.2, which have a significant amount of spectral overlap. This spectral overlap causes interference between different colour bands, known as colour cross-talk, at the receiver end even with the use of optical filters. However, the use of optical filters is necessary for certain modulations as indicated in [16]. Colour calibration techniques [8] are used to mitigate the cross-talk which are introduced in later chapters, where multicolour VLC systems are studied.

2.4 VLC Channels

The indoor VLC channels is comprised of a line-of-sight (LOS) path and a diffuse path [46]. In a scenario where both the LOS and diffuse signals are present at the receiver, the channel is termed a hybrid link. There are many cases in which the LOS could be blocked, e.g. due to a person standing between the Tx and Rx, which can completely block the

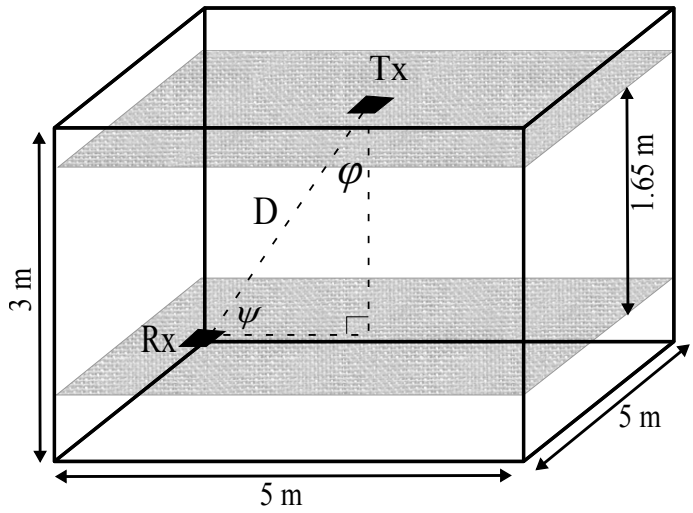

Figure 2.3: An example set-up of indoor VLC system

LOS. In this case, the Rx will detect the signal(s) reflected off indoor objects and walls, and the link is termed diffuse. The diffuse signals in VLC generally contain low power in comparison to the LOS signals due to low reflectivity of indoor objects for visible light [53]. However, in cases where the Rx is at higher distance from the Tx, the LOS and diffuse optical powers detected at the Rx become more comparable and hence more dispersion is perceived. A pure LOS link is available in VLC systems where no reflections are present at the Rx.

In VLC, the spectral properties of the optical front-ends such as LEDs, PDs and optical filters also affect the overall system performance [54]. These properties are spectral power distribution of LEDs, responsivity of PDs and transmissivity of optical filters. These properties lead to cross-talk between multicolour systems and insertion losses in all VLC systems.

Different mathematical models have been developed by various researchers to represent the optical wireless channels accurately for different indoor environments considering the characteristics of optical front-ends. These include the Gfeller and Bapst's model [27], Barry's models [53][55], the Ceiling-Bounce model [56], Ulbricht's integrating sphere model [57], Monte-Carlo and modified Monte-Carlo models [58][59], statistical impulse response model [60][61], Dustin model [62] and Iterative site based model [63]. In what follows, the three indoor VLC links used in this research, the effective channel responsivity, colour cross-talk and insertion losses are further detailed through mathematical models.

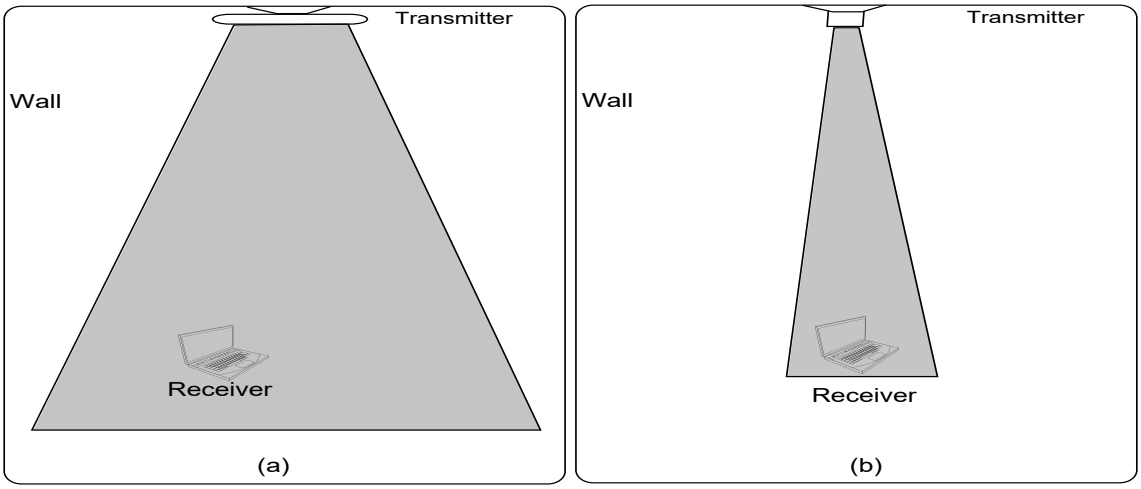

Figure 2.4: Representation of Indoor LOS Links, a) with Wide Beam and b) with Narrow Beam

2.4.1 Line-of-Sight Link

A typical indoor set-up of a VLC system is shown in Fig. 2.3, where the Tx is located at a ceiling height and the Rx is situated in a plane at the height of a desk. The physical distance between the Tx and Rx is represented by D. The angle of irradiance is notated as ϕ and the angle of incidence as ψ.

The LOS links can have variable beam-widths. Fig. 2.4 shows two different LOS links, one with a wide and other with a narrow beam-width [64]. In a wide beam-width LOS, whilst the user mobility can be higher without requiring a tracking system, the link is susceptible to blocking and shadowing [10]. On the other hand, in narrow beam-width LOS link the user mobility is dependant upon a tracking system. However, the SNR at the receiver is high as the optical power is focused towards the receiver, this also enhances the operating range of the LOS systems [64].

The LOS links do not suffer from large multipath dispersion, as the diffuse reflected signals are not significant, hence, LOS links are suitable for high data rate hotspots [65]. However, small amounts of ISI can still be caused by multiple LOS links from an array of LEDs at the Tx [46] due to the physical separation between the sources.

In a LOS link, the Tx is assumed to be completely or partially within the field-of-view (FOV) of the Rx and the channel DC path gain (η) is given as equation (2.5) [66][27][67].

$$\eta = \begin{cases} \frac{(m+1)A_{PD}}{2\pi D^2} \cos^m(\phi) \cos(\psi) g(\psi), & \psi < \Psi \\ 0, & \psi > \Psi \end{cases} \tag{2.5}$$

Equation (2.5) shows that the η is dependant on the Lambertian emission order m, given

as $-\log_2[\cos(\phi_{\frac{1}{2}})]$, where $\phi_{\frac{1}{2}}$ is the LED's semi-angle at half-power, A_{PD} is the physical surface area of the PD, Ψ is the FOV of PD and $g(\psi)$ is the optical concentrator gain given as [66]:

$$g(\psi) = \frac{n_{OC}^2}{\sin^2(\Psi)}, \tag{2.6}$$

where, n_{OC}^2 is the refractive index of the optical concentrator.

2.4.2 Diffuse Link

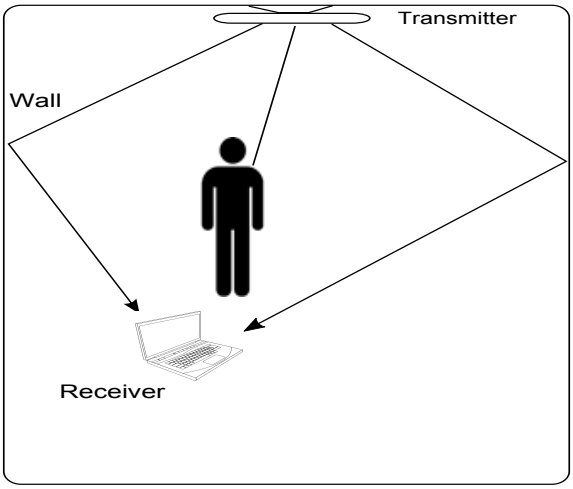

Figure 2.5: Representation of Indoor Diffuse Links where the LOS is blocked

Fig. 2.5 shows a diffuse indoor link where the LOS is blocked or shadowed by a person in a room. Although the diffuse links are flexible in terms of mobility, they suffer from multipath dispersion as the transmitted optical signal is reflected off various objects in a room, the walls, the ceiling and the floor. This multipath behaviour causes temporal dispersion of a transmitted pulse and inter-symbol interference (ISI) between multiple transmitted pulses. The indoor diffuse channel is generally modelled as a low-pass impulse response ($h_{Dif}(\tau)$) [22],[68], and can be given as a function of the diffuse channel gain ζ as [69][57]:

$$h_{Dif}(\tau) = \frac{\zeta}{\tau_c} \exp\left(-\frac{\tau - \Delta\tau_{dif}}{\tau_c}\right) u(\tau - \Delta\tau_{dif}), \tag{2.7}$$

where τ_c[1] is the time constant of the exponentially decaying diffuse channel, $\Delta\tau_{dif}$ is the signal delay of the diffuse path, $u(\tau - \Delta\tau_{dif})$ is the unit impulse as a function of $\Delta\tau_{dif}$

[1] Also known as the RC time constant as the diffuse indoor channel has a low pass filter like behaviour.

and ζ is given as:

$$\zeta = \frac{A_{PD}}{A_{Room}} \frac{\rho}{(1-\rho)}, \tag{2.8}$$

where, ρ is the average reflectivity of the indoor objects and walls, A_{Room} is the room surface area given as:

$$A_{Room} = 2(l \cdot w + l \cdot h + w \cdot h), \tag{2.9}$$

where l, h and w represent the length, height and width of the room, respectively. The τ_c in equation (2.7) can be calculated as [57]:

$$\tau_c = -\langle t \rangle / \ln(\rho), \tag{2.10}$$

where $\langle t \rangle$ is the mean time between two reflections which can be approximated as [57]:

$$\langle t \rangle = 4(l \cdot w \cdot h)/(cA_{Room}), \tag{2.11}$$

where, c is the speed of light.

For a diffuse link the electrical channel root-mean-square (rms) delay spread τ_{rms} can be estimated from τ_c, as $\tau_{rms} = \tau_c/2 = -\langle t \rangle / 2\ln(\rho)$. A more generalised formula for the τ_{rms} calculation is given in section 2.4.5. The multipath behaviour limits the data transmission rates in a diffuse link as the data samples at frequencies above the cut-off frequency or -3dB frequency (f_c) of the channel which is given as:

$$f_c = \frac{1}{2\pi\tau_c} = \frac{1}{4\pi\tau_{rms}} \tag{2.12}$$

There are various channel equalisation techniques that have been developed for the OWC and VLC. These techniques allow sampling frequencies much higher than f_c [18][17]. These techniques are discussed in later chapters.

2.4.3 Hybrid Link

A hybrid VLC link, as shown in Fig. 2.6, is composed of a LOS path and multiple delayed paths reflected off the walls, ceiling, floor and other indoor objects. The impulse response of such a channel can be modelled as [46]:

$$h(\tau) = \eta\delta(\tau - \Delta\tau_{LOS}) + \frac{\zeta}{\tau_c} \exp\left(-\frac{\tau - \Delta\tau_{Dif}}{\tau_c}\right) u(\tau - \Delta\tau_{Dif}), \tag{2.13}$$

where ΔT_{LOS} is the signal delay of the LOS path, and $\delta(\tau - \Delta\tau_{LOS})$ represents the Dirac delta pulses as a function of $\Delta\tau_{LOS}$. The VLC hybrid link can be characterised by K-

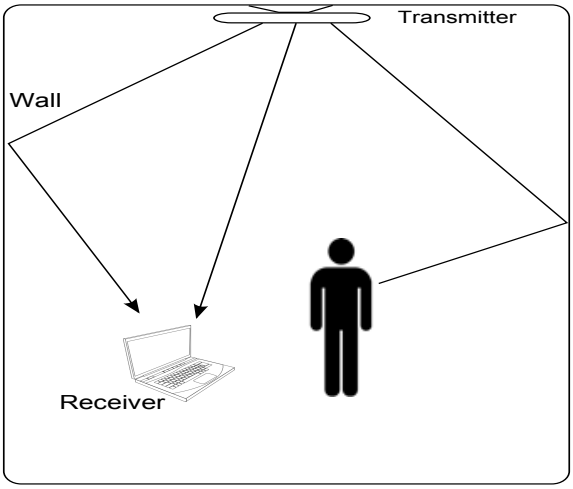

Figure 2.6: Representation of Indoor Hybrid Links containing both the LOS and diffuse channel paths

factor, which can be given as [57]:

$$K = (\eta/\zeta)^2 \tag{2.14}$$

In general, η can be much larger than ζ as ρ at visible wavelengths is much lower than at IR wavelengths [53]. Therefore, VLC suffers less dispersion in hybrid links than IR communications. However, this also implies that more power is lost in VLC due to low ρ.

2.4.4 Cross-talk and Insertion Loss

In VLC, the insertion losses arise due to the spectral properties of the LEDs, PDs and optical filters. These losses lead to poor SNR at the Rx, hence poor system performance in terms of bit error rate or packet error rate (BER/PER). The effective responsivity of a SISO VLC system using white light LED, blue filter and a PD can be given as:

$$g = \frac{\int_{\lambda^{\mathcal{T}}_{min}}^{\lambda^{\mathcal{T}}_{max}} \mathcal{S}(\lambda)\mathcal{T}(\psi,\lambda)\Re(\lambda)d\lambda}{\int_{\lambda^{\mathcal{S}}_{min}}^{\lambda^{\mathcal{S}}_{max}} \mathcal{S}(\lambda)d\lambda}, \tag{2.15}$$

where, $\mathcal{S}(\lambda)$ is the relative spectral power distribution (SPD) of the LED, $\mathcal{T}(\psi,\lambda)$ is the transmissivity of the optical filter and $\Re(\lambda)$ is the responsivity of the PD.

The cross-talk is an issue for MIMO VLC systems and multi-colour SISO systems. As this thesis focuses on the SISO VLC systems, details of MIMO cross-talk are not covered. In a multicolour VLC system, e.g. a tri-chromatic (RGB) system, the colour cross-talk

and insertion losses (CIL) matrix can be represented as G:

$$G = \begin{bmatrix} g_{1,1} & g_{1,2} & g_{1,3} \\ g_{2,1} & g_{2,2} & g_{2,3} \\ g_{3,1} & g_{3,2} & g_{3,3} \end{bmatrix} \tag{2.16}$$

In equation (2.16), each element of G represent the effective responsivity between the transmit band i and the receive band j. The value for each element of G can be calculated based on equation (2.15) as shown in equation (2.17).

$$g_{i,j} = \frac{\int_{\lambda_{min}^{\mathcal{T}_i}}^{\lambda_{max}^{\mathcal{T}_i}} \mathcal{S}_j(\lambda)\mathcal{T}_i(\psi,\lambda)\Re(\lambda)d\lambda}{\int_{\lambda_{min}^{\mathcal{S}_j}}^{\lambda_{max}^{\mathcal{S}_j}} \mathcal{S}_j(\lambda)d\lambda} \tag{2.17}$$

For the study of various multicolour VLC systems, the CIL matrix is used as a part of the optical channel. The effects due to colour cross-talk can be equalised based on colour-calibration (CC) technique [8], which is detailed in forthcoming chapters.

2.4.5 Channel Delay Spread

Indoor VLC channels are classified as multipath propagation channels, especially when the $\phi_{\frac{1}{2}}$ and Ψ are wide, i.e. the LED radiation pattern and PD FOV are wide. As mentioned previously multipath propagation arises when multiple copies of one transmitted pulse are present at the receiver and each copy has a different time of arrival which leads to ISI. There is no multipath fading in VLC as the diameter of a PD is ∼1000 times the wavelength of visible light radiations [22]. However, multipath distortion is still present due to multipath propagation.

A measure of ISI is the channel delay spread, which is effectively the time difference between the arrival of the first and the last copy of a transmitted pulse. In its *rms* form, the channel delay spread can be calculated as [70]:

$$\tau_{rms} = \sqrt{\bar{\tau^2} - \bar{\tau}^2}, \tag{2.18}$$

where, $\bar{\tau}$ is the mean excess delay, given as:

$$\bar{\tau} = \sum_{j=0}^{J-1} |h_j|^2 \tau_j \Big/ \sum_{j=0}^{J-1} |h_j|^2, \tag{2.19}$$

and $\bar{\tau^2}$ is the mean square excess delay spread, given as:

$$\bar{\tau^2} = \sum_{j=0}^{J-1} |h_j|^2 \tau_j^2 \Big/ \sum_{j=0}^{J-1} |h_j|^2 \tag{2.20}$$

In equations (2.19) and (2.20), h_j is the j^{th} path in an oversampled VLC channel and τ_j is its respective time of arrival. Given static Tx, Rx and reflectors in a VLC system, the τ_{rms} is fixed. However, as the location of Tx or Rx is changed or reflectors with different reflectivity are present, the τ_{rms} changes too. In the process of performance evaluation of various VLC signalling schemes, avariety of channel set-ups with different τ_{rms} were used.

2.5 Noise at the Receiver

Noise is present in all type of optical communications. The noise at the receivers in VLC is mainly categorised into shot noise and thermal noise. The shot noise is also known as quantum noise and it is caused by the random absorption of photons from the average light intensity entering the PD or APD from the VLC source itself, ambient sunlight, electronic displays (monitors) and any other artificial lighting-only sources. The shot noise current is a summation of random noise currents from these light sources with a Poisson distributed probability density function (pdf) [10]. However,as the number of random variables from multiple noise sources tends to infinity, the pdf of the shot noise current can be approximated to be Gaussian [26]. The shot noise power can be given as [37]:

$$\sigma_s^2 = 2qI_pB_{eff}, \tag{2.21}$$

where q is the charge on an electron, B_{eff} is the effective single-sided noise bandwidth of the receiver and I_p is the average current generated by the photodetector in the receiver. In a noiseless system I_p is given as:

$$I_p = \bar{\mathfrak{T}}\bar{\Re}(P_{Signal} + P_{Background}), \tag{2.22}$$

where, P_{Signal} is the optical power detected at the Rx from the Tx, $P_{Background}$ is the light received form other background sources, $\bar{\Re}$ is the average responsivity of the PD and $\bar{\mathfrak{T}}$ is the average transmissivity of the optical filter (which need not be included if no filter is used). Overall, I_p is limited by the optical response of the optical filter and the PD.

For a Rx with wide FOV PD, the amount of ambient light detected along with the desired modulated optical signal will be large. Therefore, the SNR at the receiver will be degraded. However, different techniques are used to control the effect of ambient noise.

Narrowband optical filters can be used at the front of a photodetector [10], which filter out any unwanted optical radiation. Other techniques include the use of a narrow FOV photodetector, but this means high alignment sensitivity between the source and receiver.

Thermal noise occurs due to random motion of electrons in any conductor at a finite temprature [37]. In an optical receiver, thermal noise is associated with the resistance of the photodetector and any other electrical component that is present in the receiver, such as the pre-amplifier. The thermal noise power of a receiver can be given as [37]:

$$\sigma_t^2 = 4k_b T B_{eff}/r; \tag{2.23}$$

where k_b is the Boltzmann constant and T is the temperature (Kelvins) of the noise equivalent input resistance r.

As the thermal noise current is signal independent with Gaussian statistics [22], the variances of shot and thermal noise processes can be added [37]. Hence, the total noise power can be given as:

$$\sigma^2 = \sigma_s^2 + \sigma_t^2 = (qI_p + 2kT/R_L)2B_{eff} \tag{2.24}$$

2.5.1 SNR and Channel Capacity

The signal to noise ratio is an important measure of the link reliability in communications systems. Given that we have a LOS link based VLC system, the electrical SNR is defined as:

$$\mathrm{SNR}_e = \frac{\bar{\mathfrak{T}}^2 \bar{\Re}^2 \eta^2 P_{Signal}^2}{\sigma^2}, \tag{2.25}$$

and the optical SNR is given as the *rms* value of the instantaneous SNR:

$$\mathrm{SNR}_o = \frac{\bar{\mathfrak{T}} \bar{\Re} \eta P_{Signal}}{\sigma} = \sqrt{\mathrm{SNR}_e} \tag{2.26}$$

SNR is also an important measure of channel capacity, which is generally given as Shannon's well known formula [71]. For a real bipolar electrical channel, the channel capacity can be given as [10]:

$$C = \frac{1}{2} B_{eff} \log_2(1 + \mathrm{SNR}_e) \tag{2.27}$$

In this thesis, the capacity of the bipolar electrical channel (equation 2.27) is used as a reference against which the throughput of the considered VLC signalling schemes is compared in uncoded and FEC modes.

2.6 Review of VLC Signalling Techniques

After nearly two decades of research on IR communications, in year 2000, work in VLC system development was published by researchers from Keio University in Japan [33][72], where the general idea of using white LEDs for wireless communication was proposed for the first time [73, 74, 75]. Since then many organisations, focusing research and development in VLC, appeared such as visible light communications consortium (VLCC) [30], Japan electronics and information technology industries associations (JEITA) [76], home gigabit access (OMEGA) [31], Pure Li-Fi [77] and the task group IEEE 802.15.7 [78]. Since the pioneering work, various modulation schemes, FEC schemes and standards have been developed for VLC and tested both through simulations and prototyping. This section provides an overview of these innovations in VLC systems and describes which modulation and FEC schemes are investigated in this research.

2.6.1 Standards

In wireless communications, standards are developed to implement and operate systems in a manner which maximises safety, quality, efficiency and universal adaptation of that system. The standardisation of VLC systems also began in Japan when JEITA published two VLC standards in 2007, namely visible light communication system (CP-1221) [79] and visible light ID system (CP-1222) [80]. In 2013, JEITA published another VLC standard know as visible light beacon system (CP-1223) [81]. The first IEEE VLC standard, IEEE 802.15.7 [8], was published in 2011, by task group IEEE 802.15.7 [78]. This VLC research only focuses on the IEEE standard and other non-standardised VLC techniques as detailed above. In the rest of the thesis, the word "standard" is used to refer to IEEE 802.15.7.

IEEE 802.15.7 standard has defined various MAC and PHY layers for short-range optical wireless communication using visible spectrum and this research only focuses on the PHY layers of the standard, especially PHY-III which uses multicolour LEDs. The three PHY layers offer data rates from 11.67 kbit/s to 96 Mbit/s [8][32], incorporating dimming modes and flicker mitigation. PHY-I uses OOK and variable PPM (VPPM) modulation schemes with concatenated Reed-Solomon (RS) & binary convolutional (BC) codes, and recommends the use of system bandwidths less than 1 MHz. PHY-II uses the two modulation schemes with RS codes at bandwidths between 3.75-120 MHz. PHY-I and PHY-II also use run length limited (RLL) Manchester and 4B6B codes to provide DC balance, clock recovery and flicker mitigation [8]. PHY-III uses a colour shift keying (CSK) modulation scheme with RS codes, at 12 and 24 MHz bandwidths. CSK in PHY-III mitigates intensity flicker by keeping the total optical powers constant across colour-bands. The standard complies to all applicable eye safety regulations too [8].

The IEEE standard is currently under revision and the new standard 802.15.7a (or 802.15.7r1) could include low rate (several kbit/s) optical camera communication (OCC) systems [82][83] and high rate (several Mbit/s) bi-directional Li-Fi systems [84]. It is not clear at the moment what the high data rate Li-Fi system might be. However, due to the significant amount of work being carried out on OFDM and DMT based WDM system the author believes that it could be a WDM based system.

A part of this thesis is focused on improving the performance of standardised multi-colour CSK system by increasing the number of colour-bands, as well as exploring FEC and equalisation techniques to improve the capacity over representative VLC channels while using standard LED switching rates. The other part investigates the effects of high peak-to-average power ratios (PAPRs) of the optical multi channel modulation schemes on their capacity and shows how rate-adaptive coded modulation techniques can be used to enhance the capacity of multiple and single channel modulation schemes.

2.6.2 Modulation Schemes

As mentioned previously, VLC systems are based on IM/DD, whereby the intensity of the source(s) is varied by M levels to transmit $k = \log_2(M)$ information bits per intensity level. M is also known as the modulation order. IM/DD requires signals at the input of the source to be real and unipolar in VLC. Ideally, as an IM/DD system, VLC can utilise all the modulation schemes that are originally designed for conventional OWC systems. These include on-off keying (OOK) (or 2-PAM) [85][86], multi-level pulse amplitude modulation (M-PAM) [86], pulse position modulation (M-PPM) [87], differential PPM (DPPM) [88] and digital pulse interval modulation (DPIM) [89]. All these schemes are categorised as single-carrier (or single-channel) modulation (SCM) schemes. Multiple sub-carrier modulation (MSM) schemes using binary and quaternary phase shift keying have also been developed for OWC [90][91].

In addition to the above mentioned modulation schemes, there are various SCM schemes that are specifically developed for VLC which utilise multi-colour LEDs such as CSK, colour intensity modulation (CIM) [92] and metameric modulation (MM) [93]. Use of multi-carrier (or multi-channel) modulation (MCM) schemes has also been proposed for VLC, such as those based on orthogonal frequency division multiplexing (OFDM) [94][95] or discrete multi-tone (DMT) [96][97] systems. Due to their origins in RF wireless and wired systems, the MCM schemes are modified for IM/DD VLC channels. It must be noted that the word “carrier” or “channel” in SCM and MCM systems refer to baseband electrical domain signals. Both SCM and MCM systems use one optical carrier while working with phosphorescent LEDs or multiple optical carriers while working with multi-

colour LEDs. In what follows, the MCM and SCM schemes studied in this research are introduced.

Multi-channel Schemes

In optical MCMs, the transmitted data stream is divided into a number of sub-streams and sent over multiple sub-channels with significantly smaller bandwidth than the total available bandwidth [71]. MCM schemes partition a frequency selective channel into a number of parallel sub-channels which experience flat fading and reduce the amount of ISI on each sub-channel [71]. The MCM schemes are different from the MSM technique in a way that spectral overlapping is used in MCM with mutually orthogonal sub-channels.

As mentioned previously, OFDM and DMT based MCM schemes have been proposed as signalling schemes for VLC over the past decade. Due to the origins of these schemes in RF systems, some signal generation modifications are necessary for the use of these schemes in IM/DD systems where a real and unipolar transmit signal is required. These signal generation modifications yield optical OFDM variants.

A widely studied optical OFDM scheme is DC-biased optical OFDM (DCO-OFDM) [95][98]. As apparent from its name, DCO-OFDM uses a DC-bias to obtain a unipolar transmit signal and Hermitian symmetry is needed in the frequency domain (FD) at the transmitter[99]. Due to high peak-to-average power ratio (PAPR), the DC-bias and hence the optical power requirements increase with modulation order in DCO-OFDM [95][100]. Therefore, the other variants of optical OFDM are designed to tackle this problem by eliminating the use of the DC-bias through different techniques. These alternative schemes are asymmetrically clipped optical OFDM (ACO-OFDM) [100][101], Flip-OFDM [102][103] and Unipolar-OFDM (U-OFDM) [7]. Another variant named ADO-OFDM (a clipped DC-biased optical OFDM) [104] has also been designed which combined the aspects of ACO and DCO systems.

There are several DMT MCM schemes proposed for use over IM/DD channels. The channel adaptive sub-carrier bit-loading aspect of DMT differentiates it from OFDM for which "water-filling" like algorithms are used [71]. These schemes are also divided into two categories; the DC-biased approach is called DC-DMT [105] and two non DC-biased approaches, PAM-DMT [106] and AC-DMT [107].

In this research, DCO-OFDM, ACO-OFDM, Flip-OFDM and U-OFDM schemes are studied. For the performance comparison of MCM and SCM systems M-PAM with DC-bias and DCO-OFDM schemes are used. A new MCM scheme named DC-biased Optical Vector Coding (DCO-VC) is also introduced here, which uses optimal channel partitioning vectors by using channel state information (CSI) at the transmitter [108]. Adaptive bit-

loading is not used for any system in this research, however both MCM and SCM can use this optimisation technique [109].

Single Channel Schemes

In SCM systems, the entire bandwidth is treated as single channel and data is transmitted at high rate over the single channel. In this research, OOK, M-PAM and M-CSK SCM schemes are studied.

OOK is the simplest form of modulation technique for IM/DD systems. There are two main types of OOK, non-return to zero OOK (NRZ-OOK) and return to zero OOK (RZ-OOK). In NRZ-OOK, an optical pulse with duration equal to the bit duration is transmitted to represent digital bit "1" and for the same duration absence of optical pulse represents bit "0". In RZ-OOK, optical pulse duration is usually smaller than the bit duration and it is varied according to the duty-cycle. OOK has been widely adopted as a bench mark modulation scheme in OWC research. In this research too, the OOK scheme has been used as a reference modulation scheme in its NRZ form and its performance is compared to M-CSK systems.

M-PAM modulation is the simplest multi-level IM/DD modulation scheme. M-PAM has its origins in RF communication systems, where its bipolar alphabets can be given as $\{\pm 1, \pm 3, \ldots, \pm(M-1)\}$. In IM/DD systems, either a DC-bias is added to the bipolar baseband M-PAM signals or unipolar alphabets $\{0, 1, \ldots, (M-1)\}$. In both cases, the alphabets can be normalised to attain certain average optical or electrical powers. M-PAM in its simplest form, i.e. 2-PAM, it is an equivalent NRZ-OOK scheme. M-PAM is used to realise a bench-mark multi-level VLC systems whose performance is compared against the multi-level MCM schemes. Additionally, a WDM system based on unipolar M-PAM scheme is also studied to make comparison with multicolour CSK systems. More details on M-PAM systems can be found in chapter 3.

CSK, as mentioned previously, is an IEEE standardised modulation scheme designed for multicolour LEDs. In CSK, different colours represent different data symbols, which are produced as a mixture of light irradiated from each source within a multicolour LED. For colour mixing, CSK uses CIE 1931 colour co-ordinates [110], where each colour can be represented by a pair of chromaticity values and each chromatic pair gives a set of intensity values for each light source for a particular colour. CSK is a major part of this research where use of more than a three colour source is explored to utilise the chromatic space more efficiently and enhancing system bit error performance. CSK is detailed in chapter 5 and 6, where the standardised and proposed CSK systems are compared through simulations and analytical approximations.

OOK, and especially the multilevel schemes M-PAM suffer ISI while working at high LED switching rates over the optical wireless channels which severely degrades the system bit or packet error performance [111][90]. In this research it is found that M-CSK, as a SCM scheme, suffer the same problem. This limits the maximum transmission data-rates in SCM schemes [112][85]. To continue the use of SCM schemes at high data-rates, channel equalisation becomes important. There are different equalisation techniques that are uses in SCM schemes. These include, decision feedback equalisation (DFE), minimum mean square equalisation (MMSE) and zero forcing equalisation (ZFE). In this thesis frequency domain equalisation (FDE) techniques are used for M-PAM and M-CSK systems while operating over representative VLC channels, due to the simplicity of equalising in the FD when compared to the time domain (TD) [113][114].

2.6.3 FEC Schemes

FEC techniques play an important role in enhancing the performance of a communications system. There is very little amount of work that has been currently done when studying the application of various FEC schemes in VLC or any other OWC. However, it is apparent from the VLC literature [17][16] that FEC schemes have a role to play in enhancement of the overall bit error performance of VLC systems, especially in MCM schemes, where clipping distorts the transmit signal. The IEEE standard suggests the use of different FEC schemes for the three PHY layers. PHY-III, which has been studied expensively in this research, uses half-rate RS code. Recently, use of three-stage concatenated codes has been proposed for PHY-III [115]. In this thesis, the rate-adaptive BC codes are studied for use in PHY-III, SCM M-PAM and MCM DCO-OFDM & DCO-VC (See chapter 4 & 6 for more information), which are less complex than the concatenated coding techniques but at the same time more effective in bit error correction than the fixed rate RS codes. The BC codes have been used many current wireless communication techniques such as Wi-Fi and WiMAX.

2.6.4 Key Modulation Performance Characteristics

Modulation schemes in any communication system are usually compared according to their link reliability, power efficiency and bandwidth efficiency. These performance characteristics are used throughout this thesis to analyse different VLC modulation schemes and are defined as:

- *Link Reliability*: The link reliability is the ability of a modulation scheme to provide a minimum acceptable error probability rate in a relevant channel conditions. Mod-

ulation schemes with high immunity to ISI are generally considered to have high link reliability.

- *Power Efficiency*: The power requirement of a modulation scheme is a big concern, especially at the user equipment (UE), where the power resources are limited due to the size of the battery. A power efficient modulation scheme will require lowest SNR values to achieve a certain bit/packet error performance at a certain data rate. FEC techniques are used to further enhance the link reliability and power efficiency of modulation schemes at the cost of reduced bandwidth efficiency.

- *Bandwidth Efficiency*: The carrier bandwidth in VLC is very large, ∼300 THz. However, the actual system bandwidth is limited by the response time of the source & detector, and the *rms* delay spread of the wireless channel. Therefore, it is important that the modulation schemes achieve highest possible bit rates over the available system bandwidth.

Based on the above three characteristics of a communication system, this thesis evaluates the system throughput (Mbit/s) performance of considered systems and compares it on the electrical SNR scale.

2.7 Summary

VLC has attracted many researchers around the globe to enable use of visible spectrum for indoor wireless communication and provide a solution for increasing network capacity requirements and demand for high data transmission rates. Given the LEDs are being used more and more as lighting source due to their energy efficiency, utilising these pre-installed sources for wireless communication through VLC enable dual use of these devices and the spectrum.

VLC can make use of both the phosphorescent and multicolour white LEDs. While the multicolour LEDs are more expensive due to manufacturing complexity they offer the use of WDM to increase the data transmission rates and precise control over the output light through CSK. Use of optical filter(s) becomes essential at the receiver, irrespective of the used source type and choice on detector type can be made based on the operating range and bandwidth requirements.

Various SCM and MCM schemes have been developed for VLC in the past 15 years in addition to an international standard and several Japanese standards. Given the existing IEEE standard offers data rates up to 96 Mbit/s only, this standard is currently under revision to enhance the transmission rates as well as to introduce low rate outdoor OCC

systems. This thesis studies the existing standardised and non-standardised VLC modulation, FEC and channel equalisation techniques introduced in this chapter and proposes novel solutions to enhance the throughput of VLC systems in the upcoming chapters.

Chapter 3

Single and Multi Channel Modulation Schemes for VLC

3.1 Introduction

In VLC, to mitigate ISI due to the signal spreading over time in wireless channels and to enable high LED switching rates, channel equalisation becomes important. multi-channel modulation (MCM) schemes have been widely deployed in wired and wireless communication networks due to their ability to combat effectively moderate to severe ISI over a communication channel. VLC, which has been mainly proposed for indoor wireless communication, suffers multipath dispersion as multiple copies of a transmitted pulse are present at the receiver due to reflection from indoor objects and walls [46]. The conventional MCM schemes cannot be used directly in IM/DD optical systems as the transmit signal has to be real and unipolar. Therefore, to overcome dispersion, various optical MCM schemes based on OFDM have been developed for VLC such as DCO-OFDM, ACO-OFDM [100], Flip-OFDM [103] and U-OFDM [7], which provides a real and unipolar transmit signal. PAM based single channel modulation (SCM) with FDE have also been proposed as a low PAPR alternative [107][109].

This chapter details the working of DC-biased optical M-PAM (DCO-PAM) based SCM and the above mentioned four different OFDM based optical MCM schemes. A new MCM scheme proposed in this research, named DCO-VC, which uses optimal channel partitioning and a DC-bias is also presented. The DCO-PAM system uses bipolar M-PAM modulation alphabets and a DC-bias to obtain a unipolar transmit signal. This is done to compare the DC-bias requirements of SCM and MCM schemes. It is shown that in the process of obtaining a real and unipolar transmit signal these schemes sacrifice at least one-half of the system capacity and in case of a DC-biased system an increase in

power requirements. The theoretical spectral efficiency of the considered SCM and MCM systems is compared and the bit error rate (BER) performance of each of the considered systems is evaluated for an AWGN channel and compared over the SNR scale. Both, the analytical and simulation based BER results are presented.

The performance of SCM and MCM systems is compared without any significant signal distortion due to the limited dynamic range of the VLC transmitter. Therefore, for the DC-biased systems a DC-bias is set to minimise the negative clipping and no positive clipping is considered for all the schemes to provide a BER of 10^{-6}. In practical scenarios, either power back-off or digital pre-distortion can be employed to mitigate the signal distortion due to the limited dynamic range of the optical transmitters. Therefore, minimising signal clipping during simulations provided an unconstrained performance comparison between the considered systems in a scenario where signal distortion must be kept to a minimum to achieve certain data throughput. For design purposes, the power back-off needed to minimise the clipping can be inferred from the results.

The analysis of results show that the DCO-PAM SCM system is more energy efficient than the MCM schemes over the AWGN channel to achieve a certain spectral efficiency for any considered SNR. The results also show that the DC-biased MCM systems compared to non DC-biased MCM systems will provide a power efficient communication link as the spectral efficiency is increased. Spectral efficiency comparisons between all the schemes show that the transmitter and receiver complexity of the OFDM systems will increase rapidly with increasing spectral efficiency as much higher modulation orders are required in comparison to the PAM based systems. Especially, the non DC-biased OFDM systems will have twice the ADC/DAC resolution requirements when compared to the DCO-OFDM schemes. Therefore, overall the AWGN channel based results will show that the DC-biased systems are more power efficient and have lower hardware complexity than the non DC-biased systems.

3.2 SCM Systems

SCM techniques existed in digital communication systems as primary modulation technique [116] a long time before the MCM schemes appeared in 1966 [117]. The MCM scheme's ability to overcome ISI in multipath propagation and to work as a multi-user system has made it the ultimate choice for signalling in communication systems [114]. In the form of OFDM and DMT, MCM has been widely used in wireless and wired communications. A major drawback of MCM is the high PAPR, which degrades the overall system performance due to non-linear front-end device, such as the power amplifier (PA) in a radio transmitter [118] or a LED in VLC. This drawback of MCM kept the interest in

low PAPR SCM systems alive and the introduction of low complexity channel equalisation techniques such as frequency domain equalisation (FDE) [119] enabled SCM to work well over multipath channels with OFDM equivalent complexity [114][113]. In order to keep the power consumption to low levels at the user equipment (UE), the mobile communication standards such as 3GPP-LTE and LTE-Advanced (LTE-A) also deploy SCM with FDE in the uplink [120].

In VLC, in addition to the effects of transmitter non-linearities, as mentioned earlier the IM/DD techniques requires the transmit signal to be real and unipolar. Although effective in ISI mitigation, the optical OFDM schemes trade power and/or bandwidth to satisfy the signalling requirements of the IM/DD channel. Therefore, FDE has been proposed with different optical SCM schemes such as OOK [121, 122], PPM [123] and M-PAM [107], in order to provide a low PAPR solution to mitigate ISI and to enhance the throughput of OWC systems at high data transmission rates. Many recent investigations have found the SCM-FDE systems to be more power efficient than the OFDM/DMT based optical MCM systems [124][109][107][105]. However, the BER & PER performance of M-PAM based SCM-FDE scheme has not been studied and compared against the optical MCM systems for high spectral efficiencies and throughputs, which is explored in this thesis along with a rate adaptive FEC coding for these systems to improve the system capacities over representative VLC channels in the next chapter.

3.2.1 Optical PAM System with FDE

As mentioned earlier, for IM/DD channels, either the bipolar M-PAM signal is converted to a unipolar signal through addition of a DC-bias equivalent to the minimum sample value of the bipolar signal or simply unipolar modulation alphabets are used. In principle the two systems are the same. However, in a DC-biased optical PAM (DCO-PAM) the used DC-bias values are apparent and comparison to DC-biased MCM systems becomes easier, which are studied with FEC schemes in the next chapter. Therefore, in this thesis a DCO-PAM system shown in Fig. 3.1[1] was considered.

In DCO-PAM, at the transmitter (Tx), the random binary data is grouped into $k = \log_2(M)$ bits and mapped to one of M different bipolar M-PAM symbols (or alphabets). Each bipolar M-PAM symbol takes the form of $\{-(M-1)+n\}$, where $n = 0, 2, 4, \ldots, 2(M-1)$. In order to enable FDE, the modulated serial signal is then parsed into blocks of length N which is also the size of the fast Fourier transform (FFT) used in FDE at the receiver (Rx) and a CP of length μ is added to each of the blocks which can be given as

[1]Note that this system is the same as a unipolar PAM based SCM-FDE systems in [107][109]. Except that here a DC-bias is added to a bipolar PAM signal to show the power lost in attaining a unipolar signal.

$\boldsymbol{x} = [x_0, x_1, \ldots, x_{N+\mu-1}]^T$. Then, after digital to analogue conversion (DAC) a certain DC-bias (B_{dc}) is added to the bipolar signal $x_b(t)$ and a unipolar signal $x_u(t)$ is obtained.

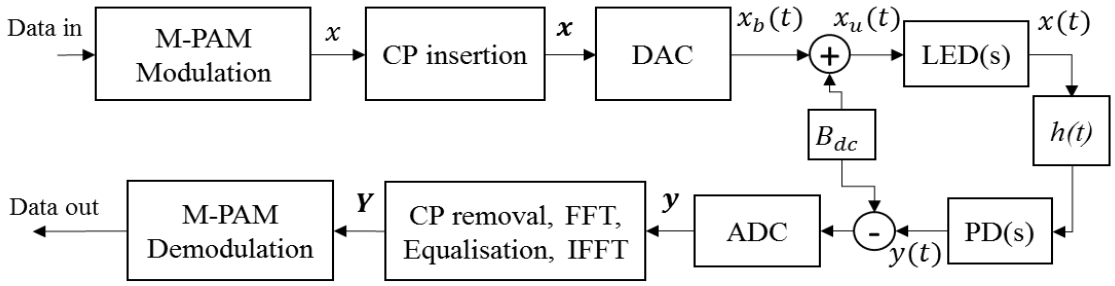

Figure 3.1: Transceiver schematic of FDE based DCO-PAM system.

B_{dc} can be set for the transmit bipolar signal, $x_b(t)$, based on its mean electrical power as in the literature [100][104], which can be given as:

$$B_{dc} = \xi\sqrt{E\{x_b^2(t)\}}, \tag{3.1}$$

where ξ is a constant of proportionality and $E\{.\}$ is the expectation function. In dB, the B_{dc} is given as $10\log_{10}(\xi^2) + 10\log_{10}(E\{x_b^2(t)\})$. Given B_{dc}, the average optical power of the transmit signal can be given as $10\log_{10}(\xi^2 + E\{x_b^2(t)\})$ in dB. Any negative samples, that are left after adding B_{dc} are clipped to zero, so that a clipped unipolar signal $x_u(t)$ can be obtained:

$$x_u(t) = x_b(t) + B_{dc} + n_{clip}(t), \tag{3.2}$$

where n_{clip} is the additive clipping noise with variance $\sigma^2_{n_{clip}}$. Since for DCO-PAM, B_{dc} is equal to the least value of the bipolar alphabet, there is no clipping needed and hence $n_{clip} = 0$.

At the Rx, post DD, the received signal $y(t)$ can be given as:

$$y(t) = \mathfrak{T}\mathfrak{R}(x(t) * h(t)) + n(t), \tag{3.3}$$

where, "$*$" denotes the convolution process, $\mathfrak{T}$ is the transmissivity of the Rx optical filter, $\mathfrak{R}$ is the responsivity (A/W) of the PD, $h(t)$ is the VLC channel impulse response (CIR. The CIR is detailed in section 2.4, where it is represented by $h(\tau)$, a function of channel delay τ, as it does not change with time. Lastly, $n(t)$ represents the AWGN with a constant variance of $\sigma_n^2 = N_o/2$, where N_o is the single-sided noise power spectral density and has units of W/Hz.

Each received DCO-PAM symbol, after B_{dc} removal and analogue to digital conversion

(ADC), is represented by $\boldsymbol{y}$. The CP is then removed from each received block $\boldsymbol{y}$, which then undergo FFT of size N for FDE. Excluding the CP, each transmitted and received block of DCO-PAM can be mathematically related as:

$$\boldsymbol{y} = \boldsymbol{W}\boldsymbol{x} + \boldsymbol{n} \tag{3.4}$$

In equation (3.4), $\boldsymbol{W}$ is the $N \times N$ channel circulant convolutional matrix, which can be diagonalised as $\boldsymbol{W} = \boldsymbol{F}^H \boldsymbol{\Lambda} \boldsymbol{F}$ [122], where $\boldsymbol{F}$ is the FFT matrix and $\boldsymbol{\Lambda}$ is a diagonal matrix with diagonal entries equal to the FFT of the optical channel impulse response $h(\tau)$. Here, $(.)^H$ represents the Hermitian transpose. The AWGN vector is given as $\boldsymbol{n} = [n_1, n_2, ...n_{N-1}]^T$. The equalised received DCO-PAM block $\boldsymbol{Y}$ is obtained through zero-forcing as, $\boldsymbol{Y} = \boldsymbol{F}^H \boldsymbol{Z} \boldsymbol{F} \boldsymbol{y}$, where, $\boldsymbol{Z}$ is the frequency domain equaliser matrix given as, $\mathbf{Z} = \boldsymbol{\Lambda}^H (\boldsymbol{\Lambda}\boldsymbol{\Lambda}^H)^{-1}$. After this, the M-PAM demodulation takes place and the binary data is retrieved from $\boldsymbol{Y}$. The minimum mean square error (MMSE) can be used as an alternative equalisation technique. However, given that the VLC channels are not highly frequency selective, ZFE has been found to provide near MMSE equivalent performance [107]. Given its lower implementation complexity, ZFE was used for DCO-PAM and the other MCM schemes which are introduced in the next sections.

3.3 MCM Systems

The MCM system overcomes multipath distortion and fading by partitioning the information data into a number of orthogonal sub-channels. VLC systems do not suffer multipath fading [22], however, multipath distortion is experienced due to the dispersive nature of the channel. Therefore, different types of OFDM and DMT based MCM systems have been proposed for VLC to overcome dispersion and allow multi-user communication. As mentioned earlier, only OFDM based systems are studied in this thesis and a new DCO-VC MCM system is proposed. In what follows, the workings of these MCM systems are detailed.

3.3.1 Optical OFDM Techniques

Before understanding the working principle of optical OFDM systems, it is important to be familiarised with the conventional RF OFDM scheme. OFDM is implemented by applying the inverse discrete Fourier transform (IDFT) and discrete Fourier transform (DFT) at the transmitter and receiver respectively [71]. In a hardware system the DFT and IDFT are realised by the Fast Fourier Transform (FFT) and its inverse, respectively.

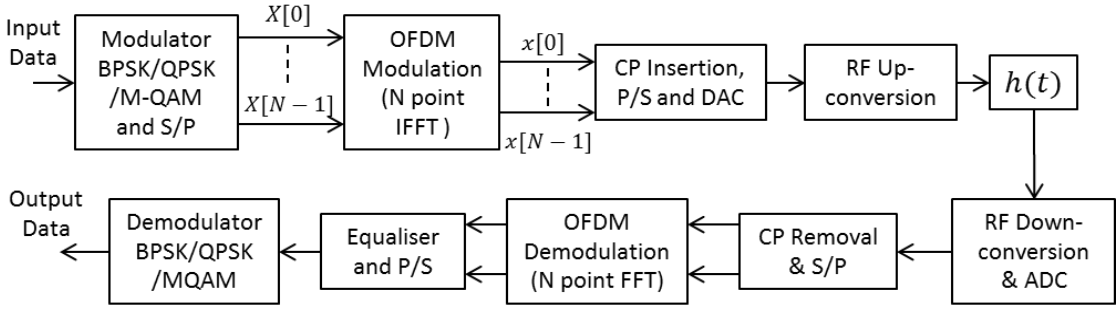

Figure 3.2: Transceiver schematic of an OFDM system.

Fig. 3.2 shows a block diagram of the OFDM transceiver. The random binary data is grouped into k bits and modulated by an M-ary quadrature amplitude modulation (M-QAM) scheme. Other baseband modulation schemes such as BPSK and QPSK are also used widely. This baseband modulation results in a stream of serial data symbols which are divided into N orthogonal sub-streams for OFDM modulation. Every N parallel data symbols, $X[0], X[1], \ldots, X[N-1]$, represent a FD OFDM symbol, which is transformed into a TD OFDM symbol, $x[n] = x[0], x[1], \ldots, x[N-1]$ through an IFFT [71], where:

$$x[n] = \frac{1}{\sqrt{N}} \sum_{i=0}^{N-1} X[i] e^{j2\pi ni/N}, \quad 0 \leq n \leq N-1 \tag{3.5}$$

Then a cyclic prefix (CP) of μ samples is added to each TD OFDM symbol to avoid ISI. The length of the CP is decided based on the finite impulse response (FIR) $h[n] = h[0], h[1], \ldots, h[\mu]$ of a discrete time channel with certain *rms* delay spread, τ_{rms} as:

$$\mu = \frac{\tau_{rms}}{T_s} - 1, \tag{3.6}$$

where, T_s is the sampling time. Then, after parallel to serial conversion and DAC a complex bipolar baseband OFDM signal is obtained which is then up-converted to a certain RF carrier and transmitted.

At the receiver side, the CP is removed and the FFT is used to obtain each received FD OFDM symbol $Y[0], Y[1], \ldots, Y[N-1]$ and each data symbol is obtained after a channel equalisation process, which in its simplest form is implemented as a zero-forcer through $Y[i]/H[i]$ operation where $H[i]$ is the channel gain of the i^{th} sub-channel calculated from the estimated frequency response of the channel. Then the baseband demodulation takes place and the binary data is recovered.

The use of OFDM MCM for optical wireless communications has been proposed by many academic researchers [98, 101, 100, 7]. Fig. 3.3 shows a block diagram of a generic

uncoded optical OFDM system. The conventional OFDM modulator is modified in order to satisfy some conditions of IM/DD systems. These conditions are, the output of the OFDM modulator must be real and positive. The output of an OFDM modulator is usually complex and to obtain a real output each FD OFDM symbol at the input of the OFDM modulator must satisfy the Hermitian symmetry [25]. This results in a FD OFDM symbol which satisfies the following condition:

$$\begin{cases} X[0] = X[\frac{N}{2}] = 0, & \text{DC Subcarrier} \\ \\ X[\frac{N}{2} - n] = X^H[\frac{N}{2} + n], & n = 1, 2, \ldots, \frac{N}{2} - 1 \end{cases} \tag{3.7}$$

Given the Hermitian symmetry at the input, a real signal at the output of the OFDM modulator is obtained. However, this signal is still a bipolar signal. There are different ways to attain a unipolar transmit signal which are discussed below.

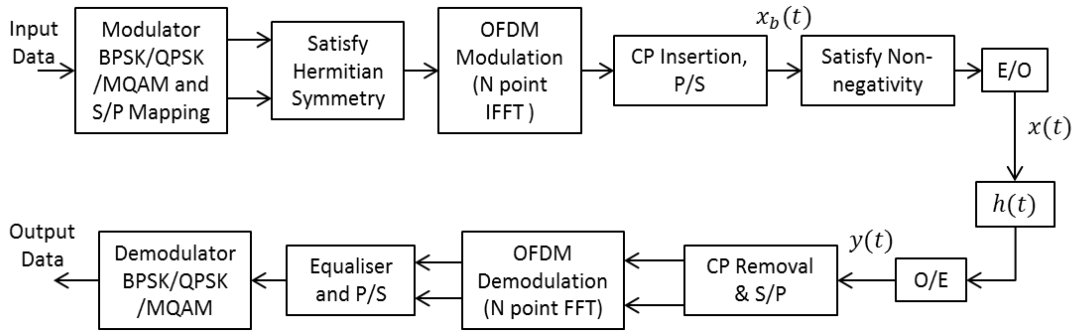

Figure 3.3: Block Diagram of a generic uncoded Optical OFDM system.

DCO-OFDM

As discussed in the previous paragraph the output of the opical OFDM modulator is bipolar and its non-negativity has to be satisfied before it can modulate the intensity of an LED. As it is named, the DCO-OFDM adds a DC-bias, B_{dc}, to the bipolar signal $x_b(t)$ (see Fig. 3.4 for an example). As mentioned in the previous section, any remaining negative sub-carriers are clipped at zero, which adds a clipping noise N_{clip} to $x(t)$. The resulting real and positive signal can be described as equation 3.2.

The DC-bias added to $x_b(t)$ in Fig. 3.4 is slightly less than the minimum value of $x_b(t)$. This means that the 5^{th} and 8^{th} samples had to be clipped at zero (see Fig. 3.4 (b)) which adds noise, N_{clip}, to $x(t)$. It is clear that increasing B_{dc} up to the minimum value of $x_b(t)$ minimises the clipping noise. However, large B_{dc} means higher power requirement which is undesirable. Additionally, B_{dc} is dependent on the limited dynamic range of the LED.

Uncontrolled B_{dc} can distort the transmit signal due to the non-linear characteristics of the transmitter circuit [125], especially when the transmit signal has high PAPR.

This device non-linearity issue is similar to that in RF communications due to the transmit PA. There are different techniques used to minimise the signal distortion due to device non-linearities. These techniques include interpolation & clipping [126], digital pre-distortion and power back-off [127][128]. These signal conditioning techniques are not studied in this thesis, however, the effect of negative signal clipping due to insufficient B_{dc} are included in this evaluation.

A key performance metric to concentrate on here is the bandwidth efficiency. Due to the Hermitian symmetry constraint, the spectral efficiency of DCO-OFDM is halved. A FD OFDM symbol of length N only carries $N/2$ sub-carriers which actually contain data [100], the other half of the sub-carriers are just carrying a copy of this data. In order to avoid the use of a DC-bias, some other optical OFDM signalling schemes have also been designed which are detailed in the following sections.

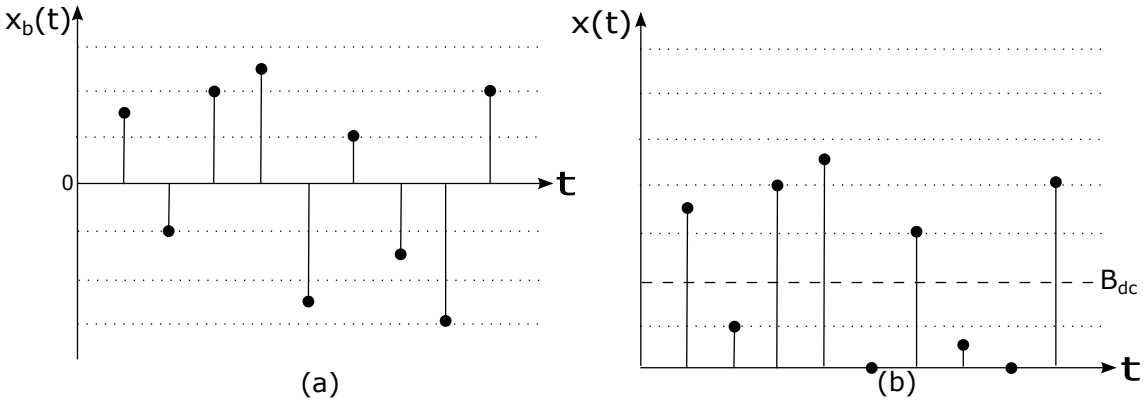

Figure 3.4: Time Domain Optical OFDM output (a) Before adding B_{dc} (b) After adding B_{dc} [7].

ACO-OFDM

ACO-OFDM provides a unipolar transmit signal without the use of DC-bias. However, this comes at the cost of further spectral efficiency degradation. In ACO-OFDM, another constraint in addition to the Hermitian symmetry constraint (3.7) is imposed at the input of the OFDM modulator [100], whereby only the odd frequency sub-carriers are modulated

[100] and the even sub-carriers are set to zero. The two constraints can be represented as:

$$\begin{cases} X[\frac{N}{2}-n] = X^H[\frac{N}{2}+n], & n = 1:1:(\frac{N}{2}-1) \\ \\ X[n] = 0, & n = 1:2:(N-1) \end{cases} \tag{3.8}$$

The Hermitian symmetry and the odd frequency sub-carrier modulation means that only $N/4$ out of N sub-carriers can carry actual information and hence the spectral efficiency of ACO-OFDM is half the spectral efficiency of DCO-OFDM [100][101] and 1/4 of the RF OFDM. However, modulating only the odd frequency carriers allows clipping of all the negative sub-carriers in bipolar signal $x_b(t)$. As the clipping noise falls on the even frequency sub-carriers, the odd frequency sub-carries do not suffer any distortion but their amplitude is reduced by a factor of 2 [129]. Therefore in the receiver, the frequency domain signal is either multiplied by 2 or the detection threshold levels are reduced by a factor of 2 before the demodulation takes place. Although ACO-OFDM does not suffer from negative clipping, positive clipping can still distort the transmit signal and cause irreducible BER problem due o limited transmitter dynamic range.

Recently, spectrally and energy efficient OFDM (SEE-OFDM) [130] has been designed, where multiple ACO-OFDM signals are summed at the transmitter before transmission. SEE-OFDM is found to have twice the spectral efficiency of ACO-OFDM (i.e. equal to that of DCO-OFDM) and it also improves the SNR requirements for a certain BER when compared to ACO-OFDM.

U-OFDM

Unipolar OFDM (U-OFDM) is one of the most recently developed optical MCM scheme [7]. Any Optical OFDM modulation scheme will require more power than RF OFDM modulation for the same bit error rate (BER). As explained previously, this is due to the energy used in making the output of the OFDM modulator real and positive. In U-OFDM, the bipolar output, $x_b(t)$, is acquired in a similar manner as in the DCO-OFDM scheme. However, the non-negativity in U-OFDM is satisfied in a completely different fashion. In U-OFDM, the bipolar signal, $x_b(t)$, is encoded in a special way to obtain the unipolar signal.

Fig. 3.5 illustrates the bipolar and unipolar U-OFDM time domain signal. Each time sample of the signal $x_b(t)$ is replaced by a pair of new time samples [7]. If a time sample of $x_b(t)$ is positive, the first sample of the new pair is set "active" and its value is the same as the original sample of signal $x_b(t)$. The second sample is set "inactive" and its value is zero. If the original time sample has a negative value, the first time sample of the new

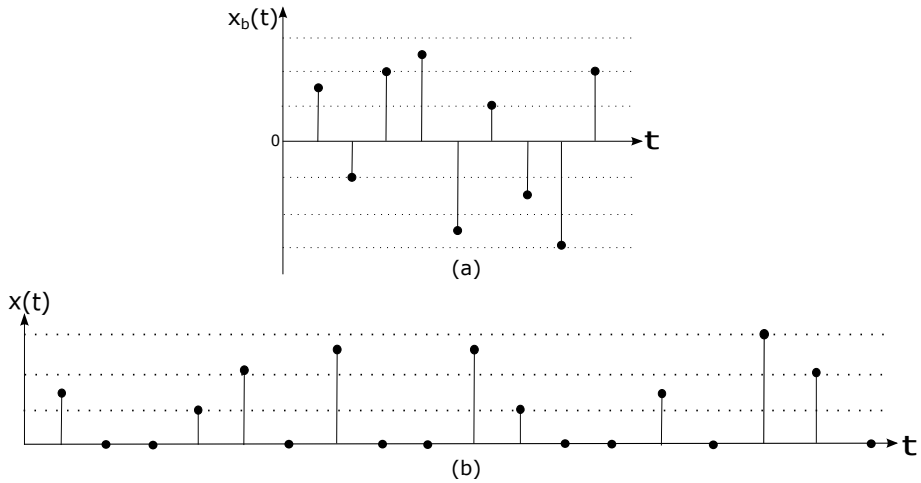

Figure 3.5: The Time Domain Optical U-OFDM Output [7]. a) the bipolar signal and b) the unipolar signal.

pair is set "inactive", so its value is zero and the second time sample "active", which is an inverted version of the original time sample [7].

At the receiver, each pair of time domain signals is decoded into one time sample. Out of each pair, the time sample with the highest magnitude is marked "active" and the other "inactive". The magnitude and polarity of the new time sample is determined by the magnitude and the position of the "active" time sample respectively [7].

Satisfying the Hermitian symmetry and encoding the bipolar OFDM output (by a rate of 1/2) means that for an OFDM block size of N only $N/4$ sub-carriers carry actual information. Hence the spectral efficiency of U-OFDM is the same as ACO-OFDM and half of that in DCO-OFDM. In order to improve the spectral efficiency of U-OFDM, recently, an enhanced U-OFDM (eU-OFDM) [131] system has been proposed which transmits multiple summed U-OFDM signals. eU-OFDM provides the same spectral efficiency as DCO-OFDM (i.e. twice that of U-OFDM).

Flip-OFDM

Flip-OFDM is very similar to U-OFDM as it also does not require any DC-bias or clipping of the negative sub-carriers while the Hermitian symmetry of each OFDM block is obtained in exactly the same manner as in DCO-OFDM. However, Flip-OFDM does not encode the bipolar signal $x_b(t)$ to obtain the unipolar signal $x(t)$. Flip-OFDM generates the unipolar signal in a simpler way. Fig. 3.6 illustrates the unipolar Flip-OFDM time domain signal. The signal $x_b(t)$ is first separated into two parts, one carrying positive sub-carriers and the other carrying negative sub-carriers [102, 103]. These two parts can be written as follows

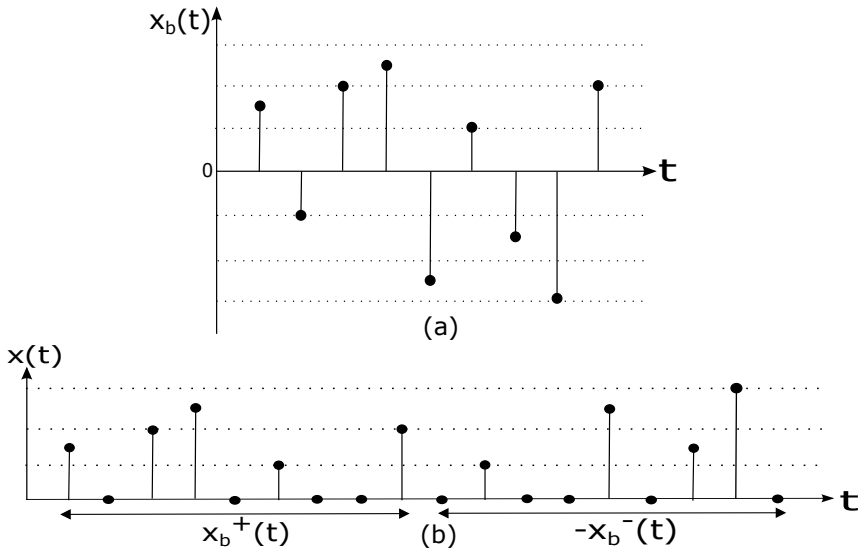

Figure 3.6: Time Domain Optical Flip-OFDM Output. a) the bipolar signal and b) the unipolar signal.

[102, 103]:

$$x_b^+(t) = \begin{cases} x_b(t) & \text{if } x_b(t) \geq 0 \\ 0 & \text{otherwise} \end{cases} \tag{3.9}$$

$$x_b^-(t) = \begin{cases} x_b(t) & \text{if } x_b(t) < 0 \\ 0 & \text{otherwise} \end{cases} \tag{3.10}$$

The signal $x(t)$ is a combination of both $x_b^+(t)$ and $x_b^-(t)$ as shown in Fig. 3.6, where the positive sub-carriers in each TD OFDM symbol are transmitted first, followed by the negative samples. Flip-OFDM also has the same spectral efficiency as U-OFDM and ACO-OFDM.

3.3.2 Optimal Channel Partitioning Vectors: Vector Coding

Vector coding (VC) is known as the optimal channel partitioning MCM technique [108]. Unlike OFDM, VC requires the CSI at the transmitter [71]. While the indoor VLC channel has a static nature, CSI will be readily available at the transmitting end. This is well matched to the requirement of VC. VC uses singular value decomposition (SVD) of the circulant channel matrix $\boldsymbol{H}_{N\times(N+\mu)}$, where N is the number of sub-channels and μ is the prefix length. For a finite impulse response (FIR) h_n, $0 \leq n \leq \mu$, of a discrete-time

channel, the circulant channel matrix can be written as [108][71]:

$$\boldsymbol{H} = \begin{bmatrix} h_0 & h_1 & \dots & h_\mu & 0 & \dots & 0 \\ 0 & h_0 & \dots & h_{\mu-1} & h_\mu & \dots & 0 \\ \vdots & \vdots & \ddots & \ddots & \ddots & \ddots & \vdots \\ 0 & \dots & 0 & h_0 & \dots & h_{\mu-1} & h_\mu \end{bmatrix} \tag{3.11}$$

The SVD of the above matrix $\boldsymbol{H}$ can be given as:

$$\boldsymbol{H} = \boldsymbol{U}\boldsymbol{S}\boldsymbol{V}^H, \tag{3.12}$$

where,$\boldsymbol{U}$ and $\boldsymbol{V}$ are two unitary matrices of size $N \times N$ and $(N+\mu)\times(N+\mu)$, respectively. $\boldsymbol{S}$ is a diagonal matrix of the same size as H and it contains the singular values ($\boldsymbol{s}_i$) of $\boldsymbol{H}$ on its diagonal elements [108][71]. VC uses matrix $\boldsymbol{V}$ at the transmitter for precoding and to create N parallel independent sub-channels. The rows of matrix $\boldsymbol{U}$ are used as discrete matched filters at the receiver.

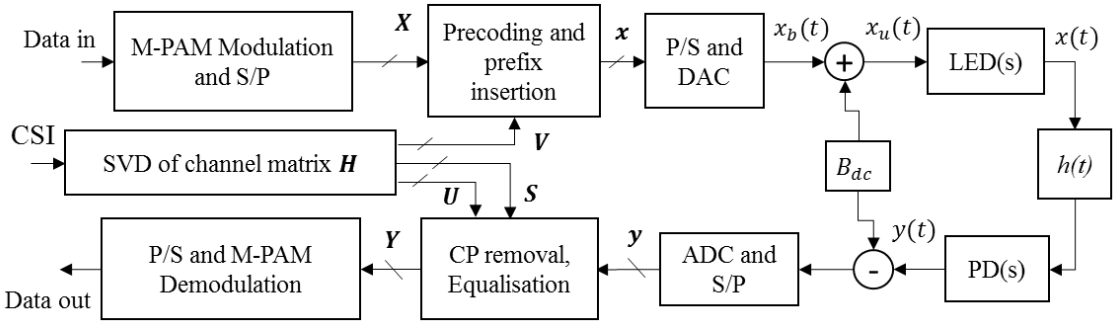

Figure 3.7: Transceiver schematic of an uncoded DCO-VC system.

Fig. 3.7 shows the schematic of a DCO-VC system. The random binary data in sets of k bits is modulated using a baseband modulation scheme. In this research, an M-PAM modulation scheme has been used in order to obtain a real and bipolar vector precoded signal. M-QAM modulation can also be used in VC, however, this will provide a complex output from the VC modulator. The PAM data is grouped into vectors of length N and these groups are known as DCO-VC blocks or symbols. Each DCO-VC symbol can be represented as $\boldsymbol{X} = [X_0, X_1, \dots, X_{N-1}]^T$ and the precoding that takes place as each DCO-VC symbol is multiplied by matrix $\boldsymbol{V}$ to obtain the precoded data vector $\boldsymbol{x}$, as $\boldsymbol{x} = \boldsymbol{V}\boldsymbol{X}$. As the size of $\boldsymbol{V}$ is $(N+\mu)\times(N+\mu)$, in order for this multiplication to take place either μ zeros are appended to the end of each DCO-VC symbol block to make their length equal to $(N+\mu)$ or the original DCO-VC symbols of length N are multiplied by the first N

columns of V [108]. Each precoded data vector can be given as $\boldsymbol{x} = [x_0, x_1, \ldots, x_{N+\mu-1}]^T$ and also includes a CP of length μ. The precoded vectors are then converted from parallel to serial and then DAC takes place which gives the real bipolar DCO-VC signal to which B_{dc} (see equation 3.1) is added and the real unipolar VC signal, $x_u(t)$ is obtained. The transmitted and received signals in DCO-VC can also be given by $x(t)$ and $y(t)$, hence, equation (3.3) applies.

At the Rx, after B_{dc} removal, ADC and serial to parallel conversion, each DCO-VC symbol can be mathematically represented as:

$$\boldsymbol{y} = \boldsymbol{H}\boldsymbol{x} + \boldsymbol{n} \tag{3.13}$$

In equation (3.13), $\boldsymbol{n}$ represents the AWGN vector. Equation (3.13) can be rewritten as $\boldsymbol{y} = \boldsymbol{U}\boldsymbol{S}\boldsymbol{V}^H\boldsymbol{V}\boldsymbol{X} + \boldsymbol{n}$ and the matched filter operation at the receiver can be represented as:

$$\boldsymbol{U}^H\boldsymbol{y} = \boldsymbol{U}^H\boldsymbol{U}\boldsymbol{S}\boldsymbol{V}^H\boldsymbol{V}\boldsymbol{X} + \boldsymbol{U}^H\boldsymbol{n} \tag{3.14}$$

By rewriting equation (3.14), the received filtered vectors can be represented as $\tilde{\boldsymbol{y}} = \boldsymbol{S}\boldsymbol{X} + \boldsymbol{U}^H\boldsymbol{n}$, where $\tilde{\boldsymbol{y}} = \boldsymbol{U}^H\boldsymbol{y}$ and $\boldsymbol{U}^H\boldsymbol{n}$ has unchanged noise variance since $\boldsymbol{U}$ is a unitary matrix. Equivalent zero-forcing equalisation in DCO-VC is realised by dividing each received sub-channel $\tilde{\boldsymbol{y}}_i$ by $\boldsymbol{s}_i$, which gives $\boldsymbol{Y}$. This is not an optimal way to equalise because sub-channel gains less than 1 enhance the noise in that sub-channel. However, this was done to provide a fair comparison between the considered schemes. An optimal way to detect a signal in DCO-VC would be to adjust the detector threshold according to known $\boldsymbol{S}$ at the Rx. Once $\boldsymbol{Y}$ is obtained, the baseband demodulation takes place and the binary data is retrieved.

3.4 Performance Evaluation over AWGN Channel

In communications, the basic performance assessment of a system is carried out for an AWGN channel, which assumes a path-loss and multipath free wireless channel. This section evaluates and compares the performance of DCO-PAM, DCO-VC, DCO-OFDM, ACO-OFDM, Flip-OFDM and U-OFDM systems over AWGN channel. The BERs of DCO-PAM and DCO-OFDM systems are evaluated though both simulations and analytical formulations, while the BER performance of non DC-bias systems is evaluated through simulations and compared to the results obtained in the literature. In addition to the performance comparison, this study validates the system simulators for the considered SCM and MCM schemes.

3.4.1 Performance of DC-biased MCM and SCM Systems

As mentioned earlier, in DC-biased systems, the transmit unipolar signal $x_u(t)$ is obtained from the bipolar signal by adding a DC-bias. Ideally, a DC-bias equivalent to the minimum sample value of the transmit bipolar signal would convert it to a unipolar signal, avoiding any negative clipping or distortion. However, in practical VLC systems, the DC-bias is set according to the dynamic range (DR) of the transmitter, such that the average optical power of the transmit signal is approximately half of the DR. Therefore, the actual DC-bias used in practical systems may lead to some signal samples to be outside the DR after DC-bias addition, especially for the signalling schemes with high PAPR. These samples will be distorted due to the non-linear characteristics of the transmitter, leading to a poor BER performance. To avoid this distortion, signal conditioning techniques like digital pre-distortion and power back-off [127][128] have been proposed as mentioned earlier.

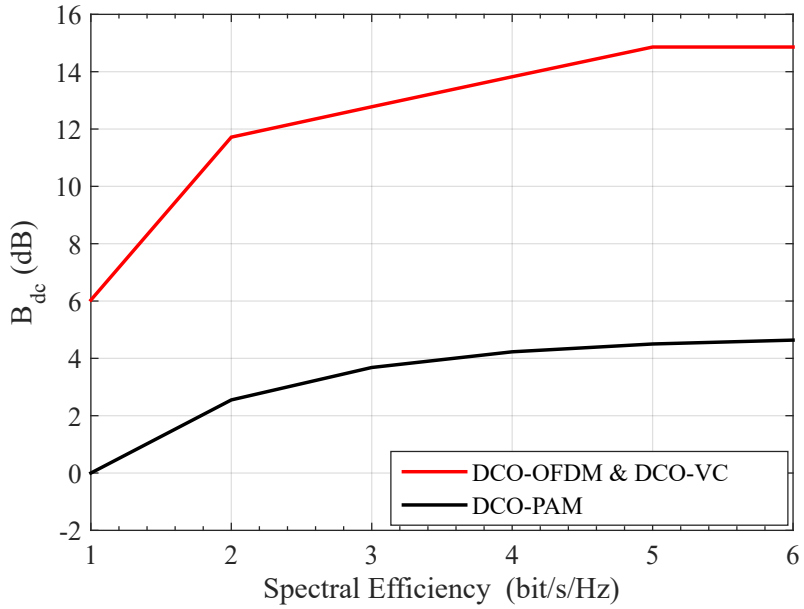

Figure 3.8: Comparison of B_{dc} values used for considered DCO-PAM, DCO-OFDM and DCO-VC schemes to achieve target BER of 10^{-6}.

In this research the performance of DC-biased signalling schemes are compared with negligible clipping effect, whereby no signal conditioning technique was required. The B_{dc} was set to minimise the negative clipping and a sufficient DR was assumed to avoid positive clipping which kept n_{clip} in equation 3.2 negligible. This was done to obtain a bench-mark error performance of DC-biased system with a target[1] BER of 10^{-6} and the

[1]A target BER of 10^{-6} was assumed as it is a typical BER requirement before any FEC is used in wireless communication systems.

irreducible BER floor due to clipping was set well below the target BER.

Fig. 3.8 shows the B_{dc} values used in this research, for a certain number of uncoded bits per sub-channel, to achieve the target BER of 10^{-6}. It can be seen that the DCO-OFDM & DCO-VC MCM schemes require the same levels of B_{dc}, which are much larger than those seen in the DCO-PAM scheme. This large difference in B_{dc} values is a direct consequence of a very peaky envelope of MCM signals. Fig. 3.9 shows the PAPR of DC-biased signalling schemes with a modulation order to achieve a spectral efficiency of 6 bit/s/Hz, in bipolar baseband (BB) versions (i.e. before adding B_{dc}). Given that the mean electrical power in each signalling scheme is normalised to one Watt, i.e. $E\{x_b^2(t)\} = 1$W, the plots in Fig. 3.9, in essence, show the cumulative distribution function (CDF) values of the peak power levels detected in 10000 data packets. Therefore, the difference in peak powers detected in DCO-PAM and MCM schemes is approximately 7.3 dB for 90% confidence, which leads to a large difference in the required B_{dc} levels.

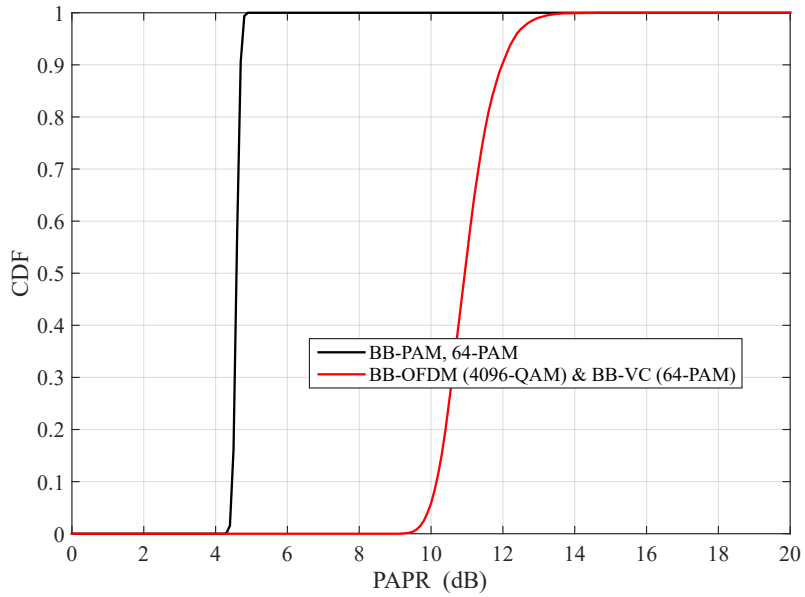

Figure 3.9: CDF plots for PAPR of the considered signalling schemes, without B_{dc}, to achieve 6 bit/s/Hz (or bits/sub-channel). Results are obtained by generating 10000 random data packets, each with 12000 bits. BB in the legends is indicative of bipolar baseband signals.

Fig. 3.10 and Fig. 3.11 shows the BER performance of 6 different modulation orders of DCO-PAM and DCO-OFDM system, respectively, which can provide a spectral efficiency of 1 to 6 bit/s/Hz. An N of 64 was used during the simulations. Both simulations and analytical results are shown, which agree well with each other. It can be seen that the SCM DCO-PAM outperforms DCO-OFDM by approximately 5 to 9 dB SNR gain for the same spectral efficiency. This large gain is mainly due to the large DC-bias required in

DCO-OFDM system. The BER performance of DCO-PAM and DCO-OFDM was also compared over the E_b/N_o scale, where E_b is the energy per bit. These results are shown in Appendix A (Fig. 1 & Fig. 2, respectively).

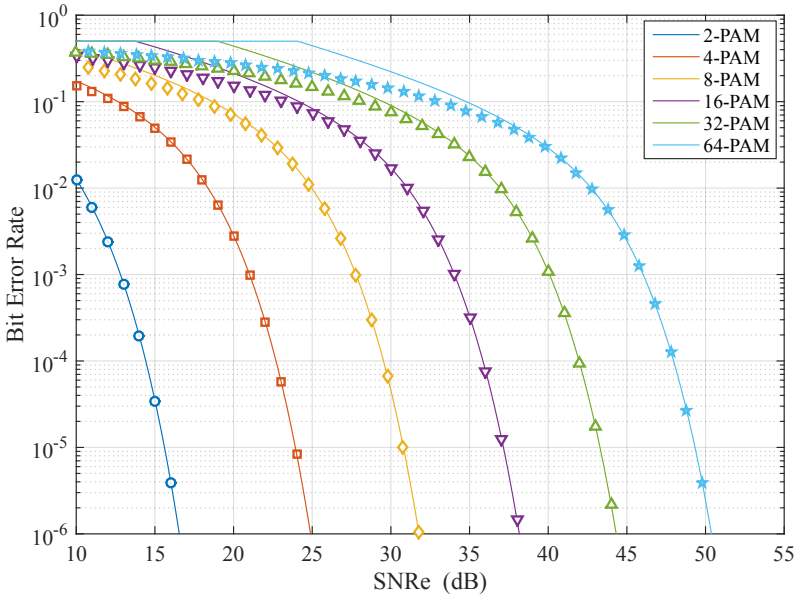

Figure 3.10: BER Performance of uncoded DCO-PAM system over AWGN channel. Solid lines and the markers represent analytical results and simulations, respectively.

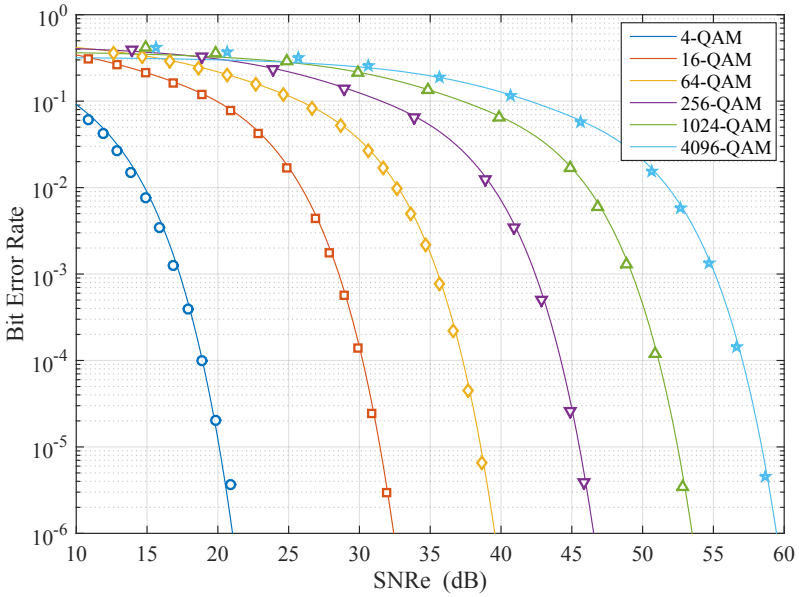

Figure 3.11: BER Performance of uncoded DCO-OFDM system over AWGN channel. Solid lines and the markers represent analytical results and simulations, respectively.

The analytical results shown in Fig. 3.10 for DCO-PAM were obtained based on union bound through:

$$\mathcal{P}_{b(\text{DCO-PAM})}=\frac{1}{Mlog_2(M)}\sum_{i=1}^{M}\sum_{\substack{j=1,\\ j\neq i}}^{M} Q\left(\sqrt{\frac{d(s_i,s_j)^2}{4\sigma_n^2}}\right), \tag{3.15}$$

where, $d(s_i, s_j)$ is the Euclidean distance between two legitimate M-PAM symbols in signal space with added B_{dc} and $Q(.)$ is the tail probability of the standard normal distribution. The bit error proability of the QAM based DCO-OFDM systems can be estimated as [132]:

$$\begin{aligned}\mathcal{P}_{b(\text{DCO-OFDM})} &= \frac{2(\sqrt{M}-1)}{\sqrt{M}\log_2(\sqrt{M})}Q\left(\sqrt{\frac{3P^2}{(M-1)\sigma_n^2}}\right)\\ &+ \frac{2(\sqrt{M}-2)}{\sqrt{M}\log_2(\sqrt{M})}Q\left(3\sqrt{\frac{3P^2}{(M-1)\sigma_n^2}}\right),\end{aligned} \tag{3.16}$$

where, P^2 is the mean electrical power of the transmit DCO-OFDM signal, and can be given as $P^2 = (\xi^2 + 1)$. It must be noted that high B_{dc} values used during simulations to achieve the target BER results in negligible n_{clip}, which can be omitted for the evaluation of the analytical bit error probabilities. For lower B_{dc} values, equations (3.15) and (3.16) should be modified taking n_{clip} into account.

Performance of DCO-VC over AWGN

The DCO-VC system is an equivalent DCO-PAM system for an AWGN channel. This is because for an AWGN channel, the channel matrix $\boldsymbol{H}$ contains ones on its diagonal elements and SVD of such a channel matrix gives identity $\boldsymbol{U}$, $\boldsymbol{S}$ and $\boldsymbol{V}^H$ matrices. Therefore, precoding and matched filtering operations do not change the transmit and receive signals, respectively. This means $\boldsymbol{x} = \boldsymbol{X}$, which contains M-PAM modulated symbols, which require the same DC-bias as the DCO-PAM system. Therefore, the DCO-VC system, is an equivalent DCO-PAM system for an AWGN channel and its performance can be given by the results in Fig. 3.10. This is not the case for a practical VLC channel, as we will see in the next chapter when multipath dispersion is present.

3.4.2 Non DC-biased Systems

Fig. 3.12 and Fig. 3.13 show the BER vs SNR_e performance of ACO-OFDM and Flip-OFDM non DC-biased systems. The BER vs E_b/N_o results are shown in Appendix A

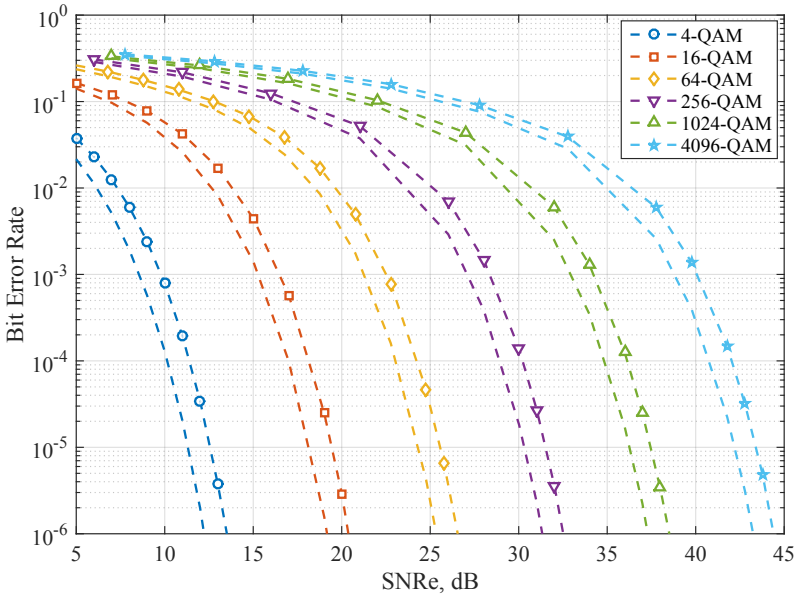

Figure 3.12: BER Performance of uncoded ACO-OFDM system over AWGN channel. Results with markers represent the performance of original system (without negative clipping at the Rx) and dashed line results represent the performance enhanced by negative clipping at the Rx.

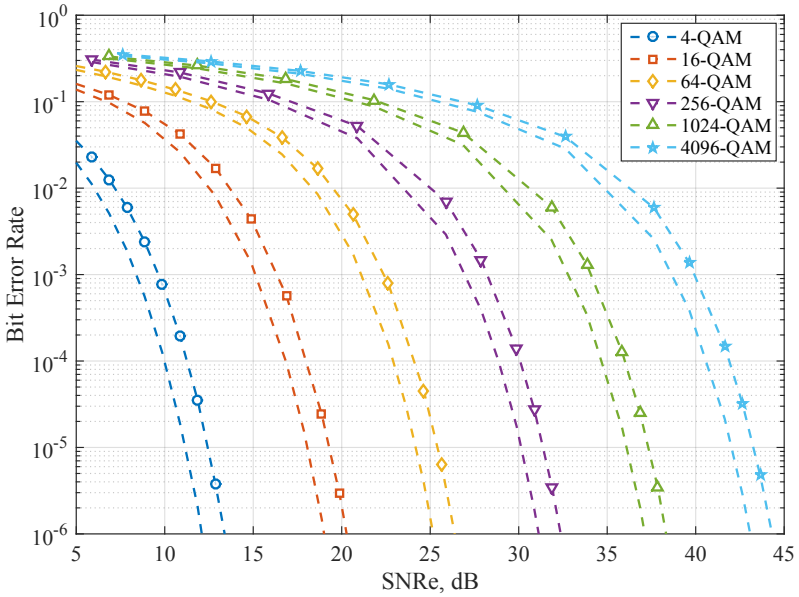

Figure 3.13: BER Performance of uncoded Flip-OFDM system over AWGN channel. Results with markers represent the performance of original system (without negative clipping at the Rx) and dashed line results represent the performance of enhanced system by negative clipping at the Rx.

(Fig. 3 & Fig. 4). For both the systems an N of 64 was used during the simulations. The results with markers are for original systems detailed in sections 3.3.1. The error rate performance of the ACO-OFDM can be improved by a slight modifications in the receiver as described in [133]. In IM/DD systems the transmitted signal is real & positive and the AWGN is bipolar. This means that the amplitude of the received samples can be negative if negative amplitude noise is added to it. Therefore, at the receiver any negative valued sample can be clipped to zero as this is simply noise [133]. This negative clipping at the Rx yields a modified ACO-OFDM system. A modified Flip-OFDM systems can also be designed in a similar manner [103]. The result without a marker are for a modified receiver with negative clipping at the Rx.

It can be seen that the ACO-OFDM systems BER performance results agree with those in [100] and [101]. The results also show that the Flip-OFDM performs equivalently to ACO-OFDM as seen in the literature [102],[103]. The modified receivers provide an SNR gain of approximately 1.25 dB when compared to the original ACO-OFDM and Flip-OFDM systems.

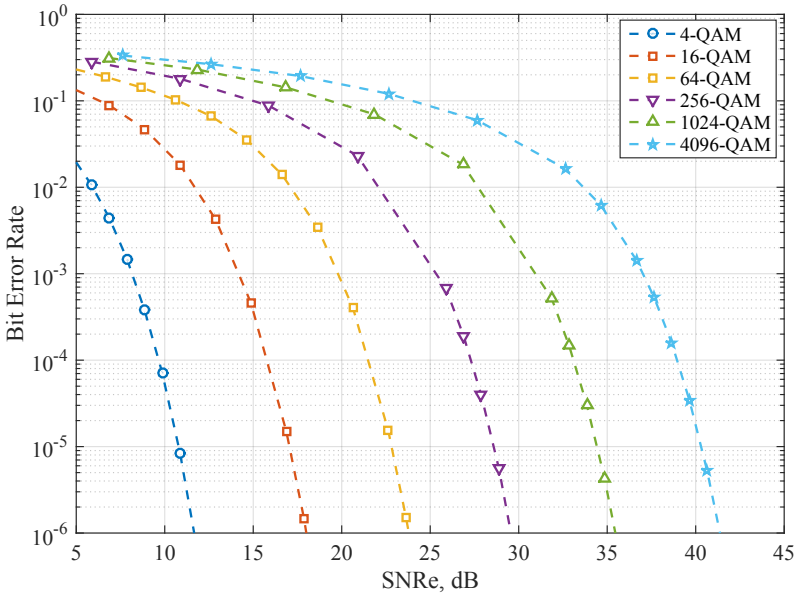

Figure 3.14: BER Performance of uncoded U-OFDM system over AWGN channel.

The BER performance of the U-OFDM system is shown in Fig. 3.14 over the SNR_e scale. Comparing the results in Figures 3.12, 3.13 and 3.14, it can be seen that U-OFDM outperforms the ACO-OFDM and Flip-OFDM by achieving an SNR gain of approximately 0.5 to 1.5 dB. This shows that U-OFDM is the most efficient non DC-biased optical MCM scheme. The BER vs E_b/N_o performance of U-OFDM is shown in the Appendix A (Fig. 5), these results agree with the results shown in [7]. The analyses in the next section evaluate

the spectral efficiency of all the considered SCM and MCMC systems.

3.4.3 Analyses of Results

The considered SCM and MCM systems provide different spectral efficiencies for the modulation orders used. This is because each system satisfies the transmit signal requirements of an IM/DD technique differently. The spectral efficiency of the DCO-PAM scheme is given as $\gamma_{(DCO-PAM)} = \frac{N}{N+\mu}\log_2(M)$. The spectral efficiency of the DCO-OFDM system can be given as:

$$\gamma_{(DCO-OFDM)} = \frac{(N/2)-1}{N+\mu}\log_2(M), \tag{3.17}$$

and the spectral efficiencies of ACO-OFDM, Flip-OFDM and U-OFDM are the same and can be given as:

$$\gamma_{(ACO/Flip/U\text{-}OFDM)} = \frac{N/4}{N+\mu}\log_2(M). \tag{3.18}$$

Table 3.1: Equivalent modulation orders of considered uncoded SCM and MCM schemes for a certain spectral efficiency.

γ (bit/s/Hz)	**Modulation Order** (M)		
	DCO-PAM	DCO-OFDM	ACO/Flip/U-OFDM
1	2-PAM	4-QAM	16-QAM
2	4-PAM	16-QAM	256-QAM
3	8-PAM	64-QAM	4096-QAM
4	16-PAM	256-QAM	64536-QAM
5	32-PAM	1024-QAM	1048576-QAM
6	64-PAM	4096-QAM	16777216-QAM

Table. 3.1 shows the different modulation orders of the considered uncoded schemes which can provide a spectral efficiency between 1 to 6 bit/s/Hz. It can be seen from this table that if $M_{(DCO-PAM)}$ is the modulation order for DCO-PAM system for a certain spectral efficiency, the modulation order for DCO-OFDM is $M^2_{(DCO-PAM)}$ and the three non DC-biased schemes is $M^4_{(DCO-PAM)}$, for the same spectral efficiency. This shows that the ADC and DAC resolution requirements will be highest for the non-DC-biased systems and lowest for the SCM DCO-PAM system. The resolution and sample rates of ADC or DAC are inversely proportional to each other. Given that VLC systems are required to operate at with high data-rates for high throughputs, the resolution requirements must be kept to a minimum. This makes the low modulation order based DC-biased system

more suitable for VLC in comparison to the non DC-biased schemes which require high modulation orders for equivalently the same spectral efficiencies.

As an example, for a spectral efficiency of 6 bit/s/Hz, ACO-OFDM, Flip-OFDM and U-OFDM will require a modulation order of 16777216-QAM, in comparison to 4096-QAM & 64-PAM for DCO-OFDM and DCO-PAM, respectively. This also affects the complexity of the system especially at the Rx side. The data in table 3.1 shows that the complexity of ACO-OFDM, Flip-OFDM and U-OFDM systems will increase rapidly with increasing spectral efficiency when compared to DC-biased systems.

Table 3.2 compares the SNR_e requirements of all the considered schemes over AWGN channel for a BER of 10^{-6} for spectral efficiencies between 1 to 3 bit/s/Hz. These SNR_e values are obtained from the BER results shown in the previous section. Clearly, the DCO-PAM system is the most efficient when compared to the optical OFDM systems. However, it is important to also notice the spread of performance of different optical OFDM systems. For 1 bit/s/Hz, the non DC-biased OFDM systems are more efficient than DCO-OFDM, especially the U-OFDM system. However, as the spectral efficiency increases to 3 bit/s/Hz DCO-OFDM is more efficient than the non DC-biased systems. This could be because the DC-bias requirements saturate with increasing spectral efficiency (see Fig. 3.8), whereas the Euclidean distances between the M-QAM symbols will continue to decrease with increasing modulation order (or spectral efficiency). Therefore, the DC-biased systems are more efficient in terms of SNR requirements and complexity when compared to non DC-biased systems.

Table 3.2: SNR_e requirements of different optical signalling schemes over AWGN channel for a BER of 10^{-6}.

γ (bit/s/Hz)	**SNR_e (dB) required for a BER of 10^{-6}**			
	DCO-PAM	DCO-OFDM	ACO/Flip-OFDM	U-OFDM
1	16.5	21	19	18
2	25	32.3	31.3	29.5
3	32	39.5	43.2	41.4
4	38	46.6	*(Too complex to determine)*	
5	44.3	53.5	*(Too complex to determine)*	
6	50.2	59.5	*(Too complex to determine)*	

3.5 Summary

The motivation behind the development of various non DC-biased optical MCM systems has been reducing the power requirements while providing a real and unipolar transmit signal for VLC and IR systems. This is because the conventional DCO-OFDM system tends to require a high DC-bias to satisfy the transmit signal requirement for an IM/DD channel. The non DC-biased systems, ACO-OFDM, Flip-OFDM and U-OFDM, eliminate the need for explicit DC-bias. However, they reduce the spectral efficiency to one half of DCO-OFDM and one quarter of the RF OFDM systems.

The BER performance result over an AWGN channel show that for a low spectral efficiency, 1-2 bit/s/Hz, the non DC-biased MCM systems outperform the DCO-OFDM scheme by an SNR requirement of 1 to 3 dB, where the non DC-biased U-OFDM system is the most efficient. However, as the spectral efficiency increases to 3 bit/s/Hz, the DCO-OFDM provides an SNR gain of 1.9 to 3.7 dB over the non DC-bias systems. The analysis of result in this chapter also show that increasing the spectral efficiency beyond 3 bit/s/Hz would mean using a QAM orders of larger than 4096 levels for the non DC biased systems. This questions the practical applicability of the the ACO-OFDM, Flip-OFDM and U-OFDM systems as modulation orders greater than 4096 levels will increase the resolution requirements of the ADC and DAC processes. The reduced spectral efficiency of the non DC-biased systems will be further affected when use of FEC becomes important to enhance the system performance as this will add further overheads.

Overall, the DC-biased systems prove to be more power and spectrally efficient for the AWGN channel. The results show that the DCO-PAM SCM scheme is the most power efficient than any optical MCM schemes considered. This is due to the low PAPR and hence the low DC-bias requirement of the DCO-PAM SCM system. In comparison to DCO-OFDM, for a certain spectral efficiency, a DCO-PAM SCM signalling could yield SNR gains between 4.5 to 9.3 dB for a VLC system.

The new MCM system, DCO-VC performs equivalent to the DCO-PAM over an AWGN channel. However, the next chapter will show that this is not the case for a representative VLC channel, where the DC-bias requirements of DCO-VC system becomes equivalent to those of DCO-OFDM.

Chapter 4

Rate-Adaptive Coded Single and Multi Channel Modulations with Frequency Domain Equalisation

4.1 Introduction

Multi-channel modulation schemes in VLC obtain a real and unipolar transmit signal at the cost of reduced capacity and/or increased power requirements due to a DC-bias, as seen in the previous chapter. This is a major drawback of optical MCM systems. In order to improve the capacity of the optical systems, this chapter compares the performance of different modulation schemes with and without the use of channel coding. The focus here is on DC-biased MCM and SCM systems as these systems are found to be more power efficient than the non DC-biased systems such as ACO-OFDM, Flip-OFDM and U-OFDM over the AWGN channels investigated in the previous chapter. Additionally, Azhar and O'Brien have found through experimentation that for certain BER DCO-OFDM offers higher bit-rates to the bandwidth limited VLC systems when compared to ACO-OFDM and U-OFDM [134].

Forward error correction schemes play a vital role to improve the error performance, hence the capacity, of a communication system for a given SNR. To the best of the author's knowledge, no work has been published which examines the performance of the optical wireless MCM and SCM systems with FEC techniques. In this chapter, the throughput performance of rate-adaptive coding (RAC) based DCO-OFDM, DCO-VC and DCO-PAM systems and their uncoded counterparts is evaluated and compared over representative hybrid (LOS+Diffuse) and only diffuse optical wireless channels.

The RAC utilise non-punctured (1/2 rate) and punctured (2/3 and 3/4) binary con-

volutional (BC) codes and a Viterbi decoder with hard-decision (HD) and soft-decision (SD) detection for the optical MCM and SCM receivers leading to RAC-HD and RAC-SD schemes,respectively. Although highly responsive LEDs have been produced [39], commercial LEDs provide a cut-off bandwidth of 2-20 MHz [46][28]. Therefore, a system bandwidth (W) of 20 MHz was considered for the MCM and SCM systems to investigate the performance enhancements with RAC based signalling.

The investigations begin by studying the performance of RAC based MCM and SCM systems over an AWGN channel through simulations and analytical approximations, which shows that the RAC significantly improves the system throughput for each of the DC-biased systems. The analytical and simulations based throughput performance evaluation for AWGN channel shows that the RAC-SD DCO-OFDM, DCO-VC and DCO-PAM systems achieve up to 5 and 9 dB electrical SNR ($\mathrm{SNR_e}$) gain when compared to the RAC-HD and uncoded transmissions, respectively. The results show that RAC-HD systems outperform the uncoded systems only for very low SNRs and as the SNR improves RAC-HD systems do not provide any coding gain.

The chapter then details the throughput performance of the considered systems examined over hybrid and NLOS channels for an indoor environment of size $(5 \times 5 \times 3)$m (see Fig. 2.3). The channel models used for the investigation include the reflectivity of different indoor objects and spectral properties of commercially available optical front-end devices. The results show that the RAC-SD schemes provide up to 9 dB $\mathrm{SNR_e}$ gain when compared to the uncoded systems. The results also show that due to low DC-bias requirements the RAC-SD DCO-PAM scheme provides the highest throughput for a certain $\mathrm{SNR_e}$ over VLC channels and achieves up to 10 and 11 dB $\mathrm{SNR_e}$ gain when compared to RAC-SD, DCO-VC and DCO-OFDM systems, respectively.

This investigation also showed that for the environment considered the maximum channel *rms* delay spread for the VLC system performance investigation is 5.7ns. In other indoor environments, it is possible that the signalling systems experience a larger *rms* delay spread. Therefore, it is important to examine the performance of the considered systems with increased temporal dispersion, which could provide different throughput performance trends to those seen in hybrid and diffuse links with low *rms* delay spreads. Towards the end, this chapter details the performance evaluation of considered systems of diffuse links with *rms* delay spreads ranging from 10ns to 50ns.

The result also showed that, despite being a suboptimal MCM, the DCO-OFDM performs almost equivalent to the optimal DCO-VC system over the considered hybrid and diffuse links. When compared in uncoded modes the DCO-VC and DCO-OFDM systems perform equivalently for less dispersive channels. However, as the channel *rms* delay spread is increased to 50ns the uncoded DCO-VC system requires up to 1 dB less $\mathrm{SNR_e}$

for the same throughput when compared to the uncoded DCO-OFDM system. On the other hand, the RAC based DCO-VC system can provide up to 3 dB SNR_e gain with increasing dispersion when compared to the RAC based DCO-OFDM system.

The DC-bias values, hence the transmit dynamic range for DCO-VC, DCO-OFDM and DCO-PAM systems were kept the same as shown in Fig. 3.8 in the previous chapter. This was done to achieve an acceptable BER performance of 10^{-6} for each coded and uncoded systems such that their SNR requirements can be compared while the schemes provide a useful data throughput. This chapter shows that reducing the DC-bias degrades the BER performance of both the uncoded and RAC based schemes which in turn degrades the throughput due to the rise of irreducible BER floor above the target BER. This happens as the reduction in DC-bias leads to high negative signal clipping and hence high clipping noise. This indicates the requirement for a more sophisticated FEC technique to minimise the effect of clipping noise in a high PAPR system, which could result in increased system complexity and latencies.

4.2 System Description

The RAC based DCO-PAM, DCO-OFDM and DCO-VC systems are different from their uncoded counterparts studied in the previous chapter in a way that they use binary convolutional (BC) channel encoding and Viterbi decoding schemes at the Tx and Rx, respectively. The RAC based MCM and SCM systems utilise non-punctured (1/2 rate) and punctured (2/3 and 3/4) BC codes as specified in [135] with Viterbi decoder. Both hard decision and soft decision detections are considered at the receiver leading to RAC-HD and RAC-SD schemes, respectively. The RAC-HD and RAC-SD systems used a 64 state BC code with the well-known industry standard generator polynomials: {171,133}. Six different modulation modes for each signalling scheme were considered; 2, 4, 8, 16, 32 and 64 PAM for DCO-PAM and DCO-VC and 4, 16, 64, 256, 1024 and 4096 QAM for the DCO-OFDM system. This was done to keep the spectral efficiency (or bits/sub-channel) the same for all the considered systems, e.g. 64-PAM based DCO-VC (or DCO-PAM) and 4096-QAM based DCO-OFDM will result in approximately the same bits/sub-channel due to the Hermitian symmetry requirement of DCO-OFDM.

Fig. 4.1, 4.2 and 4.3 show the block diagrams of RAC based DCO-OFDM, DCO-VC and DCO-PAM systems, respectively. At the Tx side of each system, random binary data is first encoded using a rate-adaptive BC code and grouped into k bits for baseband modulation, which is M-PAM for DCO-PAM & DCO-VC, and M-QAM for DCO-OFDM. After the encoding and baseband modulation the Tx real and unipolar signal $x(t)$ is obtained in each system in the same way as described in the previous chapter and the received

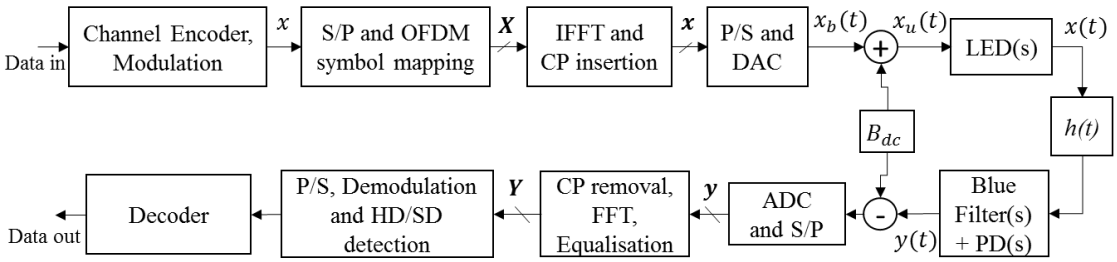

Figure 4.1: RAC based DCO-OFDM Transceiver.

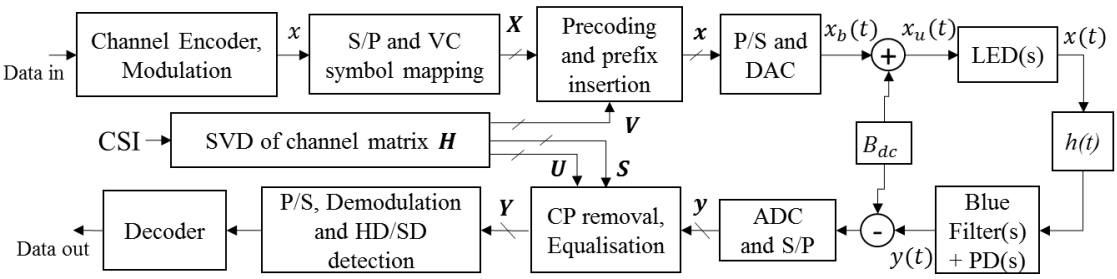

Figure 4.2: RAC based DCO-VC Transceiver.

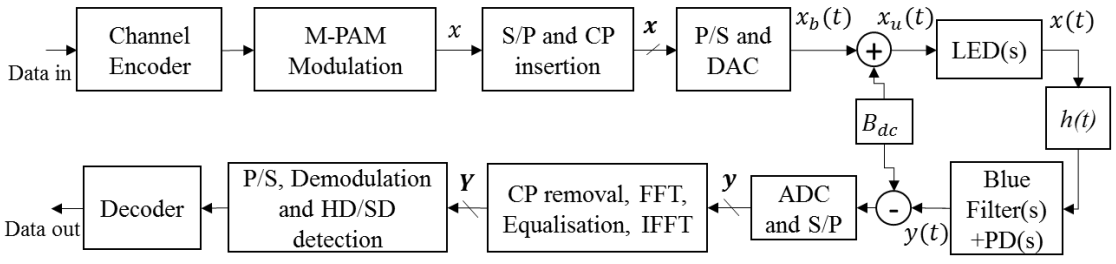

Figure 4.3: Transceiver of SCM-FDE based DCO-PAM with RAC.

signal $y(t)$ can be given by equation (3.3) from which the equalised data symbol vector $\boldsymbol{Y}$ is obtained after FD zero-forcing equalisation (ZFE) (see section 3.3.1 of Chapter 3). The baseband demodulation in terms of HD/SD detection (see section 4.2.1) and Viterbi decoding is then performed on $\boldsymbol{Y}$ to retrieve the information bits. The minimum mean square error (MMSE) can be used as an alternative equalisation technique. However, given the VLC channels are not highly frequency selective, ZFE provides MMSE equivalent performance [107].

The DC-bias B_{dc} in this chapter was set according to equation (3.1). At the beginning, the B_{dc} for each of the considered system was kept the same as shown in Fig. 3.8 to achieve a target BER of 10^{-6} as in the previous chapter to study the performance of each system without any signal distortion due to the transmitter DR. However, later in this chapter, the performance of the DCO-OFDM system has also been studied through the use of lower B_{dc} values than the optimised values in order to examine the signal clipping effect when rate-adaptive FEC is employed.

4.2.1 HD and SD information de-mappers

In considered DCO-OFDM, DCO-VC and DCO-PAM systems, the HD detection is carried out by estimating the n^{th} M-PAM or M-QAM symbol, $\boldsymbol{Y}^{'}_{n}$, from n^{th} element (or sub-channel) of $\boldsymbol{Y}$ as:

$$\boldsymbol{Y}^{'}_{n} = \arg\min_{\alpha \in \mathcal{A}} |\boldsymbol{Y}_n - \alpha|^2, \tag{4.1}$$

where, $\mathcal{A}$ contains the corresponding baseband modulation alphabets. The coded data bits are then de-mapped form $\boldsymbol{Y}^{'}_{n}$ and are forwarded to the decoder to retrieve the information bits.

In the case of SD detection in considered system, the log-likelihood ratios (LLRs) of each received binary bit are acquired from the n^{th} element (or sub-channel) of $\boldsymbol{Y}$. This can be done through either a maximum *a posteriori* probability (MAP) algorithm or by an approximate LLR computation algorithm. The MAP based LLR algorithm computes the LLR of the q^{th} binary bit b^q_n, for $0 \leq q \leq k-1$, from the n^{th} received sub-channel $\boldsymbol{Y}_n$ as [136]:

$$\mathcal{L}(b^q_n) = \frac{1}{N_o}\{\min_{\alpha \in \mathcal{A}^{q=0}} |\boldsymbol{Y}_n - \alpha|^2 - \min_{\alpha \in \mathcal{A}^{q=1}} |\boldsymbol{Y}_n - \alpha|^2\}, \tag{4.2}$$

where, $\mathcal{A}^{q=1}$ and $\mathcal{A}^{q=0}$ are the subsets of the baseband modulation constellation alphabets, and represent alphabets with q^{th} bit labelled as '1' and '0', respectively.

In our investigation, however, an approximate LLR computation method detailed in [118] was used due to high computational complexity of the MAP based LLR algorithm. As an example, for 8-PAM modulation in DCO-VC and DCO-PAM, the LLR of b^q_n from

$\boldsymbol{Y}_n$ can be obtained as [118]:

$$\mathcal{L}(b_n^q) = \begin{cases} \boldsymbol{Y}_n, & q = 0 \\ |\boldsymbol{Y}_n| - 4, & q = 1 \\ \left.\begin{array}{l} 2 - |\boldsymbol{Y}_n|, \text{ for } |\boldsymbol{Y}_n| \leq 4 \\ |\boldsymbol{Y}_n| - 6, \text{ for } |\boldsymbol{Y}_n| > 4 \end{array}\right\}, & q = 2 \end{cases} \tag{4.3}$$

These approximate LLRs are then forwarded to the decoder to obtain the decoded binary information stream. The approximate LLR algorithm in equation (4.3) can also be applied separately to the in-phase and quadrature of a 64-QAM based $\boldsymbol{Y}_n$ in DCO-OFDM to obtain the total of 6 soft bits. This approximate LLR detection is also known as the threshold detection technique. In similar manner, the approximate LLRs for different M level modulations were obtained.

4.3 Performance Evaluation of RAC Schemes over AWGN

In this section, the performance of the RAC-SD and RAC-HD based DCO-PAM and DCO-OFDM schemes is examined over AWGN channel and compared against their uncoded counterparts. The throughputs of each system are evaluated through simulations and analytical approximations, and compared against their channel capacities estimated based on modified Shannon's capacity formulas. The performance of RAC based DCO-VC system over AWGN channel will be the same as the RAC based DCO-PAM system as detailed in chapter 3, therefore, no separate throughput results are shown for the DCO-VC system.

4.3.1 Throughput of DC-biased optical signalling schemes

Fig. 4.4 and Fig. 4.5 show the throughput of DCO-PAM and DCO-OFDM systems, respectively, in uncoded, RAC-HD and RAC-SD configurations. The throughput in each of the systems can be estimated as:

$$T_{\text{DCO-PAM}} = T_{\text{DCO-VC}} = W\left(\frac{N}{N+\mu}\right)\Gamma \log_2(M)\mathcal{P}_{SR}, \tag{4.4}$$

$$T_{\text{DCO-OFDM}} = W\left(\frac{N/2-1}{N+\mu}\right)\Gamma \log_2(M)\mathcal{P}_{SR}, \tag{4.5}$$

where Γ is the code rate and $\mathcal{P}_{SR}$ is the packet success rate given as $\mathcal{P}_{SR} = (1 - BER)^{\ell}$, where ℓ is the packet length in bits. 1500 bytes long packets were transmitted and W of 20 MHz was considered during all the simulations in this investigation. The presented

throughput curves are optimised by selecting the most effective combination of Γ and M.

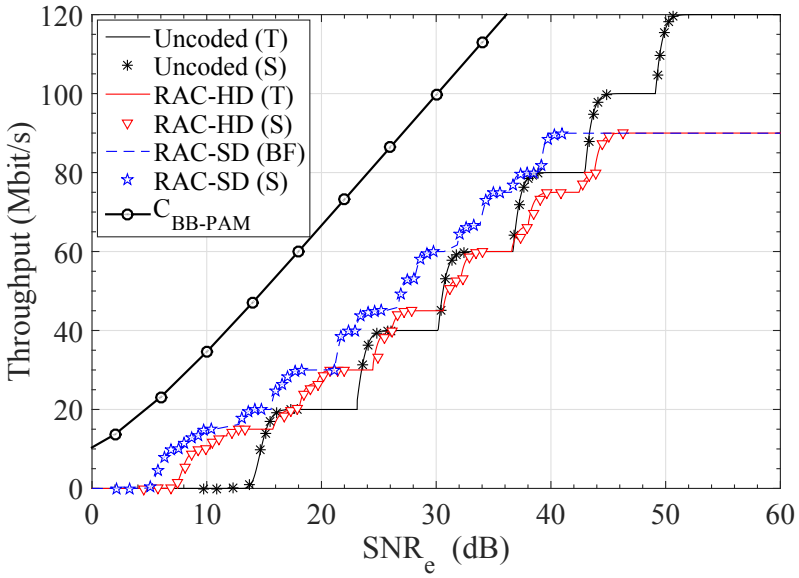

Figure 4.4: Throughput of uncoded, RAC-HD and RAC-SD DCO-PAM over AWGN channel. (T) and (S) in the legends signifies the theoretical and simulation results, respectively. The dashed line shows the best-fit (BF) throughput curve obtained by curve fitting from the simulations for RAC-SD.

The results in Fig. 4.4 and Fig. 4.5 in general show that the RAC-SD scheme is the most energy efficient over the majority of the SNR_e scale. The RAC-HD scheme can provide some gain at low SNR_e. However, as SNR_e increases above 30 and 36 dB in DCO-PAM and DCO-OFDM systems, respectively, the RAC-HD schemes yield no gain and perform worse than the uncoded schemes. On the other hand for both the DCO-PAM and DCO-OFDM, the RAC-SD schemes, provide an SNR_e gain of up to 9 dB in comparison to uncoded schemes and up to 5 dB gain when compared to RAC-HD schemes. It can be noticed that as the SNR_e increases, the gains with RAC-SD schemes are reduced. This is due to the well-known decrease in coding gain with increasing modulation order in BC coded systems. Also the higher B_{dc} requirements while working with higher M modulation modes leads to reduced coding gains. A coded system with a certain Γ, must work with a high M scheme to achieve a high throughput and will require higher B_{dc} to achieve a BER of 10^{-6}.

Overall, comparing the results in Fig. 4.4 and Fig. 4.5, it can be seen that DCO-PAM schemes are highly efficient for a certain throughput when compared to DCO-OFDM systems. This is mainly attributable to the B_{dc} value required by different modulations in each of the schemes. In Appendix B, the throughputs of both systems is given in bipolar

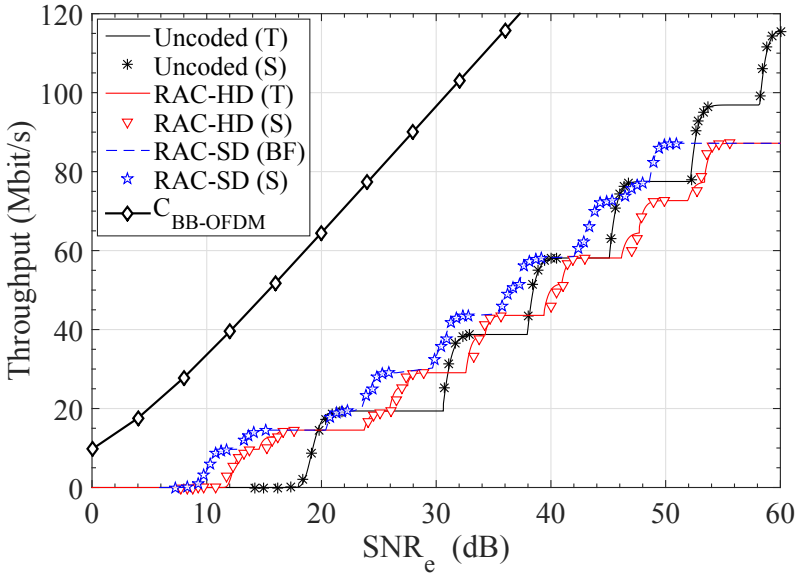

Figure 4.5: Throughput of uncoded, RAC-HD and RAC-SD DCO-OFDM over AWGN channel. (T) and (S) in the legends signifies the theoretical and simulation results, respectively. The dashed line shows the best-fit (BF) throughput curve obtained by curve fitting from the simulations for RAC-SD.

baseband (BB) configurations, i.e. unclipped signals with $B_{dc} = 0$. These results in Fig. 6 and Fig. 7 (Appendix B) for BB-PAM and BB-OFDM, respectively, show that the two systems perform equivalently, in this scenario. Hence the differentiating factor is the B_{dc} requirements for the SCM and MCM system.

4.3.2 Channel capacity of considered systems

Fig. 4.4 and Fig. 4.5, also show the Shannon capacity curves for the BB configuration of the considered systems. The BB configuration for capacity estimation was used because in VLC different B_{dc} values for different modulation orders were used for the throughput evaluation. Additionally, this shows how the system throughput is reduced by the increased B_{dc} requirements compared to the channel capacity. The channel sum capacity of the BB-PAM, BB-VC, and BB-OFDM systems can be estimated based on a modified Shannon formula as:

$$C_{\text{BB-PAM}} = \frac{WN}{2(N+\mu)} \log_2(1 + \text{SNR}_\text{e}), \tag{4.6}$$

$$C_{\text{BB-VC}} = \frac{W}{2(N+\mu)} \sum_{i=0}^{N-1} \log_2(1 + \text{SNR}_\text{e}(i)), \tag{4.7}$$

$$C_{\text{BB-OFDM}} = \frac{W}{(N+\mu)} \sum_{i=1}^{\frac{N}{2}-1} \log_2(1 + \text{SNR}_\text{e}(i)), \tag{4.8}$$

respectively. In equation (4.6) SNR_e is the average electrical SNR for DCO-PAM system. In equations (4.7) and (4.8), $\text{SNR}_\text{e}(i)$ is the electrical SNR in the i^{th} sub-channel or sub-carrier and can be given as:

$$\text{SNR}_\text{e}(i) = \frac{\mathcal{T}^2\Re^2|\boldsymbol{H}_f(i)|^2\boldsymbol{P}^2(i)}{\boldsymbol{\sigma}_n^2(i)}, \tag{4.9}$$

where, $\boldsymbol{P}^2(i)$ and $\boldsymbol{\sigma}_n^2(i)$ represent the electrical signal and noise powers in the i^{th} sub-channel or sub-carrier, respectively. $\boldsymbol{H}_f$ is the length N frequency response of the VLC channel. It can be noticed from Fig. 4.4 and Fig. 4.5, that due to low B_{dc} requirements, the RAC-SD based DCO-PAM is most efficient in operating closer to its theoretical capacity.

Throughout this thesis, the capacity of the bipolar baseband (BB) electrical channel is used as a reference. This is because in every experiment, as mentioned earlier, no limit on the peak optical power is assumed. As per [137], the optical channel capacity is limited by the maximum average and peak optical powers allowed in a transmission. This leads to different capacity bounds for optical channels, than the electrical channels found through Shannon's formulae. Fig. 11 in Appendix F shows the comparison between the capacities of the electrical and optical channels. This, as expected, shows that the capacity of the optical channels is lower than that of an electrical channel. Later in this Chapter, the effects of limited peak optical powers are also analysed which show that the signal clipping causes a rise in the error floor (or the irreducible BER floor), which will decrease the overall throughput of the system.

4.3.3 Analytical throughput estimation

The analytical throughput results for the uncoded schemes and RAC-HD schemes are also presented in Fig. 4.4 and Fig. 4.5 for the DCO-PAM and DCO-OFDM systems, respectively. Such analytical estimates are not readily available for the SD detection. In order to obtain these analytical results, the BERs of DCO-PAM and DCO-OFDM systems where first estimated theoretically and these BER were then converted to throughput using equations (4.4) and (4.5). In what follows, the analytical models used for the BER performance estimation are detailed:

Uncoded throughput

The bit error probability of the PAM based systems over the AWGN channel can be estimated through the union bound as shown in equation (3.15) and the bit error probability of the QAM based OFDM systems can be estimated through equation (3.16).

RAC-HD throughput

The bit error probability for the RAC-HD scheme can be estimated analytically as [138][139]:

$$\mathcal{P}_{b(\text{RAC-HD})} = \frac{1}{\log_2(M)} \sum_{w=d_{free}}^{d_{free}+N_{st}} \beta_w \mathcal{P}_w, \tag{4.10}$$

where w is the Hamming weight between the transmitted and received codeword, d_{free} is the free distance of the convolutional code, N_{st} is the number of significant codewords, β_w is the total number of bit errors corresponding to all the weight w codewords which are tabulated in [140][141], and $\mathcal{P}_w$ is the error probability of selecting an incorrect trellis path (or codeword) of weight w given as [142]:

$$\mathcal{P}_w = \begin{cases} \sum\limits_{j=\lceil w/2 \rceil}^{w} \binom{w}{j} \mathcal{P}_b^j (1-\mathcal{P}_b)^{w-j}, & \text{for odd } w, \\ 0.5\binom{w}{w/2} \mathcal{P}_b^{w/2} (1-\mathcal{P}_b)^{w/2} & \\ + \sum\limits_{j=w/2+1}^{w} \binom{w}{j} \mathcal{P}_b^j (1-\mathcal{P}_b)^{w-j}, & \text{for even } w \end{cases} \tag{4.11}$$

In equation (4.11), $\mathcal{P}_b$ is the bit error probability of the uncoded systems in an AWGN channel, which is given as $\mathcal{P}_{b(\text{DCO-PAM})}$ and $\mathcal{P}_{b(\text{DCO-OFDM})}$ in equations (3.15) and (3.16), respectively.

4.4 Performance Evaluation of RAC Schemes over VLC Channels

In this section, the performance of RAC DCO-OFDM, DCO-VC and FDE based DCO-PAM schemes is examined over the indoor VLC hybrid and diffuse links. The throughput performances of the uncoded and RAC-SD are compared. As the AWGN results show that SD detection is more efficient than HD, only RAC-SD based schemes were used for RAC systems in further investigations.

4.4.1 Hybrid Links

The investigation was carried out based on three different Rx locations in a considered room (as shown in Fig. 2.3), leading to three different hybrid channels. These locations are referred to as A, B and C in this chapter. The exact Rx co-ordinates for each location can be found in Table 4.2, where the *rms* delay spreads for each channel are also given which were calculated based on equation (2.18). Table 4.2 also shows the K-factor values for each hybrid VLC link, which can be computed from equation (2.14).

Table 4.1: VLC System Parameters.

Parameter	Value
A	10 mm^2
A_{Room}	110 m^2
$g_c(\psi)$	1
FOV, Ψ	70°
LED semiangle at half power, $\phi_{\frac{1}{2}}$	60°
Optical Filter Transmissivity, T [2]	0.7
PD Responsivity, R [6]	0.4 A/W

The impulse response $h(\tau)$ (in equation 2.13) for the hybrid link was obtained based on the properties of the room in Fig. 2.3, the system parameters shown in Table 4.1, and the reflectivity of the room ceiling, plaster wall, plastic wall and room floor for blue colour channel ($\lambda_c \sim 450$ nm). The ρ value observed in [53] for the blue band is approximately 0.454, which was used to evaluate $h(\tau)$. Table 6.4 show that minimum dispersion will be experienced at the centre (Location A) of the room, where K is highest as η is much larger than ζ. As the Rx is moved towards location C, K decreases and τ_{rms} increase as ζ becomes comparable to η. This behaviour of hybrid links is also seen in [57], where it is shown that the hybrid link's optical powers and cut-off bandwidths decrease as a function of η and tend to be similar to those in diffuse links as the Rx moves from the room centre (where Tx is situated) towards the walls.

Simulations Set-up

During the simulations, $N = 64$ sub-channels were used, to keep the sub-channel (or sub-block) bandwidth (W_N=$\frac{W}{N}$) much less than the channel coherence bandwidth (W_C=$\frac{0.2}{\tau_{rms}}$), i.e. $W_N << W_C$. A W of 20 MHz, and the τ_{rms} experienced over the diffuse link (sec. 4.4.2), estimates that an N of 8 could be used to decrease the system complexity, given W_N=$0.1W_C$ [71]. On the other hand, an N of 64 provides good complexity compromise

Table 4.2: The channel τ_{rms} and K values at different Rx locations while the Tx is located at $(2.5, 2.5, 2.5)$, at a symbol rate of $R_s = 20$ MS/s.

Rx Location	**Coordinates (m)**	τ_{rms} (ns)	K(dB)
A	$(2.5, 2.5, 0.85)$	0.340	23.80
B	$(1.5, 1.5, 0.85)$	0.867	14.22
C	$(0.5, 0.5, 0.85)$	3.408	0.00

and has been used in many standard communications systems such as Wi-Fi. Additionally, to achieve high throughputs, VLC systems are expected to switch LEDs beyond their cut-off bandwidths, as well as micro-LEDs suitable for VLC with cut-off bandwidths > 100 MHz have been produced [39]. This means $N > 8$ will be required, to achieve very high data throughput with $W >> 20$ MHz. The value of μ was computed as $\mu = \frac{\tau_{rms}}{T_s} - 1$ [71], where T_s is the sample duration, which gave μ of 2 for the location C hybrid link and diffuse link. Therefore, μ=2, was used for all the investigations over the indoor VLC channels.

Results and Analysis

Fig. 4.6 shows a throughput comparison of the DCO-OFDM, DCO-VC and DCO-PAM systems with uncoded and RAC-SD based transmissions over the three Rx locations considered. The results show that the RAC-SD schemes provide higher throughput than the uncoded schemes for a majority of the SNR_e values. The RAC-SD schemes provide up to 9 dB coding gain in each of the considered systems when compared to their uncoded counterparts. This shows that a BC coding based RAC scheme will significantly enhance the overall capacity of the VLC systems. It must be noted that the considered BC code has been widely used in current communication systems, such as Wi-Fi and Wi-MAX, hence the hardware implementation will not impose any significant challenge.

The results additionally show that the DCO-PAM is the most efficient signalling scheme achieving up to ∼10 dB SNR_e gain in uncoded transmissions when compared to the DCO-VC and DCO-OFDM systems. Similarly, for RAC-SD transmissions the DCO-PAM provides up to 9 and 10 dB SNR_e gains when compared to DCO-VC and DCO-OFDM, respectively. These large gains of DCO-PAM systems are due to the low B_{dc} requirements. The efficiency of uncoded DCO-PAM systems has also been reported previously in [107][109].

The results in Fig. 4.6 also show that the uncoded DCO-OFDM and DCO-VC systems require the same levels of SNR_e for certain throughput. This shows that DCO-OFDM,

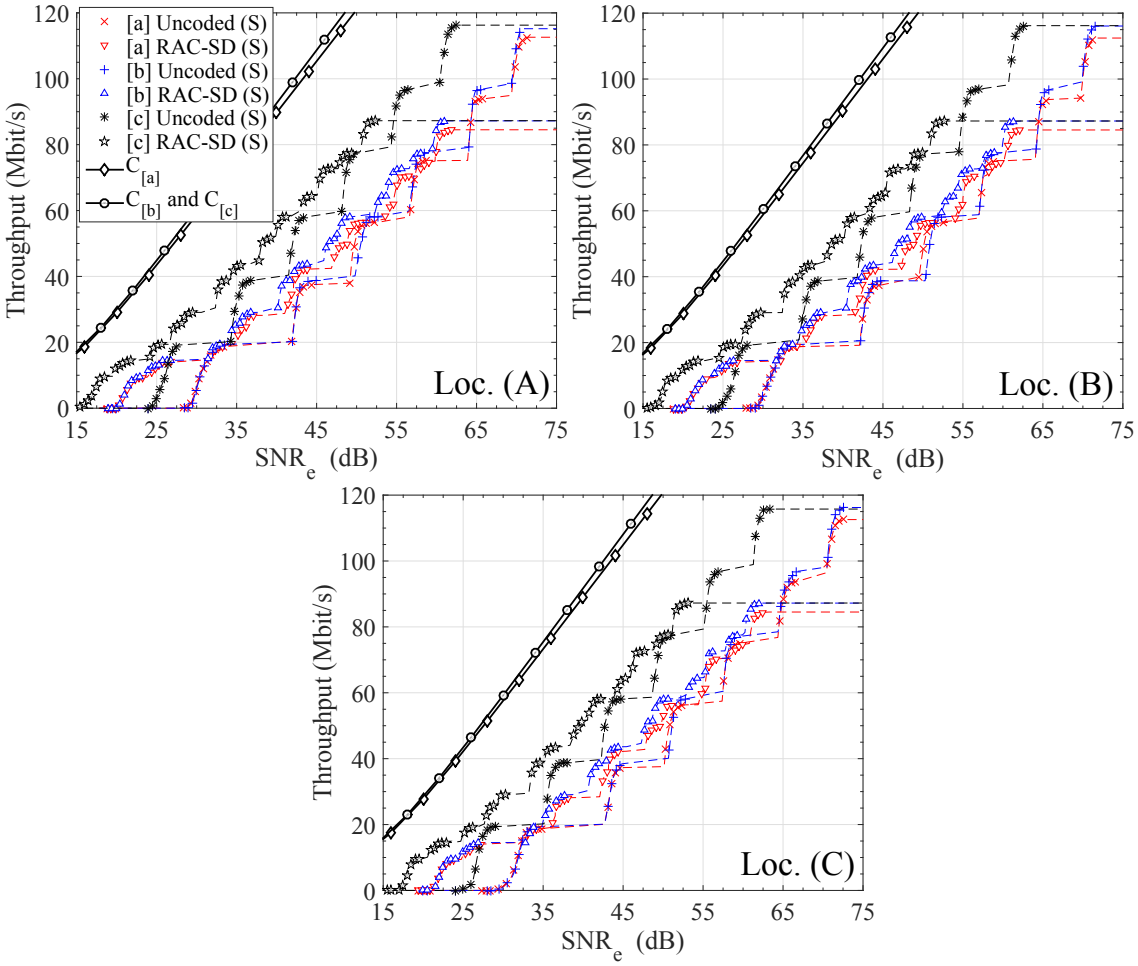

Figure 4.6: Throughput of uncoded and RAC-SD based [a] DCO-OFDM, [b] DCO-VC and [c] DCO-PAM schemes over different hybrid links in considered indoor environment. The dashed curves are obtained by curve fitting from the simulation (S) results shown by markers.

despite being a sub-optimal multi-carrier system, operates very similar to the optimal DCO-VC system. However, in RAC-SD based systems, DCO-VC requires up to ∼2 dB less SNR_e compared to DCO-OFDM for high throughputs.

It can be noticed that the performance of each system remains approximately the same across the considered Rx locations. There is approximately 0.5 dB SNR_e requirement difference for each system between locations A and C. This shows that these schemes are very effective in compensating for the temporal dispersions experienced in the considered indoor environment for a 20 MHz system bandwidth.

4.4.2 Diffuse Links: Part-I

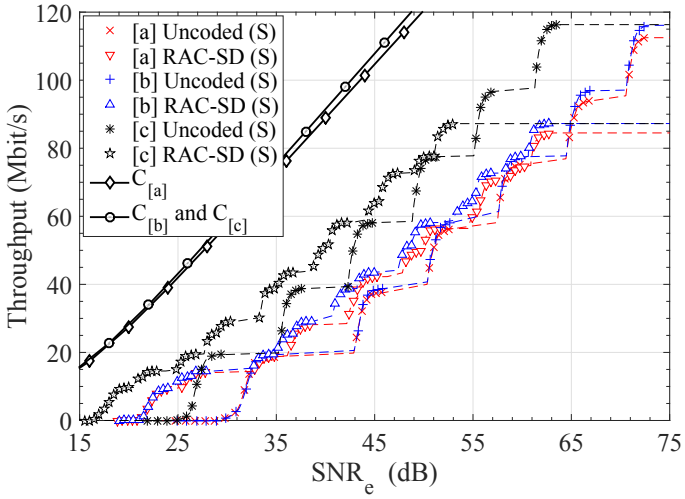

Figure 4.7: Throughput of uncoded and RAC-SD based [a] DCO-OFDM, [b] DCO-VC and [c] DCO-PAM schemes over diffuse channel. The dashed curves are obtained by curve fitting from the simulation (S) results shown by markers.

In this section the performance of the considered uncoded and RAC-SD systems is examined over a diffuse (non LOS) indoor link. In practical scenarios, the LOS in hybrid indoor links can be either blocked or may not be present due to the limited Rx FOV. In this case the VLC systems must rely upon the diffuse signals. The impulse response of diffuse indoor links has been verified through measurements in [57] and can be given as equation (2.7), which is the same as equation (2.13) when η=0. It is shown in [57], that the optical power and the cut-off bandwidth of the channel in diffuse links are uniform across a room of the type considered and depends upon average reflectivity ρ and the mean time between two reflections $\langle t \rangle$. Therefore, $h_{Dif}(\tau)$ is also uniform across the room. The τ_{rms} in this case can also be approximated as τ_{rms}=$\tau_c/2$= $-\langle t \rangle/2\ln(\rho)$ [143], where τ_c is the exponential decay time constant. For the considered room (Fig. 2.3) and the ρ value

used in the previous section, the τ_{rms} of a diffuse channel approximates to 5.7 ns, which is comparable to τ_{rms} of a hybrid link at location C.

Fig. 4.7 shows the throughput performance of the considered three systems in uncoded and RAC-SD modes. During the simulations, N was kept equal to 64 in this case as well, satisfying $W_N << W_C$ and μ of 2 was sufficient to avoid ISI. The results for the diffuse channel are similar to those at location C in the hybrid links (Fig. 4.6). This shows that all the schemes are very effective at equalising the channel dispersion over the diffuse link too. However, the diffuse channel is a lot weaker in general when compared to the LOS channels. Therefore, achieving the SNR_e values shown in Fig. 4.7 will be very difficult in a diffuse channel, making it practically challenging to achieve high data throughputs.

Overall, the RAC-SD schemes achieve higher throughputs for certain SNR_e and for the same throughput provide up to 9 dB SNR_e gain, when compared to the uncoded systems. This shows that RAC-SD schemes are equally effective over the diffuse channel as in the hybrid channels. It can be seen that the highest throughput over the diffuse link can be achieved with RAC-SD DCO-PAM system as in hybrid links. RAC-SD DCO-PAM over a diffuse link achieves up to 10 and 11 dB SNR_e gain when compared to RAC-SD DCO-VC and DCO-OFDM systems, respectively.

4.4.3 Diffuse Links: Part-II

The previous section shows that the maximum τ_{rms} experienced over the considered room (Fig. 2.3), with key system parameters shown in Table 4.1, will be 5.7ns for a diffuse link. The τ_{rms}, as previously mentioned, is directly proportional to $\langle t \rangle$ given ρ is unity. Therefore, for a room of larger size the τ_c and hence τ_{rms} will be larger. In order to study the performance of the considered three systems with higher temporal dispersion, four diffuse links each with τ_{rms} value of (I) 10ns, (II) 20ns, (III) 35ns and (IV) 50ns were used. In this case the diffuse CIR $h_{dif}(\tau)$ was obtained by directly setting the τ_c and τ_{rms} without defining the characteristics of the room.

The throughput performance of each system was evaluated through simulations over each diffuse link which is shown in Fig. 4.8. W was kept at 20 MHz and an N of 64 was used during the simulations. A μ of 2, 4, 7 and 10 was sufficient to avoid ISI over the diffuse links with τ_{rms} of 10ns, 20ns, 35ns and 50ns, respectively. The results show that the SNR requirements increase as the τ_{rms} increases and the throughput decreases due to increase in the CP length.

Overall, the results show the same trends as over the diffuse link with τ_{rms} of 5.7ns (see Fig. 4.7) and as the system performance results over hybrid links (see Fig. 4.6). The RAC-SD systems achieve up to 9 dB SNR gain when compared to the uncoded counterparts

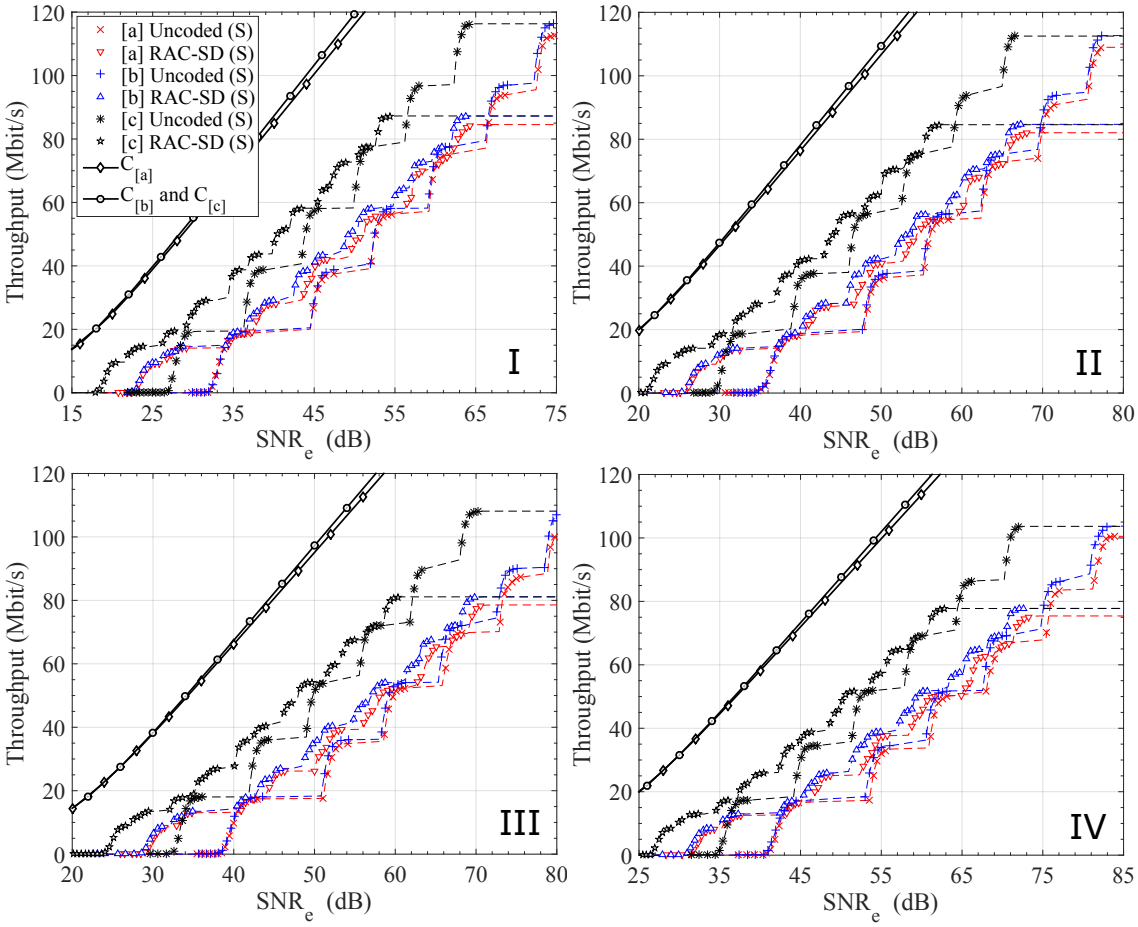

Figure 4.8: Throughput of uncoded and RAC-SD based [a] DCO-OFDM, [b] DCO-VC and [c] DCO-PAM schemes over four diffuse links with different τ_{rms}: (I) 10ns, (II) 20ns, (III) 35ns and (IV) 50ns. The dashed curves are obtained by curve fitting from the simulation (S) results shown by markers.

and the RAC-SD based DCO-PAM system is the most SNR efficient scheme of all the considered systems, which provides approximately 9 dB SNR gain over the RAC-SD based DCO-VC system and 11 dB SNR gian when compared to the RAC-SD based DCO-OFDM system. The results also show that, the DCO-VC system achieves approximately 1 and 3 dB SNR gain when compared to the DCO-OFDM system in uncoded and RAC-SD transmissions, respectively, when the τ_{rms} is increased to 50ns. This shows that the DCO-VC system could be more efficient than the DCO-OFDM system in highly dispersive channel environments.

4.4.4 Clipping Noise

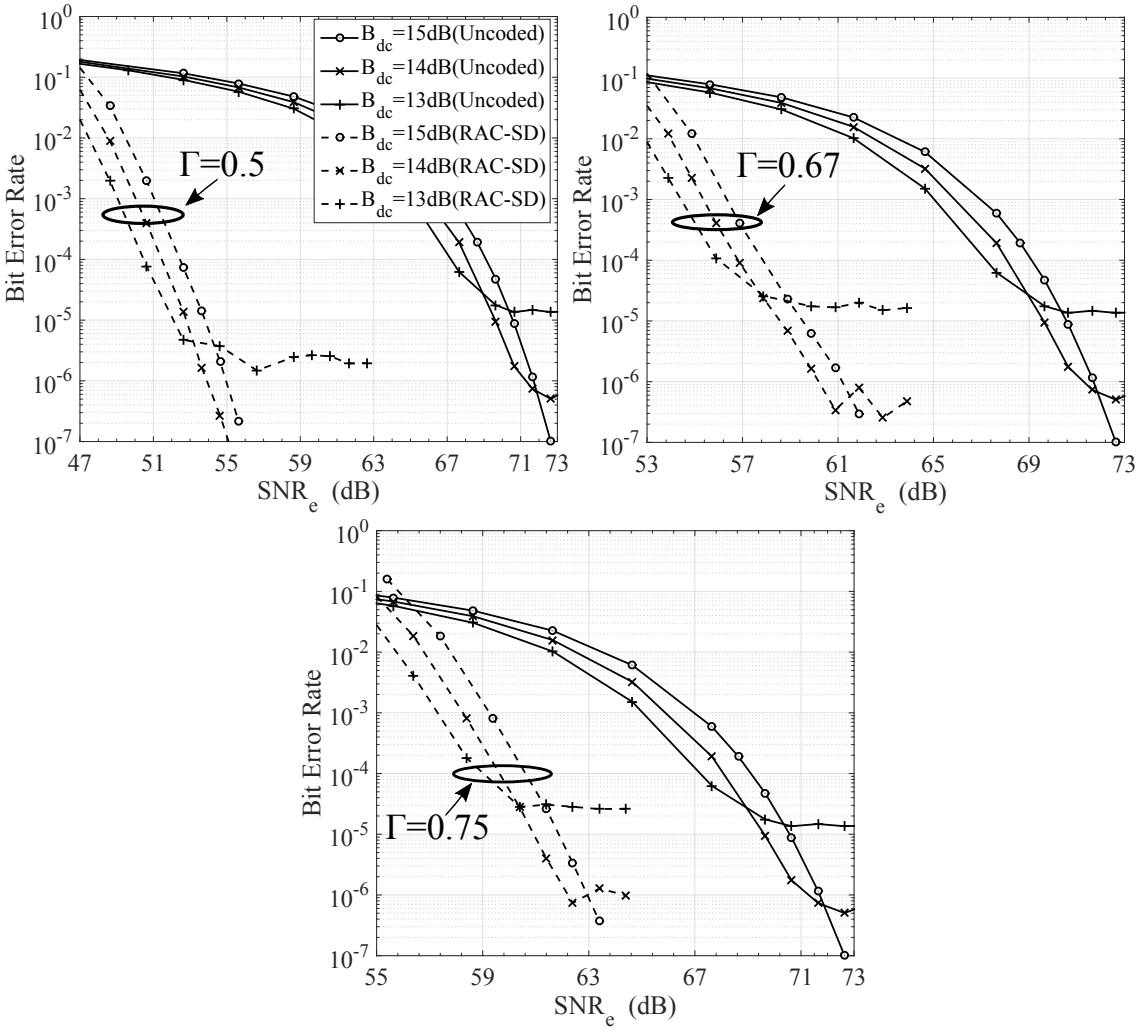

Figure 4.9: BER of 4096-QAM DCO-OFDM with different B_{dc} levels with uncoded and RAC-SD based transmissions. RAC-SD used considered three different code-rates (Γ).

As mentioned earlier, the B_{dc} for each modulation of each considered system was set such that a target BER of 10^{-6} can be achieved. The B_{dc} values used (Fig. 3.8) are very high which result in negligible clipping of the transmit signal. In order to study the effect of clipping noise, simulations were carried out using uncoded and RAC based 4096-QAM DCO-OFDM system at location C of a hybrid link. The B_{dc} was reduced from 15 dB to 14 dB and 13 dB, and the BER performance was examined which is shown in Fig. 4.9.

The results show that for the uncoded system, the irreducible error floor is raised to approximately 10^{-6} and 10^{-5} with a B_{dc} of 14 and 13 dB, respectively. This is due to increased n_{clip}. Similarly, for the RAC-SD system, the irreducible error floor is raised when B_{dc} is reduced below 15 dB, except for 1/2 rate RAC-SD system, where the noise floor remains well below 10^{-6} for a B_{dc} of 14 dB. This is because 1/2 rate BC code is stronger than the punctured codes. However, further bias reduction to 13 dB raises the error floor above the target BER even with a 1/2 rate code. The raised error floor will result in reduced system throughput as per equations (4.4) and (4.5).

These results show that the BC code used for the RAC-SD system is not capable of minimising the effect of n_{clipp} on the BER effectively, despite the gains it can provide when the optimised B_{dc} is used. Advanced FEC schemes such as iterative codes can efficiently reduce the noise floor [17][144], at the cost of increased system complexity and latencies. Another way to avoid/reduce the clipping noise would be through power back-off which will result in significant power back-off for the DCO-OFDM and DCO-VC systems, eventually leading to reduced transmit signal resolution. Therefore, it is important to use signal sets with low peak powers, such that B_{dc} requirements are reduced and signal distortion is minimised.

4.5 Summary

Building on to findings of chapter 3, which concluded DC-biased MCM and SCM systems to be more spectral and energy efficient than the non DC-biased schemes, this chapter explored the use of rate adaptive channel coding for the DC-biased MCM and SCM systems to further enhance their throughput performance over bandwidth limited VLC channels.

This chapter proposes the use of punctured BC coding and Viterbi decoding based signalling for DCO-OFDM, DCO-VC and DCO-PAM systems. The throughput performance of the coded and uncoded considered DC-biased systems has been evaluated and compared over representative indoor hybrid and diffuse channels. The results show that large DC-bias requirements and reduced spectral efficiency of the VLC MCM systems to attain a real and unipolar transmit signal leads to a low overall capacity when compared to their bipolar baseband MCM equivalents. The rate-adaptive coding based DC-biased

MCM systems, when compared to their uncoded counterparts, achieve up to 9 dB SNR_e gain over representative VLC channels.

The results show that, in uncoded mode, the newly designed MCM scheme DCO-VC performs equivalent to the DCO-OFDM system over less dispersive hybrid channels. However, as the dispersion increases the uncoded DCO-VC system outperforms the uncoded DCO-OFDM system by achieving 1 dB SNR gain. Additionally, the gain of DCO-VC system increase further to 3 dB in comparison to DCO-OFDM when the proposed FEC scheme is used with both systems. Overall, due to low DC-bias requirements, the rate-adaptive coding based DCO-PAM system achieves the highest throughputs for a certain SNR_e, when compared to DCO-VC and DCO-OFDM systems, and provides up to 11 and 12 dB SNR_e gains for the same throughput, respectively.

The chapter also studied the effect of negative signal clipping on the performance of DCO-OFDM system when DC-bias is reduced below the optimised value. This study showed that both uncoded and rate-adaptive coded schemes will fail to provide BERs lower than 10^{-6} which will lead to degraded data throughput. This shows that the MCM systems, DCO-VC and DCO-OFDM, which require large DC-bias due to their peaky signal envelope, will require large power back-off to avoid signal clipping due to the limited dynamic range of the transmit front-end. More sophisticated FEC techniques can also be employed, however, at the cost of increased complexity and latencies.

At this point in thesis, the investigations of the conventional single and multiple channel optical signalling schemes comes to end and in the upcoming chapters the focus is on the IEEE standardised multi-colour signalling systems based on colour shift keying modulation schemes which are specially designed to control the light colour at the transmitter without any intensity flicker.

Chapter 5

Colour Shift Keying Modulation Schemes

5.1 Introduction

This chapter studies colour shift keying (CSK) modulation schemes, which are specifically designed to realise VLC through multi-colour LEDs utilising multi-colour visible spectrum while meeting the indoor illumination requirements. Originally, CSK was introduced in the IEEE 802.15.7 standard [8] in PHY III, which uses three-colour or trichromatic-LEDs (TLED) and provides data rates between 11.67 kbit/s to 96 Mbit/s, incorporating intensity-flicker mitigation and dimming mode [8][32].

In this chapter, the working of CSK systems is detailed and their performance is investigated over AWGN channel. Initially, the standardised TLED CSK system and its various colour-band combinations (CBCs) are described. The different modulation orders of TLED CSK and their constellation designs are presented. The Gray mapping issues of the TLED CSK are also discussed. Then an advanced CSK scheme based on four-colour or quad-chromatic LEDs (QLED) is introduced and its different modulation orders with constellations are presented. The QLED CSK is designed to overcome the Gray mapping issues of CSK and to enhance the signalling space of the modulation scheme.

The idea of using more than three LEDs in CSK has been introduced by Butala *et al.* [93] to optimise the colour rendering effect, where the use of multiple TLED sets, each capable of generating their own gamut, has been proposed. However, Butala *et al.* [93] suggest that their system will require the receiver to be able to distinguish between the active TLED sets at the transmitter, which can increase the system complexity. On the other hand, motivation behind the QLED CSK system has been the communications perspective deficiencies of the TLED CSK system. The QLED system is similar to the

one explained in [93] as it uses multiple sets of TLED systems. However, the constellation design in QLED for each modulation ensures that multiple TLED sets will only generate the part of their gamut which is not overlapped by any other set. The QLED system realises a four-dimensional (4-D) constellation by combining four sets of three-dimensional (3-D) constellations. This allows the receiver to treat the instantaneous intensities detected as a point in the 4-D signal space and hence the receiver does not need to differentiate between TLED sets active at the transmitter.

The performance evaluation of TLED and QLED CSK systems over an AWGN channel through simulations and analytical formulations shows that the QLED system outperforms the TLED system by achieving up to 5 dB electrical SNR gain.

In CSK systems, detection at the receiver side can take place on the received intensities (in the signal space) as well as on the chromaticities which are obtained from the intensities. This chapter shows that the chromatic detection is suboptimal and increases the SNR requirements by approximately 7 dB for the TLED CSK. Hence, it should be avoided. The results also show that with detection on received chromaticities, different CBCs of TLED CSK provide a spread of BER performance which is related to the minimum Euclidean distance of each constellation in each CBC. This will require a commercial CSK system to use specific CBCs which provide the optimum BER performance, which is not desired.

In the second half of the chapter, the performance of TLED and QLED systems is studied incorporating the colour cross-talk and insertion losses which arise due to the optical properties of the front-end components such as LEDs, optical filters and PDs. The simulation based results show that even minor cross-talk can deteriorate the performance of CSK systems if not mitigated through a standard process called colour calibration. It is also shown how the QLED system based 4-CSK modulation can be used to estimate the cross-talk in CSK systems.

Towards the end of this chapter, the performance of CSK is compared to M-PAM based wavelength division multiplexing (WDM) systems and the advantages and disadvantages of WDM based VLC system are discussed. It is shown that a PAM based WDM system will provide higher data rates than the CSK systems with increasing modulation orders and number of colour bands in a multicolour VLC system. However, CSK system has more advantages from lighting perspective.

The hardware implementation issues in terms of transmit and receive resolution requirements while working with high level modulation modes are also discussed. The hardware overheads in a QLED system due to the use of four colours are also detailed along with possible solutions to keep the hardware requirements to a minimum in an LED-cluster based CSK. The intensity and colour flicker issues of CSK systems are also discussed.

5.2 TLED CSK System

This section provides a detailed background on the working of the IEEE standardised CSK systems. The constellation designs and different colour band combinations specified in standard are also presented.

5.2.1 CSK Basis

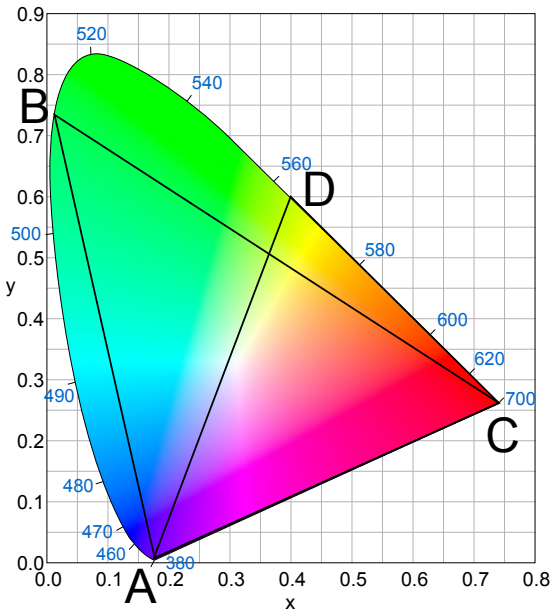

Figure 5.1: CIE 1931 colour space chromaticity diagram.

CSK, a VLC modulation scheme standardised in PHY III of IEEE 802.15.7 [8], is based on the x-y colour coordinates defined by the international commission on illumination in CIE 1931 colour space [110], shown in Fig. 5.1. The CIE 1931 colour space chromaticity diagram represents all the colours visible to the human eye with their chromaticity values x and y. The colourful region in Fig. 5.1 represents the gamut of human vision. The curved edge with wavelengths listed in nanometres is referred to as the monochromatic locus, and the straight edge, which is the line joining points A and C, is known as the purple line.

Fig. 5.1 exhibits some very interesting properties. For any two colours of different wavelengths, all the colours regenerated, by mixing the different intensities of these two colours lie on a straight line connecting the two original colours. Similarly, three different colours can regenerate all those colours which lie within the corresponding triangle on the

chromaticity plane e.g. triangle ABC and ADC in Fig. 5.1, formed by different central colour sets.

In CSK, the intensities of multi-colour LEDs are modulated for data transmission. The mixture of light produced from the LED sources allows CSK to regenerate various colours without intensity flicker, each of which can be represented by a pair of x-y coordinates and these chromaticity pairs represent different data symbols. Three colour CSK systems, which use trichromatic LEDs, are the basis of the CSK PHY in the standard [8]. In this thesis the three colour CSK systems are referred to as Trichromatic-LED (TLED) systems.

For TLED CSK, to generate the colour of each chromatic pair, the intensities required for each LED is calculated based on the linear transformation given by equation (5.1) [8].

$$\begin{bmatrix} x \\ y \\ 1 \end{bmatrix} = \begin{bmatrix} x_i & x_j & x_k \\ y_i & y_j & y_k \\ 1 & 1 & 1 \end{bmatrix} \begin{bmatrix} I_i \\ I_j \\ I_k \end{bmatrix} \tag{5.1}$$

In equation (5.1), the coordinates (x_i, y_i), (x_j, y_j) and (x_k, y_k) refer to the central wavelength chromaticity values (CWCV) of the light sources within a multi-colour LED, e.g. given by the co-ordinates of ABC or ADC triangles in Fig. 5.1. These triangles define the chromatic constellation of the TLED CSK systems. The subscripts $(.)_i$, $(.)_j$ and $(.)_k$ denote three different colour-bands (CBs) of a TLED CSK system. The (x_i, y_i), (x_j, y_j) and (x_k, y_k) also represent one CSK symbol each, with the remaining symbols each denoted by x-y chromatic pair. The CB intensities within a multi-colour LED are represented by I_i, I_j and I_k.

5.2.2 Colour band combinations of TLED CSK

A visible light wavelength band plan for CSK is given in [8], where seven different wavelength bands have been defined. These wavelength band plans are detailed in Table 5.1, with their centre band and CWCVs. These seven bands or CBs can be arranged in to 35 different trichromatic combinations. However, a valid combination must form a triangular constellation which covers a significant amount of colour space on the chromaticity co-ordinate diagram. Hence the standard provides nine valid combinations, each comprising three CBs [8]. These nine sets are known as colour-band combinations (CBCs) and are detailed in [145].

The constellation triangles of nine CBCs are shown in Fig. 5.2. Each cover a different region of the chromatic space, therefore, their constellation areas differ from each other. As CBC-1, CBC-2, CBC-7, CBC-8 and CBC-9 exhibit a large difference between their constellation shapes and use at least one different communication CB from each other,

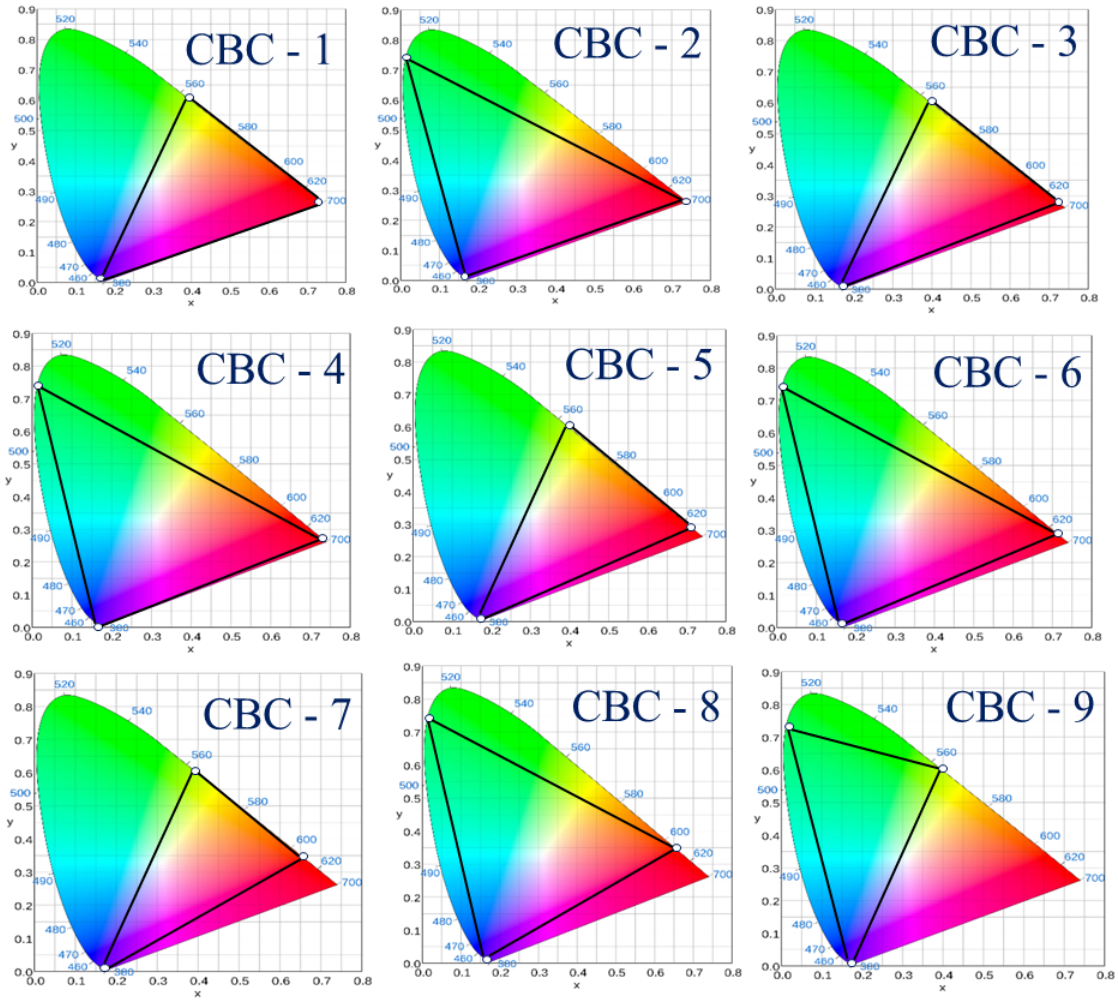

Figure 5.2: Constellation triangles of nine CBCs of TLED CSK defined in the IEEE 802.15.7.

Table 5.1: Wavelength band plan of standardise TLED CSK [8]

Band (nm)	Centre (nm)	CWCV
380-478	429	(0.169, 0.007)
478-540	509	(0.011, 0.733)
540-588	564	(0.402, 0.597)
588-633	611	(0.669, 0.331)
633-679	656	(0.729, 0.271)
679-726	703	(0.734, 0.265)
726-780	753	(0.734, 0.265)

these CBs were used for the performance evaluation of standardised TLED CSK systems in this research.

5.2.3 TLED modulation orders and constellations

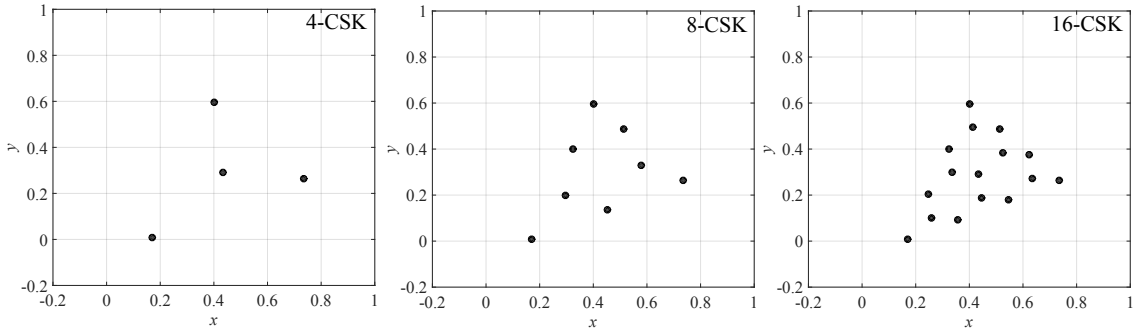

Figure 5.3: Transmit constellations of CBC-1 based TLED CSK modulations over chromatic space [8].

The IEEE standard specifies three orders of modulation for each of the nine CBCs of TLED CSK, which are 4-CSK, 8-CSK and 16-CSK. In TLED CSK, the symbol constellation on chromatic space is of triangular shape, as can be seen from different CBCs shown in Fig. 5.2. As an example, the constellations of the three standardised modulations of CBC-1 are shown over chromatic space in Fig. 5.3, where each chromatic CSK symbol is represented by a black dot.

The study of conventional CSK systems and their performance comparison to more advanced CSK systems was based on the standardised modulation orders shown in Fig. 5.3. However, the constellation size can be further increased using the symbol point allocation

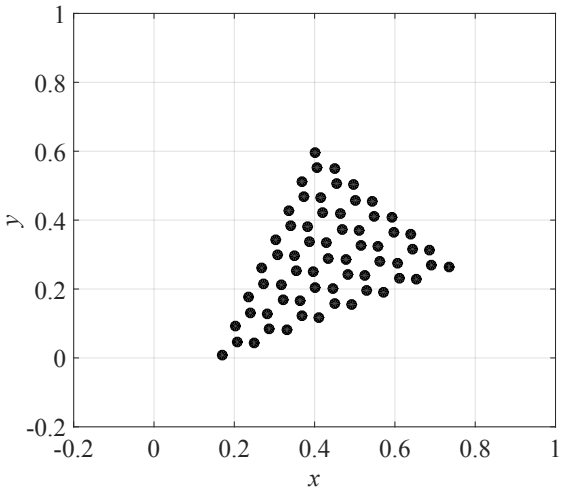

Figure 5.4: Transmit constellation of CBC-1 based TLED 64-CSK modulation over chromatic space [8].

design rules of TLED systems [8]. To study the performance of higher order TLED systems, a new 64-CSK constellation was designed which is shown in Fig. 5.4 based on the design of 16-CSK constellation and the details of its chromatic points can be found in Appendix D (Table 3).

$k = \log_2(M)$ bits are mapped to each CSK symbol, where M is the modulation order (or level). The chromaticity values of each symbol and the data bits mapped to them are detailed in Table 5.2 for CBC-1 based TLED CSK. In principle, the colour perceived by the human eye in CSK is represented by the average of the chromaticity values of symbols in a CSK constellation [92]. Therefore, different target colours can be generated by varying the symbol chromaticity values. Researchers have proposed different constellation design algorithms for CSK to optimise the colour rendering effect [93], to provide more control over the target colour and to increase modulation order above 16 levels [146][147]. A different approach to CSK was realised by the author to improve the system BER performance by utilising a fourth colour. This scheme is known as QLED CSK and it is detailed in section 5.3.

Gray mapping in TLED CSK

As the constellation shape in the TLED CSK is triangular, achieving a 1^{st} and 2^{nd} order Gray mapping is a cumbersome task. In Appendix C, Fig. 8 shows the symbol mapping for three different modulation sizes in TLED CSK system. For each constellation, all the nearest neighbour symbols have a hamming distance of one, except for (0 1 0) to (1 1 1) in Fig. 8(b) and (1 0 0 0) to (1 1 0 1) in Fig. 8(c). Therefore, the Gray mapping for the

Table 5.2: Bit mapping and chromaticity pairs of CBC-1 of three modulations of TLED CSK [8]

4-CSK	**8-CSK**	**16-CSK**
[data bits]-(x,y)	[data bits]-(x,y)	[data bits]-(x,y)
[00]-(0.402,0.597)	[000]-(0.324,0.400)	[0000]-(0.402,0.597)
[01]-(0.435,0.290)	[001]-(0.297,0.200)	[0001]-(0.413,0.495)
[10]-(0.169,0.007)	[010]-(0.579,0.329)	[0010]-(0.335,0.298)
[11]-(0.734,0.265)	[011]-(0.452,0.136)	[0011]-(0.324,0.400)
	[100]-(0.402,0.597)	[0100]-(0.623,0.376)
	[101]-(0.169,0.007)	[0101]-(0.513,0.486)
	[110]-(0.513,0.486)	[0110]-(0.435,0.290)
	[111]-(0.734,0.265)	[0111]-(0.524,0.384)
		[1000]-(0.734,0.265)
		[1001]-(0.169,0.007)
		[1010]-(0.247,0.204)
		[1011]-(0.258,0.101)
		[1100]-(0.546,0.179)
		[1101]-(0.634,0.273)
		[1110]-(0.446,0.187)
		[1111]-(0.357,0.093)

TLED system is not complete and should be improved.

5.3 QLED CSK System

The QLED CSK, like TLED CSK is a CIE 1931 colour space based modulation scheme. However, in QLED CSK, the intensity of the light illuminated by four different colour LEDs is modulated. Therefore, QLED CSK is a four dimensional M-ary modulation scheme (considering detection on the light intensity in the signal space (see section 5.5.2)). The four different sources are blue, cyan, yellow and red (BCYR) LEDs. The use of BCYR LEDs in CSK forms a quadrilateral constellation shape instead of triangular and allows simple symbol mapping and constellation design as in M-QAM schemes. Fig. 5.5 shows the operational colour space of the QLED CSK in a quadrilateral region denoted by "abcd" vertices on the CIE 1931 xy colour co-ordinates. Multi-colour LEDs with highly saturated

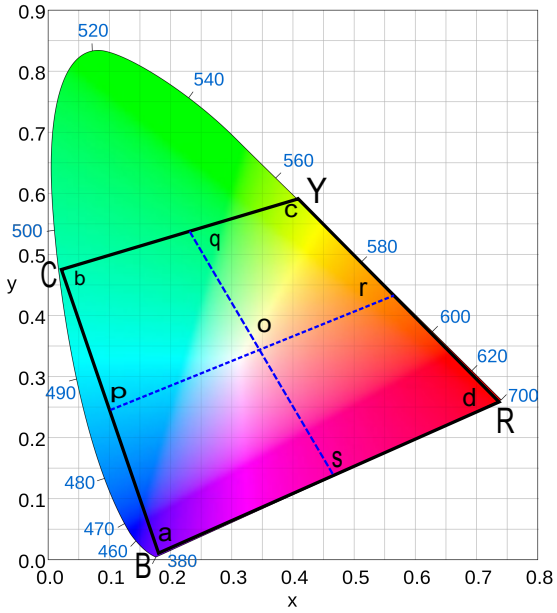

Figure 5.5: Operational colour space of the QLED CSK system on the CIE 1931 x-y colour co-ordinate diagram.

colours are available commercially, by Philips [1], which can be approximately operated at chromaticity points shown by "abcd" vertices in Fig. 5.5 and can be used for colour mixing.

For the transformation between the intensities and chromaticities, extending the set of linear equations (5.1), to incorporate the light from the fourth LED gives:

$$\begin{bmatrix} x \\ y \\ 1 \end{bmatrix} = \begin{bmatrix} x_i & x_j & x_k & x_l \\ y_i & y_j & y_k & y_l \\ 1 & 1 & 1 & 1 \end{bmatrix} \begin{bmatrix} I_i \\ I_j \\ I_k \\ I_l \end{bmatrix} \tag{5.2}$$

However, the above set of linear equations (5.2), does not have a solution and gives negative values for intensities, given a set of chromaticities. Therefore, the QLED system had to be designed in such a way that it only uses up to three LEDs at any instance and uses the same equation as the TLED CSK (5.1), for the intensity to chromaticity conversion and vice-versa. This novel QLED system switches between four TLED CSK systems in order to illuminate the colours inside the "abcd" quadrilateral region in Fig. 5.5. The QLED system requires at least three LEDs to irradiate at specific intensities in order to illuminate any colour present inside the "abcd" quadrilateral, two LEDs for any colour

on the border lines and one at the central wavelength position (or at the vertices). The "abcd" quadrilateral is further divided into four smaller regions. The colours within these small regions can be illuminated by three LEDs e.g. BCY LEDs for the top left ("pbqo" region), CYR LEDs for the top right ("oqcr" region), YRB LEDs for the bottom right ("sord" region) and RBC LEDs for the bottom left ("apos" region) regions, respectively. Therefore, only up to three out of four LEDs will be "ON" at any time instance in the QLED system and hence, the total optical power used will be equal to the TLED CSK case. However, the additional LED means the overall electrical power requirements will increase as the extra LED will need a certain level of biasing due to switching requirements.

Fig. 5.6 shows the symbol mapping and the symbol point allocation design rule for QLED 4, 8 and 16 CSK, in which symbol number along with the assigned data bits are shown. All three constellations are Gray mapped. For 4-CSK and 16-CSK the Gray mapping is the same as in [148] for QPSK and 16-QAM, respectively. The symbol mapping for 64-CSK, 256-CSK, 1024-CSK and 4096-CSK can be kept exactly the same as that of an equivalent level M-QAM modulation, which are not shown for brevity. The motivation behind the design of the QLED scheme was to enable a simple Gray mapping for the CSK systems. However, in the process, a fourth signalling dimension was added to the system, which enlarged the chromatic and signalling (intensity) spaces. Hence improved the Euclidean distances between the data symbols. This is further detailed in the performance evaluation in section 5.5.

In 4-CSK modulation, the symbols are located at the CWCVs of BCYR light sources. For 8-CSK, symbols S_0, S_3, S_5 and S_6 are located at the CWCVs and symbols S_1, S_2, S_4 and S_7 divide the line connecting CWCVs in equal sections. For 16-CSK, 64-CSK, 256-CSK, 1024-CSK and 4096-CSK four symbols are located on the CWCVs, symbols located on the lines joining CWCVs divide the lines into equal parts and the symbols located within the constellation border are approximately at equal distance from their nearest neighbours, as desired.

5.3.1 QLED constellations

Table 5.3 shows the pair of chromaticities used to represent each QLED CSK symbol for 4-CSK and 8-CSK (see Appendix D for 16-CSK and 64-CSK). Table 5.3 also shows the intensities, which can be calculated from chromaticities using equation (5.1). It must be noted that the CWCVs used in equations (5.1) varies for different symbols and depends on the symbol position (i.e. the chromaticity value for the symbol) on the "abcd" quadrilateral region in Fig. 5.5. The intensities used in 64-CSK, 256-CSK, 1024-CSK and 4096-CSK can be calculated in the similar manner. The chromatic space based transmit

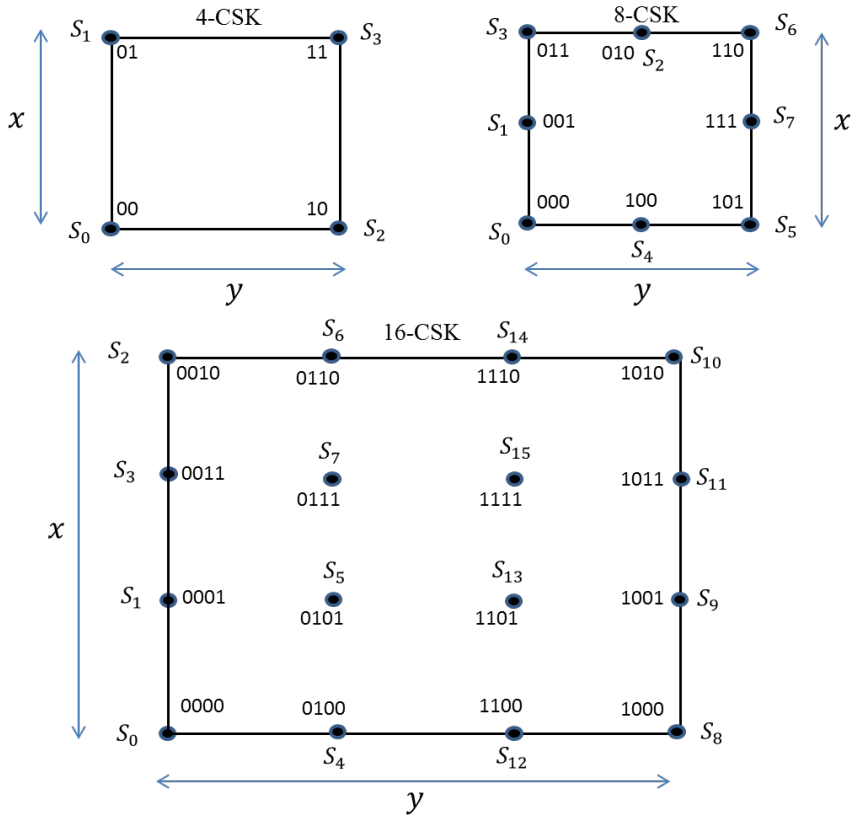

Figure 5.6: QLED CSK symbol mapping and symbol point allocation

constellation diagrams of the seven different modulation levels of QLED CSK are shown in Fig. 5.7.

Table 5.3: Unique chromaticity values and BCYR intensities for different symbols of QLED 4-CSK and 8-CSK modulations

	Symbol	x	y	I_i (w/m^2)	I_j (w/m^2)	I_k (w/m^2)	I_l (w/m^2)
4-CSK	S_0	0.169	0.007	1	0	0	0
	S_1	0.011	0.460	0	1	0	0
	S_2	0.734	0.265	0	0	0	1
	S_3	0.402	0.597	0	0	1	0
8-CSK	S_0	0.169	0.007	1	0	0	0
	S_1	0.09	0.2335	0.5	0.5	0	0
	S_2	0.2065	0.5285	0	0.5	0.5	0
	S_3	0.011	0.460	0	1	0	0
	S_4	0.4515	0.1360	0.5	0	0	0.5
	S_5	0.734	0.265	0	0	0	1
	S_6	0.402	0.597	0	0	1	0
	S_7	0.568	0.431	0	0	0.5	0.5

5.4 Intensity and Colour Flicker in CSK

In CSK, the instantaneous light intensity is kept constant, as can be seen from equation (5.1) & (5.2) which shows that the sum of light intensities from each colour source is equal to one, i.e. $I_i + I_j + I_k = I_i + I_j + I_k + I_l = 1$. This eliminates any intensity flicker related issues in CSK [13][32]. This is a big advantage of CSK when compared to PAM, PPM and OFDM based intensity modulation schemes which require continuous flicker management and can be very complex while working with arrays of LEDs [146].

Although the intensity flicker is not an issue for CSK, the scheme requires a careful design of each constellation to provide the right average light chromaticity or colour temperature which can affect the human circadian rhythm and cognitive functions such as alertness, mood, executive function and memory [149][150]. For example, under the illumination of an average warm white colour temperature ($\sim$ 3500K) humans can feel very relaxed and an average cool white colour temperature ($\sim$ 17000K) can oppositely make humans feel very active [151]. A day-light colour temperature of $\sim$ 6500K, which

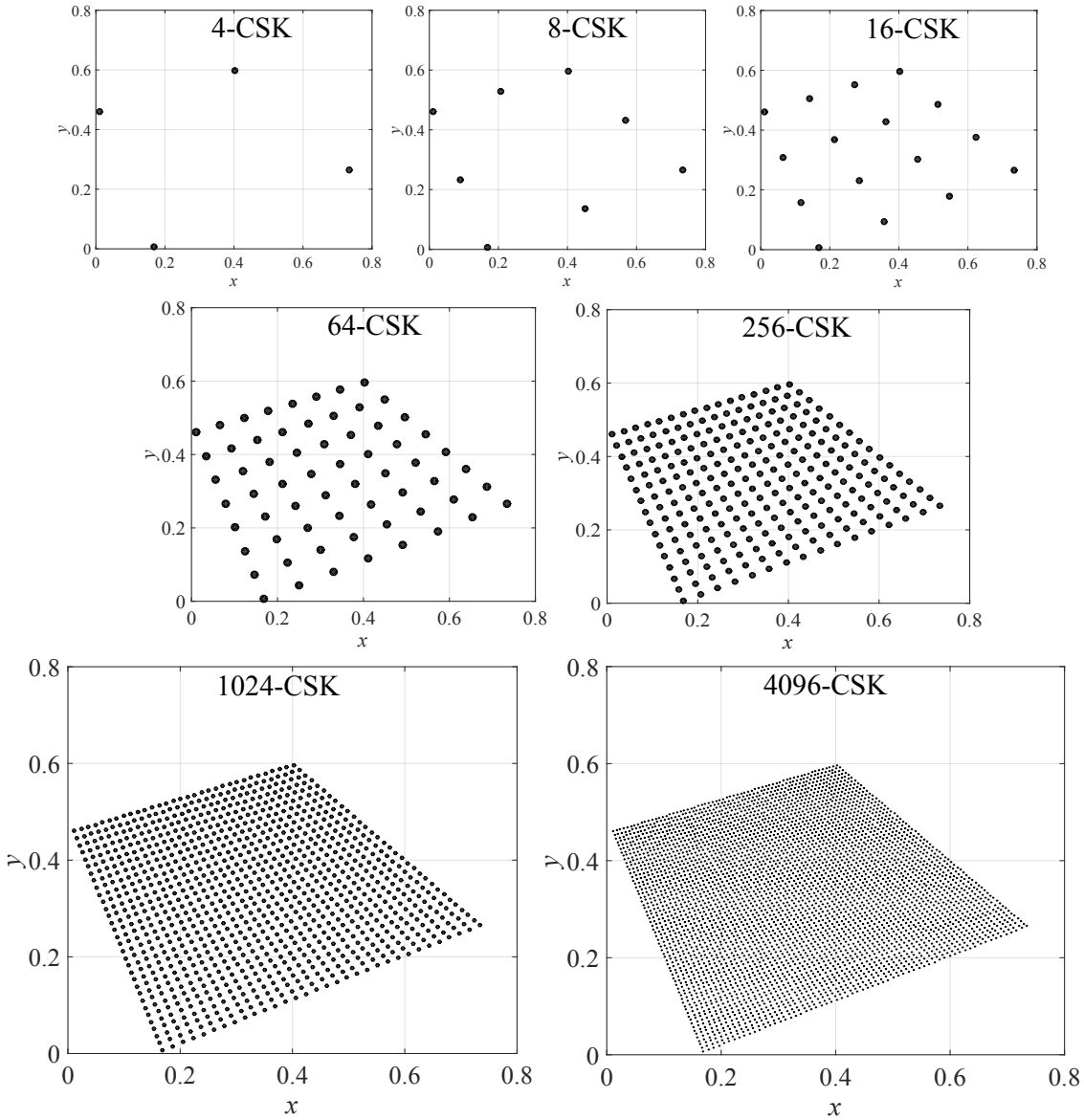

Figure 5.7: Transmit constellations of seven different QLED CSK modulations over chromatic space.

approximates to an average chromaticity value of around $[x = 1/3, y = 1/3]$, should be targeted in a CSK modulation.

5.5 Performance of Uncoded CSK Systems over AWGN

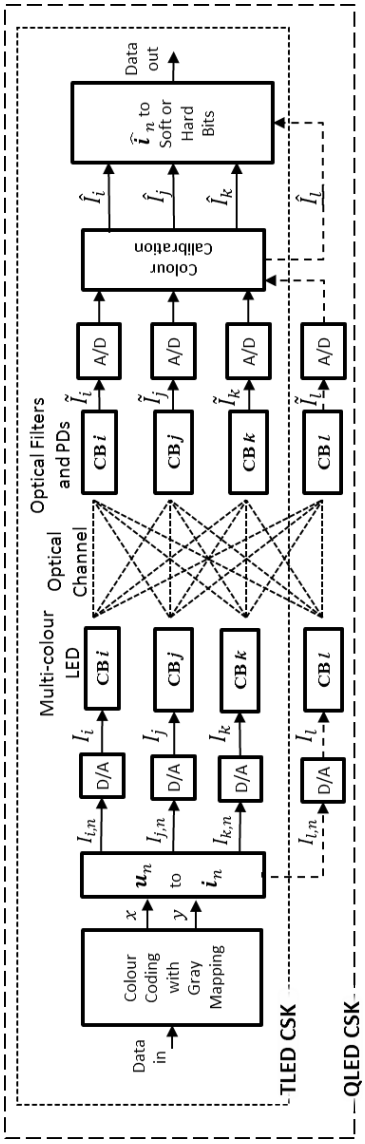

Figure 5.8: Transceiver schematic of the uncoded TLED and QLED CSK systems.

This section details working of the uncoded standardised TLED and advanced QLED CSK systems and analyses their performance over AWGN channel, assuming multipath free channel environment without CIL. Fig. 5.8 shows the transceiver schematic of both

schemes while working without the use of a FEC technique. At the Tx, the randomised binary data is grouped in to $k = \log_2(M)$ bits and mapped to a specific pair of chromaticity values given by vector $\boldsymbol{u}_n$=$[x_n, y_n]^T$ according to a bit mapping design, where n represents the n^{th} chromaticity pair. Throughput this chapter, the TLED system used bit mapping defined by the standard [8] and the QLED system used M-QAM based Gray mapping [150]. Based on $\boldsymbol{u}_n$, the n^{th} intensity vector $\boldsymbol{i}_n$=$[I_{i,n}, I_{j,n}, I_{k,n}, I_{l,n}]^T$ is obtained for a QLED system as an example. The $I_{i,n}$, $I_{j,n}$, $I_{k,n}$ and $I_{l,n}$ represent the intensity of each CB in the multi-colour LED for the n^{th} chromaticity based CSK symbol. After digital to analogue (D/A) conversion, the transmit signals I_i, I_j, I_k and I_l are obtained which modulate the intensity of each LED source.

$$\begin{bmatrix} \tilde{I}_i(t) \\ \tilde{I}_j(t) \\ \tilde{I}_k(t) \\ \tilde{I}_l(t) \end{bmatrix} = \overbrace{\begin{bmatrix} g_{1,1} & g_{1,2} & g_{1,3} & g_{1,4} \\ g_{2,1} & g_{2,2} & g_{2,3} & g_{2,4} \\ g_{3,1} & g_{3,2} & g_{3,3} & g_{3,4} \\ g_{4,1} & g_{4,2} & g_{4,3} & g_{4,4} \end{bmatrix}}^{\boldsymbol{G}} \begin{bmatrix} h(t)*I_i(t) \\ h(t)*I_j(t) \\ h(t)*I_k(t) \\ h(t)*I_l(t) \end{bmatrix} + \begin{bmatrix} n_i(t) \\ n_j(t) \\ n_k(t) \\ n_l(t) \end{bmatrix} \tag{5.3}$$

At the receiving end the narrowband optical filters pass light of the desired wavelength to the PDs. The received signals at the output of the PDs can be given by equation (5.3), where '$*$' is the convolution operator, $h(t)$ is the channel impulse response (CIR), which is detailed in section 2.4, where it is represented by $h(\tau)$, a function of channel delay τ, as it does not change significantly with time.

In equation (5.3) $\boldsymbol{G}$ is a square cross-talk and insertion loss (CIL) matrix, where $g_{m,n}$ represents the effective responsivity between the receive CB m and transmit CB n. For more information on $\boldsymbol{G}$, the reader is referred to section 2.4.4. The independent identically distributed AWGN per detector is given by $[n_i, n_j, n_k, n_l]^T$. Each CB has a noise variance of σ^2, where σ is the standard deviation of noise, related to the single-sided noise power spectral density, N_o as σ=$\sqrt{N_o/2}$.

After analogue to digital (A/D) conversion, the colour calibration (CC) as suggested in the standard [8] takes place to compensate for the cross-talk between the multi colour channels. The instantaneous sets of received intensities after CC can be given as, $[\hat{I}_i, \hat{I}_j, \hat{I}_k, \hat{I}_l]^T$ = $\boldsymbol{G}^{-1}[\tilde{I}_i, \tilde{I}_j, \tilde{I}_k, \tilde{I}_l]^T$ and the n^{th} received intensity vector can be denoted as $\hat{\boldsymbol{i}}_n = [\hat{I}_{i,n}, \hat{I}_{j,n}, \hat{I}_{k,n}, \hat{I}_{l,n}]^T$. At this point, the data bits are obtained from each $\hat{\boldsymbol{i}}_n$ through maximum likelihood detection (MLD) as:

$$\boldsymbol{i}_n^{'} = \underset{\boldsymbol{i} \in \mathbb{J}}{\arg\min} \, ||\hat{\boldsymbol{i}}_n - \boldsymbol{i}||^2, \tag{5.4}$$

where, $\mathbb{J}$ contains the intensity based alphabets of the CSK constellation. The final data bits are then de-mapped from $\boldsymbol{i}_n^{'}$.

For an AWGN only channel based investigation, equation (5.3) can be rewritten as:

$$\begin{bmatrix} \tilde{I}_i(t) \\ \tilde{I}_j(t) \\ \tilde{I}_k(t) \\ \tilde{I}_l(t) \end{bmatrix} = \begin{bmatrix} I_i(t) \\ I_j(t) \\ I_k(t) \\ I_l(t) \end{bmatrix} + \begin{bmatrix} n_i(t) \\ n_j(t) \\ n_k(t) \\ n_l(t) \end{bmatrix}, \tag{5.5}$$

Therefore, CC is not needed and $[\hat{I}_i, \hat{I}_j, \hat{I}_k, \hat{I}_l]^T = [\tilde{I}_i, \tilde{I}_j, \tilde{I}_k, \tilde{I}_l]^T$.

TLED Results

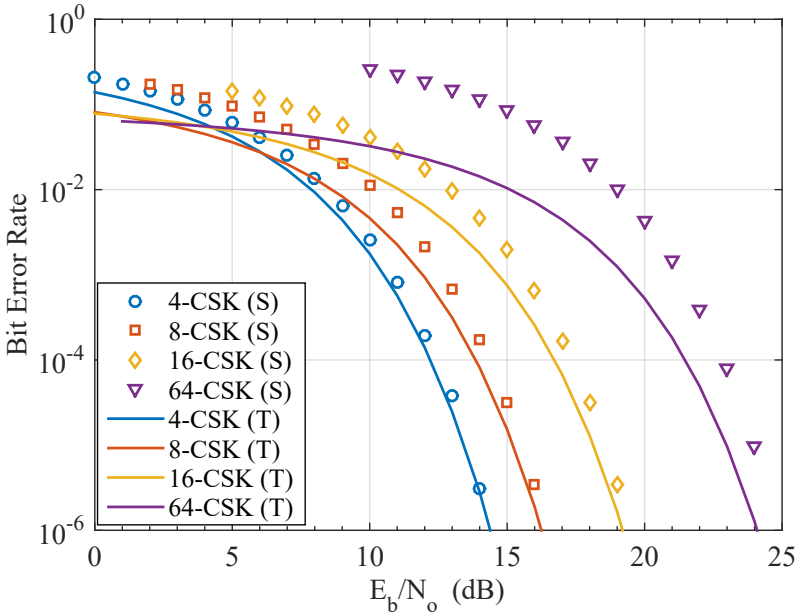

Figure 5.9: Theoretical (T) and simulations (S) based BER performance of TLED system over AWGN channel.

Fig. 5.9 shows the BER vs E_b/N_o performance of a TLED CSK system over AWGN channel, where E_b is the average energy per bit. Both the theoretical and simulation results are shown for four different modulation orders, where 4-CSK, 8-CSK and 16-CSK are standardised orders and 64-CSK with random bit mapping is introduced by the author [152]. There is reasonable agreement between the theoretical and simulation results for 4-CSK, 8-CSK and 16-CSK for high E_b/N_o levels or high SNRs. However, there is a difference between the theoretical and simulation results at low levels of SNR and there is a mismatch between the two results for 64-CSK even at high SNR. This issue is discussed in section 5.5.1 along with description of different approaches to calculate the theoretical bit error probabilities of CSK systems.

Although the BER performance of standardised TLED system, which is based on CBC-1 is evaluated, it can be said that the performance of nine different CBCs of TLED CSK will be approximately the same. This is obtained because the minimum Euclidean distances (d_{min}) of each constellations in nine CBCs are identical in the signal or intensity space, which are given in Table 5.4.

Table 5.4: Minimum Euclidean Distance, d_{min}, for various CBCs of TLED CSK measured in signal space (in Watts).

CBC Number	**Minimum Euclidean Distance** (d_{min})		
	4-CSK	8-CSK	16-CSK
CBC-1, CBC-3 & CBC-5	0.8157	0.4722	0.2702
CBC-2, CBC-4 & CBC-6	0.8158	0.4708	0.2712
CBC-7	0.8150	0.4719	0.2675
CBC-8	0.8165	0.4701	0.2380
CBC-9	0.8161	0.4701	0.2707

QLED Results

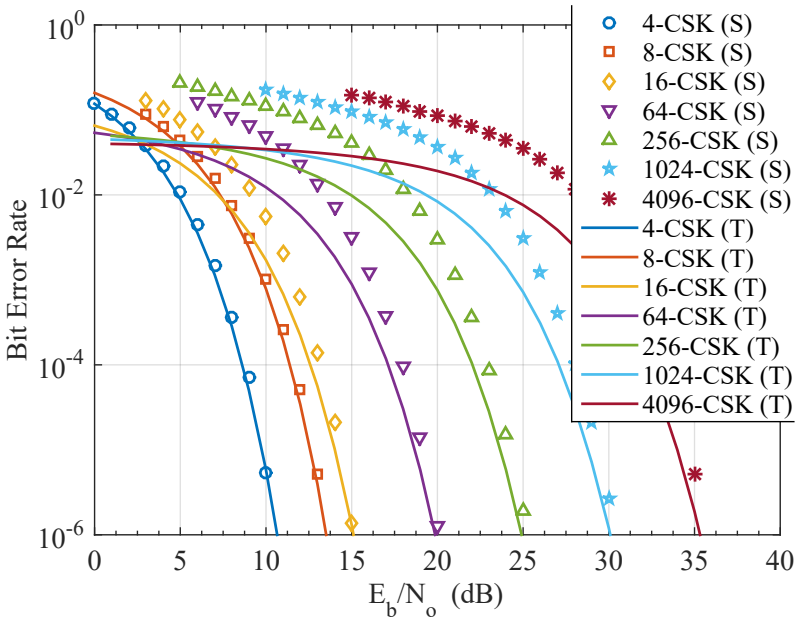

Figure 5.10: Theoretical (T) and simulations (S) based BER performance of QLED system over AWGN channel.

Fig. 5.10 shows the BERs for each of the seven different modulation orders of uncoded QLED CSK modulations over the AWGN channel. A gain of approximately 4, 2.9, 4.4

and 5 dB can be noted for 4-CSK, 8-CSK, 16-CSK and 64-CSK, when compared to the results in Fig. 5.9 of the TLED CSK. In Fig. 9 the analytical error performance of the QLED CSK have also been compared with the simulation results and a good agreement between the two can be observed in the high E_b/N_o region, as expected. The calculations for the analytical results have been detailed in section 5.5.1.

This high gain of the QLED CSK is mainly due to four dimensional signalling using BCYR LEDs, which increases the Euclidean distance between the symbols when compared to the three dimensional TLED CSK scheme. The four symbols of 4-CSK in the QLED system are orthogonal to each other as can be noted from Table 5.3. As the constellation size increases above four, the orthogonality in QLED CSK is not held any more. The 1st and 2nd order Gray mapping of symbols is also another advantage of the QLED CSK system. The Euclidean distances between the CSK symbols in the signal space (or intensity space) are larger than in the chromatic space (x-y space), however, the nearest to furthest neighbours of each symbol remain almost the same in both of the spaces. Therefore, the Gray mapping of symbols in the chromatic space works well even when the decision is made in the signal space.

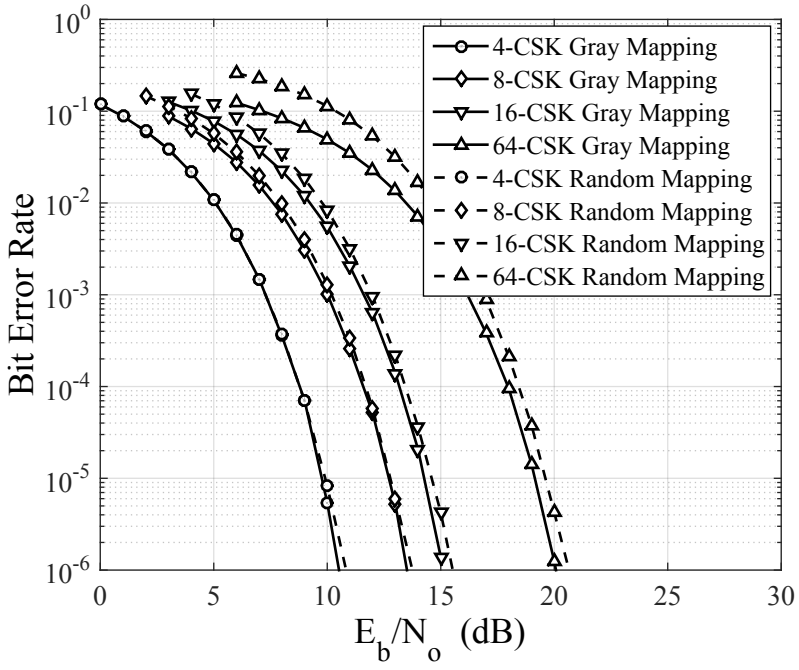

Figure 5.11: Simulations based BER performance of QLED system over AWGN channel with Gray and random bit mapping.

In order to check whether the Gray mapping improved the system performance, the QLED CSK system was tested using random symbol mapping for each transmitted symbol.

This revealed that the Gray mapping achieves SNR gains up to ∼0.8 dB as the modulation order increases above 4-CSK. This can be seen from Fig.5.11, where the BER of up to 64-CSK of QLED system is compared with the use of Gray and random bit mapping. The result show that the Gray mapping does not improve any performance for 4-CSK system as its an orthogonal signalling scheme. However, for the modulation orders above 4-CSK the Gray mapping can be seen to gradually improve the bit error performance. This improved performance with Gray mapping has the potential to further yield significant channel coding gain when CSK system is used with a FEC scheme.

5.5.1 Analytical Error Probabilities

The maximum likelihood detection (MLD) for QLED and TLED systems in signal space is based on the minimum Euclidean distance (d_{min}) detection rule as shown in equation (5.4). The analytical error probability of an MLD system can be estimated based on d_{min} and the number of nearest neighbours N_n situated at d_{min}, for each symbol [153]. The symbol error probability of a CSK system based on these parameters can be given as [154][150]:

$$\mathcal{P}_s = \frac{1}{M}\sum_{i=1}^{M}\left\{N_{ni}Q\left(\sqrt{\frac{d_{min}^2}{2N_0}}\right)\right\} \tag{5.6}$$

In the above equation, $Q(.)$ is the tail probability of the standard normal distribution and generally given as

$$Q(x) = \frac{1}{\sqrt{2\pi}}\int_x^\infty e^{-\frac{u^2}{2}}du$$

and N_0 is the one-sided noise power spectral density for the AWGN channel that has standard deviation of noise $\sigma = \sqrt{\frac{N_0}{2}}$. By using the data given in Table 5.5, to obtain the values for N_n and d_{min}, the analytical symbol error probabilities of 4-CSK modulation for the QLED can be calculated as:

$$\mathcal{P}_s = 3Q\left(\frac{1}{\sqrt{N_0}}\right) \tag{5.7}$$

and the analytical error probabilities of 4-CSK modulation for the TLED can be calculated as:

$$\mathcal{P}_s = 0.5Q\left(\frac{0.8157}{\sqrt{2N_0}}\right) + 0.5Q\left(\frac{0.817}{\sqrt{2N_0}}\right) \tag{5.8}$$

The bit error probability can be approximated as

$$\mathcal{P}_b \approx \frac{\mathcal{P}_s}{k}$$

Table 5.5: Minimum Euclidean Distance Between Symbols of TLED and QLED 4-CSK Modulation Schemes in signal space, given as (QLED/TLED)

Symbol	S_0	S_1	S_2	S_3
S_0	0/0	$\sqrt{2}$/0.8157	$\sqrt{2}/\sqrt{2}$	$\sqrt{2}/\sqrt{2}$
S_1	$\sqrt{2}$/0.8157	0/0	$\sqrt{2}$/0.8170	$\sqrt{2}$/0.8170
S_2	$\sqrt{2}/\sqrt{2}$	$\sqrt{2}$/0.8170	0/0	$\sqrt{2}/\sqrt{2}$
S_3	$\sqrt{2}/\sqrt{2}$	$\sqrt{2}$/0.8170	$\sqrt{2}/\sqrt{2}$	0/0

In the QLED CSK system, the four symbols of 4-CSK are mutually orthogonal. Therefore, the theoretical bit error probability for the 4-CSK in the QLED system can also be given as [155]:

$$\mathcal{P}_b = \frac{M}{2} Q\left(\sqrt{\frac{kE_b}{N_0}}\right) \tag{5.9}$$

As the modulation order is further increased in the four dimensional space for 8, 16, 64, 256, 1024 and 4096 CSK, the symbols do not hold mutual orthogonality any more.

Similarly, using equation (5.6), the analytical BERs for remaining CSK modulation orders were calculated, and compared against the simulations in Fig. 5.10 and Fig. 5.9. The analytical results reasonably agree with the simulations, given the analytical approach is well known to give accurate BER at high SNR. However, at low SNR, there is a mismatch between the theoretical and simulation results. This is because equation (5.6) estimates the bit error probability based on the possibility of a symbol being received as its nearest neighbour due to AWGN, which is true when either the d_{min} is large or the SNR is high. Therefore, at low SNR or low E_b/N_o, for higher modulation orders such as 16-CSK to 4096-CSK where d_{min} is small, there is a disagreement between the analytical and the simulated BER curves.

Additionally, the analytical BER for the 64-CSK of TLED system does not match with the simulations even at high SNRs. This is due to the use of random symbol mapping for 64-CSK TLED scheme in simulations [152], which usually results in a degraded performance.

A tighter error bound

Another approach to estimate the analytical BER is through the union bound, whereby, the d_{min} and N_n based performance bound can be modified to obtain a tighter bound by assuming that an error can result in reception of a transmitted symbol $\boldsymbol{i}$ as any other

symbol in the constellation $\mathcal{I}$, not only as nearest neighbour of $\boldsymbol{i}$ as in equation (5.6). This gives a new expression for the average bit error probability ($\mathcal{P}_b$) of the CSK systems given as:

$$\mathcal{P}_b = \frac{1}{Mlog_2(M)} \sum_{n_1=1}^{M} \sum_{\substack{n_2=1,\\ n_2 \neq n_1}}^{M} Q\left(\sqrt{\frac{d(\boldsymbol{i}_{n_1}, \boldsymbol{i}_{n_2})^2}{2N_o}}\right) \tag{5.10}$$

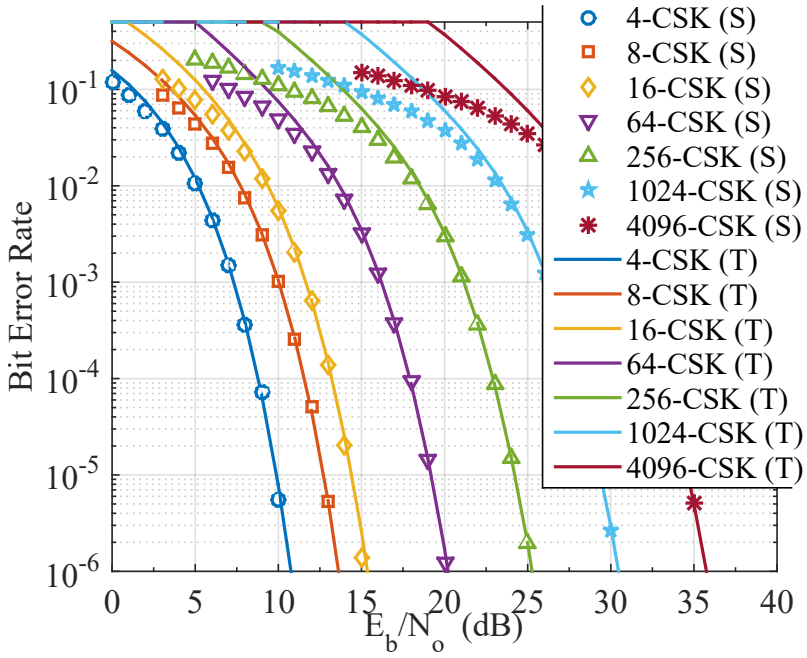

Figure 5.12: Union bound based Theoretical (T) and simulations (S) based BER performance of QLED system over AWGN channel.

Through equation (5.10), the BERs of all the different QLED modulations were approximated and compared against the simulation results, which are plotted in Fig. 5.12. Clearly, the union bound approach yields tighter error probabilities. Therefore, this estimation was adopted to obtain the analytical results for the FEC based CSK systems, which are detailed in section 6.3.

5.5.2 Detection in Chromatic Space

In CSK, there are two different detection techniques that can be used at the receiver. The first one is the detection in the signal space, directly on the received intensities. This is the detection approach used so far (see section 5.5). The second detection technique is the chromatic detection, whereby the received intensities ($\hat{\boldsymbol{i}}_n$), are converted to chromaticity using equations (5.1) or (5.2) in TLED and QLED systems, respectively and the minimum

Euclidean distance detection takes place on the received chromaticities. This approach is described in standard [8] and other publication [13][156][157]. The received chromatic pairs for a TLED system can be given as:

$$\begin{bmatrix} \hat{x} \\ \hat{y} \end{bmatrix} = \begin{bmatrix} x_i & x_j & x_k \\ y_i & y_j & y_k \end{bmatrix} \begin{bmatrix} \hat{I}_i \\ \hat{I}_j \\ \hat{I}_k \end{bmatrix} \tag{5.11}$$

At this point, the data bits are obtained from each received chromatic pair $\hat{\boldsymbol{u}}_n = [\hat{x}_n, \hat{y}_n]$ through minimum Euclidean distance detection rule as:

$$\boldsymbol{u}_n^{'} = \arg\min_{\boldsymbol{u} \in \mathcal{U}} ||\hat{\boldsymbol{u}}_n - \boldsymbol{u}||^2, \tag{5.12}$$

where, $\mathcal{U}$ contains the chromaticity based alphabets of the CSK constellation. The final data bits are then de-mapped from $\boldsymbol{u}_n^{'}$.

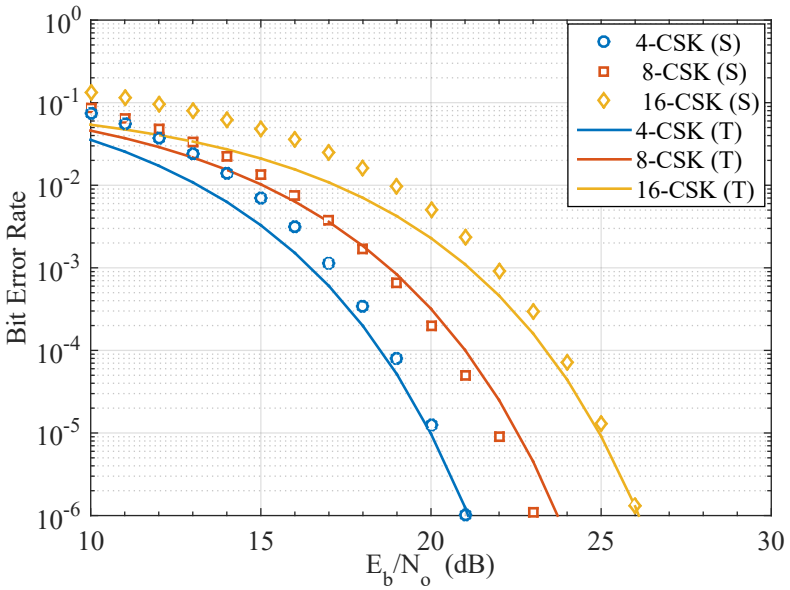

Figure 5.13: Theoretical (T) and simulations (S) based BER performance of TLED system over AWGN channel with detection in chromatic space.

Fig. 5.13 show the performance of CBC-1 based TLED CSK system with detection in chromatic space. Comparing these results with the signal space detection based results in Fig. 5.9, it can be seen that the system performance degrades by a very large margin as the E_b/N_o requirements are increased by up to 6.8 dB for the same k or M. This is because the chromatic detection is a sub-optimal detection as the conversion from received intensities to chromaticities causes the AWGN added to every pair of x and y chromaticities to be

correlated. This can be demonstrated by studying the behaviour of the noise added to the chromatic pairs.

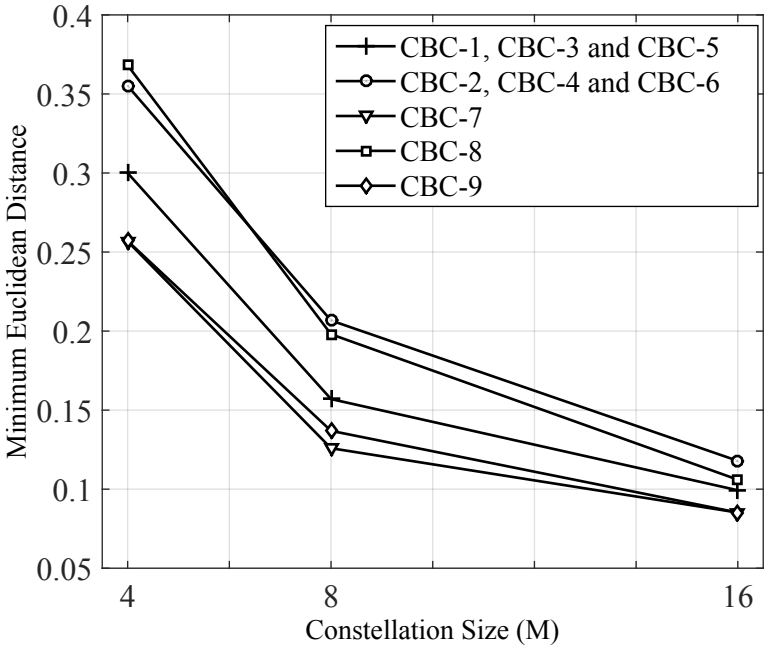

Figure 5.14: d_{min} values comparison for different CBCs of TLED CSK.

Equation 5.11 can be re-written as:

$$\begin{bmatrix} \hat{x} \\ \hat{y} \end{bmatrix} = \begin{bmatrix} x \\ y \end{bmatrix} + \begin{bmatrix} n_x \\ n_y \end{bmatrix}, \tag{5.13}$$

where, n_x and n_y are the AWGN present in the $\hat{x}$ and $\hat{y}$, respectively, and are given as:

$$\begin{bmatrix} n_x \\ n_y \end{bmatrix} = \begin{bmatrix} x_i n_i + x_j n_j + x_k n_k \\ y_i n_i + y_j n_j + y_k n_k \end{bmatrix} \tag{5.14}$$

From equation (5.14), it can be seen that n_x and n_y contain CWCV weighted noise from each CB, which makes the noise in the received chromatic pairs to be roughly three times the noise in the intensity based symbols. Additionally, it can be seen that the time variation in n_x and n_y will be similar due to the presence of instantaneous n_i, n_j and n_k in both $\hat{x}$ and $\hat{y}$ despite different magnitude of CWCV. This means the chromaticity co-ordinates will be corrupted with similar amount of noise leading to error magnitudes in $\hat{x}$ and $\hat{y}$ being identical and to be larger than the error magnitude in the received intensities. Therefore, chromatic detection should be avoided in CSK.

The theoretical error probabilities for TLED CSK system with detection in chromatic space are also shown in Fig. 5.13, which were estimated based on equation (5.6). Chromatic detection also leads to the performance of different CBCs of CSK to be different [157]. This is due to d_{min} being different across the nine CBCs in the chromatic space as oppose to being the same as in signal space. Fig.5.14 shows the d_{min} values for different CBCs of TLED system plotted against M. It can be seen that CBC-2 and CBC-7 yields the highest and lowest d_{min} values. The spread of chromatic d_{min} values means the BER performance will not be the same for different CBCs.

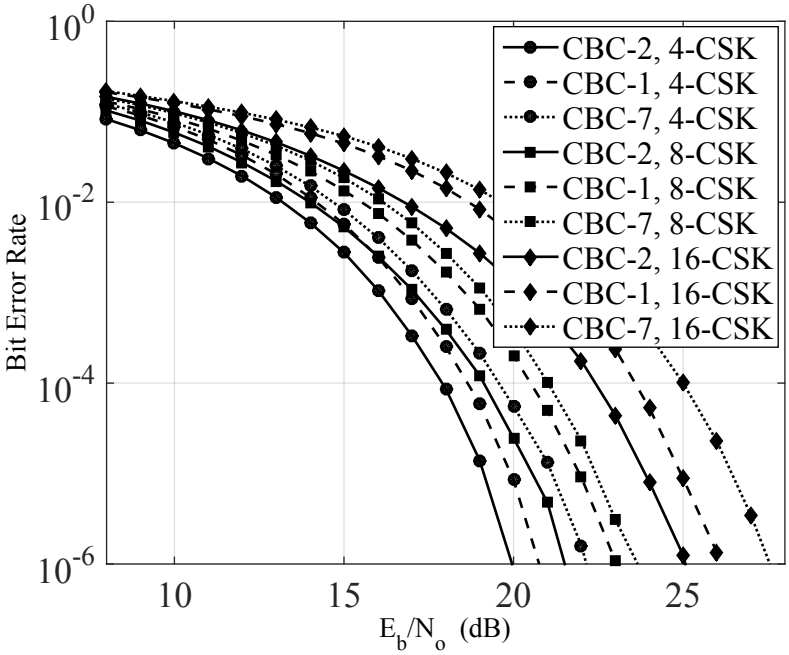

Figure 5.15: Simulations based BER performance of CBC-1, CBC-2 and CBC-7 based TLED system over AWGN channel with detection in chromatic space.

In order to illustrate the performance of the different CBCs, the BER and PER performances of CBC-1, CBC-2 and CBC-7 were determined in an AWGN channel as these CBCs offer the average, the largest and the smallest d_{min} values, respectively. CBC-1 is also the only colour-band combination that has been thoroughly detailed in [8] with bit mapping of each constellation. Fig. 5.15 shows the BER performance of different modulation schemes for selected CBCs on an E_b/N_o scale. The BER curves confirm the predictions made from the d_{min} comparison in Fig. 5.14. The BER results show a spread of system performances of the standardised CSK which is directly related to the chromatic region covered by different CBCs of CSK. CBC-2 outperforms CBC-1 and CBC-7 by achieving 0.8 to 1.5 dB and 2 to 2.5 dB of electrical SNR gains, respectively. The BER

and PER of these three CBCs are also compared over optical SNR scale in Appendix E, where the results show similar trends.

It must be noted that if chromatic detection based CSK systems are to be commercialised, the CSK designers must keep in mind the spread of BER performance that different CBCs can yield. However, detection in signal space should be considered for high performance VLC signalling. The CSK investigations in the rest of the thesis are based on signal space detection.

5.6 Performance of Uncoded CSK Systems over AWGN with Cross-talk and Insertion Losses

So far the performance of CSK systems has been studied purely based on AWGN. This section studies the effects of cross-talk, insertion losses and colour calibration (CC) on the TLED and QLED CSK systems. The optical properties of front-end components as detailed in section 5.6.1 were used to evaluate the cross-talk and insertion losses (CIL) matrix $\boldsymbol{G}$ for both the CSK systems. In this investigation, signal space detection is used at the receiver as it is the optimal detection for CSK.

5.6.1 Optical Properties of Front-End Devices

As detailed in section 2.4.4, the SPD of LEDs, the transmissivity of optical filters and the responsivity of PDs together introduce colour cross-talk and insertion losses in a multi-colour VLC system. The CIL matrix $\boldsymbol{G}$ in equation (5.3) represent the cross-talk and insertion in CSK systems through estimating the effective responsivity in each CB and cross different CBs through equation (2.17).

In order to estimate $\boldsymbol{G}$ for TLED and QLED CSK, optical properties of commercially available optical front-end components were used. The spectral response of LED sources [1] LXML-PR01 (Blue), LXML-PE01 (Cyan), LXM2-PL01 (Yellow) and LXM3-PD01 (Red) for QLED, and LXML-PR01 (Blue), LXM2-PL01 (Yellow) and LXM3-PD01 (Red) for the TLED, were used for the evaluation of G. The optical bandpass filters were assumed to be FB450-40 (Blue) [2], FB500-40 (Cyan) [3], BP590 (Yellow) [4] and FB650-40 (Red) [5] for QLED, and FB450-40, BP590 and FB650-40 for the TLED CSK. Finally, the spectral response of PC10-6b [6] PD was used.

For TLED system, the matrix G was estimated to be:

$$G = \begin{bmatrix} 0.271 & 0.030 & 0 \\ 0 & 0.255 & 0 \\ 0 & 0 & 0.200 \end{bmatrix} \tag{5.15}$$

and for the QLED system:

$$G = \begin{bmatrix} 0.271 & 0.030 & 0 & 0 \\ 0 & 0.255 & 0.002 & 0 \\ 0 & 0.003 & 0.220 & 0.007 \\ 0 & 0 & 0.003 & 0.200 \end{bmatrix} \tag{5.16}$$

From equations (5.15) and (5.16), it can be seen that the cross-talk between CBs will be very small and the next section shows that this cross-talk can be mitigated with the use of CC. However, the insertion loss will be very high, which will increase the optical power requirements per CB by roughly 70% to 80%.

5.6.2 BER Performance with CIL

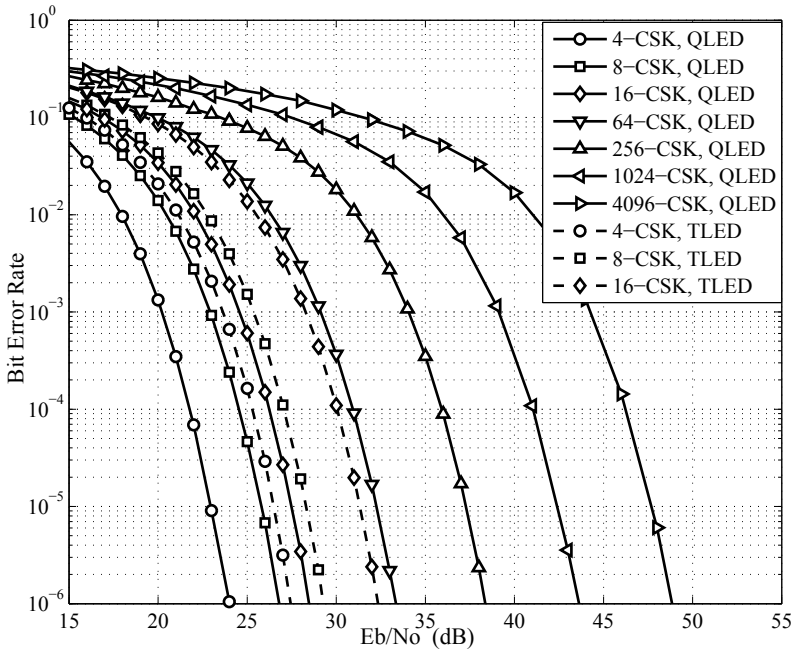

Figure 5.16: BER performance of QLED and TLED CSK schemes over AWGN channel including G, with the use of CC.

Fig. 5.16 shows the BER performance of the colour calibrated TLED and QLED schemes over AWGN channel with the inclusion of CIL. It can be seen that the overall E_b/N_o requirements increase by a large factor due to the insertion losses, when compared to the performance with AWGN only which is shown in Fig. 5.9 and Fig. 5.12, respectively. However, all the modulation formats can successfully achieve a BER of 10^{-6}, which has been made possible by the CC.

Fig. 5.17 shows the BER performance of all the CSK schemes, over the same channel condition, however, without the use of CC. The results in Fig. 5.17 show that all the

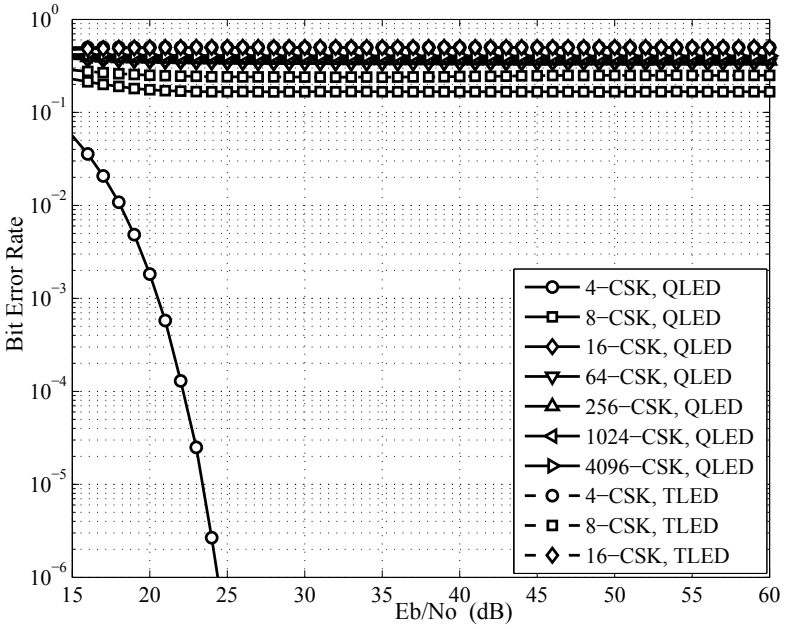

Figure 5.17: BER performance of QLED and TLED CSK schemes over AWGN channel including G, without the use of CC.

schemes will fail to work in this case except the 4-CSK of QLED, which is an equivalent four-dimensional orthogonal signalling scheme, in which at any instance of time only one LED illuminates light and the rest of the three LEDs are off. This enables the QLED's 4-CSK to operate over a cross-talk channel, without using CC. This shows that a high rate 4-CSK of QLED is robustly available to provide data links to various user terminals where the matrix G is not available and enable data links for the higher-order modulations.

Analytical BER performance

The theoretical BER performance of TLED and QLED systems over AWGN with the inclusion of CIL can be estimated with a slight modification of the union bound error

estimation equation (5.10) as:

$$\mathcal{P}_b = \frac{1}{Mlog_2(M)} \sum_{n_1=1}^{M} \sum_{\substack{n_2=1,\\ n_2 \neq n_1}}^{M} Q\left(\sqrt{\frac{d(\boldsymbol{G}\boldsymbol{i}_{n_1}, \boldsymbol{G}\boldsymbol{i}_{n_2})^2}{2N_o}}\right), \tag{5.17}$$

where all the notations have the same meaning as in equation (5.10), except that the Euclidean distance between two legitimate intensity alphabets is calculated including $\boldsymbol{G}$, which is represented by $d(\boldsymbol{G}\boldsymbol{i}_{n_1}, \boldsymbol{G}\boldsymbol{i}_{n_2})$. Fig. 5.18 shows the analytical and simulation based BER performance TLED and QLED systems over optical SNR (SNR_o), which agree with each other. Details of SNR_o calculations can be found in Appendix E.

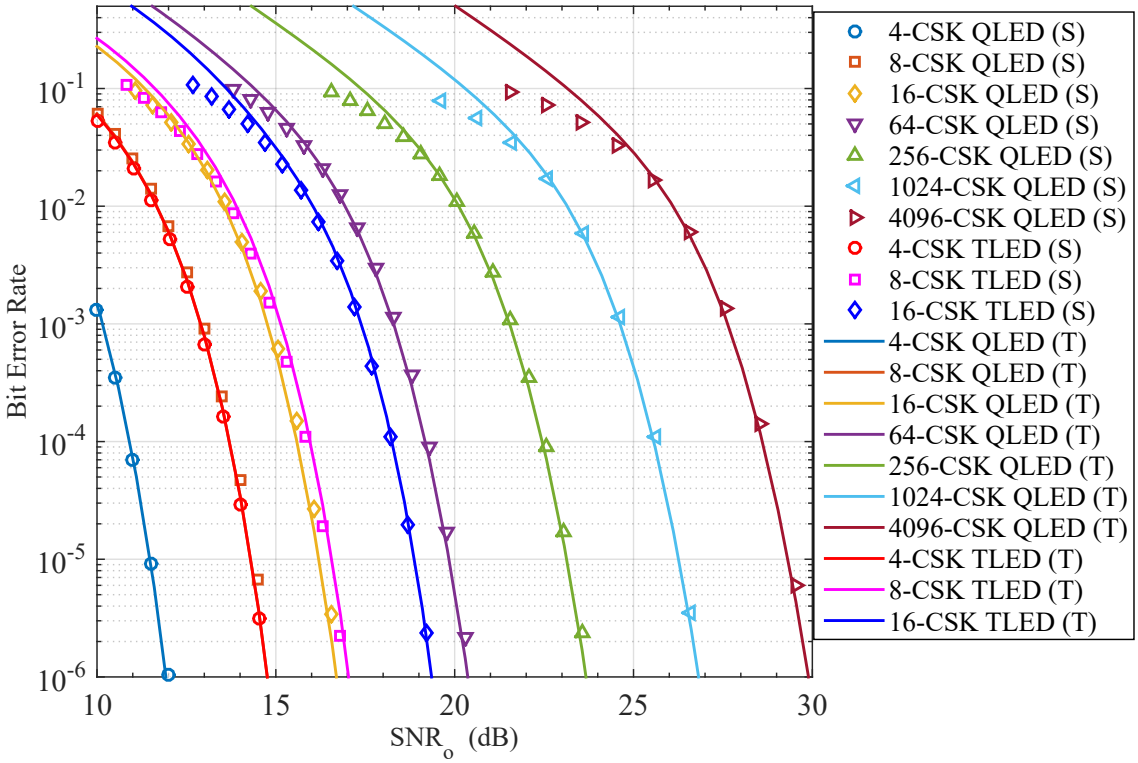

Figure 5.18: Theoretical and simulations based BER performance of QLED and TLED CSK schemes over AWGN channel including G, with CC.

5.7 Concurrent Transmissions over Multi-colour LEDs

CSK, as detailed so far in this chapter, modulates the intensity of multi-colour LEDs per $k = \log_2(M)$ bits of data. This means a set of instantaneous intensities, e.g. $\boldsymbol{i} = [I_i, I_j, I_k, I_l]^T$ for QLED CSK which refer to a certain colour (or $x-y$ pair) on chromatic

constellation, represent k bits of data. Therefore, the instantaneous intensity changes per CB are not independent. This limits the overall data-rate that can be achieved in a multi-colour VLC system, in which each CB can independently use intensity modulation scheme such as OOK or unipolar M-PAM and the overall data can be divided across the CBs to realise concurrent data transmissions over multi-colour channels. This process will increase the overall data rate by the number of concurrent transmissions or CBs. This process is known as wavelength division multiplexing (WDM) [158], which is widely used in fibre optic communications [159].

In this section, the bit error performance of CSK and WDM based three-colour VLC systems is studied. For three CBs, the TLED scheme based on CBC-1 was utilised as a CSK systems with signal space detection. On the other hand for WDM, unipolar M-PAM signalling was used [122].

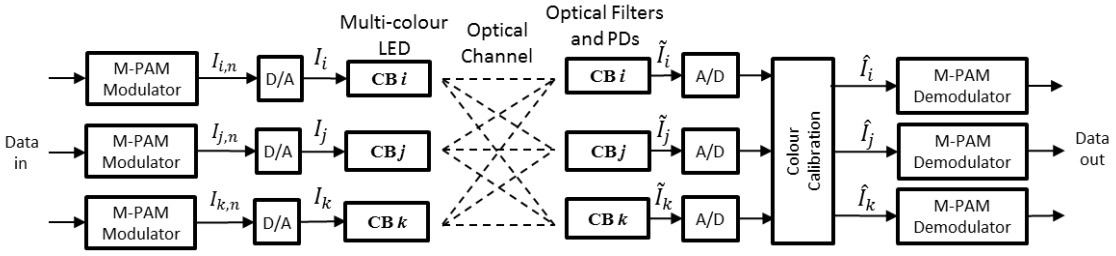

Figure 5.19: Three colour based WDM system using unipolar M-PAM signalling.

Fig. 5.19 shows schematic diagram of a M-PAM based WDM system for three CBs. At the Tx side, the binary data in each CB is grouped into k bits and each group of bits is mapped to an intensity alphabet $I \in [0, 1, \ldots, (M-1)]$, which gives the n^{th} intensity value in each CB as $I_{i,n}$, $I_{j,n}$ and $I_{k,n}$. The instantaneous intensity vector across the CBs can still be represented as $\boldsymbol{i}_n = [I_{i,n}, I_{j,n}, I_{k,n}]^T$, as in TLED CSK systems. The average intensity or optical power levels are normalised in each CB to 1/3 Watt as in TLED CSK system. This was done to keep the overall optical power in both system equal, which is 1 Watt. Then after the D/A conversion, the transmit intensity signals are obtained.

At the Rx side, the colour calibration takes place as in CSK systems and then the binary data is obtained in M-PAM demodulator, through an Euclidean distance detection rule.

5.7.1 WDM and CSK Performance Comparison

Table 5.6 compares the number of bits in the n^{th} intensity vector $\boldsymbol{i}_n$ for CSK and WDM systems, which for a CSK system is given by $\log_2(M)$ as mentioned previously and for the WDM system by $N_b * \log_2(M)$, where N_b is the number of CBs. Three different modulation

Table 5.6: Comparison of information bits per $\boldsymbol{i}_n$ in CSK and WDM system

M-CSK	Bits per $\boldsymbol{i}_n$ (CSK)	M-PAM	Bits per $\boldsymbol{i}_n$ (WDM)
4	2	2	3
8	3	4	6
16	4	8	9

orders for each system were used. Clearly, the amount of information that is carried in WDM system is higher than that in a CSK system even with a lower modulation order, due to parallel transmissions.

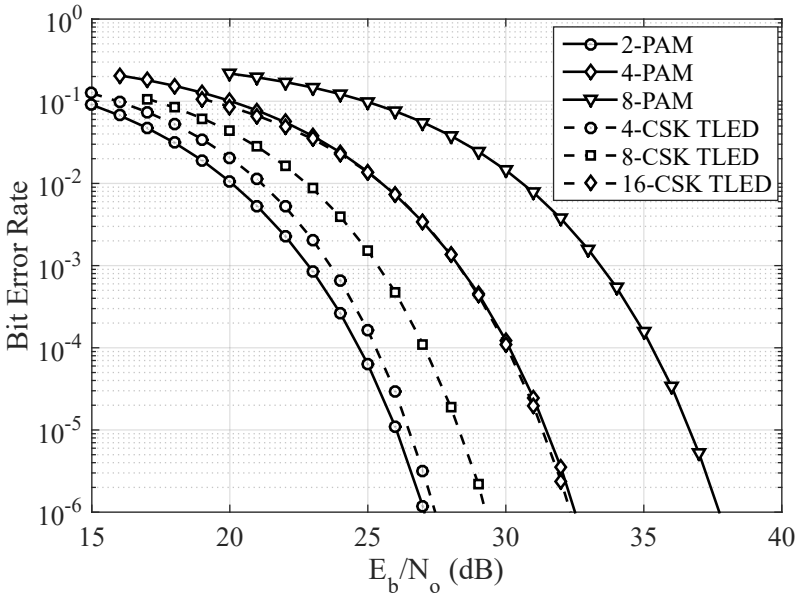

Figure 5.20: Simulations based BER performance of TLED CSK and M-PAM based WDM (concurrent transmission) systems over AWGN channel including G, with CC.

The BER performance of TLED CSK and WDM systems were compared over AWGN channel with CIL and the results are shown in Fig. 5.20. To understand these results, one must compare the performance of modulation orders which provide a same number of information bits per $\boldsymbol{i}_n$. For example, the 2-PAM based WDM and 8-CSK system will carry 3 bits in every intensity change that will take place across the CBs and the BER performance of these two systems shows that the optical power requirements of 2-PAM based WDM system will be approximately 2 dB less than the 8-CSK scheme. Therefore, for the same spectral efficiency, the WDM-PAM system will be more energy efficient than the CSK system. The 4-PAM and 8-PAM based WDM systems will require higher SNR_o, however these systems will provide higher data rates too as can be seen from Table 5.6.

Therefore, overall the WDM systems will provide much higher data rates as the modulation orders expand or as the N_b increases. However, as lighting system as well as being a communication system, CSK system becomes more useful as detailed below:

- *Intensity Flicker*: As detailed in section 5.4, CSK keeps the sum of instantaneous intensities across the CBs constant at all times. This eliminates the requirement of any flicker management in CSK. However this is not the case in OOK or M-PAM or OFDM based WDM system, where the intensity in each CB is modulated independently and the sum of intensities at the transmitter will be time varying. This imposes visible and invisible flicker issues for WDM systems, especially for low frequencies [160] and while working with large arrays of LEDs [146][147].

- *Colour Flicker*: It must be noted that CSK provides control over the output colour, which is important to control the colour temperature in CSK systems (see section 5.4). An average chromaticity value of around $[x = 1/3, y = 1/3]$ is targeted in CSK systems through constellation design to provide a colour temperature of ∼6500K. There is no direct way of controlling the colour temperature in WDM systems, other than varying the average power in each CB which will lead to the BER performance in each CB to be different and hence could require power adaptive bit loading on each CB.

5.8 Key Observations for CSK Systems

5.8.1 Implementation Issues for Higher Level Signalling

The limited dynamic range of LEDs and their sensitivity to small changes in the drive current can become a major hurdle in the implementation of the higher modulation order VLC systems, such as 64, 256, 1024 and 4096 level schemes. For example, an M-ary PAM based VLC system would require the LED to operate with M different intensity levels. This is not the case in CSK systems as each symbol can be constructed from different sets of the multi-colour LEDs used. Specifically, the QLED system is designed in a way that intensity levels required per LED (or colour) are much less than the modulation order M.

As detailed in section 5.3, the QLED CSK systems require at most three out of four LEDs to irradiate at specific intensity levels for any symbol in the constellation [150]. Also, the constellations of QLED CSK are designed such that each LED of QLED only irradiate for three quadrants of the constellations. This means, each LED of QLED is not required to irradiate at specific distinguishable intensities for every symbol in the constellation. For an even k, the number of intensity symbols in a 2^k level QLED constellation that emerge

from distinguishable intensity levels of each colour can be given as:

$$U_{QLED} = \frac{3M}{4} - 2\sqrt{M} + 3 \tag{5.18}$$

Equation (5.18) is derived from the total number of symbols in three quadrants of the constellation and the number of symbols where the intensity is the same. Table 5.7 shows U_{QLED}, the distinguish intensity levels per LED for TLED CSK ($U_{TLED} = M - 2\sqrt{M} + 3$) and M-PAM ($U_{PAM} = M$). Table 5.7 shows that the actual distinguishable intensity levels required per CB (or colour) in a QLED system are 28% to 50% less than M. Hence, simpler control of LED intensity levels with limited dynamic range is achieved.

Table 5.7: Distinguish intensity levels per LED for different VLC schemes.

M	**4**	**16**	**64**	**256**	**1024**	**4096**
U_{PAM}	4	16	64	256	1024	4096
U_{TLED}	3	11	51	227	963	3971
U_{QLED}	2	7	35	163	707	2947

Furthermore, the resolution of ADC and DAC has to be sufficiently high for error free transmission and reception. There is a trade-off between the resolution and sampling rates that these converters can have. For higher sampling rates the resolution is decreased and vice-versa. VLC systems rely upon higher sampling rates for high data transmission rates. Therefore, to keep the ADC or DAC design simple and energy efficient, the resolution has to be kept to moderate levels. QLED CSK's low U_{QLED} means that the resolution requirements will be low even at high modulation levels, hence simpler and faster ADC or DAC conversions are achievable which helps to reduce the power consumption.

5.8.2 Hardware Overhead in QLED System

The additional LED at the transmitter, PD and a filter at the receiver means the overall system cost could increase by $\approx$ 33% for a QLED system, assuming equivalent unit prices. However, the QLED scheme, when compared to TLED scheme, has an SNR gain of approximately 2.9 to 5 dB for the same data rates at a reasonable BER. This SNR gain could be traded by having less number of LED clusters in a QLED lighting scheme. For example, a TLED cluster of 9 LEDs (3 x TLED) could be replaced with an 8 LED cluster of QLED (2 x QLED) for approximately the same luminance levels, data rate and performance. This way in fact, the QLED scheme can reduce the overall costs for a CSK system.

At the same time, given a low unit price of these optical front ends, if the same number of LED clusters are used for both the TLED and QLED CSK, the QLED scheme will have higher flexibility for the data-rate vs operating range trade-off. For example, comparing the results in Fig. 5.9 and Fig. 5.10, we can notice that the 16-CSK QLED system has approximately the same E_b/N_o requirements as 4-CSK TLED. Hence, QLED CSK will almost double the data-rates for the same indoor SNR.

5.9 Summary

This chapter studies the standardised TLED CSK systems and evaluate their bit error performance based on detection in the signal and chromatic spaces. The AWGN channel based simulation and analytical investigations show that the chromatic detection is sub-optimal and increase the SNR requirements of the system when compared to the intensity detection in the signal space.

An advanced QLED CSK system has been presented and recommended over the existing TLED CSK system based on their error performance comparison in an AWGN channel. The QLED system has enhanced minimum Euclidean distance between the data symbols at the transmitter due to the use of four LEDs and also allows 1^{st} and 2^{nd} order Gray mapping. The performance evaluation shows that, comparing to a TLED scheme, the QLED scheme has an electrical SNR gain of up to 5 dB over AWGN. The analytical error performance analysis for both of the CSK schemes has also been presented for an AWGN channel.

The effects of cross-talk and insertion losses are also studied, which shows that CC is very important for CSK systems to achieve low bit error rates. The results show that 4-CSK in a QLED system can operate in the presence of cross-talk without the use of CC due to its orthogonal nature which makes the scheme an ideal signalling channel for CC estimation.

Use of concurrent transmissions over multiple CBs is also discussed to achieve higher throughput at the cost of reduced control over lighting abilities of a VLC system. It is also shown that four CB based constellation designs of QLED CSK minimise the DAC and ADC resolution requirements when compared to TLED CSK and M-PAM systems.

Chapter 6

Rate-Adaptive Coded Colour Shift Keying Systems with Frequency Domain Equalisation

6.1 Introduction

Using the standardised TLED and advanced QLED CSK systems detailed in the previous chapter as fundamental CSK systems, this chapter introduces the use of forward error correction (FEC) and channel equalisation techniques for CSK to enhance the system BER performance and overall capacity while operating over representative VLC channels. Investigations show that the two CSK systems, without the use of any channel coding and channel equalisation technique, are unable to fully utilise their spectral capabilities over the indoor hybrid and non-line-of-sight (NLOS) channels and incur large power penalties even for low modulation orders. The higher modulation order [152] CSK signals experience temporal dispersion in an indoor environment even with very strong line-of-sight (LOS). As the receiver (Rx) is horizontally moved away from the transmitter (Tx), even the low modulation orders of CSK suffer temporal dispersion due to the increased channel *rms* delay spread and reduced LOS gain. This leads to large reduction in the achievable throughput and a large increment in the SNR requirements even for low order modulation formats.

In order to combat multipath dispersion and enhance the system capacity, the use of rate-adaptive coded CSK (RAC-CSK) with frequency domain equalisation (FDE) is proposed. The RAC-CSK is found to significantly enhance the throughput of the CSK schemes when using the same standard specified bandwidth of 24 MHz. It is shown that the RAC-CSK when used with FDE, maximises the system capacity, over the representative

VLC channels. The FDE based RAC-CSK, when realised through the QLED scheme, could increase the throughput of the CSK systems beyond 250 Mbit/s when the standard specific system bandwidth is utilised.

The use of FDE for CSK is considered as it is well known for providing a low complexity means to combat temporal dispersion of a single carrier (SC) modulation based data signal [113]. As in optical OFDM [161][162], the FDE based CSK schemes will have high spectral efficiency and low computational complexity. Importantly, the FDE based RAC-CSK will have the advantage of low peak to average power ratios (PAPR) at the transmitter, which will reduce both the DC bias and the signal conditioning requirements caused by the non-linear I-V characteristics of LEDs, such as pre-distortion and power back-off [127][128].

The performance evaluation begins by comparing the throughput of the standard specific uncoded-CSK, Reed-Solomon coded CSK (RS-CSK) and RAC-CSK over the AWGN channel. The VLC standard IEEE 802.15.7 specifies the use of a fixed half-rate Reed-Solomon (RS) coding for the CSK systems, for which a hard-decision (HD) detection was used due to simpler decoding structure. The alternative FEC scheme RAC-CSK utilises the well known non-punctured (1/2 rate) and punctured (2/3 and 3/4 rate) binary convolutional (BC) codes with both HD and soft-decision (SD) detections. The HD and SD detection based RAC-CSK systems are referred to as RAC1-CSK and RAC2-CSK, respectively, in this thesis. Although a rate-adaptive RS-CSK system can also be realised, our focus on rate-adaptive BC codes is primarily due to SD detection. The analytical and simulation based throughput performance evaluation of the considered systems for an AWGN channel show that RAC-CSK outperforms the RS-CSK and uncoded-CSK achieving up to 10 and 3.7 dB SNR gains, respectively. The RS-CSK does not achieve any useful coding gain and provides low throughputs when compared to Uncoded and RAC-CSK schemes.

In the latter half of the chapter, the performance of considered systems is examined over hybrid (LOS+Diffuse) and NLOS channels. Results show that, FDE based RAC-CSK enables the use of higher modulation modes of CSK and enhances the system throughput by up to 200% and 50% for the QLED and TLED schemes, respectively, when compared to uncoded-CSK. Overall, the RAC-CSK with FDE in comparison to the uncoded-CSK, provides SNR gains between 5 to 27 dB over hybrid links and up to 12 dB over diffuse links.

The throughput of FDE based RAC-CSK can be further improved by using system bandwidth's greater than 24 MHz and/or by switching the LED at faster rates and equalising for the LED's response [28]. However, LED response equalisation is not considered in this research.

Finally, the uncoded QLED and TLED systems with FDE are studied over various diffuse links for certain normalised delay spreads. This was done to further evaluate the

effectiveness of FDE for CSK systems. The results show that the power requirements of both TLED and QLED systems, without the use of FDE, tend to infinity as the normalised delay spread increases. This is due to ISI which leads to an irreducible BER. On the other hand, the use of FDE combats ISI and reduces the power requirements of CSK systems at the cost of small overhead due to the cyclic prefix (CP).

The optical channel models detailed in Chapter 2 are used in this investigation including the reflectivity of different indoor objects for multi-colour CSK bands and the cross-talk & insertion losses incurred due to the optical properties of commercially available front-end devices.

6.2 FEC based CSK System with FDE

Fig. 6.1 shows a generic block diagram of the FDE based QLED and TLED schemes to realise RAC-CSK and RS-CSK. At Tx side the binary data is first encoded using a channel encoder, which in this chapter is either RS or punctured BC. The coded data is then grouped into $k = log_2(M)$ bits, where M is the modulation order, and mapped to dedicated chromatic pairs, given by vectors $\boldsymbol{u}_n = [x_n, y_n]^T$, where n represents the n^{th} chromatic pair. Then, from each $\boldsymbol{u}_n$, the intensity vector $\boldsymbol{i}_n = [I_{i,n}, I_{j,n}, I_{k,n}, I_{l,n}]^T$ for a QLED system can be obtained, where $I_{i,n}$, $I_{j,n}$, $I_{k,n}$ and $I_{l,n}$ represent the intensity of each CB for a certain $\boldsymbol{u}_n$.

In order to enable FDE in CSK systems, block wise transmission is used. Therefore, intensity values in each CB, are parsed into transmit intensity vectors of length N, e.g. for CB "i", a vector denoted by $\boldsymbol{v}_i = [I_{i,0}, I_{i,1}, ...I_{i,N-1}]^T$. Similarly, $\boldsymbol{v}_j$, $\boldsymbol{v}_k$ and $\boldsymbol{v}_l$ are obtained for the remaining CBs. Then a cyclic prefix (CP) of length μ is added to the front of each of these vectors, which, for example, gives the transmit vector for CB "i" as $[I_{i,N-\mu}, I_{i,N-(\mu-1)}, ...I_{i,N-1}, I_{i,0}, I_{i,1}, ...I_{i,N-1}]^T$. Therefore, each block contains a total N_{SB} sub-blocks, where $N_{SB} = N + \mu$. After digital to analogue (D/A) conversion, the transmit signals I_i, I_j, I_k and I_l are obtained which modulate the intensity of each LED source.

At the receiving end the narrow-band optical filters pass light of the desired wavelength to the PDs. The received signals at the output of the PDs can be given by equation (5.3) in section 5.5. After analogue to digital (A/D) conversion, the colour calibration as suggested in the standard [8] takes place to compensate for the cross-talk between the multi-colour channels. The instantaneous sets of intensities after calibration can be given as, $[\hat{I}_i, \hat{I}_j, \hat{I}_k, \hat{I}_l]^T = \boldsymbol{G}^{-1}[\tilde{I}_i, \tilde{I}_j, \tilde{I}_k, \tilde{I}_l]^T$. Then, after CP removal, the received intensity blocks per CB $\hat{\boldsymbol{v}}_i$, $\hat{\boldsymbol{v}}_j$, $\hat{\boldsymbol{v}}_k$ and $\hat{\boldsymbol{v}}_l$ are converted to the frequency domain using the fast Fourier transform (FFT) of size N, so that the FDE can take place. The transmit $\boldsymbol{v}_i$ and receive

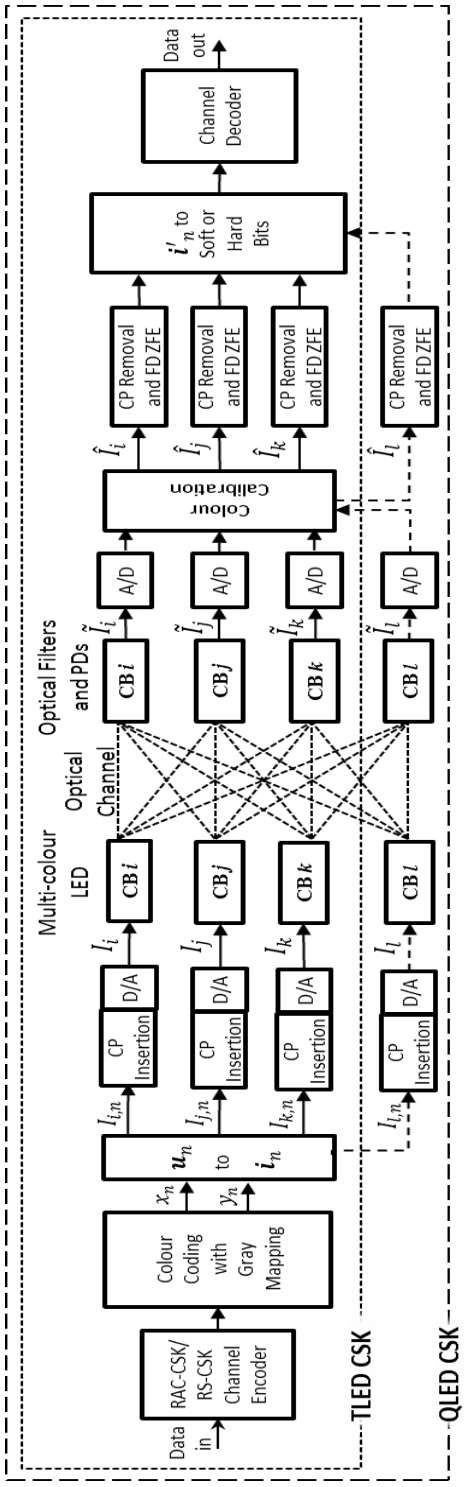

Figure 6.1: Generic schematic of the Rate-Adaptive Coded TLED and QLED CSK systems with Frequency Domain Equalisation.

$\hat{\boldsymbol{v}}_i$ vectors can be related as:

$$\hat{\boldsymbol{v}}_i = \boldsymbol{H}\boldsymbol{v}_i + \boldsymbol{n}_i \tag{6.1}$$

In equation (6.1), $\boldsymbol{H}$ is the $N \times N$ channel circulant convolutional matrix, in this case for CB "i", which can be diagonalised as $\boldsymbol{H} = \boldsymbol{F}^H \boldsymbol{\Lambda} \boldsymbol{F}$ [122], where $\boldsymbol{F}$ is the FFT matrix and $\boldsymbol{\Lambda}$ is a diagonal matrix with diagonal entries equal to the FFT of the CIR of the respective CB. The AWGN vector for CB "i" is denoted as $\boldsymbol{n}_i = [n_{i,0}, n_{i,1}, ...n_{i,N-1}]^T$.

In this research, the FDE is based on frequency domain (FD) zero-forcing equaliser, $\boldsymbol{Z} = \boldsymbol{\Lambda}^H(\boldsymbol{\Lambda}\boldsymbol{\Lambda}^H)^{-1}$. The equalised vector $\boldsymbol{v}_i^{'}$ is obtained as, $\boldsymbol{v}_i^{'} = \boldsymbol{F}^H \boldsymbol{Z} \boldsymbol{F} \hat{\boldsymbol{v}}_i$. Similarly, the vectors $\boldsymbol{v}_j^{'}$, $\boldsymbol{v}_k^{'}$ and $\boldsymbol{v}_l^{'}$ are obtained and the n^{th} received intensity vector is given as, $\boldsymbol{i}_n^{'} = [I_{i,n}^{'}, I_{j,n}^{'}, I_{k,n}^{'}, I_{l,n}^{'}]^T$. At this point, the hard and soft data bits are obtained from each $\bar{\boldsymbol{i}}_n$ as detailed in section 6.2.3.

6.2.1 Description of Modulation and FEC Schemes

The investigation of the RAC-CSK systems was based on the standardised three modulation schemes of the TLED (4, 8 and 16 level CSK) and seven modulation schemes of the QLED (4, 8, 16, 64, 256, 1024 and 4096 level CSK) with Gray mapping defined in [150]. The band-plan for TLED and QLED systems used is shown in Table 6.1.

Table 6.1: A band plan of TLED and QLED CSK.

CB	TLED-Colour	QLED-Colour	CWCV	Centre(nm)
i	Red	Red	{0.734, 0.265}	660
j	Green	Yellow	{0.402, 0.597}	570
l	–	Cyan	{0.011, 0.460}	500
k	Blue	Blue	{0.169, 0.007}	450

The FDE based RAC-CSK is realised through a rate-adaptive BC code using HD (RAC1-CSK) and SD (RAC2-CSK) detections, and their performance is compared with standard specific fixed-rate RS-CSK and the uncoded-CSK. Although a rate-adaptive RS-CSK system can also be realised, our focus on rate-adaptive BC codes is primarily due to lower complexity SD detection. The RS-CSK utilised the standard specific RS(64,32) 1/2 rate encoder with HD detection. Both the RAC1-CSK and RAC2-CSK systems used the 64 state BC code with well-known industry standard generator polynomials: {171,133} and code rates 1/2, 2/3 and 3/4 through puncturing patterns specified in [135]. These code-rates and different modulation orders of the CSK systems lead to various aggregate bit rates (equivalent spectral efficiencies or bits per channel use), $\mathrm{AR} = \Gamma \log_2(M)$, where Γ is the FEC code rate. These ARs are given in Table 6.2. A standard specific system

bandwidth (W) of 24 MHz was used throughout the performance evaluation of the coded CSK systems.

Table 6.2: Aggregate bit rates (AR) of the RS-CSK and RAC-CSK.

Modulation Order M	**RS-CSK**	**RAC-CSK, 1/2 rate**	**RAC-CSK, 2/3 rate**	**RAC-CSK, 3/4 rate**
4	1.01	1	1.33	1.5
8	1.52	1.5	2	2.25
16	2.03	2	2.67	3
64	3.04	3	4	4.5
256	4.06	4	5.33	6
1024	5.07	5	6.67	7.5
4096	6.09	6	8	9

6.2.2 Properties of Front-End Devices

For a complete performance evaluation of uncoded-CSK, RS-CSK and RAC-CSK systems, the properties of front-end devices must be taken into consideration. As detailed in section 5.6.1, the CIL matrix $\boldsymbol{G}$ can be obtained from the SPD of of LEDs, the transmissivity of optical filters and the responsivity of PDs, which introduce colour cross-talk and insertion losses in a multi-colour VLC system. Assuming the same optical front-end components as in section 5.6.1, the same matrix values for TLED (equation (5.15)) and QLED (equation (5.16)) systems were used in this chapter as well.

6.2.3 Hard and soft decision detection

The procedure to obtain the received data bits differs for the HD and SD detections. In the case of the RS-CSK and RAC1-CSK, the HD detection is used to estimate the final intensity vector $\boldsymbol{i}_n^{''}$, as:

$$\boldsymbol{i}_n^{''} = \underset{\boldsymbol{i}\in\mathcal{I}}{\arg\min} \, ||\boldsymbol{i}_n^{'} - \boldsymbol{i}||^2, \tag{6.2}$$

where, $\mathcal{I}$ contains the intensity based alphabets of the CSK constellation. The data bits are then de-mapped from $\boldsymbol{i}_n^{''}$ and fed to the RS or Viterbi decoder to decode the information bits.

In RAC2-CSK, the soft information bits, for the Viterbi decoder, can be obtained by using the maximum *a posteriori* probability (MAP) algorithm, whereby, the log-likelihood-ratio (LLR) of the q^{th} binary bit of the n^{th} received intensity vector b_n^q, for $0 \leq q \leq k-1$,

can be obtained as [163][136]:

$$\mathcal{L}(b_n^q) = \log\left(\mathcal{P}(b_n^q = 1|\boldsymbol{i}_n^{'})\Big/\mathcal{P}(b_n^q = 0|\boldsymbol{i}_n^{'})\right). \tag{6.3}$$

In equation (6.3), $\mathcal{P}(b_n^q = 1|\boldsymbol{i}_n^{'})$ is the *a posteriori* probability (APP) when b_q is equal to 1. As in [163][136], using the max-sum approximation of $\log\sum_z f(z) \approx \max_z \log f(z)$, equation (6.3) can be simplified as:

$$\mathcal{L}(b_n^q) = \max_{\boldsymbol{i}\in\mathcal{J}^{q=1}} \log p(\boldsymbol{i}_n^{'}|\boldsymbol{i}) - \max_{\boldsymbol{i}\in\mathcal{J}^{q=0}} \log p(\boldsymbol{i}_n^{'}|\boldsymbol{i}), \tag{6.4}$$

where, $\mathcal{J}^{q=1}$ and $\mathcal{J}^{q=0}$ are the subsets of the intensity based alphabets of the CSK constellation, and represent alphabets with the q^{th} bit labelled as '1' and '0', respectively. Given colour calibration and FDE has taken place, in equation (6.4), the conditional probability density function (pdf), $p(\boldsymbol{i}_n^{'}|\boldsymbol{i})$ can be expressed as, $p(\boldsymbol{i}_n^{'}|\boldsymbol{i}) = (1/\sqrt{2\pi}\sigma_T)\exp(-||\boldsymbol{i}_n^{'}-\boldsymbol{i}||^2/2\sigma_T^2)$, where, σ_T^2=$3\sigma^2$ for a three colour system and σ_T^2=$4\sigma^2$ for a four colour system. Therefore, to obtain the LLRs, equation (6.4) can be further simplified as:

$$\mathcal{L}(b_n^q) = \frac{1}{2\sigma_T^2}\{\min_{\boldsymbol{i}\in\mathcal{J}^{q=0}} ||\boldsymbol{i}_n^{'} - \boldsymbol{i}||^2 - \min_{\boldsymbol{i}\in\mathcal{J}^{q=1}} ||\boldsymbol{i}_n^{'} - \boldsymbol{i}||^2\}. \tag{6.5}$$

6.3 Performance of FEC based CSK Systems over AWGN

Prior to the study of FDE based RAC-CSK systems, the performance of RAC-CSK systems was examined through simulations and analytical formulations over the AWGN channel and was compared to the standard specific fixed rate RS-CSK and Unocded-CSK systems. This was done to identify the more efficient coded CSK system and to validate the CSK simulators. As mentioned in the previous chapter, the AWGN channel based investigation is carried out assuming multipath free environment and without any CIL i.e. identity $\boldsymbol{G}$. Therefore, the system can be mathematically represented by equation (5.5).

Fig. 6.2 and Fig. 6.3 show the absolute throughput (T) for the TLED and QLED schemes in AWGN, respectively, using the uncoded-CSK, RS-CSK, RAC1-CSK and RAC2-CSK transmissions. Throughout the investigation, a standard specific CSK system bandwidth (W) of 24 MHz was used to see how the RAC-CSK systems improve the system performance given this fixed W. The T is calculated as:

$$T = W\Gamma\log_2(M)\mathcal{P}_{SR}, \tag{6.6}$$

where, $\mathcal{P}_{SR}$ is the packet success rate given as $\mathcal{P}_{SR} = (1 - \text{BER})^{\ell}$ for a packet length ℓ in bits. 1500 bytes long packets were transmitted during all the simulations considered in

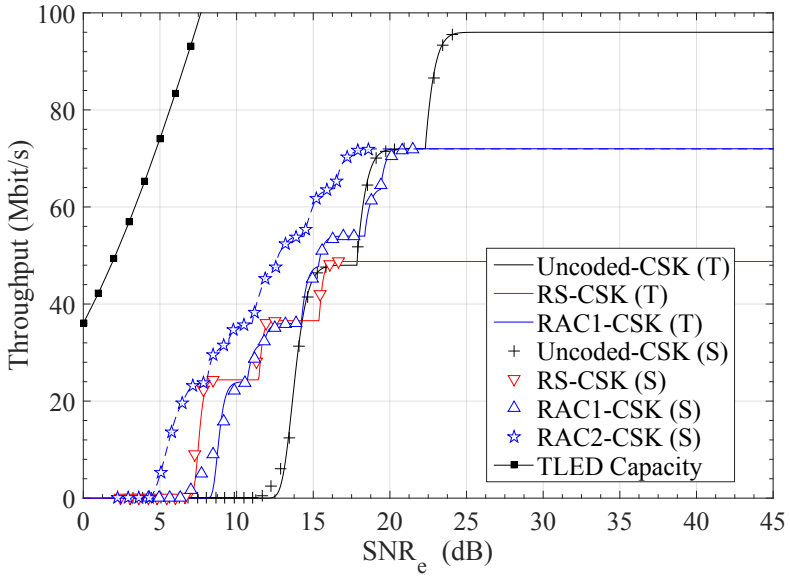

Figure 6.2: Theoretical (T) and simulation (S) results of the T of the coded and uncoded TLED CSK systems over an AWGN channel. The dashed line shown with RAC2-CSK results is obtained through curve fitting of simulation results.

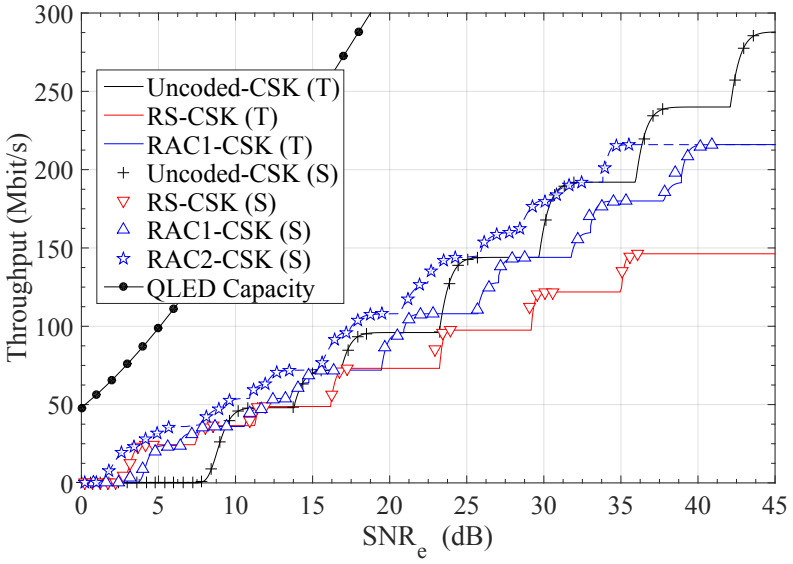

Figure 6.3: Theoretical (T) and simulation (S) results of the T of the coded and uncoded QLED CSK systems over an AWGN channel. The dashed line shown with RAC2-CSK results is obtained through curve fitting of simulation results.

this paper. In the case of RAC-CSK, the T curves are optimised by selecting the most effective combinations of Γ and M.

The T of different techniques is compared against the average electrical-SNR per CB (SNR_e) and results show that for both CSK systems the RAC2-CSK transmission provides the maximum T for the majority of the SNR_e values considered. In the TLED system, RAC2-CSK scheme achieves a maximum SNR gain of 3.7, 3 and 2.7 dB over the uncoded-CSK, RS-CSK and RAC1-CSK, respectively. Similarly, in the QLED system, the RAC2-CSK achieves a maximum SNR gain of 2.5, 10 and 5 dB over the uncoded-CSK, RS-CSK and RAC1-CSK, respectively.

Overall, for SNR_e above 22.5 dB in TLED and 36.5 dB in QLED, the uncoded-CSK achieves the highest T. Although, the HD schemes do not provide any significant gain over the uncoded-CSK, the RAC1-CSK achieves higher T when compared to the RS-CSK for SNR_e values above 16 dB and 19 dB for TLED and QLED systems, respectively. It is well known in communications that half-rate RS encoders are not optimum for the Gaussian channels [155]. A reason for RS codes to be specified for use in CSK PHY could be low complexity HD detection in the chromatic space.

6.3.1 Analytical Performance of RS-CSK and RAC-CSK

In Fig. 6.2 and Fig. 6.3, the theoretical results for the uncoded-CSK, RAC1-CSK and the RS-CSK are also shown and they agree closely with the simulation results. These theoretical throughput results are obtained from the theoretical bit error probabilities. The bit error probability of the uncoded-CSK systems can be estimated through the union bound as shown in section 5.5.1 (equation (5.10)). Details of the theoretical estimation of the bit error probabilities of RAC1-CSK and RS-CSK are derived in the following subsections.

RAC1-CSK

The bit error probability for the RAC1-CSK scheme can be estimated analytically as shown in chapter 4 through equations (4.10) and (4.11).

RS-CSK

The analytical bit error probability of a GF(2^κ) RS-CSK can be given as [138]:

$$\mathcal{P}_{b(\text{RS})} = \frac{2^{\kappa-1}}{2^\kappa - 1}\mathcal{P}_{s(\text{RS})}, \tag{6.7}$$

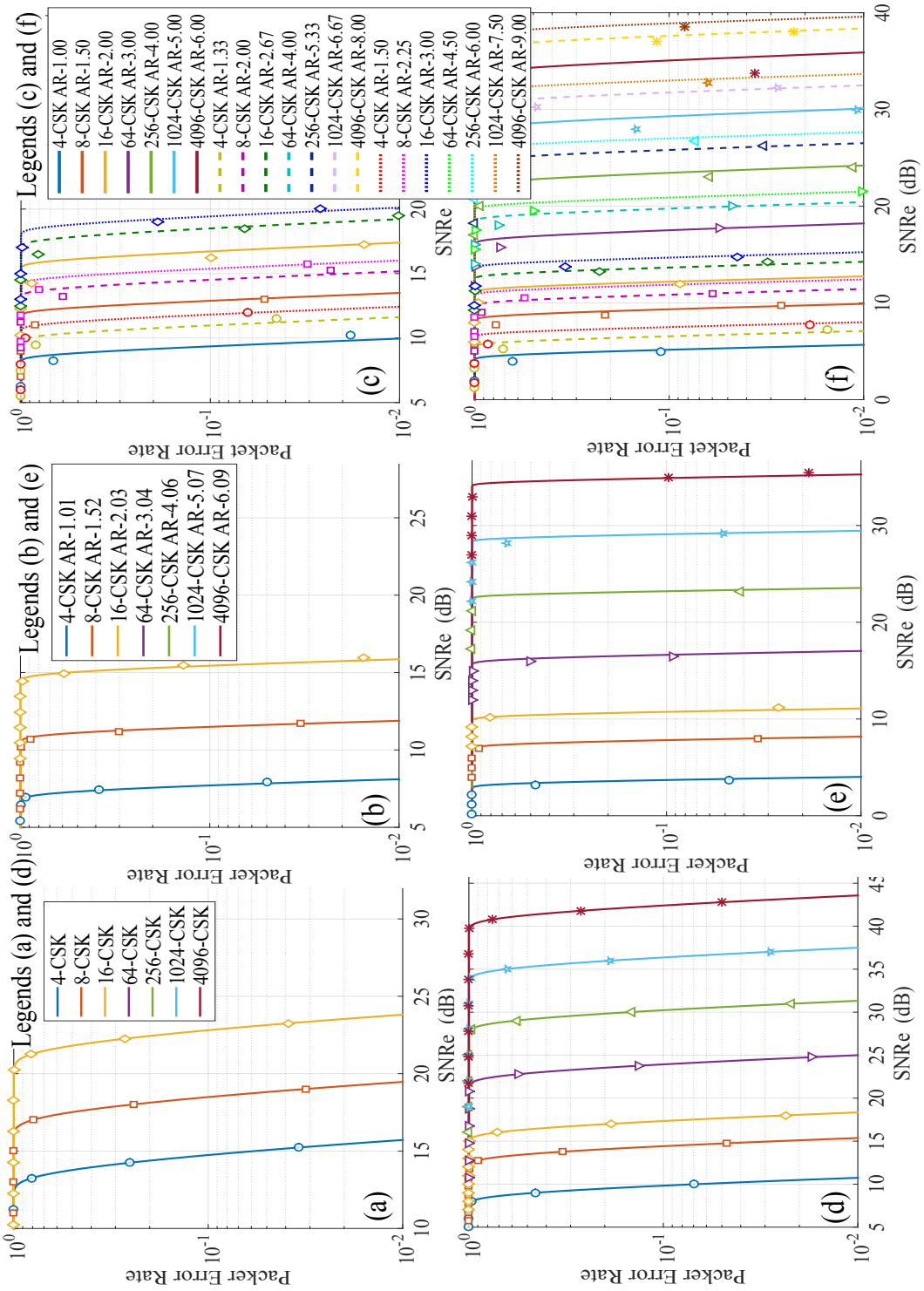

Figure 6.4: Theoretical (Lines) and simulation (Markers) results of the PER of a) the uncoded-CSK TLED, b) the uncoded-CSK QLED, c) the RS-CSK TLED, d) the RS-CSK QLED, e) the RAC1-CSK TLED, f) the RAC1-CSK QLED over AWGN. The aggregate bit rate, $\mathrm{AR} = \Gamma \log_2(M)$.

where, κ is the number of bits in a RS symbol and $\mathcal{P}_{s(\mathrm{RS})}$ is the symbol error probability of the RS codes, which can be given as [138]:

$$\mathcal{P}_{s(\mathrm{RS})} = \frac{1}{2^{\kappa}-1} \sum_{j=\epsilon+1}^{2^{\kappa}-1} j \binom{2^{\kappa}-1}{j} (\hat{\mathcal{P}}_{s(\mathrm{RS})})^{j} (1-\hat{\mathcal{P}}_{s(\mathrm{RS})})^{2^{\kappa}-1-j}, \tag{6.8}$$

where, ϵ is the error correction capability of the RS code with minimum distance D_{min} and is given by:

$$\epsilon = (D_{min} - 1)/2 \tag{6.9}$$

In equation (6.8), the $\hat{\mathcal{P}}_{s(\mathrm{RS})}$ is the upper bound on the symbol error probability of the RS codes and it can be approximated as $\hat{\mathcal{P}}_{s(\mathrm{RS})}=1-(1-\mathcal{P}_b)^{\kappa}$ [164]. The bit error probabilities of equation (4.10), (6.7) and (5.10) for the RAC1-CSK, RS-CSK and uncoded-CSK, respectively, can be easily converted to the packet error and/or success probabilities. For completeness, the packet error rates (PER) for QLED and TLED CSK transmissions, obtained through simulations and theoretical formulations, are presented in Fig. 6.4.

Fig. 6.2 and Fig. 6.3 also show the Shannon capacity curves for TLED and QLED systems for an AWGN channel. For bandwidth W, the capacity of CSK systems, based on Shannon's capacity formula, can be obtained from equation (6.10), where the $1/2$ term indicates the use of real signalling sets and N_b is the total number of CBs used in the CSK system.

$$C = \frac{1}{2} N_b W \log_2(1 + \mathrm{SNR_e}) \tag{6.10}$$

6.4 Performance of CSK systems over Indoor VLC Channels

In this section, the performance of RAC-CSK is examined over indoor VLC hybrid and diffuse links. The throughput performances of uncoded-CSK, RAC2-CSK only and RAC2-CSK with FDE are compared. The RAC2-CSK has been selected as the coded CSK systems as it achieves the highest throughputs in AWGN channels, outperforming RS-CSK and RAC1-CSK.

Experimental Set-up

An indoor environment as shown in Fig. 2.3 of size ($5 \times 5 \times 3$) m was assumed. The transmitter Tx situated at the ceiling height and a receiver Rx at desk level height as in [46][66]. It is assumed that the unit normal vectors of Tx and Rx are (0,0,-1) and (0,0,1), respectively. The indoor wireless VLC channel between Tx and Rx is composed of a LOS

path and multiple delayed paths reflected off the walls, ceiling, floor and other indoor objects. The impulse response of such a hybrid channel containing LOS and multiple reflected paths can be modelled as equation (2.13).

Five different hybrid links were used for the performance evaluation, each with different Rx locations A, B, C, D and E, as shown in the top view of the room in Fig. 6.5. The Tx is situated at the centre of the room shown in Fig. 2.3 at location (2.5, 2.5, 2.5) m. The details of the Rx locations can be found in Table 6.4. Different system parameters are listed in Table 6.3. The ϕ and ψ can be calculated from the orientation and position of the Tx and Rx in the model room. In this research, the CSK systems have been studied without the use of an optical concentrator, therefore, $g_c(\psi)$ is unity.

Table 6.3: VLC System Parameters.

Parameter	Value
A	10 mm^2
A_{Room}	110 m^2
$g_c(\psi)$	1
PD FOV, Ψ	70°
LED semiangle at half power, $\phi_{\frac{1}{2}}$	60°

6.4.1 Performance over Hybrid Channels

Table 6.4: The τ_{rms} and K values of different CBs for different Rx locations while the Tx is located at $(2.5, 2.5, 2.5)$, at standard specific symbol rate of 24 MS/s.

Rx Location	Coordinates (m)	CB-Blue/Cyan		CB-Green/Yellow		CB-Red	
		τ_{rms} (ns)	K(dB)	τ_{rms} (ns)	K(dB)	τ_{rms} (ns)	K(dB)
A	$(2.5, 2.5, 0.85)$	0.363	23.8	0.395	23.0	0.489	21.0
B	$(2, 2, 0.85)$	0.508	20.8	0.552	20.0	0.685	18.0
C	$(1.5, 1.5, 0.85)$	1.089	14.2	1.184	13.4	1.465	11.4
D	$(1, 1, 0.85)$	2.237	6.8	2.436	6.0	3.029	4.0
E	$(0.5, 0.5, 0.85)$	4.061	0.0	4.412	-0.8	5.443	-2.8

The impulse response $h(\tau)$ (equation 2.13) for each CB in TLED and QLED CSK was obtained based on the properties of the room in Fig. 2.3, the system parameters shown in Table 6.3, and the ρ values of the room ceiling, plaster wall, plastic wall and room floor for

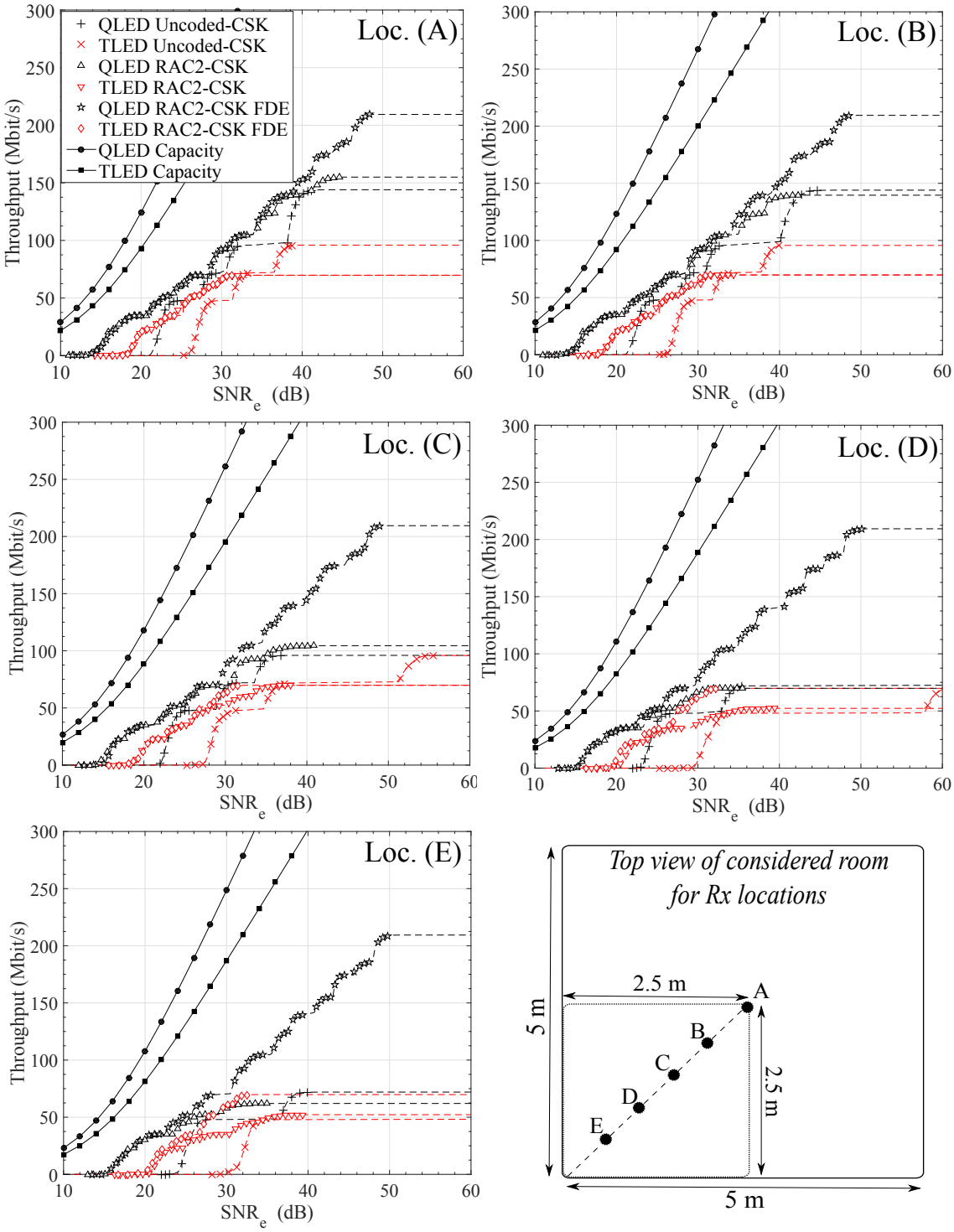

Figure 6.5: The throughput of uncoded-CSK, RAC2-CSK and RAC2-CSK with FDE for both TLED and QLED schemes at Rx locations A, B, C, D and E in the model room (of Fig. 2.3). The markers signifies simulation results and the dashed curves are obtained by curve fitting from the simulation results.

different colour channels. The ρ values observed in [53] for CBs Blue/Cyan, Yellow/Green and Red are 0.454, 0.477 and 0.534, respectively, which were used to evaluate each $h(\tau)$. The values of $\boldsymbol{G}$ for TLED and QLED systems provided in equation (5.15) and (5.16), respectively, were used.

The channel *rms* delay spreads (τ_{rms}) and K-factor experienced at each Rx location in each CB were calculated through equation (2.18) and (2.14), respectively. These two characteristics are shown in Table 6.4, which show that minimum dispersion will be experienced at the centre (Location A) of the room, where K is largest as η is much larger than ζ. As the Rx is moved towards location E, K decreases and τ_{rms} increase as ζ becomes comparable to η. Additionally, at each location, τ_{rms} is lowest for the blue CB where ρ is smallest and τ_{rms} is highest for Red CB where ρ is highest.

For the FDE based RAC-CSK system, an N of 64 was used, to keep the sub-block (or sub-carrier) bandwidth ($W_N{=}\frac{W}{N}$) much less than the channel coherence bandwidth ($W_C{=}\frac{0.2}{\tau_{rms}}$), i.e. $W_N << W_C$. The standard specific W, and the τ_{rms} experienced in the worst hybrid links (Location E) and diffuse link (sec. 6.4.2), estimates that an N of 8 could be used to decrease the system complexity, given $W_N{=}0.1W_C$ [71]. On the other hand, an FFT size of 64 provides good complexity compromise and has been used in many standard communications systems such as Wi-Fi. Additionally, to achieve high throughputs, VLC systems are expected to switch LEDs beyond their cut-off bandwidths, as well as μ-LEDs suitable for VLC with cut-off bandwidths greater than 100 MHz have been produced [39]. This means N much greater than 8 will be required, to achieve very high throughputs for CSK systems with $W >> 24$ MHz. The value of μ was computed as $\mu{=}\frac{\tau_{rms}}{T_s}{-}1$ [71], where T_s is the sample duration, which gave μ of 2 for the location E hybrid link and diffuse link. Therefore, $\mu{=}2$, was used for all the investigations over the indoor VLC channels investigated.

Fig. 6.5 shows the throughput (T) vs $\mathrm{SNR_e}$ plots of the uncoded-CSK, RAC2-CSK, and RAC2-CSK with FDE for TLED and QLED schemes at the considered Rx locations. The T for the uncoded-CSK and RAC2-CSK can be estimated from equation (6.6), which can be modified for FDE based RAC2-CSK as:

$$T = \frac{N\mathcal{P}_{SR}W}{N_{SB}}\Gamma\log_2(M) \tag{6.11}$$

and the capacity curves are obtained by modifying equation (6.10) as:

$$C = \frac{1}{2}\frac{N_bW}{N_{SB}}\sum_{n=0}^{N-1}\log_2(1+\mathrm{SNR_e}(n)), \tag{6.12}$$

where, $\mathrm{SNR_e}(n)$ is the average electrical SNR for the i^{th} sub-block per CB and is given for TLED system as:

$$\begin{aligned}\mathrm{SNR_e}(n) &= \frac{\left\{\mathfrak{T}_i\Re_i\boldsymbol{\nu}_{i,n}\boldsymbol{p}_{i,n}\right\}^2}{3\boldsymbol{\sigma}^2_{i,n}} + \frac{\left\{\mathfrak{T}_j\Re_j\boldsymbol{\nu}_{j,n}\boldsymbol{p}_{j,n}\right\}^2}{3\boldsymbol{\sigma}^2_{j,n}} \\ &+ \frac{\left\{\mathfrak{T}_k\Re_k\boldsymbol{\nu}_{k,n}\boldsymbol{p}_{k,n}\right\}^2}{3\boldsymbol{\sigma}^2_{k,n}} \end{aligned} \tag{6.13}$$

where, $\mathfrak{T}_i$ and $\Re_i$ are the transmissivity of filters and responsivity of the PDs of CB "i", respectively. $\boldsymbol{\nu}_{i,n}$, $\boldsymbol{p}_{i,n}$ and $\boldsymbol{\sigma}_{i,n}$ represent the channel gain, signal power and noise power of the n^{th} sub-block in CB "i", respectively, with $\boldsymbol{\nu} = |\mathrm{diag}(\boldsymbol{\Lambda})|$.

The results in Fig. 6.5 show that as the Rx is shifted from the centre of the room towards the corner, T of QLED and TLED uncoded-CSK systems is affected severely and the $\mathrm{SNR_e}$ requirements increase rapidly for certain T. At location A, where the Tx and Rx are directly facing each other ($\phi, \psi = 0°$), it can be seen that maximum T of QLED uncoded-CSK is restricted to ∼140 Mbit/s. This is because the higher level QLED modulations [152] (256, 1024 and 4096 CSK) suffer irreducible BER due to ISI. The signal spreading at location A is very low due to high η, which allows lower order modulations to operate successfully. As the Rx is moved to location E, the T of QLED and TLED uncoded-CSK is reduced to ∼70 and ∼48 Mbit/s, respectively. This happens as the lower order modulations also suffer irreducible BER over relatively more dispersive channels at Rx locations away from the room centre.

From the RAC2-CSK T curves in Fig. 6.5, it can be seen that across the considered Rx locations, without FDE, RAC2-CSK reduces the $\mathrm{SNR_e}$ requirements by up to approximately 7 and 9 dB for QLED and TLED systems, respectively. The $\mathrm{SNR_e}$ reduction is higher at low T and lower at high T. However, it can be noticed that RAC2-CSK without FDE is not able to utilise the higher order modulations of CSK systems to maximise the capacity. Therefore, the use of FDE is essential. The results for RAC2-CSK systems with FDE show the best achievable T at any given $\mathrm{SNR_e}$. The effectiveness of FDE can be seen from the behaviour of FDE based RAC2-CSK results, which show a very similar $\mathrm{SNR_e}$ requirements for CSK systems at any of the considered locations. Overall, across all the Rx locations, the RAC2-CSK with FDE enhances the system T between 50% to 200% for the QLED scheme and T up to 50% for the TLED scheme.

Table 6.5 shows the maximum achievable $\mathrm{SNR_e}$ gains through FDE based RAC2-CSK in comparison with the uncoded-CSK for same T, which are obtained from the results in Fig. 6.5. It can be seen that over the considered Rx locations, the combined FDE and

Table 6.5: Maximum SNR gain achievable through RAC-CSK with FDE in hybrid links for T between 25 Mbit/s and 200 Mbit/s.

	A	**B**	**C**	**D**	**E**
QLED SNR_e Gain (dB)	5	5.5	6	8	10
TLED SNR_e Gain (dB)	6.5	7	8	27	11

coding gains can reach 10 and 27 dB[1] for QLED and TLED schemes, respectively. Further coding gains can be obtained through the use of more complex concatenated convolutional and RS codes, and Turbo codes. This is a topic of further research for the authors. The BC code of constraint length 7 used in our investigation has been widely used in wireless communication systems. Therefore, practical implementation of proposed CSK systems will be straightforward.

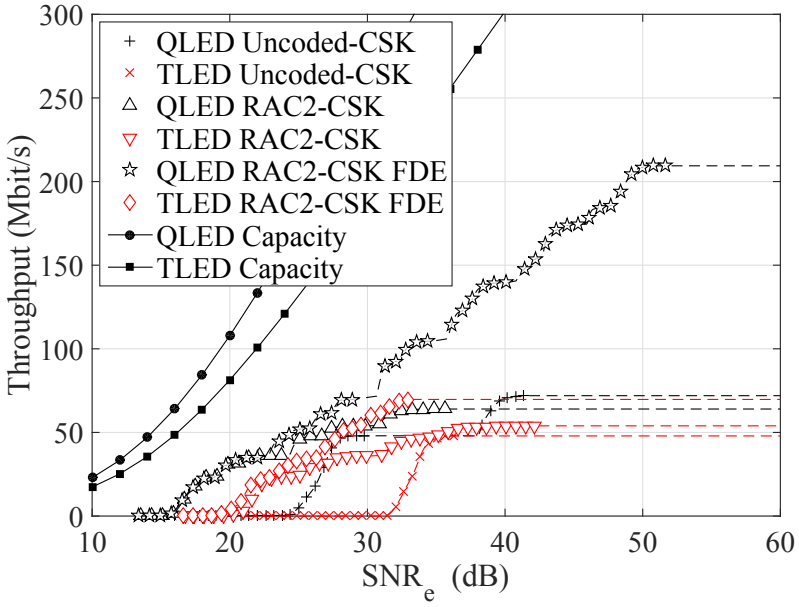

Figure 6.6: The throughput of uncoded-CSK, RAC2-CSK and FDE based RAC2-CSK for both TLED and QLED schemes for a diffuse link in the model room (of Fig. 2.3). The markers signifies simulation results and the dashed curves are obtained by curve fitting from the simulations.

Interleaving can be used to further enhance the performance of the RAC-CSK systems. The performance of RAC2-CSK with a random bit-interleaver was tested at locations A

[1]The SNR_e gain at location "D" for the TLED system is very high due to high SNR_e requirement of the uncoded-CSK scheme to operate at ∼72 Mbit/s at this location. At location "E", TLED's uncoded-CSK cannot operate at 72 Mbit/s due to high levels of ISI. Therefore, the maximum SNR_e gain is seen at a lower T of ∼48 Mbit/s.

and E of the room. The of depth the interleaver was set equivalent to the data packet size. This experiment showed that the SNR_e requirements can be further reduced by up to 1 dB. Therefore, bit and/or block interleavers specifically designed for CSK VLC systems could be used to further enhance the system performance.

6.4.2 Performance over Diffuse Channel

In this section the performance of FDE based RAC-CSK systems is examined over NLOS indoor link. In practical scenarios, the LOS in hybrid indoor links can be either blocked or may not be present due to the limited Rx FOV. In this case the VLC systems must rely upon the diffuse signals. The impulse response of diffuse indoor links has been verified through measurements in [57] and can be given as equation (2.7), which is the same as equation (2.13) when η=0.

It is shown in [57], that the optical power and the cut-off bandwidth of the channel in diffuse links are uniform across a room of the type considered and depends upon ρ and $\langle t \rangle$. Therefore, $h_{Dif}(\tau)$ is also uniform across the room. The τ_{rms} in this case can also be approximated as $\tau_{rms}=\tau_c/2 = -\langle t \rangle / 2\ln(\rho)$ [143]. For the considered room (Fig. 2.3) and the ρ values used in the previous section, the τ_{rms} for each of the CB (from i to l) in QLED CSK approximate to 5.7, 5.7, 6.1 and 7.2 ns. These values are similar to those noted in hybrid links at location E. This behaviour of hybrid links is also seen in [57], where it is shown that the hybrid link's optical powers and cut-off bandwidths decrease as a function of η and tend to be similar to those in diffuse links as the Rx moves from the room centre (where Tx is situated) towards the walls.

Fig. 6.6 show the throughput performance of the uncoded-CSK, RAC2-CSK only and FDE based RAC2-CSK. For the FDE based RAC2-CSK systems, N was kept at 64 in this case thereby satisfying $W_N << W_C$ and μ of 2 was sufficient to avoid ISI. The results for the diffuse channel are similar to those at location E in the hybrid links (Fig. 6.5) for the FDE based system. However, the systems without FDE require approximately 1-2 dB more SNR_e for the same T. This is because the delay spreads are relatively higher in the diffuse link.

Overall, the results over a diffuse channel show that through the FDE based RAC2-CSK systems, a maximum SNR_e gain of $\sim$12 dB can be achieved for both the TLED and QLED schemes when compared to the uncoded-CSK systems. Additionally, the overall T is enhanced by up to 200% and 50% for QLED and TLED schemes, respectively, with the use of FDE based RAC2-CSK.

6.5 Uncoded CSK over Different Diffuse Links

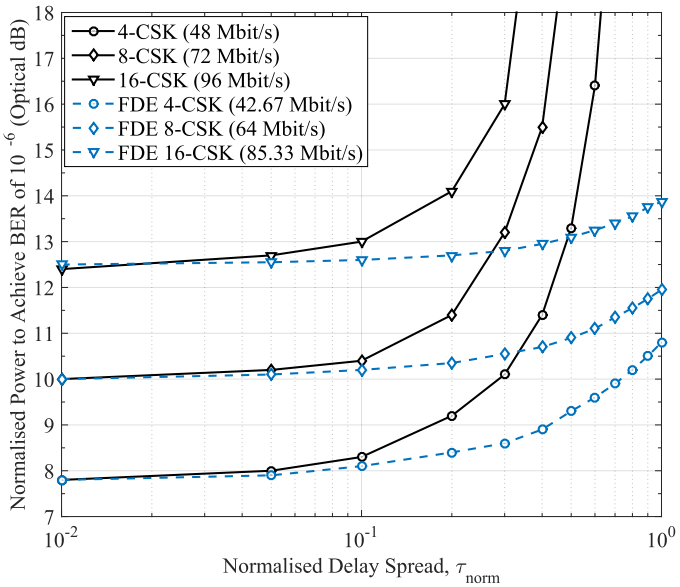

Figure 6.7: Dependence of unequalised and equalised multipath normalised power requirements on normalised delay spread, for TLED CSK modulations, to achieve a BER of 10^{-6}. All the power requirements are normalised relative to the optical power required by OOK over an AWGN channel, which is ∼7dB.

In this section, the performance of uncoded TLED and QLED CSK systems over a non-LOS (Diffuse) optical wireless channels with and without the use of FDE is investigated. This was done to examine further the effectiveness of FDE for CSK system, while operating over highly dispersive diffuse links. In this case, the channel impulse response remains same (equatio (2.7)), however, ζ was kept at unity and τ_c was varied, which produced a range of channel normalised delay spread τ_{norm} values for a fixed bit rate, T_b. τ_{norm} and T_b are related as $\tau_{norm} = \tau_c/2T_b$. The standard specific switching rate of 24 MHz (or Mega symbol per second) was assumed. This gives uncoded and unequalised data rates of up to 96 Mbit/s (64-CSK) for the TLED scheme and 288 Mbit/s (4096-CSK) for the QLED scheme. The data rates for different modulation orders of CSK can be calculated as:

$$\text{Data Rate} = \left(\frac{N}{N_{SB}}\right) W \log_2(M) \tag{6.14}$$

During the simulations, values used for N and μ were 64 and 8, respectively. To minimise the effect of cross-talk on the performance of the TLED and QLED systems, at the receiver, colour calibration as suggested by the standard [8], was used.

Fig. 6.7 and Fig. 6.8 show the optical power requirements of the uncoded-unequalised

Table 6.6: Normalised optical power requirements of uncoded-unequalised and uncoded-FDE based TLED and QLED CSK systems for a D_t of 0.1, 0.5 and 1.

Modulation Schemes			Optical Power Requirements (dB) for $\tau_{norm} = 0.1$	Optical Power Requirements (dB) for $\tau_{norm} = 0.5$	Optical Power Requirements (dB) for $\tau_{norm} = 1$
Unequalised	TLED	4-CSK	8.3	16.4	∞
		8-CSK	10.4	∞	∞
		16-CSK	13	∞	∞
	QLED	4-CSK	5.4	7.6	20.5
		8-CSK	8.3	11.8	∞
		16-CSK	10.2	14.6	∞
		64-CSK	13.7	∞	∞
		256-CSK	17.9	∞	∞
		1024-CSK	22.1	∞	∞
		4096-CSK	∞	∞	∞
FDE-ZFE	TLED	4-CSK	8.1	9.3	10.8
		8-CSK	10.2	10.9	11.95
		16-CSK	12.6	13.1	13.87
	QLED	4-CSK	5.3	6.4	7.9
		8-CSK	8.15	8.8	9.9
		16-CSK	10	10.55	11.3
		64-CSK	13.62	13.95	14.42
		256-CSK	16.9	17.07	17.5
		1024-CSK	20.06	20.22	20.52
		4096-CSK	23.14	23.32	23.52

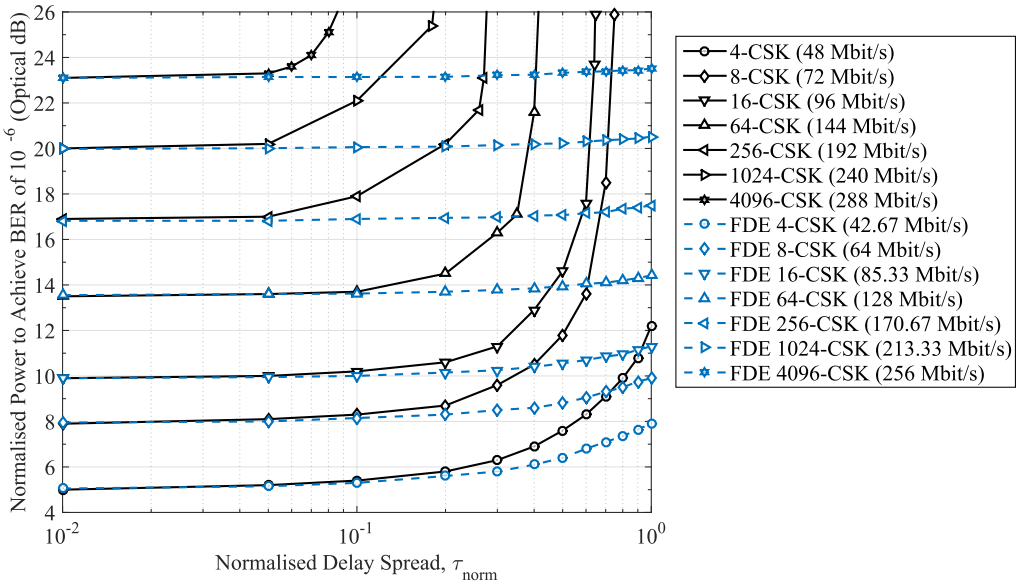

Figure 6.8: Dependence of unequalised and equalised multipath normalised power requirements on normalised delay spread, for QLED CSK modulations, to achieve a BER of 10^{-6}. All the power requirements are normalised relative to the optical SNR required by OOK over an AWGN channel, which is ∼7dB.

and uncoded-FDE based TLED and QLED CSK schemes, respectively, over a scale of τ_{norm}. The results show that the FDE based CSK modulation schemes offer a large amount of reduction in the optical power requirements, as τ_{norm} increases, when compared to the unequalised CSK schemes. The FDE enables both QLED and TLED CSK to operate at their highest data rates using a finite amount of optical power over the diffuse optical channels with large delay spreads. Fig. 6.7 and Fig. 6.8 also show that the data rates of each modulation scheme reduce by ∼12% when FDE is used due to the CP overhead. This gives a highest data rate of 85.33 Mbit/s for the TLED and 256 Mbit/s for the QLED scheme.

Using the results in Fig. 6.7 and Fig. 6.8, Table 6.6 compares the optical power requirements of both the CSK schemes, with and without the use of an equaliser, for three optical channels with different τ_{norm}. Table 6.6 shows that FDE does not only allow higher data rate transmission for CSK schemes by enabling good data links for higher order modulations, but it also reduces the power requirements of the lower order modulation modes which require high optical powers without the use of FDE. The power reductions with FDE range from 0.08 dB to ∞[1].

Table 6.6 also shows that for the target BER of 10^{-6} the QLED CSK is more robust to

[1] ∞ amount of power reduction correspond to a condition, where the unequalised CSK systems suffer irreducible bit error rate due to ISI

channel dispersion effects than the TLED CSK. It can be seen that the 4-CSK of QLED scheme is the only modulation which can achieve the target BER without using FDE for a finite amount of optical power over a channel with $\tau_{norm} = 1$. Whereas with the use of FDE, the QLED scheme can provide the same data rates as the TLED scheme requiring 2.05 to 2.9 dB less optical power. This power gain of QLED scheme is mainly due to larger Euclidean distances between symbols restored after equalisation.

6.6 Summary

This chapter proposes the use of RAC-CSK with low complexity FDE for the standardised TLED and advanced QLED schemes, while operating over indoor hybrid and NLOS links. It is shown through simulations and analytical approximations that RAC-CSK systems will provide the highest throughputs for a certain electrical SNR and that the standard specific RS-CSK is unable to provide any significant channel coding gains.

The performance analysis of the conventional CSK systems suggests that the higher modulation modes will not be able to operate even in the presence of strong LOS and as the signal dispersion is increased from moderate to high levels even lower modulation modes suffer ISI and incur irreducible BERs/PERs. This restricts the multi-colour VLC schemes' ability to operate at their maximum capacities. The FDE based RAC-CSK systems enable the higher modulation modes of CSK to operate over hybrid and NLOS links. Though RAC-CSK with FDE will increase the overall system complexity and signalling overhead, it will enhance the system throughputs by up to 200% and reduce the SNR requirements by up to 27 dB depending on the severity of dispersion. These gains will be vital when extending the bandwidth of CSK to achieve even higher data rates.

Chapter 7

Conclusions

This research started with an aim to explore and extend the capabilities of physical layer techniques for VLC systems which enables the use of visible spectrum for wireless communication to support future communication networks meet foreseen data demands. The objective of this research was to explore the state-of-the-art VLC modulation, coding and channel equalisation techniques, and evaluate their key performance characteristics, identify performance limiting factors and propose novel solutions.

Being a hybrid communication and lighting system, VLC signalling schemes must also fulfil the lighting requirements especially when used with multi-colour LEDs where control of LED array's output colour becomes critical. Therefore, the thesis was focused on both the conventional single and multiple channel VLC signalling sets, such as optical OFDM and PAM schemes, as well as IEEE standardised CSK schemes which are specifically designed to meet indoor illumination requirements while working with multi-colour LEDs.

Throughout the thesis, focus has been the bit and/or packet error rate performance enhancement of VLC physical layers, while the system operates over representative VLC channels, thereby improving the throughput for a given SNR. Novel MCM and multi-colour SCM schemes have been proposed which enhance the overall data throughputs when compared to the existing schemes. The use of well-known rate-adaptive FEC scheme is proposed for both SCM and MCM systems which significantly enhances their throughput over LOS and NLOS indoor links. In order to mitigate ISI in CSK systems, use of frequency domain channel equalisation has been proposed, which allows the multi-colour VLC scheme to work with very high modulation orders over dispersive VLC channels.

After providing an overview of VLC systems, standards and representative channel models the investigations begin by studying the performance of various non DC-biased MCMs, DC-biased MCM and DC-biased SCM systems over an AWGN channel. It is shown that due to low PAPRs, the DC-bias requirements of multilevel DCO-PAM SCM are lower than the multilevel DCO-OFDM MCM, which leads to an SNR gain of up to 9.3

dB for the SCM scheme over the AWGN channel. A key outcome from Chapter 3 is the spectral efficiency and SNR requirement comparison of DCO-OFDM and non DC-biased ACO-OFDM, Flip-OFDM and U-OFDM MCM systems, which shows that with increasing spectral efficiency, the DCO-OFDM system becomes more power efficient than the non DC-biased counterparts. It was also shown that for spectral efficiencies above 3 bit/s/Hz, the complexity of non DC-biased systems will make them impractical.

A new optimal channel partitioning MCM system named DCO-VC has been proposed. The DCO-VC system uses the CSI at the transmitter to decompose the VLC channel into orthogonal sub-channels which are modulated with M-PAM alphabets. The PAPRs and hence the DC-bias requirements for DCO-VC and DCO-OFDM systems are found to be the same. The throughput performance of DCO-OFDM, DCO-VC and DCO-PAM systems has also been evaluated and compared over representative LOS and NLOS VLC channels. The uncoded system throughputs for the DCO-OFDM and DCO-VC system for LOS and less dispersive NLOS channels are found to be the same. However, for highly dispersive NLOS channels the uncoded DCO-VC system outperforms the uncoded DCO-OFDM by an electrical SNR gain of up to 1 dB.

In order to enhance the throughput of SCM and MCM systems, use of rate-adaptive BC codes with Viterbi decoder has also been proposed. It is shown through simulations and analytical formulations that well-known industry standard punctured BC codes can reduce the SNR requirements of DCO-OFDM, DCO-VC and DCO-PAM systems by up to 9 dB over representative VLC channels. Both hard and soft decision detection were investigated for coded SCM and MCM systems. While the hard decision detection provided some SNR gain at very low throughputs, the soft decision detection was found to be the most efficient across a wide range of throughputs for each system.

Analysis of throughput results obtained for coded DCO-OFDM and DCO-VC systems for VLC channels showed that BC coding gain was higher for DCO-VC systems than that for DCO-OFDM. The coded DCO-VC system could provide up to 3 dB SNR gain when compared to the coded DCO-OFDM system. Overall, due to low DC-bias requirements the DCO-PAM system was found to be the most power efficient for any throughput when compared to DCO-OFDM and DCO-VC systems providing up to 12 and 11 dB electrical SNR gains, respectively. This and the low hardware complexity of the DCO-PAM SCM signalling makes them practically more suitable for VLC systems.

The effects of negative signal clipping have also been studied. The signal clipping arises due to a limited dynamic range of the transmitter which restricts the DC-bias levels used to obtain a unipolar transmit signal. The investigation showed that the uncoded and BC coded MCM systems, which require large DC-bias will suffer from irreducible BER issues as the transmit signal is distorted by the negative clipping when the DC-bias is reduced.

This showed that the high PAPR MCM systems will require large power back-off to avoid signal clipping which will also affect the BER performance as power back-off will reduce the Euclidean distance between the transmit data symbols. This also showed that the used punctured BC codes cannot correct the errors occurring due to signal clipping, which highlights the need for more sophisticated FEC techniques such as turbo codes. However, this will increase the physical layer complexity and latencies.

After exploration and enhancement of non standardised SCM and MCM systems, the thesis focuses on the IEEE standardised multi-colour CSK systems. First the performance of standardised TLED CSK systems and its nine CBCs was evaluated based on chromatic and intensity space detections. This showed that the TLED CBCs have variable BER performance with suboptimal chromatic space detection and all the CBCs perform equally with intensity or signal space detection. In order to enhance the BER and throughput performance of CSK systems, a QLED scheme has been proposed and recommended over the TLED scheme. The new QLED scheme enables a four-dimensional signalling for CSK which improves the minimum Euclidean distance between data symbols at the transmitter due to the use of four LEDs. This also allows 1^{st} and 2^{nd} order Gray mapping over the quadrilateral chromatic constellation space of the QLED system. The performance evaluation showed that, the QLED scheme has an electrical SNR gain of up to 5 dB over the AWGN channel when compared to the TLED system. The QLED CSK, due to enhanced constellation space and QAM like symbol mapping, is able to work with very high modulation modes such as 4096-CSK. The theoretical error performance analysis for both of the CSK schemes have also been presented for an AWGN channel.

Later the BER performance of QLED and TLED systems was evaluated for an AWGN channel with the insertion losses and colour cross-talk which arise due to the optical properties of the LEDs, PDs and optical filters. This study shows that the colour calibration is very important for CSK systems. The analysis of results showed that other than 4-CSK modulation of the QLED system, no TLED or QLED CSK modulation was able to operate in the considered channel without the use of colour calibration. This showed that the QLED system can operate with 4-CSK even without the knowledge of the cross-talk matrix and hence can be used to evaluate cross-talk to enable operation of higher modulation modes for higher throughputs.

Use of concurrent transmissions over multiple colour bands has also been discussed to achieve higher throughput through WDM at the cost of reduced control over lighting abilities of a VLC system. Hardware implementation issues of CSK systems are also discussed. It is shown that the four colour band based constellation designs of QLED CSK minimise the DAC and ADC bit resolution requirements when compared to TLED CSK and M-PAM systems.

Finally, use of RAC-CSK with low complexity FDE for the standardised TLED and advanced QLED schemes has been proposed, while operating over indoor hybrid and NLOS links. It is shown through simulations and analytical approximations that rate-adaptive coding will enhance the throughputs of CSK systems and that the standard specific RS-CSK is unable to provide any significant channel coding gains. The performance analysis of uncoded and unequalised CSK systems suggested that the higher modulation modes will not be able to operate even in the presence of strong LOS and the lower modulation modes also cannot provide a reliable data-link when the temporal dispersion is increased due to a weak LOS. This minimises the throughput capabilities of the CSK schemes. The FDE based RAC-CSK systems enable the higher modulation modes of CSK to operate over hybrid and NLOS links. Rate-adaptive FEC with FDE will increase the overall system complexity of the CSK physical layer and its signalling overhead, however, it will enhance the system throughputs by up to 200% and reduce the SNR requirements by up to 27 dB depending on the severity of dispersion. These gains will be vital when extending the bandwidth of CSK to achieve even higher data rates.

Overall, novel modulation, coding and channel equalisation techniques have been proposed to enhance the capabilities of standardised and non standardised VLC systems, such that the commercialisation of VLC products can accelerate. It has been shown that the DC-bias requirement is the most important consideration for the power efficiency of VLC signalling sets and the higher dimensional signalling improves the throughput and power efficiency of multi-colour CSK systems.

Future Recommendations

1. **Hardware Demonstration:** Although thoroughly investigated through simulations and analytical analysis, the newly developed systems DCO-VC and QLED CSK require a practical investigation through hardware implementation. A performance comparison between the IEEE standardised TLED and proposed QLED CSK systems through hardware implementation should be carried out to verify the power efficiency of the proposed system. Similarly, the throughput performance of the DCO-OFDM, DCO-VC and DCO-PAM systems should be compared through prototyping to verify the SNR gains of DCO-PAM and DCO-VC over DCO-OFDM system. The effect of limited transmitter dynamic range on the performance of SCM and MCM systems must also be evaluated through a hardware demonstration where the mean optical power and the DC-bias will be fixed for different modulation modes considered signalling schemes.

2. **Effectiveness of FDE for SCM:** In this thesis, the use of FDE for the DCO-PAM

and CSK SCM systems has been investigated considering system bandwidths of 20 and 24 MHz, respectively. In order to improve the data rates, the VLC systems are expected to operate at electrical bandwidths of hundreds of MHz. This will increase the temporal dispersion of signals transmitted in a VLC system leading to severe ISI. Therefore, the performance of FDE based SCM systems must be investigated considering higher bandwidths to evaluate the effectiveness of this simple channel equalisation technique and a comparison against the MCM systems should be made.

3. **MIMO for CSK:** The standardised and proposed CSK system have been studied for a SISO set-up in this thesis. Generally, the indoor lighting is realised through multiple arrays of LEDs, each capable of acting as a separate CSK transmitter for a multi-colour MIMO set-up. The author would be particularly interested in studying the multi-colour MIMO channel matrices to examine how a MIMO CSK system would benefit from the multiple different colour channels.

4. **PAPR Reduction for MCM Schemes:** We have seen through Chapters 3 and 4 that the high PAPR of the MCM systems increases their DC-bias requirements. The high PAPR of MCM systems is a well-known issue and various techniques are under investigation to mitigate this problem such as use of block coding and artificial intelligence. However, there are overheads and latencies associated with these techniques. Author is highly interested in investigating novel PAPR reduction techniques for MCM systems to reduce their overall power consumption.

5. **ADC/DAC for High Speed VLC:** The VLC systems are expected to operate at multi GHz electrical bandwidths. This requires multiple giga sample per second (GSPS) ADC and DAC systems. There is a well-known trade-off between the power consumption, resolution and sampling rates of the ADC/DAC devices. The author is interested in investigating ADC/DAC architectures to propose novel high sampling, power efficient ADC/DAC solutions for VLC systems.

Appendix A - BER Performance of SCM and MCM Systems Over AWGN Channel

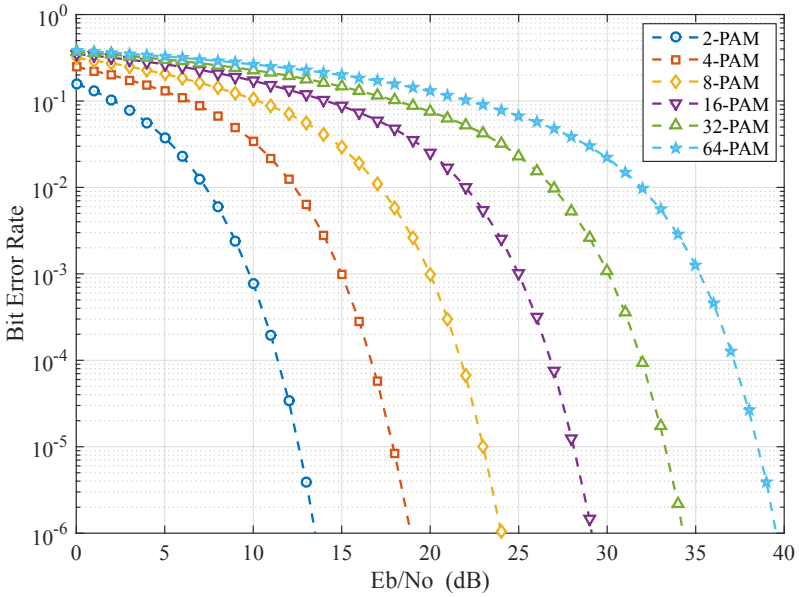

Figure 1: BER Performance of uncoded DCO-PAM system over AWGN channel. Solid lines and the markers represent analytical results and simulations, respectively.

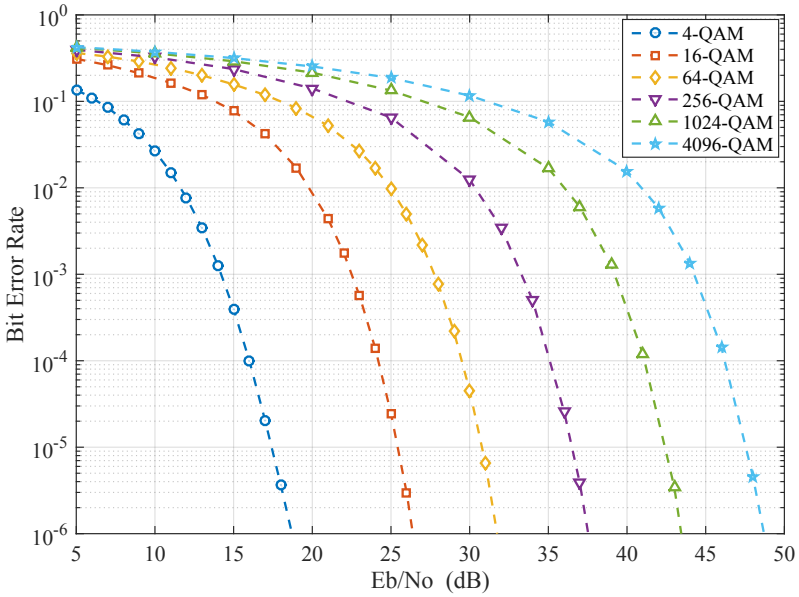

Figure 2: BER Performance of uncoded DCO-OFDM system over AWGN channel. Solid lines and the markers represent analytical results and simulations, respectively.

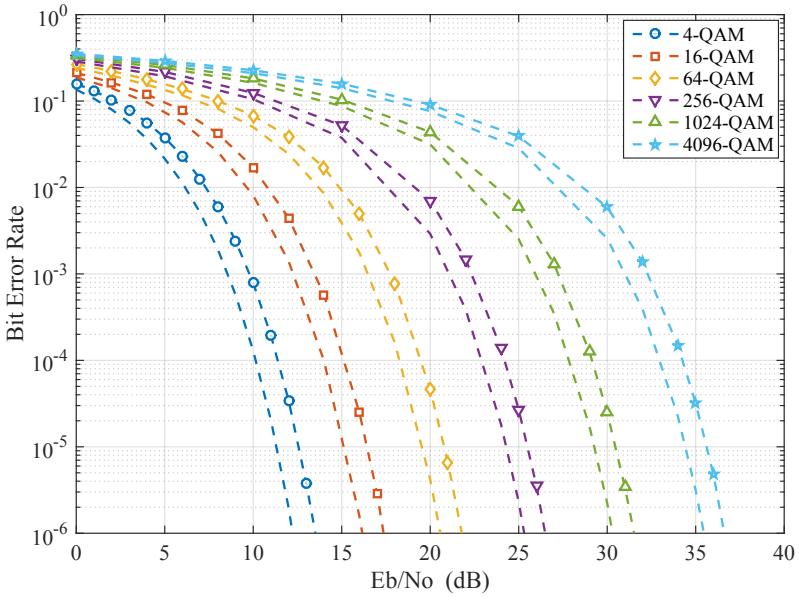

Figure 3: BER Performance of uncoded ACO-OFDM system over AWGN channel. Results with markers represent the performance of original system (without negative clipping at the Rx) and dashed line results represent the performance enhanced with negative clipping at the Rx.

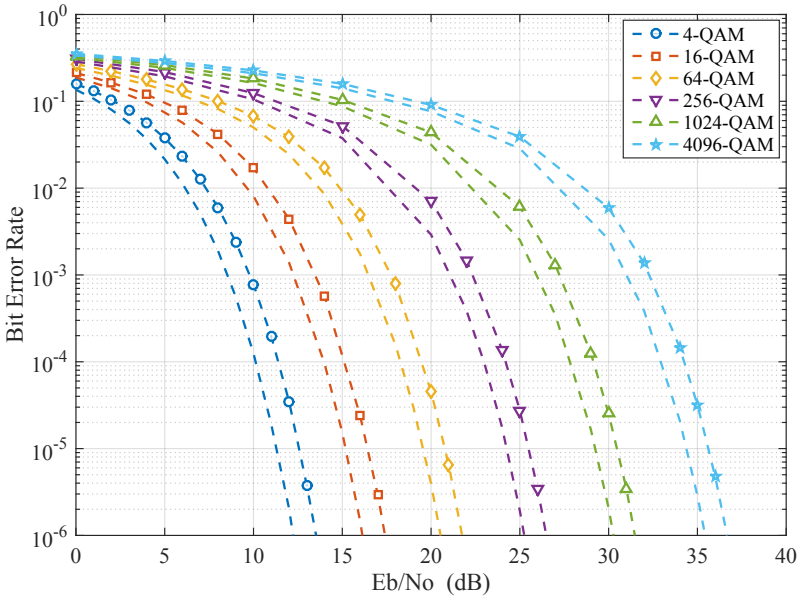

Figure 4: BER Performance of uncoded Flip-OFDM system over AWGN channel. Results with markers represent the performance of original system (without negative clipping at the Rx) and dashed line results represent the performance of enhanced system with negative clipping at the Rx.

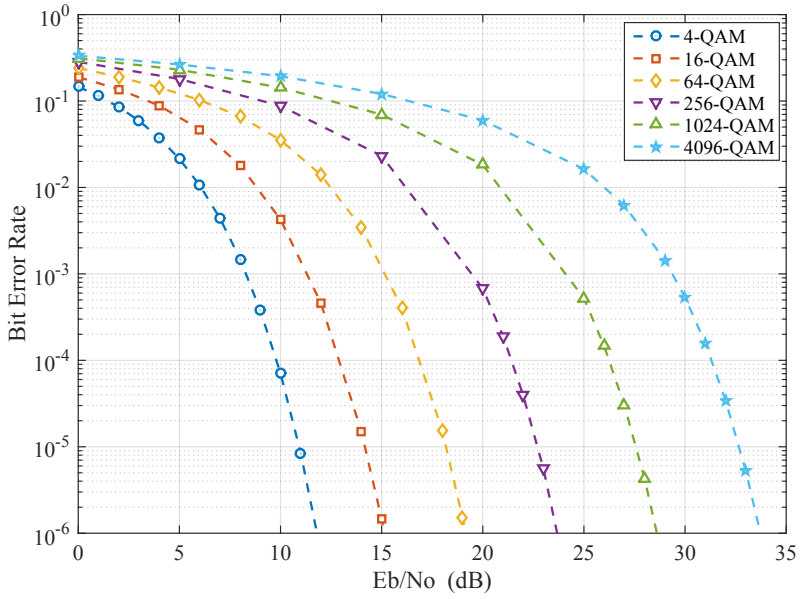

Figure 5: BER Performance of uncoded U-OFDM system over AWGN channel.

Appendix B - Throughput Performance of Bipolar Baseband SCM and MCM Systems

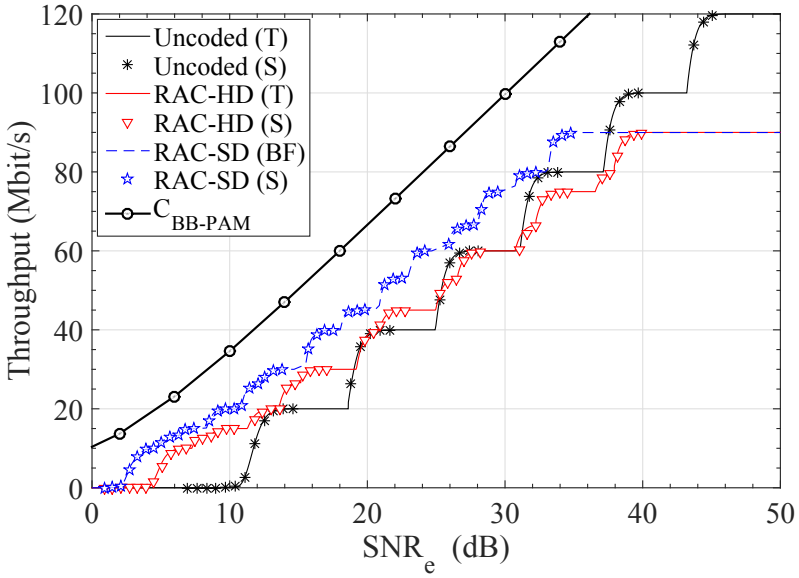

Figure 6: Throughput of uncoded, RAC-HD and RAC-SD BB-PAM over AWGN channel.

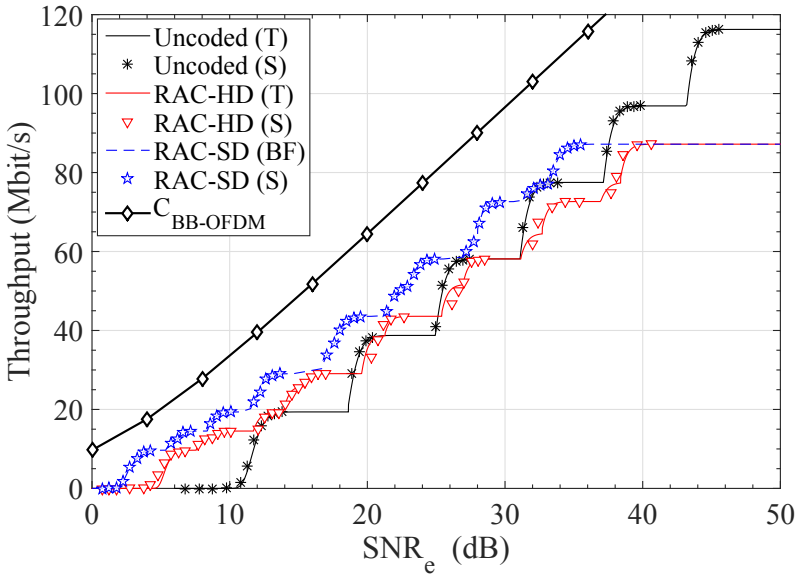

Figure 7: Throughput of uncoded, RAC-HD and RAC-SD BB-OFDM over AWGN channel.

Appendix C - Bit Mapping of TLED CSK

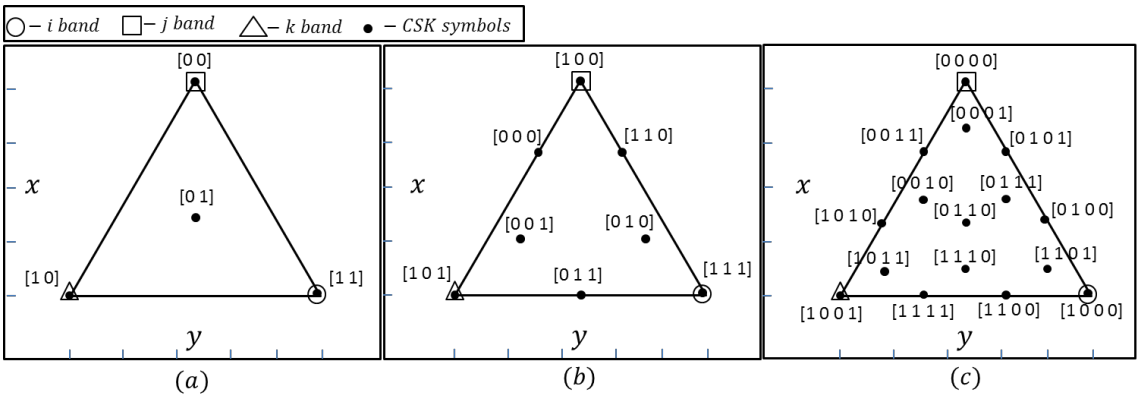

Figure 8: TLED M-CSK system's symbol mapping; (a) 4-CSK, (b) 8-CSK, (c) 16-CSK [8]

Appendix D - Chromatic and Intensity Values of CSK Systems

Table 1: Unique chromaticity values and intensities for each symbol of QLED 16-CSK modulation

Symbol	x	y	I_i (w/m^2)	I_j (w/m^2)	I_k (w/m^2)	I_l (w/m^2)
S_0	0.1690	0.0070	1	0	0	0
S_1	0.1163	0.1580	0.6667	0.3333	0	0
S_2	0.0110	0.4600	0	1	0	0
S_3	0.0637	0.3090	0.3333	0.6667	0	0
S_4	0.3573	0.0930	0.6667	0	0	0.3333
S_5	0.2853	0.2306	0.3787	0.3247	0	0.2966
S_6	0.1413	0.5057	0	0.6667	0.3333	0
S_7	0.2134	0.3681	0.3202	0.2915	0.3882	0
S_8	0.7340	0.2650	0	0	0	1
S_9	0.6233	0.3757	0	0	0.3333	0.6667
S_{10}	0.4020	0.5970	0	0	1	0
S_{11}	0.5127	0.4863	0	0	0.6667	0.3333
S_{12}	0.5457	0.1790	0.3333	0	0	0.6667
S_{13}	0.4544	0.3031	0.2934	0	0.3428	0.3638
S_{14}	0.2717	0.5513	0	0.3333	0.6667	0
S_{15}	0.3630	0.4272	0	0.3955	0.2563	0.3483

Table 2: Unique chromaticity values for each symbol of QLED 64-CSK modulation

Symbol	x	y	**Symbol**	x	y
S_0	0.1690	0.0070	S_{32}	0.7340	0.2650
S_1	0.1464	0.0717	S_{33}	0.6866	0.3124
S_2	0.1013	0.2011	S_{34}	0.5917	0.4073
S_3	0.1239	0.1364	S_{35}	0.6391	0.3599
S_4	0.0110	0.4600	S_{36}	0.4020	0.5970
S_5	0.0336	0.3953	S_{37}	0.4494	0.5496
S_6	0.0787	0.2659	S_{38}	0.5443	0.4547
S_7	0.0561	0.3306	S_{39}	0.4969	0.5021
S_8	0.2497	0.0439	S_{40}	0.6533	0.2281
S_9	0.2236	0.1061	S_{41}	0.6094	0.2780
S_{10}	0.1714	0.2306	S_{42}	0.5216	0.3778
S_{11}	0.1975	0.1683	S_{43}	0.5655	0.3280
S_{12}	0.0669	0.4796	S_{44}	0.3461	0.5774
S_{13}	0.0930	0.4173	S_{45}	0.3900	0.5297
S_{14}	0.1452	0.2929	S_{46}	0.4778	0.4277
S_{15}	0.1191	0.3551	S_{47}	0.4339	0.4776
S_{16}	0.4111	0.1176	S_{48}	0.4919	0.1544
S_{17}	0.3779	0.1749	S_{49}	0.4551	0.2092
S_{18}	0.3115	0.2895	S_{50}	0.3815	0.3189
S_{19}	0.3447	0.2322	S_{51}	0.4183	0.2641
S_{20}	0.1786	0.5187	S_{52}	0.2344	0.5383
S_{21}	0.2118	0.4614	S_{53}	0.2712	0.4835
S_{22}	0.2782	0.3468	S_{54}	0.3448	0.3738
S_{23}	0.2450	0.4041	S_{55}	0.3080	0.4286
S_{24}	0.3304	0.0807	S_{56}	0.5726	0.1913
S_{25}	0.3007	0.1405	S_{57}	0.5323	0.2436
S_{26}	0.2414	0.2600	S_{58}	0.4516	0.3484
S_{27}	0.2711	0.2003	S_{59}	0.4919	0.2960
S_{28}	0.1227	0.4991	S_{60}	0.2903	0.5579
S_{29}	0.1524	0.4394	S_{61}	0.3306	0.5055
S_{30}	0.2117	0.3198	S_{62}	0.4113	0.4008
S_{31}	0.1820	0.3796	S_{63}	0.3710	0.4531

Table 3: Unique chromaticity values for each symbol of TLED 64-CSK modulation

Symbol	x	y	**Symbol**	x	y
S_0	0.1690	0.0070	S_{32}	0.5110	0.3705
S_1	0.7340	0.2650	S_{33}	0.3828	0.3810
S_2	0.4020	0.5970	S_{34}	0.4636	0.4178
S_3	0.2497	0.0439	S_{35}	0.4162	0.4653
S_4	0.3304	0.0807	S_{36}	0.2070	0.0474
S_5	0.4111	0.1176	S_{37}	0.2877	0.0843
S_6	0.4919	0.1544	S_{38}	0.3684	0.1211
S_7	0.5726	0.1913	S_{39}	0.4492	0.1580
S_8	0.6533	0.2281	S_{40}	0.5299	0.1948
S_9	0.2023	0.0913	S_{41}	0.6106	0.2317
S_{10}	0.2356	0.1756	S_{42}	0.6913	0.2685
S_{11}	0.2689	0.2599	S_{43}	0.6439	0.3160
S_{12}	0.3021	0.3441	S_{44}	0.5964	0.3634
S_{13}	0.3354	0.4284	S_{45}	0.5490	0.4108
S_{14}	0.3687	0.5127	S_{46}	0.5016	0.4582
S_{15}	0.6866	0.3124	S_{47}	0.4542	0.5057
S_{16}	0.6391	0.3599	S_{48}	0.4067	0.5531
S_{17}	0.5917	0.4073	S_{49}	0.3734	0.4688
S_{18}	0.5443	0.4547	S_{50}	0.3401	0.3845
S_{19}	0.4969	0.5021	S_{51}	0.3069	0.3003
S_{20}	0.4494	0.5496	S_{52}	0.2736	0.2160
S_{21}	0.2830	0.1282	S_{53}	0.2403	0.1317
S_{22}	0.3637	0.1650	S_{54}	0.3210	0.1686
S_{23}	0.4445	0.2019	S_{55}	0.4017	0.2054
S_{24}	0.5252	0.2387	S_{56}	0.4825	0.2423
S_{25}	0.6059	0.2756	S_{57}	0.5632	0.2791
S_{26}	0.3163	0.2125	S_{58}	0.5157	0.3266
S_{27}	0.3970	0.2493	S_{59}	0.4350	0.2897
S_{28}	0.4777	0.2862	S_{60}	0.3543	0.2529
S_{29}	0.5584	0.3230	S_{61}	0.3876	0.3371
S_{30}	0.3496	0.2968	S_{62}	0.4683	0.3740
S_{31}	0.4303	0.3336	S_{63}	0.4209	0.4214

Appendix E - BER/PER Performance of Different CBCs of TLED CSK

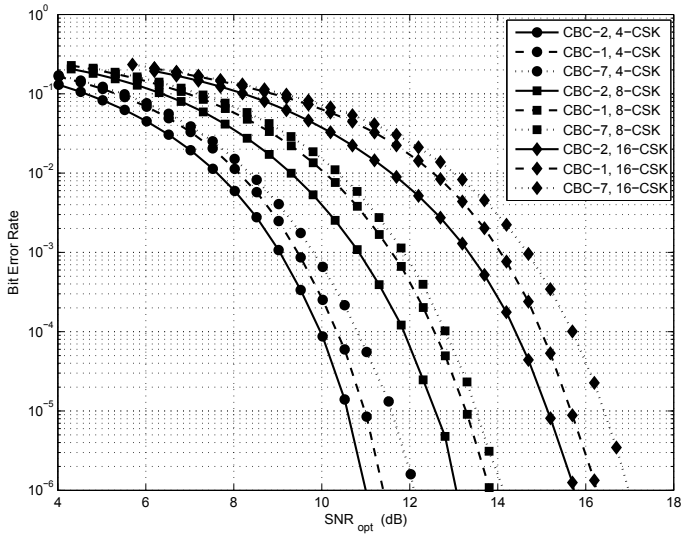

Figure 9: BER comparison between CBC-1, CBC-2 and CBC-7 for 4, 8 and 16 CSK modulations using Optical SNR scale.

In optical communications, it is informative to compare system performance on the optical SNR scale. The BER for the selected CBCs have been compared on the optical

SNR scale in Fig. 9. The optical SNR has been calculated as:

$$\mathrm{SNR_{opt}} = \frac{\bar{P}_{opt}}{\bar{N}_{opt}} \equiv \frac{\bar{P}_{opt}}{(\bar{P}_e/\mathrm{SNR_e})^{0.5}} \tag{1}$$

In equation 1, $\bar{P}_{opt}$ denotes the mean optical power that has been calculated as the sum of the mean optical power emitted by each of the three LEDs of the CSK system and it is computed as $\bar{P}_{opt} = E\{I_i(t)\} + E\{I_j(t)\} + E\{I_k(t)\}$. Practically in circuits and simulations, the equivalent mean optical noise $\bar{N}_{opt}$ is calculated as the *rms* value of the electrical noise in the CSK system, $\bar{N}_{opt} = \sqrt{\bar{N}_e} = \sqrt{E\{n_i^2(t)\} + E\{n_j^2(t)\} + E\{n_k^2(t)\}}$. Equation 1 also shows the relation between the $\mathrm{SNR_{opt}}$ and $\mathrm{SNR_e}$ to demonstrate the dependence on the bit rate, where $\bar{P}_e$ is the overall mean electrical power of a CSK signal at the transmitter, given as $\bar{P}_e = E\{I_i^2(t)\} + E\{I_j^2(t)\} + E\{I_k^2(t)\}$. Fig. 9 shows the BER versus optical SNR performance for CBC-1, CBC-2 and CBC-7 for all the modulation schemes.

Fig. 10 shows the packet error rate (PER) curves for the selected CBCs on an optical SNR scale. For the PER results, a packet size of 1500 bytes has been used. The PER curves display the same trends as the BER curves. For a PER of 10^{-2}, CBC-2 outperforms CBC-1 and CBC-7 by the same SNR margin as in the BER curves.

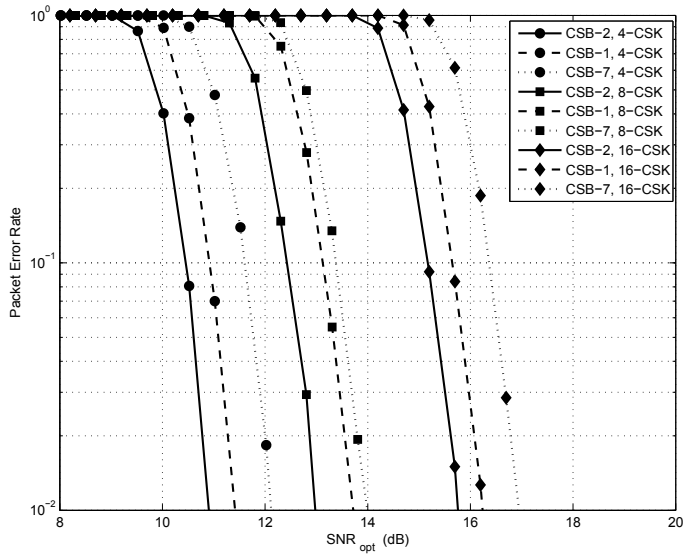

Figure 10: PER comparison between CBC-1, CBC-2 and CBC-7 for 4, 8 and 16 CSK modulations using Optical SNR scale, for a packet size of 1500 bytes.

Analysis of Results

Table 4 compares the energy requirements of CBC-1, CBC-2 and CBC-7 for a BER of 10^{-6}. It depicts the performance spread of the PHY III of IEEE 802.15.7 for an AWGN channel, and suggests that CSK designers will need to decide which CBC to use in a commercial CSK product, if chromatic detection is used. Table 4 shows that CBC-2 requires 0.8 to

Table 4: Energy requirements of different CSK CBCs for a BER of 10^{-6} in an AWGN channel.

CBC Number	Multilevel CSK	E_b/N_o (dB)	SNR_{opt} (dB)	Penalty *w.r.t.* CBC-2 $\{E_b/N_o$, $\text{SNR}_{\text{opt}}\}$ (dB)
CBC-1	4-CSK	20.8	11.3	{0.8, 0.4}
	8-CSK	23	13.8	{1.5, 0.8}
	16-CSK	26	16.2	{1, 0.5}
CBC-2	4-CSK	20	10.9	
	8-CSK	21.5	13	
	16-CSK	25	15.7	
CBC-7	4-CSK	22.2	12.1	{2.2, 1.2}
	8-CSK	23.5	14.1	{2, 1.1}
	16-CSK	27.5	16.9	{2.5, 1.2}

1.5 dB less E_b/N_o or 0.4 to 0.8 dB less SNR_{opt} than CBC-1 which has an average value of d_{min}. At the same time CBC-2 requires 2 to 2.5 dB less E_b/N_o or 1.1 to 1.2 dB less SNR_{opt} than CBC-7 which has the smallest d_{min} value. Therefore, CBC-2 is the most energy efficient of all the CBCs and will, consequently, give better operating range.

Appendix F - Capacity Bounds of Optical Intensity Channels

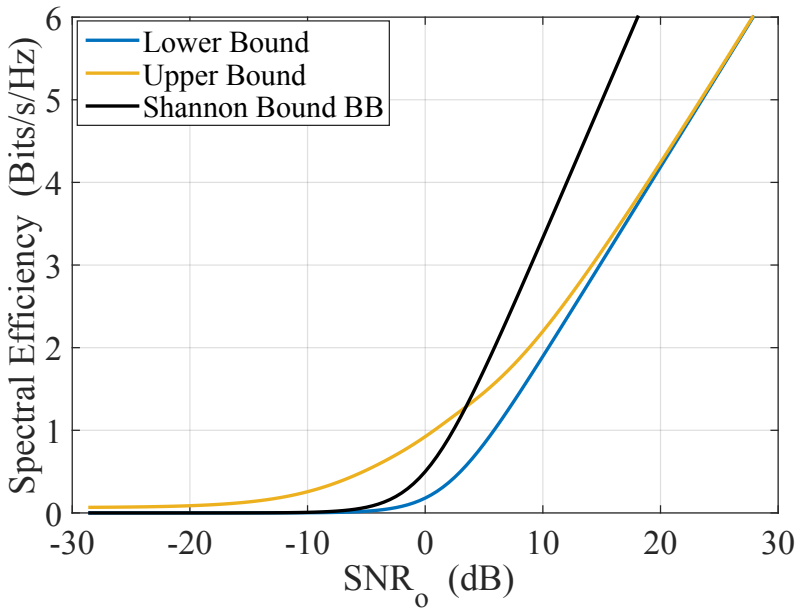

Figure 11: Capacity comparison between the bipolar baseband channel and optical intensity channel based on AWGN.

Fig. 11 shows the capacity comparison between the bipolar baseband channel and optical intensity channel over an optical SNR scale. The lower and upper bound curves show the capacity limits of the optical channel [137], while the curve labelled Shannon Bound BB shows the capacity of the electrical bipolar baseband channel.

References

[1] Philips Lumileds. Luxeon Rebel and Luxeon Rebel ES [Online]. Available: http://www.philipslumileds.com/products/luxeon-rebel/luxeon-rebel-color, 2014. xi, 18, 86, 102

[2] Thorlabs. FB450-40 Bandpass Filter [Online]. Available: http://www.thorlabs.de/thorproduct.cfm?partnumber=FB450-40, 2014. xi, 18, 69, 102

[3] Thorlabs. FB500-40 Bandpass Filter [Online]. Available: http://www.thorlabs.de/thorproduct.cfm?partnumber=FB500-40, 2014. xi, 18, 102

[4] Midopt. BP590 Bandpass Filter [Online]. Available: http://midopt.com/bp590.html, 2014. xi, 18, 102

[5] Thorlabs. FB650-40 Bandpass Filter [Online]. Available: http://www.thorlabs.de/thorproduct.cfm?partnumber=FB650-40, 2014. xi, 18, 102

[6] First Sensor. PC10-6b PIN PD [Online]. Available: http://www.first-sensor.com/en/datasheet/501229, 2014. xi, 18, 20, 69, 102

[7] D. Tsonev, S. Sinanovic, and H. Haas. Novel unipolar orthogonal frequency division multiplexing (u-ofdm) for optical wireless. In *Vehicular Technology Conference (VTC Spring), 2012 IEEE 75th*, pages 1 –5, may 2012. doi: 10.1109/VETECS.2012.6240060. xi, 32, 37, 42, 44, 45, 46, 55

[8] IEEE Standard for Local and Metropolitan Area Networks–Part 15.7: Short-Range Wireless Optical Communication Using Visible Light. *IEEE Std 802.15.7-2011*, pages 1–309, 6 2011. doi: 10.1109/IEEESTD.2011.6016195. xiii, xv, xvi, 7, 14, 18, 21, 27, 30, 78, 80, 81, 83, 84, 85, 92, 99, 101, 113, 128, 142

[9] Shlomi Arnon, John R. Barry, George K. Karagiannidis, Robert Schober, and Murat Uysal. *Advanced Optical Wireless Communication Systems*. Cambridge, 2012. xvi, 15, 16

[10] S. Hranilovic. *Wireless Optical Communication Systems*. Springer, 2005. xvi, 15, 16, 19, 20, 23, 28, 29

[11] CISCO Visual Networking Index (VNI). The zettabyte era [online]. available: http://www.cisco.com, May 2012. 2

[12] K.K. Wong, T. O'Farrell, and M. Kiatweerasakul. The performance of optical wireless ook, 2-ppm and spread spectrum under the effects of multipath dispersion and artificial light interference. *International Journal for Communication Systems*, 13 (7-8):551–576, 2000. 2

[13] S. Rajagopal, R.D. Roberts, and Sang-Kyu Lim. IEEE 802.15.7 visible light communication: modulation schemes and dimming support. *Communications Magazine, IEEE*, 50(3):72–82, march 2012. ISSN 0163-6804. doi: 10.1109/MCOM.2012.6163585. 2, 13, 89, 99

[14] T. S. Rappaport, S. Sun, R. Mayzus, H. Zhao, Y. Azar, K. Wang, G. N. Wong, J. K. Schulz, M. Samimi, and F. Gutierrez. Millimeter wave mobile communications for 5g cellular: It will work! *IEEE Access*, 1:335–349, 2013. ISSN 2169-3536. doi: 10.1109/ACCESS.2013.2260813. 2

[15] J. Grubor, S. Randel, K.-D. Langer, and J. Walewski. Bandwidth-efficient indoor optical wireless communications with white light-emitting diodes. In *Communication Systems, Networks and Digital Signal Processing, 2008. CNSDSP 2008. 6th International Symposium on*, pages 165–169, 2008. doi: 10.1109/CSNDSP.2008.4610769. 2

[16] Giulio Cossu, Wajahat Ali, Raffaele Corsini, and Ernesto Ciaramella. Gigabit-class optical wireless communication system at indoor distances (1.5 – 4 m). *Opt. Express*, 23(12):15700–15705, Jun 2015. doi: 10.1364/OE.23.015700. URL `http://www.opticsexpress.org/abstract.cfm?URI=oe-23-12-15700`. 2, 3, 17, 21, 34

[17] D. Tsonev, Hyunchae Chun, S. Rajbhandari, J.J.D. McKendry, S. Videv, E. Gu, M. Haji, S. Watson, A.E. Kelly, G. Faulkner, M.D. Dawson, H. Haas, and D. O'Brien. A 3-gb/s single-led ofdm-based wireless vlc link using a gallium nitride μled. *Photonics Technology Letters, IEEE*, 26(7):637–640, April 2014. ISSN 1041-1135. doi: 10.1109/LPT.2013.2297621. 2, 25, 34, 76

[18] Lubin Zeng, D. O'Brien, Hoa Minh, G. Faulkner, Kyungwoo Lee, Daekwang Jung, Yunje Oh, and Eun Tae Won. High data rate multiple input multiple output (mimo) optical wireless communications using white led lighting. *Selected Areas in Communications, IEEE Journal on*, 27(9):1654–1662, 2009. ISSN 0733-8716. doi: 10.1109/JSAC.2009.091215. 2, 20, 25

[19] Ahmed Taha Hussein and Jaafar MH Elmirghani. Mobile multi-gigabit visible light communication system in realistic indoor environment. *Journal of Lightwave Technology*, 33(15):3293–3307, 2015. 2, 15

[20] Ariel Gomez, Kai Shi, Crisanto Quintana, Mitsuhisa Sato, Grahame Faulkner, Benn C Thomsen, and Dominic O'Brien. Beyond 100-gb/s indoor wide field-of-view optical wireless communications. *Photonics Technology Letters, IEEE*, 27(4): 367–370. 2

[21] Gordon Povey. How green is visible light communication [online], August 2011. URL `http://visiblelightcomm.com/how-green-is-visible-light-communications/`. 3, 13

[22] J.M. Kahn and J.R. Barry. Wireless infrared communications. *Proceedings of the IEEE*, 85(2):265–298, feb 1997. ISSN 0018-9219. doi: 10.1109/5.554222. 4, 13, 14, 20, 24, 27, 29, 41

[23] S. Haruyama Y. Ito and M. Nakagawa. "rate-adaptive transmission on a wavelength dependent channel for underwater wireless communication using visible light leds". 105:127–132, Feb 2006. 5

[24] Zhengyuan Xu and B.M. Sadler. Ultraviolet communications: Potential and state-of-the-art. *Communications Magazine, IEEE*, 46(5):67–73, 2008. ISSN 0163-6804. doi: 10.1109/MCOM.2008.4511651. 13, 14

[25] H. Elgala, R. Mesleh, and H. Haas. Indoor optical wireless communication: potential and state-of-the-art. *Communications Magazine, IEEE*, 49(9):56–62, September. ISSN 0163-6804. doi: 10.1109/MCOM.2011.6011734. 13, 43

[26] W. Popoola Z. Ghassemlooy and S. Rajbhandari. *Optical Wireless Communication: System and Channel Modelling with MATLAB*. CRC Press, New York, 2013. 13, 14, 28

[27] F.R. Gfeller and U. Bapst. Wireless in-house data communication via diffuse infrared radiation. *Proceedings of the IEEE*, 67(11):1474 – 1486, nov. 1979. ISSN 0018-9219. doi: 10.1109/PROC.1979.11508. 13, 22, 23

[28] Lubin Zeng, D. O'Brien, Hoa Le-Minh, Kyungwoo Lee, Daekwang Jung, and Yunje Oh. Improvement of date rate by using equalization in an indoor visible light communication system. In *ICCSC, 2008*, pages 678–682, May 2008. doi: 10.1109/ICCSC.2008.149. 13, 16, 60, 112

[29] D. O"Brien, L. Zeng, Hoa Le-Minh, G. Faulkner, J.W. Walewski, and S. Randel. Visible light communications: Challenges and possibilities. In *PIMRC 2008. IEEE 19th Int. Symp.*, pages 1–5, 2008. doi: 10.1109/PIMRC.2008.4699964. 13

[30] VLCC. Visible light communication consortium [online](accessed: Sep 2015). URL `http://www.vlcc.net/`. 13, 14, 30

[31] Home gigabit access, omega [online](accessed: Sep 2015). URL `http://www.ict-omega.eu/`. 14, 30

[32] R.D. Roberts, S. Rajagopal, and Sang-Kyu Lim. Ieee 802.15.7 physical layer summary. In *GLOBECOM Workshops (GC Wkshps), 2011 IEEE*, pages 772–776, 2011. doi: 10.1109/GLOCOMW.2011.6162558. 14, 30, 78, 89

[33] Yuichi Tanaka, Shinichirou Haruyama, and Masao Nakagawa. Wireless optical transmissions with white colored led for wireless home links. In *Personal, Indoor and Mobile Radio Communications, 2000. PIMRC 2000. The 11th IEEE International Symposium on*, volume 2, pages 1325–1329. IEEE, 2000. 14, 30

[34] T. O'Farrell. Design and evaluation of a high data rate optical wireless system for the diffuse indoor channel using barker spreading codes and rake reception [optical wireless communications]. *Communications, IET*, 2(1):35–44, 2008. ISSN 1751-8628. doi: 10.1049/iet-com:20060372. 14

[35] J.B. Carruthers and J.M. Kahn. Modeling of nondirected wireless infrared channels. *Communications, IEEE Transactions on*, 45(10):1260–1268, Oct. ISSN 0090-6778. doi: 10.1109/26.634690. 15

[36] Ahmed Taha Hussein and Jaafar MH Elmirghani. 10 gbps mobile visible light communication system employing angle diversity, imaging receivers, and relay nodes. *Journal of Optical Communications and Networking*, 7(8):718–735, 2015. 15

[37] G. P. Agarwal. *Fiber-Optic Communication Systems.* John Wiley and Sons, Inc., 2002. ISBN 0-471-22114-7. 16, 20, 28, 29

[38] S. M. Sze and Kwok K. Ng. *Physics of Semiconductor Devices.* John Wiley & Sons Inc., 2007. 16

[39] Jonathan JD McKendry, David Massoubre, Shuailong Zhang, Bruce R Rae, Richard P Green, Erdan Gu, Robert K Henderson, AE Kelly, and Martin D Dawson. Visible-light communications using a cmos-controlled micro-light-emitting-diode array. *J. Lightw. Technol, IEEE*, 30(1):61–67, 2012. 16, 60, 70, 124

[40] Energy Alliance. Lightbulb efficiency comparison chart [online](accessed: June 2016). URL `http://greatercea.org/lightbulb-efficiency-comparison-chart/`. 16

[41] Lumens to watts conversion chart, 2015. URL `http://www.thelightbulb.co.uk/resources/lumens_watts`. 16

[42] Efficient blue light-emitting diodes leading to bright and energy-saving white light sources. Royal Swedish Academy of Sciences, 2014. 16

[43] P.A. Haigh, Z. Ghassemlooy, S. Rajbhandari, and I. Papakonstantinou. Visible light communications using organic light emitting diodes. *Communications Magazine, IEEE*, 51(8):148–154, August 2013. ISSN 0163-6804. doi: 10.1109/MCOM.2013.6576353. 17

[44] J W Park, D C Shin, and S H Park. Large-area oled lightings and their applications. *Semiconductor Science and Technology*, 26(3):034002, 2011. URL `http://stacks.iop.org/0268-1242/26/i=3/a=034002`. 17

[45] P.A. Haigh, Z. Ghassemlooy, I. Papakonstantinou, F. Arca, S.F. Tedde, O. Hayden, and E. Leitgeb. A 1-mb/s visible light communications link with low bandwidth organic components. *Photonics Technology Letters, IEEE*, 26(13):1295–1298, July 2014. ISSN 1041-1135. doi: 10.1109/LPT.2014.2321412. 17

[46] J. Grubor, S. Randel, K.-D. Langer, and J.W. Walewski. Broadband information broadcasting using led-based interior lighting. *Lightwave Technology, Journal of*, 26 (24):3883–3892, Dec 2008. ISSN 0733-8724. doi: 10.1109/JLT.2008.928525. 17, 21, 23, 25, 37, 60, 121

[47] OSRAM. Details on photobiological safety of led light sources [online](accessed: June 2016). URL `http://www.osram-os.com/Graphics/XPic9/00079436_0.pdf/Details`. 17

[48] AC Boucouvalas. Iec 825-1 eye safety classification of some consumer electronic products. 1996. 19

[49] IEC825. *Safety of Laser Products. Equipment classification, requirements and user guide*. International Eletrotechnical Commission, 1993. 19

[50] D.J.T. Heatley, D.R. Wisely, I. Neild, and P. Cochrane. Optical wireless: the story so far. *Communications Magazine, IEEE*, 36(12):72–74, 79–82, Dec 1998. ISSN 0163-6804. doi: 10.1109/35.735881. 19

[51] David A Rockwell and G Stephen Mecherle. Wavelength selection for optical wireless communications systems. In *ITCom 2001: International Symposium on the Convergence of IT and Communications*, pages 27–35. International Society for Optics and Photonics, 2001. 19

[52] JS Ng, CH Tan, JPR David, and GJ Rees. Effect of impact ionization in the ingaas absorber on excess noise of avalanche photodiodes. *Quantum Electronics, IEEE Journal of*, 41(8):1092–1096, 2005. 20

[53] Kwonhyung Lee, Hyuncheol Park, and J.R. Barry. Indoor channel characteristics for visible light communications. *Communications Letters, IEEE*, 15(2):217–219, February 2011. ISSN 1089-7798. doi: 10.1109/LCOMM.2011.010411.101945. 22, 26, 69, 124

[54] P.M. Butala, H. Elgala, T.D.C. Little, and P. Zarkesh-Ha. Multi-wavelength visible light communication system design. In *Globecom Workshops (GC Wkshps), 2014*, pages 530–535, Dec 2014. doi: 10.1109/GLOCOMW.2014.7063486. 22

[55] J.R. Barry, J.M. Kahn, W.J. Krause, E.A. Lee, and D.G. Messerschmitt. Simulation of multipath impulse response for indoor wireless optical channels. *Selected Areas in Communications, IEEE Journal on*, 11(3):367–379, 1993. ISSN 0733-8716. doi: 10.1109/49.219552. 22

[56] J.B. Carruthers and J.M. Kahn. Modeling of nondirected wireless infrared channels. *Communications, IEEE Transactions on*, 45(10):1260–1268, 1997. ISSN 0090-6778. doi: 10.1109/26.634690. 22

[57] V. Jungnickel, V. Pohl, S. Nonnig, and C. Von Helmolt. A physical model of the wireless infrared communication channel. *Selected Areas in Communications, IEEE Journal on*, 20(3):631–640, 2002. ISSN 0733-8716. doi: 10.1109/49.995522. 22, 24, 25, 26, 69, 72, 127

[58] F.J. Lopez-Hernandez, R. Perez-Jimeniz, and A. Santamaria. Monte carlo calculation of impulse response on diffuse ir wireless indoor channels. *Electronics Letters*, 34(12):1260–1262, 1998. ISSN 0013-5194. doi: 10.1049/el:19980825. 22

[59] F.J. Lopez-Hernandez, R. Perez-Jimenez, and A. Santamaria. Modified monte carlo scheme for high-efficiency simulation of the impulse response on diffuse ir wireless indoor channels. *Electronics Letters*, 34(19):1819–1820, 1998. ISSN 0013-5194. doi: 10.1049/el:19981173. 22

[60] R. Perez-Jimenez, J. Berges, and M.J. Betancor. Statistical model for the impulse response on infrared indoor diffuse channels. *Electronics Letters*, 33(15):1298–1300, 1997. ISSN 0013-5194. doi: 10.1049/el:19970866. 22

[61] R. Perez-Jimenez, V.M. Melian, and M.J. Betancor. Analysis of multipath impulse response of diffuse and quasi-diffuse optical links for ir-wlan. In *INFOCOM '95. Fourteenth Annual Joint Conference of the IEEE Computer and Communications Societies. Bringing Information to People. Proceedings. IEEE*, pages 924–930 vol.2, 1995. doi: 10.1109/INFCOM.1995.515965. 22

[62] F.J. Lopez-Hermandez and M.J. Betancor. Dustin: algorithm for calculation of impulse response on ir wireless indoor channels. *Electronics Letters*, 33(21):1804–1806, 1997. ISSN 0013-5194. doi: 10.1049/el:19971224. 22

[63] J.B. Carruthers and P. Kannan. Iterative site-based modeling for wireless infrared channels. *Antennas and Propagation, IEEE Transactions on*, 50(5):759–765, 2002. ISSN 0018-926X. doi: 10.1109/TAP.2002.1011244. 22

[64] D. C. OBrien, M. Katz, P. Wang, K. Kalliojarvi, S. Arnon, M. Matsumoto, R. Green, S. Jivkova. Short-range optical wireless communications. *Wireless World Research Forum*, pages 146–151, 2007. 23

[65] K.-D. Langer and J. Grubor. Recent developments in optical wireless communications using infrared and visible light. In *Transparent Optical Networks, 2007. ICTON '07. 9th International Conference on*, volume 3, pages 146–151, July 2007. doi: 10.1109/ICTON.2007.4296267. 23

[66] T. Komine and M. Nakagawa. Fundamental analysis for visible-light communication system using led lights. *Consumer Electronics, IEEE Transactions on*, 50(1):100–107, 2004. ISSN 0098-3063. doi: 10.1109/TCE.2004.1277847. 23, 24, 121

[67] John R. Barry. *Wireless Infrared Communications*. Kluwer Academic Press, Boston, MA, 1994. 23

[68] J.B. Carruthers and J.M. Kahn. Modeling of nondirected wireless infrared channels. *Communications, IEEE Transactions on*, 45(10):1260–1268, 1997. ISSN 0090-6778. doi: 10.1109/26.634690. 24

[69] V Pohl, V Jungnickel, and C Von Helmolt. Integrating-sphere diffuser for wireless infrared communication. *IEE Proceedings-Optoelectronics*, 147(4):281–285, 2000. 24

[70] Timothy O'Farrell. Statistical fading models: Narrowband and wideband fading. URL `http://hercules.shef.ac.uk/eee/teach/resources/eee6431/Lecture_3.pdf`. 27

[71] Andrea Goldsmith. *Wireless Communications*. Cambridge Univerity Press, 2005. 29, 32, 41, 42, 47, 48, 69, 70, 124

[72] Yuichi Tanaka, Toshihiko Komine, Shinichiro Haruyama, and Masao Nakagawa. Indoor visible light data transmission system utilizing white led lights. *IEICE transactions on communications*, 86(8):2440–2454, 2003. 30

[73] Toshihiko Komine and Masao Nakagawa. Fundamental analysis for visible-light communication system using led lights. *Consumer Electronics, IEEE Transactions on*, 50(1):100–107, 2004. 30

[74] T. Komine and M. Nakagawa. Performance evaluation of visible-light wireless communication system using white led lightings. In *Computers and Communications, 2004. Proceedings. ISCC 2004. Ninth International Symposium on*, volume 1, pages 258–263 Vol.1, June 2004. doi: 10.1109/ISCC.2004.1358414. 30

[75] Toshihiko Komine and Masao Nakagawa. Integrated system of white led visible-light communication and power-line communication. *Consumer Electronics, IEEE Transactions on*, 49(1):71–79, 2003. 30

[76] Japan electronics and information technology industries association, jeita [online](accessed: Sep 2015), . URL `http://www.jeita.or.jp/`. 30

[77] Pure li-fi [online](accessed: Sep 2015). URL `http://purelifi.com/`. 30

[78] Ieee 802.15 wpan task group 7 (tg7) visible light communication [online](accessed: Sep 2015). URL `http://www.ieee802.org/15/pub/TG7.html`. 30

[79] Visible light communication system, cp-1221, jeita [online](accessed: Sep 2015), . URL `http://www.jeita.or.jp/cgi-bin/standard_e/list.cgi?cateid=1&subcateid=50`. 30

[80] Visible light id system, cp-1222, jeita [online](accessed: Sep 2015), . URL `http://www.jeita.or.jp/cgi-bin/standard_e/list.cgi?cateid=1&subcateid=50`. 30

[81] Visible light beacon system, cp-1223, jeita [online](accessed: Sep 2015), . URL http://www.jeita.or.jp/cgi-bin/standard_e/list.cgi?cateid=1&subcateid=50. 30

[82] Richard D Roberts. Undersampled frequency shift on-off keying (ufsook) for camera communications (camcom). In *Wireless and Optical Communication Conference (WOCC), 2013 22nd*, pages 645–648. IEEE, 2013. 31

[83] Nirzhar Saha, Md Shareef Ifthekhar, Nam Tuan Le, and Yeong Min Jang. Survey on optical camera communications: challenges and opportunities. *Optoelectronics, IET*, 9(5):172–183, 2015. 31

[84] IEEE 802.15 WPANTM. 15.7 Revision: Short-Range Optical Wireless Communications Task Group (TG 7r1) (Accessed Sep 2015). URL http://www.ieee802.org/15/pub/IEEE%20802_15%20WPAN%2015_7%20Revision1%20Task%20Group.htm. 31

[85] Malik D Audeh and Joseph M Kahn. Performance evaluation of baseband ook for wireless indoor infrared lan's operating at 100 mb/s. *Communications, IEEE Transactions on*, 43(6):2085–2094, 1995. 31, 34

[86] J. R. Barry. *Wireless Infrared Communication*. Kluwer Academic Press, Boston, 1994. ISBN 0-7923-9476-3. 31

[87] Rob Otte, Leo P De Jong, and Arthur HM Van Roermund. Wireless optical ppm telemetry and the influence of lighting flicker. *Instrumentation and Measurement, IEEE Transactions on*, 47(1):51–55, 1998. 31

[88] Da-shan Shiu and Joseph M Kahn. Differential pulse-position modulation for power-efficient optical communication. *Communications, IEEE Transactions on*, 47(8): 1201–1210, 1999. 31

[89] ED Kaluarachi, Zabih Ghassemlooy, and Brett Wilson. Digital pulse interval modulation for optical free space communication links. In *Optical Free Space Communication Links, IEE Colloquium on*, pages 3–1. IET, 1996. 31

[90] Jeffrey B Carruthers and Joseph M Kahn. Multiple-subcarrier modulation for nondirected wireless infrared communication. *Selected Areas in Communications, IEEE Journal on*, 14(3):538–546, 1996. 31, 34

[91] Tomoaki Ohtsuki. Multiple-subcarrier modulation in optical wireless communications. *Communications Magazine, IEEE*, 41(3):74–79, 2003. 31

[92] K.-I. Ahn and J.K. Kwon. Color intensity modulation for multicolored visible light communications. *Photonics Technology Letters, IEEE*, 24(24):2254–2257, 2012. ISSN 1041-1135. doi: 10.1109/LPT.2012.2226570. 31, 84

[93] P.M. Butala, J.C. Chau, and T.D.C. Little. Metameric modulation for diffuse visible light communications with constant ambient lighting. In *Optical Wireless Communications (IWOW), 2012 International Workshop on*, pages 1 –3, oct. 2012. doi: 10.1109/IWOW.2012.6349697. 31, 78, 79, 84

[94] Yuichi TANAKA, Toshihiko Komine, Shinichiro Haruyama, and Masao Nakagawa. Indoor visible communication utilizing plural white leds as lighting. In *Personal, Indoor and Mobile Radio Communications, 2001 12th IEEE International Symposium on*, volume 2, pages F–81. IEEE, 2001. 31

[95] Oswaldo González, Rafael Pérez-Jiménez, S Rodriguez, José Rabadán, and Alejandro Ayala. Ofdm over indoor wireless optical channel. In *Optoelectronics, IEE Proceedings-*, volume 152, pages 199–204. IET, 2005. 31, 32

[96] J. Vucic, C. Kottke, S. Nerreter, A. Buttner, K.-D. Langer, and J. Walewski. White light wireless transmission at 200 + mb/s net data rate by use of discrete-multitone modulation. *Photonics Technology Letters, IEEE*, 21(20):1511–1513, Oct 2009. ISSN 1041-1135. doi: 10.1109/LPT.2009.2028696. 31

[97] Jelena Vučić, Christoph Kottke, Stefan Nerreter, Klaus-Dieter Langer, and Joachim W Walewski. 513 mbit/s visible light communications link based on dmt-modulation of a white led. *Journal of Lightwave Technology*, 28(24):3512–3518, 2010. 31

[98] Mostafa Z Afgani, Harald Haas, Hany Elgala, and Dietmar Knipp. Visible light communication using ofdm. In *Testbeds and Research Infrastructures for the Development of Networks and Communities, 2006. TRIDENTCOM 2006. 2nd International Conference on*, pages 6–pp. IEEE, 2006. 32, 42

[99] J. Armstrong. Ofdm for optical communications. *Lightwave Technology, Journal of*, 27(3):189–204, Feb 2009. ISSN 0733-8724. doi: 10.1109/JLT.2008.2010061. 32

[100] J. Armstrong and B.J.C. Schmidt. Comparison of asymmetrically clipped optical ofdm and dc-biased optical ofdm in awgn. *Communications Letters, IEEE*, 12(5): 343 –345, may 2008. ISSN 1089-7798. doi: 10.1109/LCOMM.2008.080193. 32, 37, 40, 42, 44, 45, 55

[101] J. Armstrong, B.J.C. Schmidt, D. Kalra, H.A. Suraweera, and A.J. Lowery. Spc07-4: Performance of asymmetrically clipped optical ofdm in awgn for an intensity modulated direct detection system. In *Global Telecommunications Conference, 2006. GLOBECOM '06. IEEE*, pages 1 –5, 27 2006-dec. 1 2006. doi: 10.1109/GLOCOM.2006.571. 32, 42, 45, 55

[102] N. Fernando, Yi Hong, and E. Viterbo. Flip-ofdm for optical wireless communications. In *Information Theory Workshop (ITW), 2011 IEEE*, pages 5–9, Oct. 2011. doi: 10.1109/ITW.2011.6089566. 32, 46, 47, 55

[103] N. Fernando, Yi Hong, and E. Viterbo. Flip-ofdm for unipolar communication systems. *Communications, IEEE Transactions on*, 60(12):3726–3733, December. ISSN 0090-6778. doi: 10.1109/TCOMM.2012.082712.110812. 32, 37, 46, 47, 55

[104] S.D. Dissanayake and J. Armstrong. Comparison of aco-ofdm, dco-ofdm and ado-ofdm in im/dd systems. *Lightwave Technology, Journal of*, 31(7):1063–1072, April 2013. ISSN 0733-8724. doi: 10.1109/JLT.2013.2241731. 32, 40

[105] Michael Wolf, Sher Ali Cheema, Martin Haardt, and Liane Grobe. On the performance of block transmission schemes in optical channels with a gaussian profile. In *Transparent Optical Networks (ICTON), 2014 16th International Conference on*, pages 1–8. IEEE, 2014. 32, 39

[106] Daniel JF Barros, Sarah K Wilson, and Joseph M Kahn. Comparison of orthogonal frequency-division multiplexing and pulse-amplitude modulation in indoor optical wireless links. *Communications, IEEE Transactions on*, 60(1):153–163, 2012. 32

[107] Mike Wolf and Martin Haardt. Comparison of ofdm and frequency domain equalization for dispersive optical channels with direct detection. In *Transparent Optical Networks (ICTON), 2012 14th International Conference on*, pages 1–7. IEEE, 2012. 32, 37, 39, 41, 63, 70

[108] John M. Cioffi. Chappter 4: Multi-channel modulation. URL `http://www.stanford.edu/group/cioffi/ee379c/`. 32, 47, 48, 49

[109] Liang Wu, Zaichen Zhang, Jian Dang, and Huaping Liu. Adaptive modulation schemes for visible light communications. *Journal of Lightwave Technology*, 33(1):117–125, 2015. 33, 37, 39, 70

[110] CIE. Commission Internationale de lEclairage Proc. 1931. 33, 80

[111] KK Wong, T O'Farrell, and M Kiatweerasakul. The performance of optical wireless ook, 2-ppm and spread spectrum under the effects of multipath dispersion and artificial light interference. *International Journal of Communication Systems*, 13(7-8): 551–576, 2000. 34

[112] Gene W Marsh and Joseph M Kahn. Performance evaluation of experimental 50-mb/s diffuse infrared wireless link using on-off keying with decision-feedback equalization. *Communications, IEEE Transactions on*, 44(11):1496–1504, 1996. 34

[113] D. Falconer, S.L. Ariyavisitakul, A. Benyamin-Seeyar, and B. Eidson. Frequency domain equalization for single-carrier broadband wireless systems. *Comms. Mag., IEEE*, 40(4):58–66, Apr 2002. ISSN 0163-6804. doi: 10.1109/35.995852. 34, 39, 112

[114] Fabrizio Pancaldi, Giorgio M Vitetta, Reza Kalbasi, Naofal Al-Dhahir, Murat Uysal, and Hakam Mheidat. Single-carrier frequency domain equalization. *Signal Processing Magazine, IEEE*, 25(5):37–56, 2008. 34, 38, 39

[115] Junyi Jiang, Rong Zhang, and Lajos Hanzo. Analysis and design of three-stage concatenated color-shift keying. *IEEE Transactions on Vehicular Technology*, pages 1–12, 2014. 34

[116] Nevio Benvenuto, Rui Dinis, David Falconer, and Stefano Tomasin. Single carrier modulation with nonlinear frequency domain equalization: an idea whose time has comeagain. *Proceedings of the IEEE*, 98(1):69–96, 2010. 38

[117] Robert W Chang. Synthesis of band-limited orthogonal signals for multichannel data transmission. *Bell System Technical Journal*, 45(10):1775–1796, 1966. 38

[118] Richard van Nee and Ramjee Prasad. *OFDM for Wireless Multimedia Communications*. Artech House, Boston, London, 2000. ISBN 0-89006-530-6. 38, 63, 64

[119] Terry Walzman and Mischa Schwartz. Automatic equalization using the discrete frequency domain. *Information Theory, IEEE Transactions on*, 19(1):59–68, 1973. 39

[120] Kodzovi Acolatse, Yeheskel Bar-Ness, and Sarah Kate Wilson. Novel techniques of single-carrier frequency-domain equalization for optical wireless communications. *EURASIP Journal on Advances in Signal Processing*, 2011:4, 2011. 39

[121] Mike Wolf, Liane Grobe, Marie Ruth Rieche, Andreas Koher, and Jelena Vucic. Block transmission with linear frequency domain equalization for dispersive optical

channels with direct detection. In *Transparent Optical Networks (ICTON), 2010 12th International Conference on*, pages 1–8. IEEE, 2010. 39

[122] A Nuwanpriya, Jian Zhang, A Grant, Siu-Wai Ho, and Lin Luo. Single carrier frequency domain equalization based on on-off-keying for optical wireless communications. In *WCNC, IEEE*, pages 4272–4277, April 2013. doi: 10.1109/WCNC.2013.6555264. 39, 41, 106, 115

[123] Chia-chen Hsieh and Da-shan Shiu. Single carrier modulation with frequency domain equalization for intensity modulation-direct detection channels with intersymbol interference. In *Personal, Indoor and Mobile Radio Communications, 2006 IEEE 17th International Symposium on*, pages 1–5. IEEE, 2006. 39

[124] A. Nuwanpriya, Siu-Wai Ho, J.A. Zhang, A.J. Grant, and Lin Luo. Pam-scfde for optical wireless communications. *Lightwave Technology, Journal of*, 33(14):2938–2949, July 2015. ISSN 0733-8724. doi: 10.1109/JLT.2015.2424456. 39

[125] Hany Elgala, Raed Mesleh, and Harald Haas. An led model for intensity-modulated optical communication systems. *Photonics Technology Letters, IEEE*, 22(11):835–837, 2010. 44

[126] Jean Armstrong. New ofdm peak-to-average power reduction scheme. In *Vehicular Technology Conference, 2001. VTC 2001 Spring. IEEE VTS 53rd*, volume 1, pages 756–760. IEEE, 2001. 44

[127] H. Elgala, R. Mesleh, and H. Haas. Predistortion in optical wireless transmission using ofdm. In *HIS*, volume 2, pages 184–189, Aug 2009. doi: 10.1109/HIS.2009.321. 44, 50, 112

[128] R. Mesleh, H. Elgala, and H. Haas. An overview of indoor ofdm/dmt optical wireless communication systems. In *CSNDSP, IEEE*, pages 566–570, July 2010. 44, 50, 112

[129] J. Armstrong and A.J. Lowery. Power efficient optical ofdm. *Electronics Letters*, 42 (6):370–372, March 2006. ISSN 0013-5194. doi: 10.1049/el:20063636. 45

[130] Emily Lam, Sarah Kate Wilson, Hany Elgala, and Thomas DC Little. Spectrally and energy efficient ofdm (see-ofdm) for intensity modulated optical wireless systems. *arXiv preprint arXiv:1510.08172*, 2015. 45

[131] Dobroslav Tsonev and Harald Haas. Avoiding spectral efficiency loss in unipolar ofdm for optical wireless communication. In *Communications (ICC), 2014 IEEE International Conference on*, pages 3336–3341. IEEE, 2014. 46

[132] Kyongkuk Cho and Dongweon Yoon. On the general ber expression of one-and two-dimensional amplitude modulations. *Communications, IEEE Transactions on*, 50 (7):1074–1080, 2002. 53

[133] S.K. Wilson and J. Armstrong. Transmitter and receiver methods for improving asymmetrically-clipped optical ofdm. *Wireless Communications, IEEE Transactions on*, 8(9):4561–4567, September. ISSN 1536-1276. doi: 10.1109/TWC.2009.080524. 55

[134] A. Azhar and D. O'Brien. Experimental comparisons of optical ofdm approaches in visible light communications. In *GLOBECOM Workshops (GC Wkshps), 2013 IEEE*, Dec 2013. 59

[135] Ieee standard for air interface for broadband wireless access systems. *IEEE Std 802.16-2012 (Revision of IEEE Std 802.16-2009)*, pages 1–2542, Aug 2012. doi: 10.1109/IEEESTD.2012.6272299. 61, 115

[136] Qi Wang, Qiuliang Xie, Zhaocheng Wang, Sheng Chen, and L. Hanzo. A universal low-complexity symbol-to-bit soft demapper. *Trans. Veh. Technol, IEEE*, 63(1): 119–130, Jan 2014. ISSN 0018-9545. doi: 10.1109/TVT.2013.2272640. 63, 117

[137] Amos Lapidoth, Stefan M Moser, and Michele A Wigger. On the capacity of free-space optical intensity channels. *IEEE Transactions on Information Theory*, 55(10): 4449–4461, 2009. 67, 149

[138] John G. Proakis and Masoud Salehi. *Digital Communications*. McGraw-Hill, fifth edition, 2008. 68, 119, 121

[139] Shu Lin and Daniel J. Costello, Jr. *Error Control Coding: Fundamentals and Applications*. Prentice-Hall, Inc., 1983. 68

[140] J. Conan. The weight spectra of some short low-rate convolutional codes. *Trans. Commun., IEEE*, 32(9):1050–1053, Sep 1984. ISSN 0090-6778. doi: 10.1109/TCOM.1984.1096180. 68

[141] Jeff Foerster and John Liebetreu. FEC Performance of Concatenated Reed-Solomon and Convolutional Coding with Interleaving, June 2000. URL `http://www.ieee802.org/16/tg1/phy/contrib/802161pc-00_33.pdf`. 68

[142] S Rajbhandari, Z Ghassemlooy, and NM Aldibbiat. Performance of convolutional coded dual header pulse interval modulation in infrared links. In *6th PGNET, UK*, pages 227–231, 2006. 68

[143] Jeffrey B Carruthers and Joseph M Kahn. Modeling of nondirected wireless infrared channels. *Trans. Commun., IEEE*, 45(10):1260–1268, 1997. 72, 127

[144] . Forward error correction for high bit-rate DWDM submarine systems. ITU, ITU-T G.975.1. 76

[145] Atsuya Yokoi, Jaeseung Son, Taehan Bae. CSK constellation in all color band combinations, march 2011. URL `http://mentor.ieee.org/802.15/dcn/11/15-11-0247-00-0007-csk-constellation-in-all-color-band-combinations.pdf`. 81

[146] E. Monteiro and S. Hranilovic. Constellation design for color-shift keying using interior point methods. In *Globecom Workshops (GC Wkshps), 2012 IEEE*, pages 1224–1228, 2012. doi: 10.1109/GLOCOMW.2012.6477755. 84, 89, 108

[147] R.J. Drost and B.M. Sadler. Constellation design for color-shift keying using billiards algorithms. In *GLOBECOM Workshops (GC Wkshps), 2010 IEEE*, pages 980–984, 2010. doi: 10.1109/GLOCOMW.2010.5700472. 84, 108

[148] Supplement to ieee standard for information technology - telecommunications and information exchange between systems - local and metropolitan area networks - specific requirements. part 11: Wireless lan medium access control (mac) and physical layer (phy) specifications: High-speed physical layer in the 5 ghz band. *IEEE Std 802.11a-1999*, page i, 1999. doi: 10.1109/IEEESTD.1999.90606. 87

[149] Van Bomme WJM and Van Ven Beld GJ. Lighting for work: a review of visual and biological effects. *Lighting Research and Technology*, 36:255–269, 2004. 89

[150] R. Singh, T. OFarrell, and J.P.R. David. An enhanced color shift keying modulation scheme for high-speed wireless visible light communications. *J. Lightw. Technol., IEEE*, 32(14):2582–2592, July 2014. ISSN 0733-8724. doi: 10.1109/JLT.2014.2328866. 89, 92, 96, 108, 115

[151] Jin Young Park, Ra-Yeon Ha, Vin Ryu, Eosu Kim, and Young-Chul Jung. Effects of color temperature and brightness on electroencephalogram alpha activity in a polychromatic light-emitting diode. *Clin Psychopharmacol Neurosci*, 11:126–131, 2013. 89

[152] R. Singh, T. O'Farrell, and J.P.R. David. Higher order colour shift keying modulation formats for visible light communications. In *VTC Spring, IEEE*, pages 1–5, May 2015. doi: 10.1109/VTCSpring.2015.7145858. 93, 97, 111, 125

[153] John G. Proakis. *Digital Communications*. McGraw-Hill, third edition, 1995. 96

[154] G. Welti and J.S. Lee. Digital transmission with coherent four-dimensional modulation. *Information Theory, IEEE Transactions on*, 20(4):497–502, 1974. ISSN 0018-9448. doi: 10.1109/TIT.1974.1055247. 96

[155] Bernard Sklar. *Digital Communications: Fundamentals and Applications*. Prentice-Hall, Inc., second edition, 2001. 97, 119

[156] Bo Bai, Qunfeng He, Zhengyuan Xu, and Yangyu Fan. The color shift key modulation with non-uniform signaling for visible light communication. In *ICCC, 2012 1st IEEE Int. Conf.*, pages 37–42, 2012. doi: 10.1109/ICCCW.2012.6316471. 99

[157] Ravinder Singh, Timothy O'Farrell, and John P.R. David. Performance evaluation of ieee 802.15.7 csk physical layer. In *Globecom Workshops, IEEE*, pages 1064–1069, Dec 2013. doi: 10.1109/GLOCOMW.2013.6825133. 99, 101

[158] G Cossu, AM Khalid, P Choudhury, R Corsini, and E Ciaramella. 3.4 gbit/s visible optical wireless transmission based on rgb led. *Optics express*, 20(26):B501–B506, 2012. 106

[159] Charles Brackett et al. Dense wavelength division multiplexing networks: Principles and applications. *Selected Areas in Communications, IEEE Journal on*, 8(6):948–964, 1990. 106

[160] Arnold Wilkins, Jennifer Veitch, and Brad Lehman. Led lighting flicker and potential health concerns: Ieee standard par1789 update. In *Energy Conversion Congress and Exposition (ECCE), 2010 IEEE*, pages 171–178. IEEE, 2010. 108

[161] J. Armstrong and B. Schmidt. Comparison of asymmetrically clipped optical ofdm and dc-biased optical ofdm in awgn. *Commun. Lett., IEEE*, 12(5):343–345, May 2008. ISSN 1089-7798. doi: 10.1109/LCOMM.2008.080193. 112

[162] D.J.F. Barros, S.K. Wilson, and J.M. Kahn. Comparison of orthogonal frequency-division multiplexing and pulse-amplitude modulation in indoor optical wireless links. *Trans. Commun., IEEE*, 60(1):153–163, January 2012. ISSN 0090-6778. doi: 10.1109/TCOMM.2011.112311.100538. 112

[163] Linqi Song, Jun Wang, Changyong Pan, and Jian Fu. A normalized llr soft information demapping method in dtmb system. In *ICCS 2008. 11th IEEE Singapore Int. Conf.*, pages 1297–1301, Nov 2008. doi: 10.1109/ICCS.2008.4737392. 117

[164] T.A. Gulliver. Matching q-ary reed-solomon codes with m-ary modulation. *Trans. Commun., IEEE*, 45(11):1349–1353, Nov 1997. ISSN 0090-6778. doi: 10.1109/26.649739. 121